UNIVERSITY OF SOUTHAMPTON

FACULTY OF NATURAL AND ENVIRONMENTAL SCIENCES

Ocean and Earth Sciences

Volume [1] of [1]

Controls on the composition and extraction of rare earth elements and yttrium (REY) in deep sea polymetallic nodules and sediments

by

Amaya Menendez Gamella

Thesis for the degree of Doctor of Philosophy

September 2017

UNIVERSITY OF SOUTHAMPTON

ABSTRACT

FACULTY OF FACULTY OF NATURAL AND ENVIRONMENTAL SCIENCES

Ocean and Earth Sciences

Thesis for the degree of Doctor of Philosophy

CONTROLS ON THE COMPOSITION AND EXTRACTION OF RARE EARTH ELEMENTS AND YTTRIUM (REY) IN DEEP SEA POLYMETALLIC NODULES AND SEDIMENTS

By Amaya Menendez Gamella

Rising demand for metals is driving a search for new mineral resources and mining of seafloor deposits is likely to commence in the next few years. These include polymetallic nodules and crusts that are highly enriched in Mn, Co, Ni, Cu, Mo, Li and Te, and deep-sea clays that can contain high concentrations of the rare earth elements and yttrium (REY). The potential environmental impacts of mining these deposits are, however, poorly constrained and a better understanding of the processes that control metal enrichment in marine resources is essential. In support of this, I have undertaken detailed geochemical investigations of polymetallic nodules and crusts and deep sea sediments.

Analyses of deep-sea sediments recovered from the Atlantic Ocean reveal that REY concentrations are highest (up to ~510 ppm) in slowly accumulating pelagic red clays that contain ferromanganese micronodules. Micronodules that have a hydrogenous source, characterised by lower Mn/Fe, have higher REY concentrations than micronodules that have a diagenetic source. REY concentrations in pelagic red clays from the Atlantic are ~4 times lower than concentrations reported for Pacific clays; the area of seafloor required to extract ~10% of the global annual REY demand is ~100 km^2, assuming removal of the upper 1 m of sediment.

The bulk chemical composition of polymetallic nodules from different areas (UK Claim and APEI-6) of the Clarion Clipperton Fracture Zone in the eastern Pacific Ocean is rather similar, but high resolution in situ analyses show that the composition of individual layers within nodules is highly heterogeneous. Nodules from the UK Claim area contain a higher proportion of layers with high Mn/Fe and low Co that accumulate relatively rapidly; these layers likely accumulated in the Miocene when the UK Claim area was located closer to the equator, in the zone of high primary productivity.

Leaching of sediments and polymetallic nodules with dilute oxalic acid is effective for extracting the transition metals but is ineffective for releasing the REY. The REY are effectively extracted from Pacific nodules and sediments with dilute HCl, but the extraction efficiency is lower for samples from the Atlantic Ocean (~45% vs >~80% in the Pacific).Return of leached residues to seawater has the potential to increase the metal content of seawater above a mining site by up to four orders of magnitude. This may represent a source of toxicity to the benthic ecosystem in a mining area.

Table of Contents

Table of Tables

Chapter 2

Chapter 3

Table of Figures

Chapter 1

Chapter 2

Chapter 5

Appendices

Appendix A

Academic Thesis: Declaration Of Authorship

I, Amaya Menendez Gamella declare that this thesis and the work presented in it are my own and has been generated by me as the result of my own original research.

Controls on the composition and extraction of rare earth elements and yttrium (REY) in deep sea polymetallic nodules and sediments

I confirm that:

1. This work was done wholly or mainly while in candidature for a research degree at this University;
2. Where any part of this thesis has previously been submitted for a degree or any other qualification at this University or any other institution, this has been clearly stated;
3. Where I have consulted the published work of others, this is always clearly attributed;
4. Where I have quoted from the work of others, the source is always given. With the exception of such quotations, this thesis is entirely my own work;
5. I have acknowledged all main sources of help;
6. Where the thesis is based on work done by myself jointly with others, I have made clear exactly what was done by others and what I have contributed myself;
7. Parts of this work have been published as: Menendez, A., James, R.H., Roberts, S., Connelly, D. (2017): Controls on the distribution of rare earth elements in deep-sea sediments in the North Atlantic Ocean. *Ore Geology Reviews*, 87:100-113.

8. Signed: .....

Date: .....

Acknowledgements

The work leading to this Doctoral Thesis has been funded by the European Union Seventh Framework Programme (FP7/2007-2013) under the MIDAS project, grant agreement no. 603418. Thanks to Prof. Phil Weaver for coordinating this project and also for being an excellent landlord.

Very especially I would like to thank my main thesis supervisor, Prof. Rachael H. James at the University of Southampton. Her patient support and advice during my PhD time have been key in my development as a scientist. Rachael knew how to guide my work into the right direction, while at the same time allowing it to be my own. In particular I want to thank her for trusting in me to carry out this project, which has led me to live an amazing experience as a PhD student at Southampton. I also would like to thank to the rest of my supervisors, Prof. Stephen Roberts, Dr. Kate Peel and Prof. Doug Connelly, as they have also provided support and useful feedback to my manuscripts.

As this thesis has taken me to spend a decent number of hours in the lab, I have to give a special mention to the lab managers Dr. Matt Cooper, Dr. Andy Milton, Dr. Richard Pearce and (again) Dr. Kate Peel for their priceless guidance and patience. Also, many thanks to Mr. Bob Jones, Mr. John Ford and Mr. Dan Doran for the sectioning of my (ultradelicate) manganese nodules.To Dr. Anna Lichtchslag for her extraoficial mentoring, and for making work in the night shift during the JC120 cruise such a fun experience!

I am very grateful to so many of my fellow PhD students and friends in Southampton for so many incredibly fun moments spent together during the last 3 years…too many people to name in one page! Special mention to my lovely housemates during most of the last 3 years, Melanie Siegburg and Tim van Peer.

I want to thank Age Vellinga for his tasty meals after long thesis-writing days. Thanks for making my life amazing and exciting every day!

And last but not least, to my parents, Rosa Maria and Pedro Alberto: because I owe it all to you. Thanks for your inconditional support, which has taken me to where I am now.

Definitions and Abbreviations

ΣREY = Total Rare Earth elements + Yttrium

AED = Australasian Ecotoxicity Database

APEI= Area of Potential Environmental Interest

AUV = Autonomous Underwater Vehicle

Avg = average

AABW = Antartic Bottom Water

BC = Box Core

Bdl = Below detection limit

BSD = Backscattered

BOSCORF = British Ocean Sediment Core Research Facility

Bsf = Below seafloor

CCD = Carbonate Compensation Depth

CCFZ = Clarion Clipperton Fracture Zone

CDI = Cobalt Development Institute

Cmbsf = centimeters below seafloor

CMC = Camera-mounted Core

CRM = Certified Reference Material

DP = Deep Plain

EDS = Energy Dispersive Spectrometry

EEZ = Exclusive Economic Zone

EPR = East Pacific Rise

FL = Flat

GAC = Global Annual Consumption

GC = Gravity Core

GR = Growth Rate

GRS = Geochemical Reference Sample

HREE = Heavy Rare Earth Elements (Tb, Dy, Er, Ho, Tm, Yb, Lu)

HyBIS = Hydraulic Benthic in Situ Sampler

ICP-MS = Inductively Coupled Plasma Mass Spectrometry

IMnI = International Manganese Institute

INSD = International Nickel Study Group

ISA = International Seabed Authority

JC120 = James Cook 120 cruise

LA ICP-MS = Laser Ablation Inductively Coupled Mass Spectrometry

LED = Light-emmiting Diode

LDEO = Lamont-Doherty Earth Observatory

LREE = Light Rare Earth elements (La, Ce, Pr, Nd)

MAR = Mid-Atlantic Ridge

MC = Mega Core

MIDAS = Managing Impacts of Deep Sea Resource Exploitation

MREE = Middle Rare Earth Elements (Sm, Eu, Gd)

m-XRF = micro-focused X-Ray Fluorescence

NASC = North American Shale Composite

MOR = Mid-Oceanic Ridge

NOAA = National Oceanographic and Atmospheric Administration

OMI = Ocean Mining Inc.

OPD = Oxygen Penetration Depth

PC = Piston Core

PCZ = Prime Crust Zone

PTFE = Polytetrafluoroethylene

RC = Red Clay

RC† = Red Clay with micronodules

RD = Rock Dredge

RI = Ridge

REE = Rare Earth Elements

REY = Rare Earth Elements + Yttrium

RRS = Royal Research Ship

SEM = Scanning Electronic Microscopy

SD = Standard Deviation

SMS = Sulfide Massive Deposits

SS = Sum of Squared

TC = Trigger Core

TR = Trough

UNCLOS = United Nations Convention on the Law of the Sea

UKSRL = UK Seabed Resources Limited

USGS = U.S. Geological Survey

XAFS = X-Ray Absorption Structure

XRF = X-Ray Fluorescence

Chapter 1: Introduction

Marine ferromanganese deposits, including polymetallic nodules and crusts have been considered an important source of metals since the 1970's (Rona 2002). These deposits are highly enriched in elements such as Mn, Co, Ni, Cu, Mo, Li, Te and the rare earth elements and yttrium (REY) (e.g. Hein et al., 2013), some of which are crucial in the development of many emerging and new generation technologies. Recent studies have also shown that deep-sea clays from the Pacific Ocean may also be an economically interesting source of the REY (Kato et al., 2011).

Concentrations of metals in these marine deposits are nevertheless highly variable, and likely related to environmental conditions that prevail as they form. These potentially include sedimentation rate, oxygen levels linked to surface bioproductivity, deep oceanic currents and the geodynamic environment. Understanding of the interplay between, and the relative importance of these processes, is therefore essential for understanding the genesis and evolution of deep sea deposits, and for mineral prospecting and the management of the environmental impact of such activities.

1.1 History of the exploration of deep sea deposits

Submarine ferromanganese crusts were first discovered in 1868 in the Kara Sea, in the Arctic Ocean off Siberia (Murray and Renard, 1891). Following this discovery, during a trip around the world from 1873 to 1876 on board the oceanographic vessel Challenger, many small black- and brown- coloured spherical concretions of different shapes and sizes were collected for various locations in all of the ocean basins. These were called "manganese nodules" although the first chemical analyses of three nodules from the Pacific revealed that they also contained high concentrations of Fe, Cu, Co, Ni, Zn and Pb (e.g. Goldberg & Picciotto 1955, Dietz, 1955, Riley & Prapas Sinhaseni, 1958). These early studies suggested that ferromanganese concretions were more abundant in the Pacific Ocean than the Atlantic, and they tended to occur at depths > 2000 m. The sediments on which the nodules were sitting were characterised as red clays with "dark chocolate- coloured oozes" which were found to be rich in manganese. The internal structure of nodules was characterised as a series of concentric

layers of alternating light and dark bands, although it was noted that some very large nodules consisted of a massive black core, with layers only occurring in the outer part. The outer layers were found to be rich in hydrated oxides of manganese and iron (Riley & Prapas Sinhaseni, 1958). Their formation process was attributed to the precipitation of colloidal hydrous phases which had absorbed trace metals from seawater.

These first chemical data revealed that polymetallic nodules were a potential source of Ni, Co, Cu and Mn, and a growing interest in their economic value started to develop. In the early 1960's, nodule fields in the Central Pacific started to be explored by mining companies such as Kennecott and Newport Shipbuilding (1962). During the next few years, these companies started to produce the first maps of the occurrence of nodules (McKelvey et al., 1979).

The importance of the nodule field in the "East-West belt of the southern Pacific Northwest, between the Clarion and Clipperton fractures", known at that time as the "Horn area", was first highlighted by Horn et al., (1972). This is an area located in the Central Eastern Pacific Ocean, north of the equatorial high productivity zone (Antoine et al., 1996). It extends from approximately 20˚N, 120˚W to 5˚N, 160˚W.

Active industrial exploration of Pacific nodules and crusts began in the early 80's. This led to the establishment of the International Seabed Authority (ISA) in Jamaica, and the signature of the United Nations Convention on the Law of the Sea (UNCLOS) in 1982, and its 1994 Implementing Agreement relating to deep seabed mining; a sort of "constitution for the seas". This law set up the framework of legal rights to the exploitation of marine resources on the sea floor outside national territorial waters, by dividing the seas into various legal zones. It also defines the legal status and extent of these zones and establishes norms governing the rights and jurisdictions of the coastal and flag states in respect of these zones (Bollmann, 2010). According to these zones, a state's jurisdiction ranges as the distance from the coast increases from full territorial sovereignty (in internal waters) to limited "aquitorial" sovereignty (in the territorial sea) and limited jurisdiction (in the exclusive economic zone, EEZ, and continental shelf) (Fig. 1).

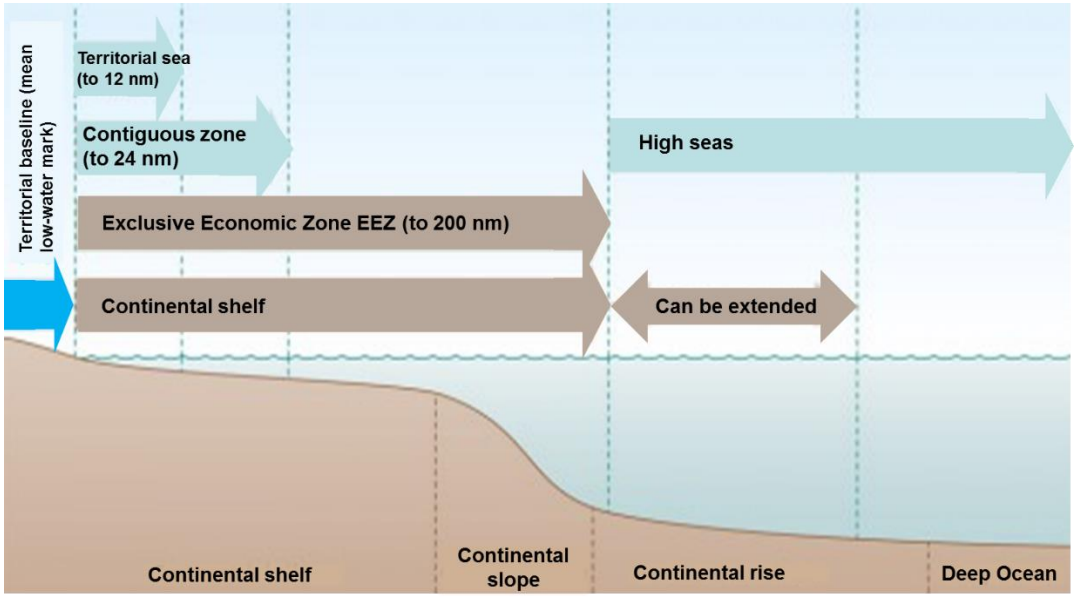

Figure 1. Delimited legal zones by UNCLOS. From Bollman, (2010).

A number of exploration licenses for large nodule fields within the Clarion Clipperton Fracture Zone have been granted by the International Seabed Authority since 2000, and regulations on prospecting and exploration of cobalt-rich crusts were adopted in 2012. Because of concerns about the effects of mining on the functioning of marine ecosystems and biodiversity (Smith & Koslow, 2007), the ISA identified nine bio-geographic sub-regions within the CCFZ in which no mining will occur. These areas are 400 km × 400 km in size, consisting of a protected core of 200 km x 200 km, surrounded by a buffer zone extending 100 km in each direction. These areas are known as “Areas of Potential Environmental Interest” (APEI), and are distributed across the CCFZ so as to capture the wide range of the different habitat types in the area (Wedding et al., 2013).

Interest in slowly-accumulating pelagic clays as a potential resource for rare earth elements and yttrium (REY) has been recently highlighted by Kato et al., (2011). These authors reported that sediment samples from the central and eastern Pacific have total REE (plus Y) concentrations of up to 1000-2230 ppm, and claimed that mining of only one square kilometre of a ~ 70- m thick layer in this area could produce a fifth of the of the current annual world consumption of these elements. These authors found that REY concentrations appear to be related to the presence of iron oxyhydroxide minerals and phillipsite which are assumed to scavenge REEs from ambient seawater. Thus, they inferred the distribution of these REE-rich sediments was likely to be the result of the interplay between input of Fe at mid-ocean ridges, the dispersal of the particle-rich

hydrothermal plume by oceanic currents and dilution of this material with biogenous carbonates and silica as well as terrigenous material.

Following this discovery, in 2013, extremely REY-rich mud, defined as mud with more than 5,000 ppm total REE and yttrium concentration (ΣREY), was discovered in the western Pacific Ocean off Minamitorishima Island, Japan. Iron (oxyhydr)oxides, manganese oxides, and apatite were identified as possible host phases for the REY (Iijima *et al.*, 2015; Fujinaga et al., 2015). Furthermore, Kon et al. (2014) claimed that the total REY contents of apatite in REY-rich mud from near Minamitorishima Island averaged up to 21,000 ppm. Despite these optimistic claims for the Pacific, marine sediments from the North Atlantic (Menendez et al., 2017) and Indian Oceans (Pattan & Parthiban, 2011; Yasukawa et al., 2015) appear to have rather lower REY concentrations (< 1000 ppm).

A significant potential advantage of both marine sediments and polymetallic nodules as a resource is that metals and the REY are relatively easily extracted from them. For example, it has been shown that the REY can be efficiently leached from polymetallic nodules in weak (0.2 M) H_2SO_4 (Parhi et al., 2013), and recent studies of Pacific deep-sea sediments indicate that the REY can be quantitatively extracted from them by leaching in dilute HCl and H_2SO_4 for periods of as short as 2-5 minutes at room temperature (Kato et al., 2011; Takaya et al., 2015). Similarly, studies of marine ferromanganese precipitates including crusts and nodules show that transition metals (Mn, Co, Ni, Cu, Zn and Pb) can easily be extracted at room temperature using low concentration solutions of hydroxylamine hydrochloride and oxalic acid/ammonia oxalate buffer (Koschinsky & Halbach, 1995). Co, Cu, Ni and Mn have also been successfully extracted within a short time from polymetallic nodules using a mixture of $FeSO_4$-H_2SO_4- H_2O (Vu et al., 2005). However, this method requires heating to ~ 90 °C. The relative simplicity of these methods has obvious and considerable benefits over extraction from land-based REY deposits

1.2 Types of deep marine deposits

1.2.1 REY- rich muds

Deep-sea sediments, including pelagic red clay, metalliferous sediments and zeolitic clay, are a potential source of REE. Of these, REY-rich mud has been defined as those clays with more than 400 ppm total REY (ΣREY) (Nakamura et al.,

2015), as this content makes them comparable to ΣREY in ion adsorption-type ore deposits in southern China (Bao and Zhao, 2008; Wu et al., 1995).

REY-rich muds are dark-brown pelagic clays characterized by low contents of terrigenous detrital materials, biogenous silica, and carbonates (Nakamura et al., 2015). Other components identified in these muds are calcium phosphates such as apatite, Fe-Mn-(oxyhydr)oxides and the zeolite phillipsite (e.g. Dubinin & Rozanov, 2001; Menendez et al., 2017).

1.2.1.1. REY-rich muds in the Pacific Ocean

Highest REY concentrations in the Pacific Ocean are found in slowly- accumulating pelagic sediments at depths greater than 4000 meters in areas more than 2000 km from land. Kato et al. (2011) identified two main regions for REY-rich muds in the Pacific: the eastern South Pacific and central North Pacific (Figure 2). REY- rich clays from the Eastern South Pacific region were found to be less than 10 meters thick, with ΣREY of 1000 - 2230 ppm, in the range of ion-adsorption-type deposits from southern China (ΣREY contents of 500–2000 ppm; Wu et al., 1995). REY-rich clays from the central North Pacific are by contrast much thicker (extending to > 30 m below the seafloor) than in the eastern South Pacific, with moderately high ΣREY contents (400 – 1000 ppm). Some of these moderately REY enriched layers were found to be up to ~ 70 meters thick east of the Hawaiian Islands.

In addition to these two main regions, REY- rich muds were also found in sediment layers from the northeastern Pacific (west of the Juan de Fuca Ridge; Figure 2). These layers have ΣREY contents comparable to those of the central North Pacific and are characterised by their location 10 – 20 m below the seafloor and their thicknesses of 5 - 30 meters, often overlaid by REY-depleted sediment layers.

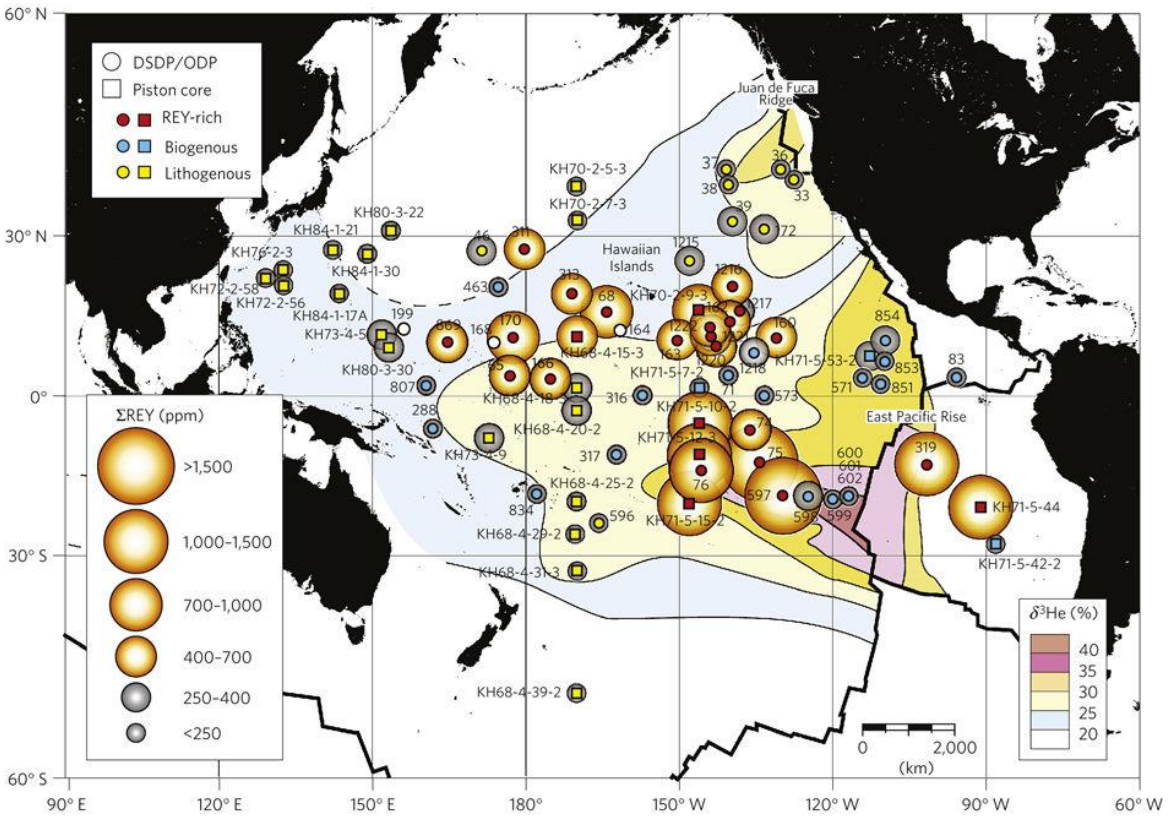

Figure 2. Distribution of average ΣREY contents in surface sediments (less than 2 m below seafloor) in the Pacific Ocean (Kato et al., 2011).

REY distribution diagrams are a useful resource to infer the nature of the geochemical processes affecting the sediments. Sediments from the Pacific Ocean are characterised by a pronounced Ce anomaly, as well as by an enrichment in the HREE relative to the LREE and have high Y/Ho ratios (e.g. Elderfield et al., 1981; Dubinin & Sval'nov 2002; Yasukawa et al., 2016). This indicates that Pacific sediments tend to incorporate relatively large quantities of biogenic apatite that is an important REY carrier phase (Toyoda et al, 1990; Dubinin & Rozanov, 2001; Dubinin, 2004). In support of this, X- ray absorption fine structure (XAFS) and micro- focused X- ray fluorescence (m- XRF) analyses have shown that La in REY-rich mud is found in association with apatite (Kashiwabara et al., 2014).

1.2.1.2. REY- rich muds in the Atlantic Ocean

To date fewer studies have been conducted in Atlantic sediments compared with the Pacific or the Indian Oceans. Most of the previous studies (e.g. Dubinin & Rozanov, 2001) have reported REE contents of deep-sea mud in the Atlantic of less than 400 ppm (below the threshold for a REY- rich mud). In a later study Dubinin et al. (2013) reported ΣREY content of up to ~ 380 ppm (average

115 ppm) for deep-sea muds in the Angola Basin. Slightly higher concentrations were found by Dubinin and Rimskaya-Korsakova (2011), who reported concentrations of up to ~ 600 ppm in sediments from the Brazil Basin. The most likely explanation for the lower average REY abundances for Atlantic deep sea clays in comparison with those reported for the Pacific Ocean is the generally higher sedimentation rates in the Atlantic Ocean, as a greater part of this ocean lies below the carbonate compensation depth (CCD) (Sverdrup et al., 1970; Biscaye et al., 1976), which reduces the time available for uptake of the REY from seawater into sediments.

1.2.1.3. REY- rich muds in the Indian Ocean

Although there are more data available for deep sediments from the Indian Ocean relative to the Atlantic, information on the lateral distribution of REY- rich muds is still sparse. Bulk sediment analyses of red clays located in the surface of the sediment column in the eastern Indian Ocean revealed relatively high ΣREY concentrations (excluding Y, Pr, Tb and Tm) of up to ~ 750 ppm (Pattan et al. 1994). Concentrations of the REY in sediment samples from the Central Indian Ocean Basin are similar, ~ 780 ppm (Pattan and Parthiban, 2011).

In more recent studies, a 50- meter thick REY- rich mud, comparable to those in the central North Pacific has been reported in the eastern Indian Ocean (Yasukawa et al., 2014). The ΣREY content of these muds was moderately high, on average ~ 630 ppm with a maximum of ~ 1100 ppm. Nevertheless, these muds were only found 70 – 120 m below the seafloor. These authors found a strong link between Ca-phosphate and the ΣREY, and suggested that that biogenic apatite is a major host mineral of REY in the Indian Ocean muds.

1.2.1.4. Genesis of REY-rich muds

In their study of deep sediments in the Pacific Ocean, Kato et al., (2011) suggested that hydrothermal activity at mid oceanic ridges (MORs) plays a role in the formation of REY- rich muds. They noted a correlation between the distribution of the REY- rich muds and helium-3 anomalies (δ^3He; an indicator of hydrothermal plumes along mid- oceanic ridges) in the water column. Formation of Fe-Mn- (oxyhydr)oxides as hydrothermal fluids mix with seawater is thought to scavenge the REY from seawater, and these (oxyhydr)oxides subsequently fall to the seafloor (Kato et al. 2011).

Biogenic Ca- phosphate is also an important control on the REY in REY- rich muds (Kashiwara et al., 2014; Yasukawa et al., 2014; Kon et al., 2014). Nevertheless it has been noted that the ΣREY also correlate with Fe_2O_3 and MnO, as well as P_2O_5, in these REY-rich sediments, suggesting that other carrier phases may also be important. These could include biogenic apatite, phillipsite, Fe- Mn- (oxyhydr)oxides and Fe- Ca- hydrophosphates (Dubinin, 2001).

Numerous studies (e.g. Kato et al., 2011; Menendez et al., 2017) have shown that there is an inverse relationship between REY and sedimentation rates in both the Pacific and the Atlantic. The most REY- enriched pelagic clays are usually found in places with very low sedimentation rates, of generally less than 0.1 cm/kyr. (Kato et al. 2011). In these environments, accumulation of biogenic Ca- phosphate is higher than that that of any other component (e.g. Hüneke and Henrich, 2011). This would explain why REY-rich muds are generally found only at depth in the ocean, below the CCD, and their absence in elevated areas of high carbonate productivity such as the East Pacific Rise (EPR) or the Mid Atlantic Ridge (MAR) or the continental slopes.

1.2.2 Polymetallic nodules

Polymetallic or manganese nodules are concretions formed of concentric layers of iron and manganese (oxyhydr)oxides, generally around a nucleus. This nucleus if present may be of different sizes and often consists of a small shell or microfossil, phosphatised fragments of shark teeth (Halbach et al., 1988), or fragmented pieces of older nodules. The morphology and thickness of the nodule layers are variable. Many nodules show discontinuous layers, with differences between their bottom side that is in contact with the sediments, and their top side that is exposed to seawater. The size of the nodules may vary too, from microscopic-sized micronodules, to large aggregates of more than 20 centimetres diameter.

Most nodules lie on the seabed at the sediment-water interface, although they be completely covered by sediments in areas with higher rates of sedimentation. Their abundances are also variable from one location to another, reaching densities of up to ~ 75 kg/m^2 in some nodule fields (e.g. Mewes et al., 2014). Nodule density is a principal control on economic potential, and nodule abundances of > 10 kg/m^2 over areas extending several tenths of square kilometre are usually considered to be economically viable (e.g. Hein et al., 2003).

1.2.2.1. Mechanisms of formation

Nodules can acquire metals from three sources, seawater (hydrogenetic), sediment pore fluids (diagenetic), and hydrothermal fluids (hydrothermal). Although some nodules only incorporate metals from one source, they are usually formed from a combination of sources. All nodules however require: 1) low sedimentation rates; 2) the presence of bottom water currents that remove fine sediment particles, but retain coarser particles such as the shells of small marine organisms or nodule fragments that then can act as nuclei for new nodules; 3) a good oxygen supply in order to form Fe- Mn- (oxyhydr)oxides; and 4) sediments with enough porosity to hold large amounts of pore water.

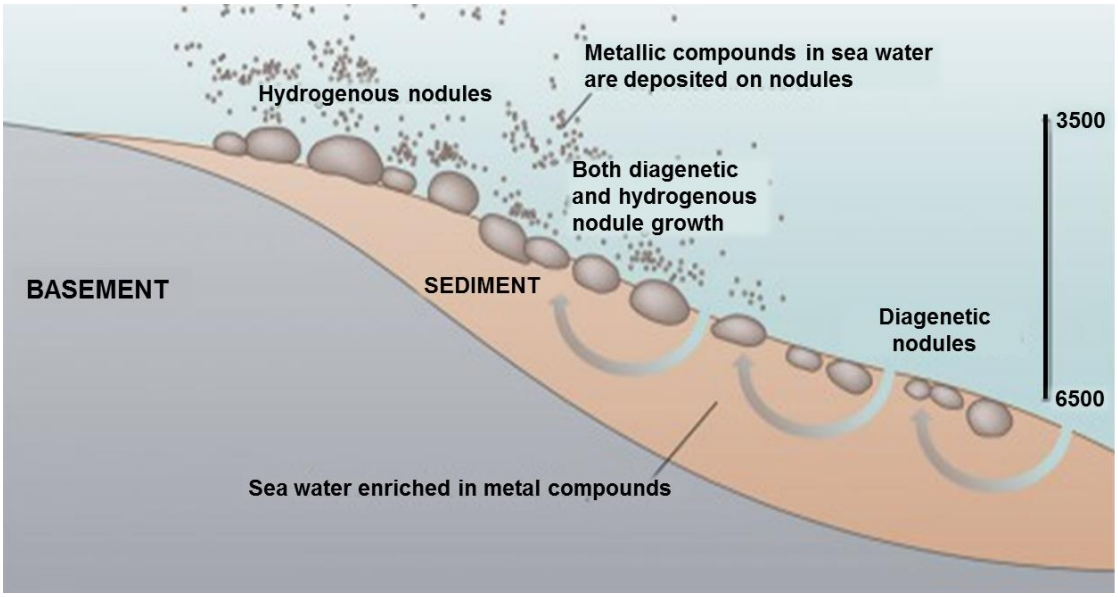

Figure 3. Scheme showing hydrogenetic and diagenetic types of nodule formation (World Ocean Review 3)

Hydrogenetic precipitation of nodules is characterised by precipitation of metals from the overlying oxic bottom waters (Koschinsky and Halbach, 1995). As these metals have previously been scavenged by colloidal particles, such as hydrated Fe- and Mn- (oxyhydr)oxides, the final precipitate consists of a fine intergrowth of hydrated Mn and Fe-oxide phases, with low Mn/Fe ratios and high Co (Burns & Burns, 1978). Typically hydrogenous deposits have rather low Mn/Fe ratios, ≤ 3, and low quantities of Ni + Cu, as these elements are excluded from (oxyhydr)oxide structures. Additionally, hydrogenous deposits tend to have positive Ce anomalies and high REY concentrations, which results from the slow surface complexation of REY from ambient seawater with colloidal Fe-Mn-(oxyhydr)oxide particles, with preferential enrichment of tetravalent Ce (Piper,

1974; Addy, 1979; de Lange et al.,1992; Nath et al., 1992; Kasten et al., 1998, Bau et al., 2014).

Diagenetic nodules result from the mobilization of Mn under oxic or suboxic conditions within sediment pore waters, and its re-precipitation as Mn- oxides when these fluids migrate into oxygen-replete pore waters at the oxic-suboxic boundary (Halbach et al., 1981). Precipitation of Mn- oxides during early oxic diagenesis coincides with release of trace metals such as Ni, Cu and Zn from the oxidation of organic matter oxidation (Dymond et al. 1984) so these metals tend to be enriched in the Mn-oxide structure (Halbach et al., 1981). By contrast, suboxic diagenesis results in higher Mn^{2+} but lower Ni and Cu fluxes (Halbach et al., 1981). Both oxic and sub-oxic diagenetic deposits are characterized by fast growth rates of up to ~ 250 mm/Ma (von Stackelberg, 2000). In contrast to slow-growing hydrogenous nodules, diagenetic nodules have lower REY concentrations because the fast growth rate inhibits complexation of the REY on the surface of the Mn-oxides (Kuhn et al., 1998; Ohta et al., 1999). Diagenetic nodules also tend to have negative Ce anomalies, because of the different redox behaviour of this element with respect to the other trivalent REEs (Sholkovitz et al., 1994; Schijf et al., 1995; Bau et al., 1997; Bau et al,. 2014).

Hydrothermally- influenced nodules are by contrast rarer, and acquire metals from hot springs associated with hydrothermal activity. Hydrothermal deposits consist typically of pure Mn oxide and have negligible levels of other metals except for Mg, Ba, K and Li (Usui & Someya, 1997). Although the REY content of hydrothermal deposits is highly variable (e.g. Kuhn et al., 1988), these deposits tend to have negative Ce anomalies, positive Eu and Y anomalies, and are strongly depleted in the light rare earth elements (LREE) relative to the heavy rare earth elements (HREE) (e.g. Mills et al., 2001, Kuhn et al,. 1988).

1.2.2.2. Occurrence

Polymetallic nodules generally occur in deep marine basins, between 4000 and 6000 meters water depth with very low sedimentation rates, of less than 1 cm/1000 yrs (e.g. Hein et al., 2013). Metal-depleted nodules have also been found in shallower areas near continental platforms and in fresh water lakes (e.g. Baturin et al., 2002, 2009). Deep water nodules are usually found below the CCD in areas of high surface productivity. This is because biogenic calcite dilutes the organic matter necessary for the diagenetic reactions in the sediment that release Mn, Ni and Cu (Cronan et al., 2006).

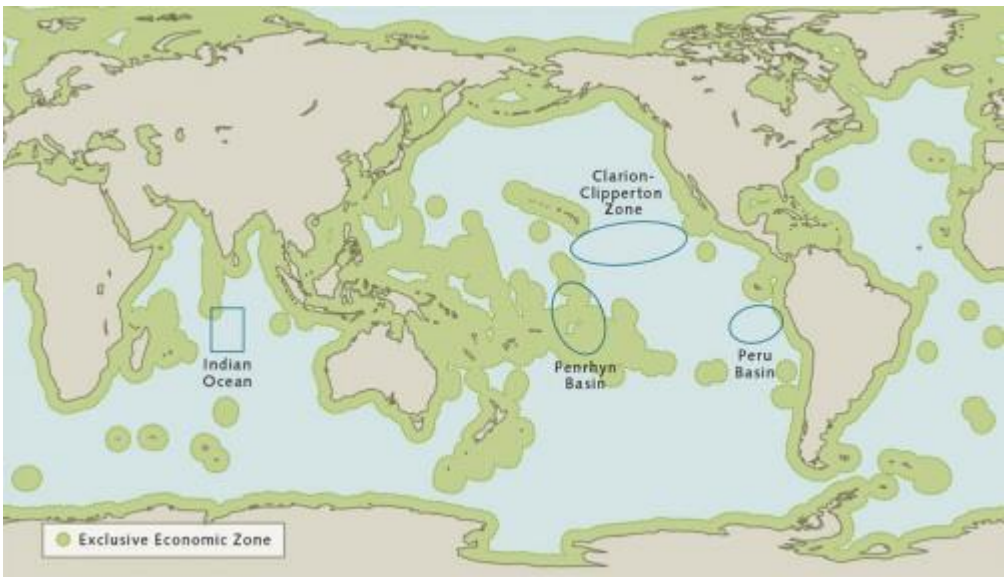

Figure 4. Distribution of nodules with densities that are great enough for industrial exploitation. From World Ocean Review 3, (2014).

The Clarion-Clipperton Fracture Zone (CCFZ) is the world's largest manganese nodule field, with an area of 9 million km^2 (Figure 3). This area is located in the Equatorial Pacific, and extends from the west coast of Mexico to the east of Hawaii (20˚N, 120˚W to 5˚N, 160˚W), being delimitated north and south by the Clarion and Clipperton Fractures, respectively. It is located just north of the equatorial zone of high productivity (Antoine et al., 1996). Data on nodule abundances over peripheral regions and areas with variable seafloor morphology suggests that nodules are not evenly distributed over the CCFZ, as densities range between 10 and 75 kg/m^2 (e.g. Mewes et al., 2014). Due to the low levels of surface productivity, the bottom sediments are generally oxic, with oxygen penetration depths of more than 3 meters in some locations (e.g. Rühlemann et al., 2011). As a result, the current growth of nodules in this area is most likely hydrogenetic, although a strong suboxic diagenetic signal may be found in nodules from some parts of the central CCFZ (Wegorzewski et al., 2014). These nodules constitute a potential resource for the diagenetically- influenced elements Mn, Ni, Cu and Zn (e.g. Wegorzewski & Kuhn, 2014).

The Peru Basin is situated about 3000 km off the Peruvian coast, in the south-eastern tropical Pacific. It is about half as large as the CCFZ, with nodule densities averaging ~ 10 kg/m^2. In contrast with the CCFZ, the Peru Basin sediments are characterised by an oxic-suboxic front at about only ~ 10 cm sediment depth (Von Stackelberg, 1997). This is a result of the high bioproductivity in the surface waters, which leads to a high flux of organic carbon into the sediments (Halbach

et al., 1988). As a result, manganese nodules in this area currently form by the supply of metals from suboxic pore waters at the bottom part of the nodules and by the supply of metals from oxic seawater on the top of the nodule (Dymond et al., 1984). They are considered to be a potential resource for the diagenetically-influenced elements Mn and Ni, as high concentrations of up to ~ 25 % and ~ 1.5 %, respectively have been reported for these elements (e.g. Glasby, 2000).

The Penrhyn Basin is the third most important nodule field in the Pacific Ocean. It is located in the vicinity of the Cook Islands on the Australian continent with a total area of ~ 750000 km^2. Average nodule densities have been estimated to be~ 25 kg/m^2, although small, isolated areas have been found with nodule densities up to ~ 58 kg/m^2 (Hein et al., 2015). The abyssal seabed sediments consist predominantly of zeolite-rich pelagic red-brown clays, located at depths greater than 4800 m, although some carbonate muds/oozes are also present in the north eastern part of the Basin. The pelagic muds consist of detrital silicates, zeolites, volcanic glass, Fe- and Mn- oxides and phosphate debris (Cronan et al., 2010). The area is characterised by low sedimentation rates and highly oxygenated conditions, due to the influence of the Antarctic Bottom Water (Hein et al., 2015). As a result, nodule growth is influenced by hydrogenetic precipitation of Mn oxide and Fe (oxyhydr)oxide from ambient bottom waters, with very little contribution from sediment pore waters (Hein et al., 2015). The nodules are therefore considered to be a good resource for the hydrogenetically- enriched metals Co, Ti, as well as for the REY. On the other hand, they have relatively low concentrations of Ni, Cu and Mn compared to the CCFZ nodules (Hein et al., 2015).

To date, only one large area of manganese nodules has been discovered in the central Indian Ocean, with an area in the range of that of the Penrhyn Basin. The estimated nodule density is ~ 5 kg/m^2 (Pattan & Parthiban, 2011), although the sediments also contain numerous micronodules. The nodules have relatively high concentrations of Mn, Ni, Cu and Zn and appear to have a mainly diagenetic source (Pattan & Parthiban, 2011).

In the Atlantic Ocean, nodules fields have been discovered in the Brazil Basin (Kasten et al., 1998; Dubinin & Rimskaya-Korsakova, 2009), and the Madeira abyssal plain in the north Western Atlantic (de Lange & Poorter, 1992). These nodules have high concentrations of Fe, Co and the REY that point to a hydrogenetic origin. However, some nodules from the Angola Basin may also contain a diagenetic component (Dubinin et al., 2013). Large nodule fields are

sparse in the Atlantic Ocean, and are confined to relatively small deep basins due to higher sedimentation rates and lower CCD relative to the Pacific.

1.2.3 Ferromanganese crusts

Unlike polymetallic nodules, all ferromanganese crusts have a hydrogenetic origin, as they precipitate from seawater onto the surface of seamounts, ridges and plateaus which provide a long-term sediment-free hard substrate for millions of years (Hein et al., 2013). The distribution of ferromanganese crusts is poorly known, but they tend to be more common in the Pacific than in the Atlantic and Indian Oceans because sediment- free ridges and seamounts are more common in the Pacific (Figure 5).

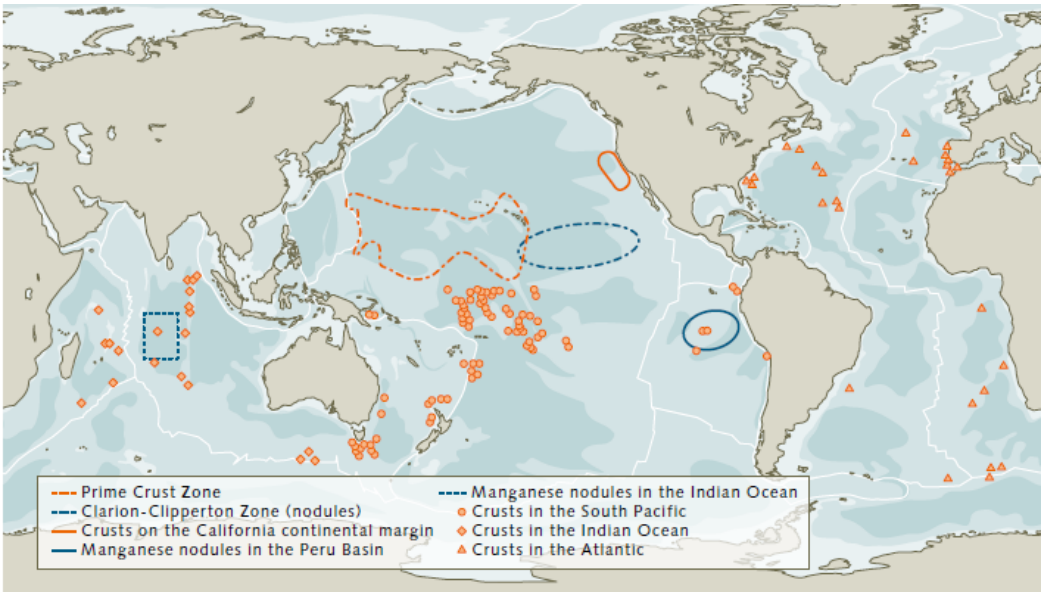

Figure 5. Locations of known ferromanganese crusts and polymetallic nodules. From World Ocean Review 3, (2014).

Crusts are generally found at depths of 400 to 7000 meters, with the thickest deposits occurring at depths of about 800 to 2500 m. The thickness of the deposits varies from less than 1 mm to 260 mm (Hein et al., 2013), being generally thicker in seamounts of an older age. Subsequently, crusts are thickest in the NW Pacific as the seamounts there are the oldest in the global ocean, of Jurassic age (Usui & Someya, 1997). Crusts in this location, also known as the Prime Crust Zone (PCZ, Figure 5) also have the highest concentrations of metals, which has attracted great interest in them, with numerous crust exploration campaigns currently taking place at that location.

The mechanism of metal enrichment in ferromanganese crusts is controlled by the sorption of considerable quantities of metals from seawater, as they have very high porosity (~ 60%) and specific- surface areas (average 325 m^2/g) and grow at extremely slow rates of up to 5 mm/Ma (Hein et al., 2000). It is thought that the morphology of seamounts and ridges facilitates the growth of ferromanganese crusts and the acquisition of metals. This is linked, for instance to the upwelling that takes place along the flanks of the seamounts, which creates turbulent mixing along the flanks and over the summit. This ultimately helps keep the seamounts free of sediments, as well as supplying nutrients to surface waters that then can be used in primary productivity (Hein et al., 2013). Organic matter produced in surface waters will sink, and be oxidised, creating an oxygen minimum zone, which acts as a reservoir for dissolved Mn and associated metals that are then enriched in the crusts. As the water column becomes more oxic, hydrogenetic growth processes are triggered, and metals are scavenged from the overlying sea water.

1.2.3.1. Mechanisms of formation

Hydrogenetic accretion of ferromanganese crusts is controlled by the colloidal scavenging of trace metals from sea water by Mn- oxides and Fe- (oxhydr)oxides. Mn- oxides capture positively charged ions on their negatively charged surfaces, while the slightly positively- charged surfaces of the Fe- (oxhydr)oxides attract negatively charged and neutral ions from seawater (Hein et al., 2013). Trace metals are incorporated by electrostatic and chemical bonding, as well as surface oxidation or substitution (Hein & Koschinsky, 2013).

Diagenetic processes such as phosphatisation may occur in old ferromanganese crusts. This process causes the impregnation of the crusts with carbonate fluorapatite during times of major global climate transitions (e.g. Bau et al., 1996; Koschinsky et al., 1997). During this process, trace metals are remobilised and the original metal content may be modified (Koschinsky et al., 1997). In particular, some of the REY such as yttrium and the heavy rare earths (HREE) may be preferentially enriched in phosphatised deposits (Bau et al., 1996). It has been pointed out by many authors that most ferromanganese crusts from the Pacific Ocean have been impregnated at some extent with carbonate fluorapatite during one or several episodes of phosphatisation in the Tertiary (Halbach et al., 1989, Grau and Kudrass, 1991; Hein et al., 1993). According to these authors, only

relatively young crusts that formed since the Miocene are not affected by the secondary phosphatisation.

1.2.3.2. Composition

First-generation ferromanganese crusts are composed of an intergrowth of the Fe-oxide vernadite and amorphous Fe-(oxyhydr)oxides, with minor amounts of goethite and detrital silicates such as quartz and feldspar (Hein et al., 2013). Older deposits (pre Middle Miocene) are likely to have undergone phosphatisation and can contain up to 20% of fluorapatite (Halbach et al., 1989).

Although Fe and Mn occur in similar amounts, it has been noted that the Mn content tends to be generally higher in open-ocean environments in the Pacific, while Fe is higher in ferromanganese crusts from the Indian and Atlantic oceans, as well as in continental margins around the Pacific (Hein et al., 2013). Elements such as cobalt and nickel may constitute an economically interesting resource in ferromanganese crusts.

1.3 Resource potential and mining of deep sea deposits

The resource potential of deep sea ferromanganese deposits and sediments relies on their high content in many economically interesting metals such as Mn, Co, Ni and Cu, as well as the REY. Furthermore, there are limitations in the current supply of the REY, because China is decreasing their exports as more if their production is being used internally (Hein et al., 2013). As the world's demand for these metals increases, this will require new sources of metals, including deep sea resources.

1.3.1 Uses of the Rare Earth Elements and Yttrium (REY)

The REY are key components of high-technology applications (e.g. laptops, cell phones and flat screen televisions; Kingsnorth, 2008) and green energy technologies (e.g. electric 'hybrid' cars, wind turbines and fluorescent lighting; Castor and Hedrick, 200). The importance of some deep sea resources such as the REY-rich muds is due to the need for a stable supply of REY, as world demand for developing technologies increases.

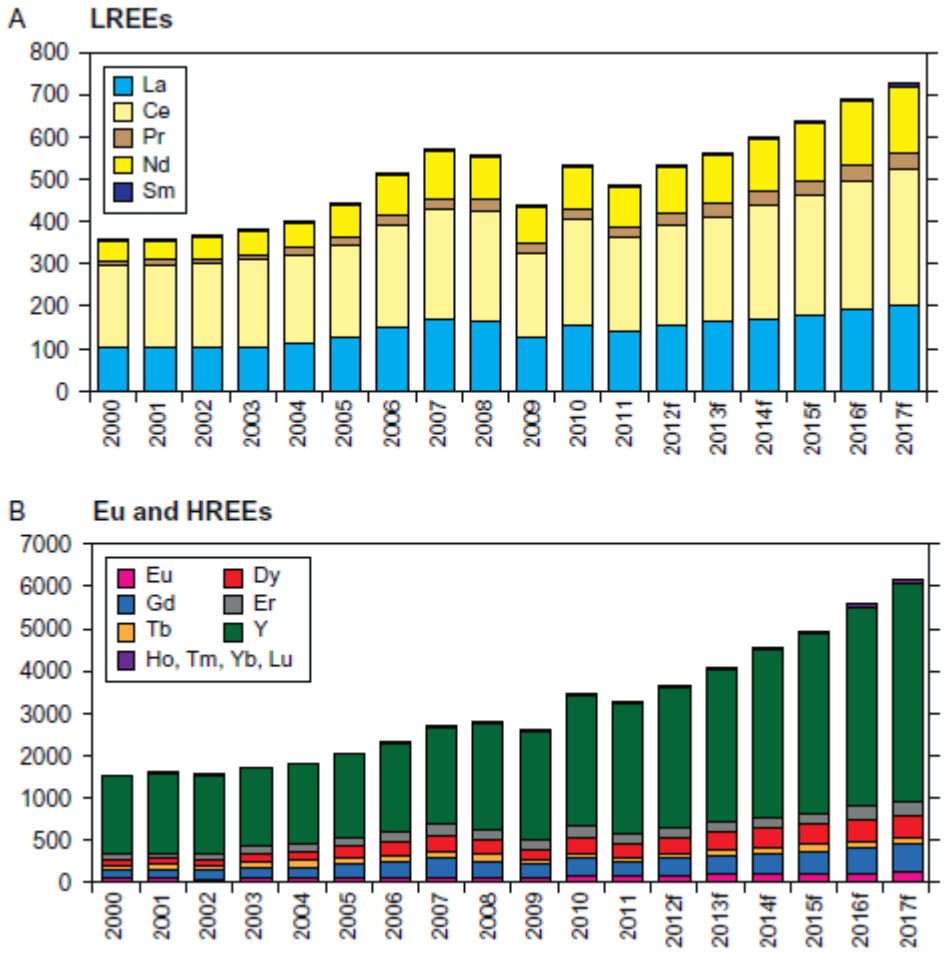

Figure 6. Global demand for rare earths and yttrium from 2000 to 2017. (A) Normalized demand for LREEs. La in 2000 = 100. (B) Normalized demand for Eu and HREEs. Eu in 2000 = 100. f = forecast. Modified from Shaw and Chegwidden (2012) in Nakamura et al., (2015).

Around 90 % of the global production of these elements is controlled by China (USGS, 2014), which owns at least half of the world's reserves (USGS, 2013). Chinese ion-adsorption ore deposits are particularly important, as they are more enriched in the heavy rare earth elements (HREE = Tb, Dy, Er, Ho, Tm, Yb, Lu) (Vulcan, 2012), which are of higher economic importance although more uncommon in REY- rich ores (Figure 6).

1.3.2 Comparison with land- based deposits

Grades of metals in land-based mines are decreasing with time. As an example, the average Cu content of ores in 1900 was of 4%, while nowadays it is only 0.5 % (Mudd, 2009), which subsequently requires more ore to be processed to produce the same amount of Cu. Additionally, land- based mines must remove a substantial amount of overburden to reach the deposits, with the opening of

deep- open pits. In connection with this, it has been reported that many nodules in the CCFZ contain > 1 % Cu, although the variability of Cu concentrations within the area is yet to be constrained. Manganese nodule fields have the additional advantage of the lack of overburden to remove in order to reach the ore bodies, as they are essentially two- dimensional deposits. Similar estimations of ore content suggest economically interesting contents of Mn, Co and Ni in nodules from the CCFZ (e.g. Hein et al. 2013).

Additionally, high contents in REE have also been reported for nodule fields (e.g. Dubinin & Rozanov, 2000; Hein et al., 2015). More importantly, marine deposits seem to be potentially more enriched in the rarer but economically more interesting heavy rare earth elements (HREE) than the land- based ores. In fact, the average content of these elements in large terrestrial ores is < 1 % of the total REY, while it has been reported that the HREE content of nodules from the CCFZ comprises up to ~ 13 % of the total REY (Hein et al., 2013).

With respect to REY- rich muds, Kato et al., (2011) made estimates that the resource potential of REY- rich muds in some of the thick beds of the Eastern South Pacific could supply up to 25,000 tonnes of REY oxides, which is comparable to one fourth of the 2012 global annual demand (USGS, 2013). This, however requires all the mud section to be mined, which in some cases reached up to ~ 70 meters thickness.

Other advantages often highlighted for deep- sea deposits over land- based mines is their distribution on the surface of the seabed, which facilitates their recovery once mining tools are on the seabed. Similarly, REY- rich muds are typically found as layered pelagic sediments with a relatively uniform distribution over extensive areas of the seafloor (e.g. Lyle et al., 2010). By contrast, land- based mines must remove a greater amount of host rock or sediments to reach the ore bodies, with the associated increases in costs and environmental impact.

Terrestrial REY deposits also tend to be associated with high concentrations of radioactive elements such as U and Th (e.g., Murakami and Ishihara, 2006; Sørensen et al., 2011), which appear as waste by- products after the processing of the ores. This has obvious and direct implications for the safety of the exploitation if these resources, as well as their environmental impact. Concentrations of these elements in REY- rich muds and ferromanganese deposits are notably lower (by up to ~ 2 orders of magnitude (e.g. Meor Yusoff & Latifah,

2002). This, therefore suggests that mining of deep sea resources is less likely to produce hazardous radioactive waste.

The extraction of metals from ferromanganese deposits and REY- rich muds is also expected to be notably faster and easier than land- based deposits. Most terrestrial hard-rock deposits must undergo complex metal extraction processes such as physical beneficiation and leaching in hot, concentrated acid or alkali solutions. This requires a high consumption of energy (e.g. Haque et al., 2014) and generally produces significant release of chemical waste into local farmlands and rivers (Hilsum, 2009). Kato et al. (2011) and Takaya (2015) reported that more than 90% of REY can be quickly and easily leached from deep-sea muds by using dilute hydrochloric acid at room temperature. Similarly, studies of marine ferromanganese precipitates including crusts and nodules show that transition metals (Mn, Co, Ni, Cu, Zn and Pb) can easily be extracted at room temperature using low concentration solutions of hydroxylamine hydrochloride and oxalic acid/ammonia oxalate buffer (Koschinsky & Halbach, 1995). Co, Cu, Ni and Mn have also been successfully extracted within a short time from polymetallic nodules using a mixture of $FeSO_4$-H_2SO_4- H_2O (Vu et al., 2005). However, this method requires heating to ~90 ˚C.

1.3.3 Mining strategies

The development of equipment and techniques to investigate and exploit the deep seabed has been one of the great challenges to science and technology over the past half-century. Deep-seabed mining differs from its land- based counterpart because it must be carried out underwater by remote methods, controlled from a floating platform at the sea surface.

To date no commercial recovery of deep sea resources has taken place in water depths greater than 200 meters (ISA technology brochure, 2014). However testing of systems for recovery of polymetallic nodules at depths greater than 5000 meters has proven that they can be easily lifted off the seabed. Most of the mining solutions have been developed and tested in the course of exploration for polymetallic nodule deposits. Many of their characteristics are however applicable to other deep marine resources.

Over time considerable improvements have been made in the technology used for the locating and sampling of the resources. The ultimate purpose of the technologies used for surveying and sampling deep sea resources is to assess

whether or not determined areas are suitable for further resource exploitation. This includes assessing if the resource abundances are great enough to be efficiently collected by the mining equipment. Additionally, the ores must concentrate metals in enough grades to be economically interesting (e.g. Hein et al., 2003).

1.3.3.1. Seafloor characterisation

Echo sounding has been used since the 1930 to characterize the topography of the seafloor. These generate sound waves within a certain radius that hit successively the sea floor beneath the vessel as it progresses, in order to provide a depth profile for the topography in the exploration region. The time interval between emission and reception of the sound wave in the sea floor is then converted to depth given the velocity of sound in the water. If equally spaced surveys are undertaken in parallel then a block of the seabed can be mapped.

Multibeam echosounders became available at the end of the 1970s (e.g. Farr, 1980). These were able to produce faster measurements, as multiple acoustic signals can map the seafloor below and to the side of the vessel. Modern multibeam echo sounders produce more than 150 measurements for each swath (averaging one every 130 m), covering a width of 20 kilometres at a depth of 4000 m (e.g. Theberge & Cherkis, 2013).

Additionally to surveying from a ship, most recent exploration campaigns have used autonomous underwater vehicles (e.g. Autosub AUV) that descend to the sea bottom, where they can collect images and nodule samples, before returning back to the surface on their own. In this way, nodule densities on the bottom can be estimated as kg of nodules per square meter. Other collection mechanisms include grabs and cameras operated by cable (e.g. Hydraulic Benthic In situ Sampler HyBIS, Boxcore, Gravity Corer GC or Mega Corer MC).

1.3.3.2. Mining technologies

The first trial of a prototype system for mining of manganese nodules took place in 1970 on the Blake Plateau, off the coast of Florida in the Atlantic Ocean, at a depth of 1000 m by Deepsea Ventures Inc. (ISA, 2014). During the following decade development and testing of different systems followed, carried out by several international consortia. The basic elements of these systems were an underwater, self-propelled nodule collector and an airlift- based raising system on

which nodules were propelled (Figure 7). In this device the ores are collected from the ocean floor and crushed to make a seawater slurry which is then pumped to the surface through a riser pipe.

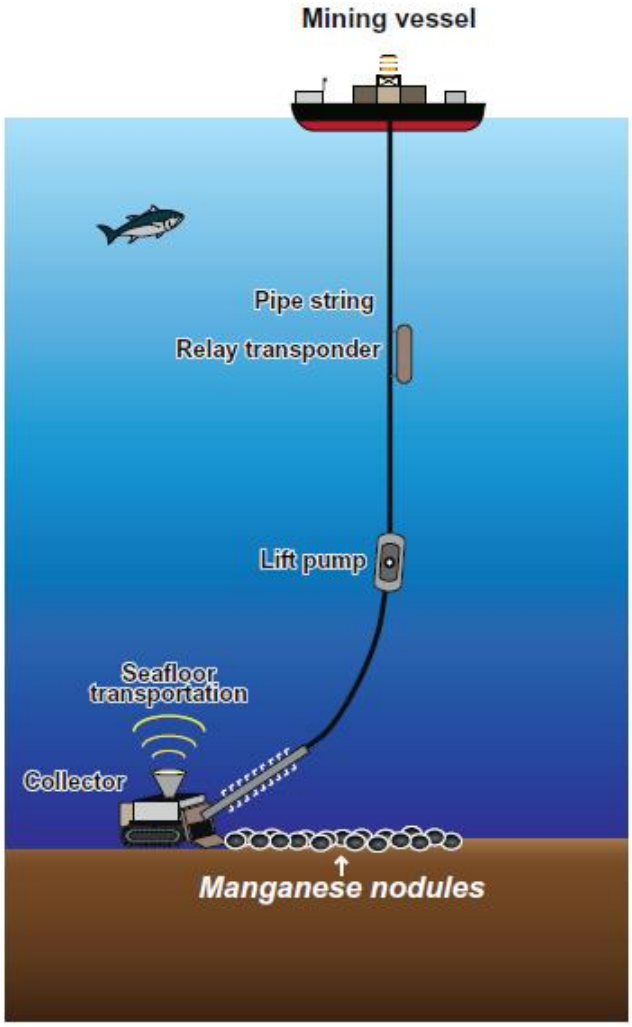

Figure 7. System used to mine manganese nodules. Modified from ISA Technology Brochure in Nakamura et al., (2015).

The air- lift system is created when compressed air is injected at the seafloor and intermediate depths to produce three- phase (gas, liquid and solid) upward flow. This system was tested by Mineral Associates with a towed collector, which managed to recover ~ 550 tons of manganese nodules during 18 h of operation. The air- lift system has the advantage that it avoids the need for an underwater mechanical pump. However wearing of the riser pipe might occur as expansion of the injected air at shallower depths causes an excessive velocity of the air flow. Both mechanisms (air- lifting and mechanical pumping) were further tested together by different mining companies such as Ocean Mining Inc. (OMI), and

about ~ 600 tons of nodules were recovered off the Central Pacific Ocean during the tests (ISA, 2014).

All of these tests were conducted over relatively short periods of time using small- scale experimental systems. Commercial mining however will require design and operating of much larger systems. Although no tests have been made for REY- rich muds, it can be inferred that similar approaches will be needed. These likely include the need for a seafloor mud collection tool similar to that of the nodules, as well as an air-lifting system to lift the slurry of mud and seawater up to a support vessel equipped with facilities for acid leaching and storage.

Once in the support vessel, the slurry is dewatered and transferred to storage tanks. Metals are then leached from the ores by different leaching methods with diluted acids, either onboard the vessel or on an onshore processing plant.

1.3.3.3. Leaching of ores

Many processes have been investigated to treat ferromanganese deposits. Initially the extraction of only nickel, copper and cobalt was considered, although after 1978 manganese was also added in order to increase the total revenue and to reduce the amount of waste (ISA, 2010). The technologies are of two types: hydrometallurgy, in which the metals are leached from the nodules by acid (hydrochloric or sulphuric) or basic (ammonia) reagents, and smelting, in which the hydroxides are reduced (stripped of oxygen) and the melted metals separated by gravity.

In the case of the REY- rich muds, Kato et al. (2011) showed that acid leaching is an effective method for effective recovery of the REY over short periods of time and room temperature.

Several consortia worked on processing nodules up to 1990 and their work is documented in the form of patents. One of these is the Cuprion process, which was developed by Kenecott. This method is similar to the Caron nickel extraction process from laterites, which is based on ammonium carbonate leaching of nickel. Unlike the Caron process, on which the laterite ore is dried and pre-reduced at high temperature with gases, in the Cuprion process this step is suppressed by instead carrying out the reduction during leaching by the cuprous ions (ISA background document, 2008). This process requires the wet ore to be ground and then slurred in a mixture of sea water and copper- and ammonium carbonate- bearing liquor. The slurry then passes through a series of reaction

vessels into which carbon monoxide is introduced. The cuprous ions are produced, which subsequently catalyses the reduction of the Mn- and Fe- oxide matrix. In this way the economic metals are dissolved and separated from the reduced residues by counter current washing. The nickel and copper are then extracted by liquid ion exchange combined with electrotwinning (separation by electrolysis), and the cobalt is removed by sulphide precipitation. However, recovery of manganese from the ferromanganese residue was found to be difficult.

Sulfuric acid leaching of ferromanganese deposits was first proposed by Fuerstenau in 1977, and later considerably improved in studies by the French Commissariat à l'Energie Atomique. It consists of the dissolution of the metals in crushed nodules by sulfuric acid at 180 °C and a pressure of 1200 kilopascals. Then bivalent manganese ions, formed by pre-reduction of some of the nodules with sulfuric gas, are introduced into a steam- pressured heating chamber to increase the recovery of cobalt. Copper, nickel and cobalt are then precipitated from the resulting solution using hydrogen sulfide.

Several companies have also studied the application of classical nickel and copper smelting processes to the treatment of polymetallic nodules. In these, following drying and calcination in a rotary kiln, the nodules are introduced into a submerged electric- arc furnace for reduction. Then a manganese- rich slag and an iron- copper- cobalt alloy are produced. Most of the remaining iron and manganese are removed from the alloy by oxidation in a converter. Following this process, a nickel- cobalt matte is obtained by adding sulfur. This can then be treated by selective extraction methods used in the nickel industry.

As we stated in section 1 of this introduction, Kato et al., (2011) showed relatively efficient rates of REY extraction from REY- rich muds after a short leaching time with weak acids. Takaya et al., (2015) further experimented with different reagents such as hydrochloric acid, sulfuric acid and nitric acid. They concluded that in addition to weak acids, strong acids, such as hydrochloric, sulfuric, and nitric acids, are also suitable for extraction of REY, as they recovered more than 90% of the REY almost instantaneously at room temperature (25 °C). They also used ammonium sulfate and sodium hydroxide as they are used for the recovery of REY from the Chinese ion- adsorption type deposits. However, these reagents did not successfully recover the REY from seafloor sediments.

1.4 Thesis Outline

Interest in the exploitation of deep sea mineral resources continues to grow, with mining of polymetallic seafloor massive sulfide deposits (SMS) expected to commence in 2019 offshore Papua New Guinea (Solwara 1, Nautilus Minerals). Nevertheless, there is still a pressing need to address issues about the environmental sustainability of underwater mining, as public policies are still under development to assess impacts, protect ecosystems and distribute resource rents (Hoagland et al., 2010). This includes the necessity to properly determine the geochemical and environmental processes that regulate the chemical composition of the deposits, which in turn will define the footprint of potential mining activities.

Regarding polymetallic nodules and REY- rich sediments, neither their occurrence nor the variability of their metal content is accurately known. It is however clear that the amount of metals in some of these deposits is equal to or higher than those of land- based ores, and has the potential to have a significant impact on the global resource supply. Additionally, the potentially lower costs associated with metal extraction from seafloor resources, coupled with lower levels of radioactive waste material, need to be better assessed.

This thesis addresses these issues by defining the baseline metal concentration and phase's association of a wide range of deep sea sediments (Chapter 2) and ferromanganese deposits from different locations (Chapter 5), with a focus on samples from areas which are likely to be considered for mining in the next few decades. Furthermore, methods for the extraction of metals from these deposits have been assessed (Chapter 3). Finally, a study of both a licensed mining area and an Area of Potential Environmental Interest in the CCFZ has been undertaken in order to determine the suitability of the APEI as a baseline from which to assess the impacts of nodule mining activities (Chapter 4).

Chapter 2: Controls on the distribution of rare earth elements in deep-sea sediments in the North Atlantic Ocean

This Chapter has been published as: Menendez, A., James, R.H., Roberts, S., Connelly, D. (2017): Controls on the distribution of rare earth elements in deep-sea sediments in the North Atlantic Ocean. *Ore Geology Reviews*, 87: 100-113.

Abstract

Deep-sea sediments can contain relatively high concentrations of rare earth elements and yttrium (REY), with a growing interest in their exploitation as an alternative to land-based REY resources. To understand the processes that lead to enrichment of the REY in deep-sea sediments, I have undertaken a detailed geochemical study of sediments recovered from the Atlantic Ocean, on a transect along ~24 °N that includes the deep Nares Abyssal Plain and the Canary and North America Basins.

Total REY concentrations (ΣREY) range from 7.99 to 513 ppm, and total concentrations of the heavy REY (Eu - Lu) range from 0.993 to 56.3 ppm. REY concentrations are highest in slowly accumulating pelagic red clays, especially in samples that contain ferromanganese micronodules. Factor analysis reveals that hydrogenous Fe- and Mn-(oxyhydr)oxides are the primary REY carrier phase in the red clays. In situ analysis of individual micronodules confirms that they have high ΣREY (up to 3620 ppm). REY concentrations are higher in micronodules that have a hydrogenous source, characterized by higher Fe/Mn, compared to micronodules that have a diagenetic source.

The ΣREY content of North Atlantic deep-sea sediments is ~4 times lower than in Pacific deep-sea sediments. I calculate that the area of seafloor required to extract ~10% of the global annual REY demand is ~100 km^2, assuming removal of the upper 1m of sediment.

2.1 Introduction

The rare earth elements (REE) are a group of 17 chemically similar metallic elements which comprise the 15 lanthanides, as well as scandium and yttrium.

They are used in the widest range of consumer products of any group of elements, and are important in many 'green' carbon-reducing technologies (Castor and Hedrick, 2006). For example, wind turbines use in the range of 0.6-1.0 tonne of neodymium magnets per megawatt of energy generated, REE phosphors are used in energy efficient lighting including LEDs, and 10-15 kg of lanthanum is used in every rechargeable battery that powers the Toyota Prius hybrid car (Lifton, 2009).

The world's most commercially important REE deposits are found in alkaline igneous rocks and carbonatites (Orris & Grauch, 2002). The estimated total world reserve of rare earth oxides on land is about 114 million tonnes, 48% of which is in China (Cordier, 2011). World production of REE is currently dominated by China, accounting for 90% of supply in 2013 (USGS, 2014). Demand for the REE is expected to grow by at least 6% per year over the next 25 years, particularly for permanent magnets and medical technologies (Alonso et al., 2012), and this, coupled with China's near monopoly of production, has led to concern about the risk of supply shortage, and prompted increased interest in REE exploration and the emergence of small land-based mines in other parts of the world (Australia, South Africa, North and South America and Scandinavia; Orris & Grauch, 2002).

Potential marine-based REE resources include deep sea sediments, polymetallic nodules, ferromanganese crusts and phosphorites. Polymetallic nodules mainly occur in deep ocean basins at depths of 4000-6000 m (Zhang et al., 2012). They have very high total REE concentrations (~700-2400 ppm; Hein & Koschinsky, 2013) as well as high concentrations of other economically interesting metals such as Ni, Co, Cu, Mo, Li and Te (Hein et al., 2013). The nodules can acquire REEs and metals from seawater ("hydrogenous" nodules) or from the sediment pore waters ("diagenetic" nodules) (Halbach et al., 1981). Ferromanganese crusts form by precipitation of dissolved components from seawater and are commonly found on top of western Pacific guyots. They are mainly formed of Mn-oxides intergrown with Fe oxyhydroxides; some older (pre-middle Miocene) crusts also contain carbonate fluoroapatite that was incorporated during diagenesis (Hein et al., 1993). The crusts have unusually high concentrations of Co (~8000 ppm; e.g. Koschinsky & Hein, 2003), and total REE concentrations (~2000 ppm; e.g. Mills et al., 2001) that are similar to polymetallic nodules. Phosphorite deposits are widespread on the seafloor of continental shelves and slopes along the western continental margins of the Pacific and Atlantic oceans, and can also occur on seamounts and plateaus (e.g. Thomson et al., 1984). Like ferromanganese crusts,

they acquire REEs from seawater, but their total REE concentration is widely variable (from a few tens to ~2000 ppm; Gonzalez et al., 2016).

Deep-sea sediments, including pelagic red clay, metalliferous sediments and zeolitic clay, are a potential source of REE. High concentrations of the REE and yttrium (REY), up to 2230 ppm total REY (ΣREY), comparable to the level in ore deposits in southern China, are reported for deep sea muds in the eastern South Pacific and central North Pacific (Kato et al., 2011). These authors suggest that the 70-m thick REY-rich mud layer in an area of 1 km^2 in the central North Pacific could supply the majority of current annual REY consumption in the world. If REY levels in Pacific sediments are applicable throughout the world's oceans, then the seafloor REY resource could potentially exceed the world's current land reserves (Kato et al., 2011).

To assess the potential for deep-sea sediments from the Atlantic Ocean as a REY resource, I have measured REY concentrations in sediments recovered from a transect at ~24 ˚N (Fig. 1). I also use these data to evaluate the processes that lead to REE enrichment. We show that ΣREY concentrations are lower than those measured in the eastern South Pacific and central North Pacific, and highlight the roles of scavenging of REY by iron- and manganese oxy(hydr)oxides and micronodule formation for enhancing REY concentrations in deep sea sediments.

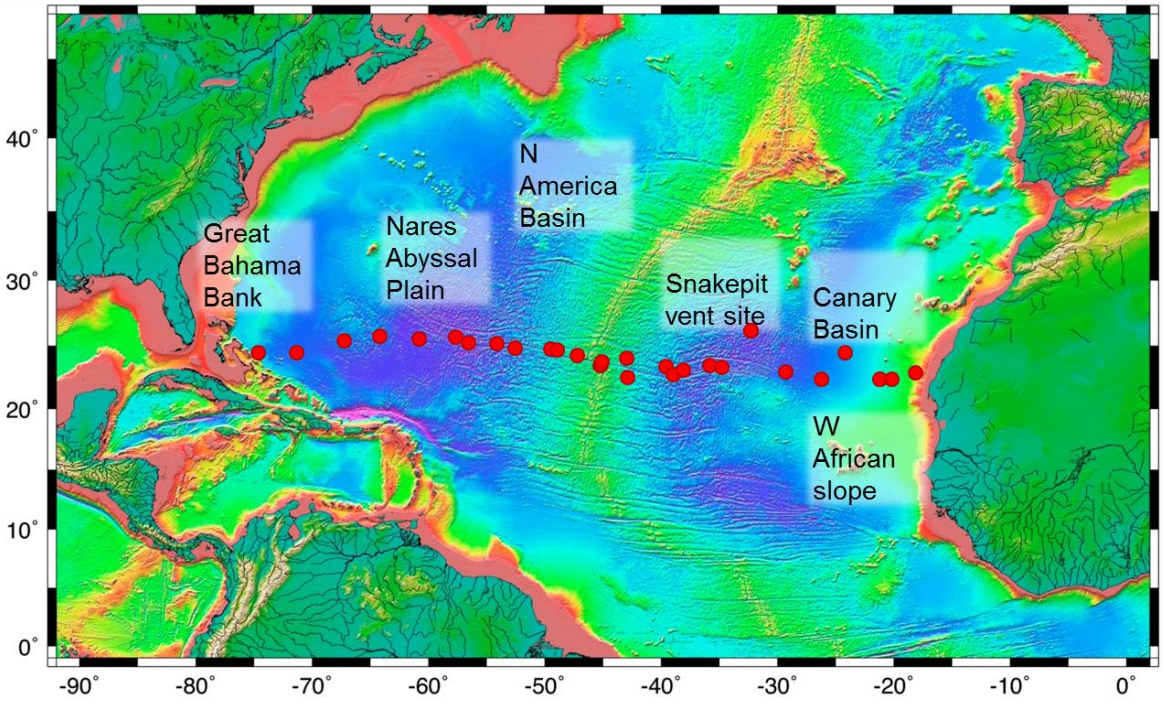

Figure 1. Location of sediment samples used in this study. The samples were taken along a transect across the North Atlantic at ~24 ˚N. Seafloor topography is from NOAA

(http://oceanexplorer.noaa.gov/explorations/05stepstones/background/plan/media/natl_topography.html).

Sample	Lat (°N)	Long (°E)	Location	Water depth (m)	Core type#	Source*	Depth bsf (cm)	Description
RC10-277	24.0	-72.9	Great Bahama Bank	5407	PC	LDEO	4-6	carbonate sand
RC11-243	24.0	-69.6	Great Bahama Bank	5407	PC	LDEO	30-32	brown clay
VM17-2	24.9	-65.5	Great Bahama Bank	5303	PC	LDEO	200-202	consolidated brown clay
VM16-15	25.3	-62.5	Nares Abyssal Plain	5810	PC	LDEO	880-882	consolidated brown clay
VM09-34	25.1	-59.2	Nares Abyssal Plain	5879	TC	LDEO	500-502	consolidated brown clay
RC10-10	25.2	-56.1	Nares Abyssal Plain	5929	PC	LDEO	500-502	consolidated brown clay
RC10-13	24.8	-55.0	Nares Abyssal Plain	5300	PC	LDEO	85-87	brown-yellowish clay
VM25-33	24.7	-52.6	North America Basin	941	PC	LDEO	40-42	orange-brown clay with micronodules
VM25-32	24.4	-51.0	North America Basin	5464	PC	LDEO	100-102	brown clay with micronodules
VM25-30	24.3	-48.0	W of Mid-Atlantic Ridge	4096	PC	LDEO		chalk
VM10-93	24.2	-47.5	Central Atlantic	3574	PC	LDEO	100-102	carbonate ooze
VM31-152	23.8	-45.8	Central Atlantic	4174	PC	LDEO	200-202	marl
VM10-89	23.0	-43.8	Central Atlantic	3523	PC	LDEO	630-632	white chalk
TH1-54S	23.1	-43.8	Central Atlantic	3840	CMC	LDEO	50-52	consolidated pink clay
VM20-242	23.4	-43.7	Central Atlantic	4565	PC	LDEO	635-637	carbonate-rich brown clay with micronodules
AT180-118	23.6	-41.6	Central Atlantic	4500	PC	LDEO	200-202	grey silty clay
VM20-241	22.1	-41.5	Central Atlantic	4372	PC	LDEO	100-102	foraminiferous marl
VM10-88	23.0	-38.2	Central Atlantic	4971	PC	LDEO	400-402	consolidated brown clay
AT181-001	22.3	-37.6	Central Atlantic	3895	PC	LDEO	65-67	chalk
RC21-2	22.7	-36.7	Canary Basin	3895	PC	LDEO	20-22	red-brown clay
VM22-212	23.0	-34.5	Canary Basin	6081	PC	LDEO	750-752	brown clay with micronodules
VM10-87	22.9	-33.5	Canary Basin	5329	PC	LDEO	420-422	consolidated grey clay
D11805-7	25.7	-31.0	Canary Basin	6129	BC	BOSCORF	15-17, 38-40	turbiditic grey clay
D10311	25.7	-31.0	Canary Basin	6133	GC	BOSCORF	5-7, 40-42	red clay
D11805-5	25.7	-31.0	W Africa cont. slope	5554	PC	BOSCORF	59-71, 96-98	turbiditic grey clay
VM27-255	22.6	-28.0	W Africa cont. slope	5554	PC	LDEO	81-83	orange clay
VM32-52	22.0	-25.0	W Africa cont. slope	5220	PC	LDEO	38-40	marl
KA74-4	24.0	-23.0	W Africa cont. slope	4838	GC	LDEO	323-325	consolidated brown clay
VM23-99	22.0	-20.0	W Africa cont. slope	4118	PC	LDEO	85-87	yellow marl
VM29-170	22.0	-20.0	W Africa cont. slope	4455	PC	LDEO	7-9	marl
VM30-54	22.0	-19.0	W Africa cont. slope	3506	PC	LDEO	140-142	marl
KM1-46	22.5	-17.0	W Africa cont. slope	1221	PC	LDEO	50-52	grey sand

Table 1: Location and description of deep-sea sediments from the North Atlantic Ocean. #: PC = piston core; GC = gravity core; BC = box core; KC = Kasten core; CMC = camera-mounted core; TC = trigger core; RD = rock dredge. *LDEO = Lamont-Doherty Earth Observatory; BOSCORF = British Ocean Sediment Core Facility. bsf = below seafloor.

2.2 Sample material

Sediment samples (~8 cm^3) were collected from cores stored at the British Ocean Sediment Core Facility, Southampton (BOSCORF) and at the Lamont-Doherty Earth Observatory, New York (LDEO). The cores were collected between 1955 and 1988 on cruises Discovery 118 (1981) and 177 (1988), Atlantis 180 and 181 (1947), Conrad 10 (1965), 11 (1968) and 21 (1978), Theta 1 (1971), Kane 74 (1974), Kevin Moran 1 (1955) and Vema 9 (1956), 10 (1956), 16 (1959), 17 (1960), 20 (1964), 22 (1966), 23 (1966), 25 (1968), 27 (1970), 29 (1973), 30 (1973) and 32 (1975). Most of these cores were split on board the ship or shortly after they were collected, and have since been stored at room temperature, in the case of the LDEO cores, and at ~4ºC in the case of the cores at BOSCORF. Core RC21-02 had been stored refrigerated at ~4 ˚C and was split for sampling in this study. The old age and partly desiccated state of some of the cores raises the possibility of chemical alteration during storage, although this effect is considered to be minor in oxic sediments (Rapin et al., 1986).

The core sites are located on a transect at ~24 ˚N across the North Atlantic Ocean, east to west from the Great Bahama Bank to the west slope of Africa. The transect crosses through the Nares Abyssal Plain, the North America Basin and the Canary Basin, and intersects the Snake Pit hydrothermal site at ~23˚N. The location of the core sites is showed in Fig. 1, and a list of the samples including water depth and a brief description is given in Table 1.

The sediment samples include fine-grained red/brown clays, grey clays, turbidites, carbonate oozes, chalks of different purities and foraminiferal marls. The red/brown clays are quite compacted and tend to be continuous in the cores, although traces of burrowing were observed in some cores. Core lithology was logged using a hand lens to assess texture and colour, structures such as bedding and burrows, carbonate content, mineralogy and the nature of the contact between different intervals. Samples were selected from the best preserved sections, and on the basis of the lithology.

Photographs of representative cores are shown in Fig. 2. Some sediments host palagonitised volcanic glass fragments and micronodules, within a fine-grained clay matrix (Fig. 3). The micronodules are ~0.1 to 5 mm in diameter, are rounded or subrounded and are generally evenly distributed throughout the sediment. Micronodules in sample VM25-033 (Fig. 3c) exhibit a dendritic morphology, and

are observed to cover large zeolite/palagonite clasts. The micronodules are numerous in some sediment samples, comprising up to 5% of the matrix.

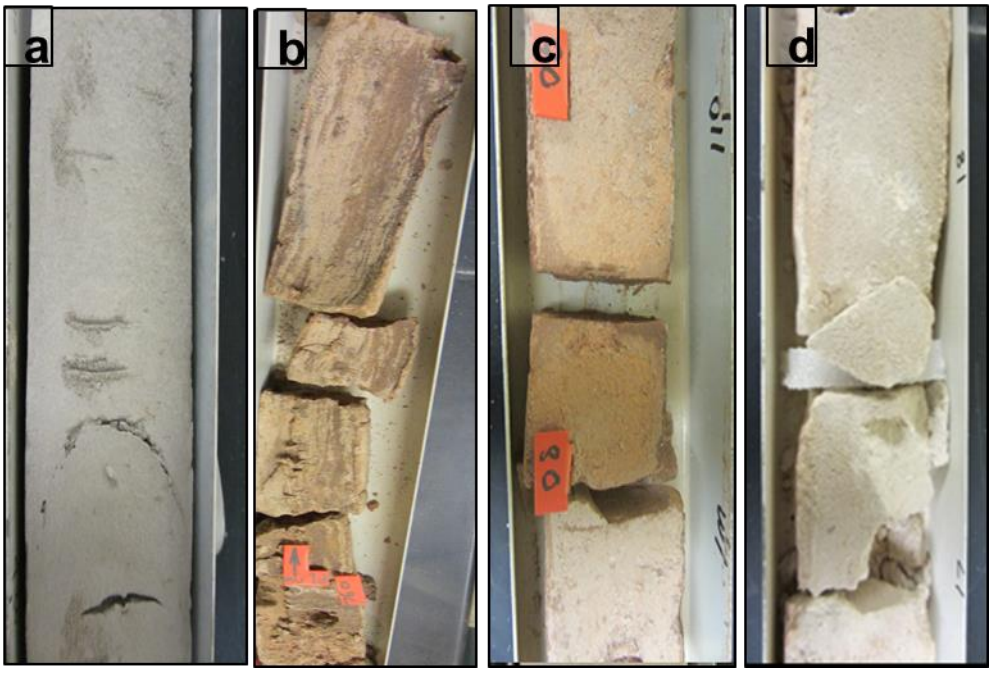

Figure 2. Representative sediment cores of a) grey clay (VM10-87), b) micronodule-rich red/brown clay (VM22-212), c) red/brown clay (VM27-255) and d) carbonate ooze (AT181-1).

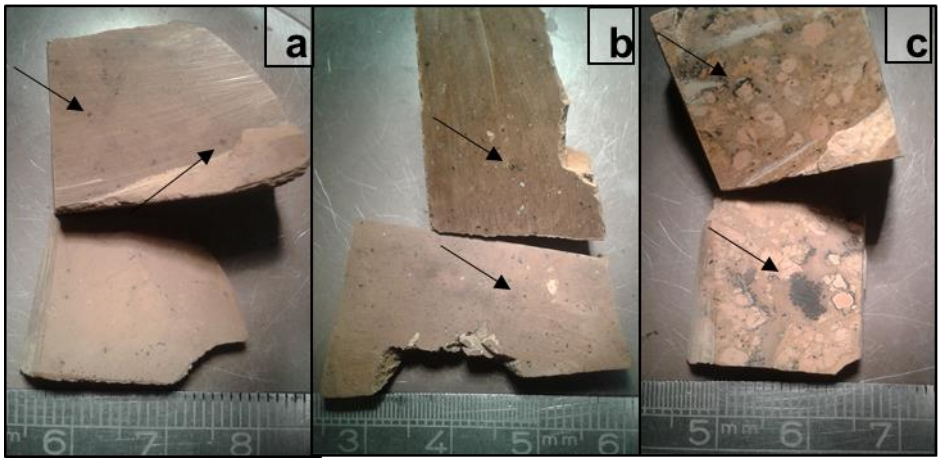

Figure 3. Micronodules in samples a) VM25-032, b) VM20-242 and c) VM25-033

2.3 Analytical methods

2.3.1 Sample dissolution

Sediment samples were taken from the inner part of the recovered cores to avoid the sampling of surface alteration products. The samples were then oven-dried at 40 ˚C (a low temperature was used to minimise the likelihood for modification of

Fe concentrations in these oxic sediments; Rapin et al., 1986) and ground in an agate mortar and dissolved in a mixture of hydrofluoric (HF), perchloric ($HClO_4$) and hydrochloric (HCl) acids, and aqua regia. For each sample, ~100 mg of powdered material was transferred to a 15 mL PTFE screw-cap vial and weighed. 5 mL of aqua regia was added to each vial, which was capped and refluxed on a hotplate at 90 ˚C overnight. The solution was then evaporated to near dryness, and 3 mL of HF and 2.25 mL of $HClO_4$ were added and heated on a hotplate at 150 ˚C overnight. The cap was removed and the samples were heated to 170 ˚C until white fumes were observed. The temperature was then increased to 180 ˚C and the sample was evaporated to near-dryness. 2 mL of $HClO_4$ was added, the cap was replaced and the solution was heated overnight on a hotplate at 150 ˚C. After evaporating to near-dryness, 10 mL of HCl was added and the sample was heated on a hotplate at 130 ˚C.

The solution was then evaporated to near dryness, and made up to 100 cm^3 in 0.5 M HNO_3 in a volumetric flask. A sub-sample of 1 mL of this solution was dried down, spiked with an internal standard consisting of 5 ppm Re and In and 20 ppm Be, and made up to 13 mL with 0.5 M HNO_3 for trace element and REY analyses. For analysis of the major elements, 0.25 mL of the solution was spiked, and made up to 5 mL with 0.5 M HNO_3.

2.3.2 Analysis of major elements, trace elements and REYs

Major element (Na, Mg, Al, K, Ca, Ti, Fe and Mn), trace element (V, Cr, Co, Ni, Cu, Zn, Rb, Sr and Ba), and REY (La, Ce, Pr, Nd, Sm, Eu, Gd, Tb, Dy, Y, Ho, Er, Tm and Lu) concentrations were determined by inductively coupled plasma mass spectrometry (ICP-MS; Thermo Scientific X-Series II) at the University of Southampton. Measurements were calibrated against 6 certified rock reference materials (BHVO-2, BAS-206, BIR-1, JB-1a, BRR-1, JB-3), and the accuracy and reproducibility of the measurements was assessed by multiple (n=9) analyses of MAG-1, BCSS-1 and MESS-1 certified reference materials, analysed as unknowns alongside the samples. Instrument drift was assessed by addition of internal standards (Re, In and Be), and analysis of an internal standard every 10 samples. The external reproducibility of the analyses was better than ±5 % for the major elements, and better than ±3 % for most of the trace elements and REEs; the reproducibility of Cu and Y analyses was ±8 % and ±15 %, respectively. Measured concentrations were within ±5% of the certified or recommended values for all elements except K (±10 %), Tb (±20 %) and Y (±15 %).

Sample	Type*	Depth (m)	Na	Mg	Al	K	Ca	Ti	Fe	Mn	CaCO3
RC10-277	Carb	5407	2.94	1.89	2.41	1.11	28.5	0.17	2.75	0.33	58.8
RC11-243	RC	5407	1.80	1.52	6.76	2.48	5.24	0.36	4.23	0.14	12.6
VM17-002	RC	5303	2.14	1.39	8.46	2.37	0.32	0.37	5.35	0.54	bdl
VM16-015	RC	5809	0.86	1.67	10.7	2.91	0.31	0.48	6.44	0.47	bdl
VM9-34	RC	5879	1.83	1.67	10.2	3.12	0.47	0.49	7.05	0.33	bdl
RC10-10	RC	5929	1.29	1.35	9.60	2.60	0.29	0.44	6.19	0.46	bdl
RC10-13	RC	5300	1.78	1.61	9.29	2.63	3.99	0.46	5.91	0.58	7.4
VM25-33	RC†	5009	1.82	2.72	8.80	2.50	0.65	0.44	7.65	0.69	bdl
VM25-32	RC†	5464	1.37	1.84	9.38	2.86	0.69	0.50	6.46	0.62	0.1
VM25-30	Carb	4096	1.88	0.76	3.07	1.05	29.0	0.18	2.31	0.21	64.3
VM10-093	Carb	3574	2.83	0.24	0.58	0.25	40.9	0.03	0.52	0.07	90.4
VM31-152	Carb	4174	3.25	0.21	0.29	0.14	28.5	0.02	0.33	0.05	93.0
VM10-89	Carb	3523	1.44	0.35	0.95	0.32	36.9	0.06	0.78	0.07	82.7
TH1-54S	Carb	3840	0.83	0.72	2.49	0.81	30.7	0.15	1.87	0.15	65.2
VM20-242	RC†	4565	0.81	2.57	7.98	2.03	6.90	0.47	7.49	1.04	11.7
AT180-118P	GC	4500	0.84	1.40	8.33	2.59	2.17	0.56	4.86	0.44	3.4
VM20-241	Carb	4372	1.16	0.59	3.15	0.92	29.4	0.20	2.55	0.90	68.4
VM10-88	RC†	4971	1.51	1.62	10.0	2.37	0.62	0.64	8.79	0.75	bdl
AT181-1	Carb	3895	1.61	2.68	0.09	0.06	39.5	0.001	0.14	0.003	94.3
RC21-02	RC	3895	1.23	1.42	8.36	2.41	4.57	0.52	5.12	0.10	9.2
VM22-212	RC†	6081	1.43	2.81	7.80	3.09	0.57	0.40	8.87	0.64	9.2
VM10-87	GC	5329	0.89	1.26	9.73	3.15	0.79	0.52	4.81	0.45	bdl
D11805_7-S1	GC	6129	2.38	1.22	4.83	1.47	21.2	0.26	2.83	0.41	0.1
D11805_7-S2	GC	6129	1.97	1.22	4.78	1.48	20.9	0.26	2.79	0.41	42.3
D10311-S1	RC	6133	1.70	2.06	9.28	2.75	0.91	0.58	5.93	0.28	46.9
D10311-S2	RC	6133	1.65	1.89	8.88	2.65	1.16	0.55	5.84	0.34	0.2
D11805_5-S1	GC	5554	1.69	1.20	4.64	1.44	20.4	0.25	2.73	0.39	0.9
D11805_5-S2	GC	5554	2.11	1.26	4.75	1.47	20.9	0.25	2.84	0.40	46.4
VM27-255	RC	5554	2.35	1.85	9.21	2.70	1.11	0.56	6.16	0.44	40.0
VM32-52	Carb	5220	1.73	1.84	8.59	2.58	3.02	0.53	5.41	0.19	90.6
KA74-0046	RC	4838	1.89	1.31	6.11	1.82	14.9	0.41	3.88	0.13	5.5
VM23-99	Carb	4118	2.33	1.18	3.90	1.28	21.7	0.22	1.97	0.07	31.3
VM29-170	Carb	4455	2.03	0.71	2.59	0.81	32.3	0.19	1.65	0.04	45.4
VM30-54	Carb	3506	1.34	0.84	2.56	0.97	25.1	0.15	1.42	0.02	71.8
KM1-046P	GC	1221	1.75	0.81	2.19	0.90	25.5	0.14	1.23	0.009	57.5

Table 2: Concentrations (wt %) of major elements in North Atlantic deep-sea sediments. *Carb = carbonate; RC = red clay; RC† = red clay with micronodules; GC = grey clay. bdl = below detection limit.

2.3.3 $CaCO_3$ analysis

Total inorganic carbon was measured by separating CO_2 from 15 mg of sediment by addition of 0.4 M phosphoric acid (H_3PO_4), and analysis of the CO_2 produced by coulometry (UIC Inc CM5015 CO_2 coulometer, equipped with an acidification module). A 99.999% purity $CaCO_3$ standard was used to calibrate the measurements, and to assess drift and reproducibility. The reproducibility of the analyses is better than ±0.5%.

Sample	Type*	Depth (m)	V	Cr	Co	Ni	Cu	Rb	Sr	Ba
RC10-277	Carb	5407	49.9	39.5	41.5	80.1	65.4	26.3	421	101
RC11-243	RC	5407	103	75.0	18.9	42.4	42.5	108	285	336
VM17-002	RC	5303	151	67.5	57.7	102	85.3	112	88.1	332
VM16-015	RC	5809	193	83.7	55.0	89.9	86.6	141	115	401
VM9-34	RC	5879	164	85.2	46.0	79.8	97.3	142	134	454
RC10-10	RC	5929	151	81.2	61.4	107	124	127	109	361
RC10-13	RC	5300	149	84.5	70.4	150	134	124	283	362
VM25-33	RC†	5009	133	74.1	64.3	466	185	98.1	113	171
VM25-32	RC†	5464	161	82.2	80.5	136	148	123	152	374
VM25-30	Carb	4096	57.8	33.8	28.8	48.4	58.9	40.8	1230	346
VM10-093	Carb	3574	14.0	8.38	8.14	12.8	21.2	7.52	1600	49.2
VM31-152	Carb	4174	7.84	4.64	5.62	9.49	12.4	3.43	935	14.8
VM10-89	Carb	3523	21.0	10.5	10.3	16.4	26.8	11.8	1420	84.2
TH1-54S	Carb	3840	46.9	28.2	21.2	32.6	45.3	31.3	1360	280
VM20-242	RC†	4565	268	66.7	131	185	205	84.8	408	343
AT180-118P	GC	4500	119	63.8	12.7	23.2	16.5	122	188	315
VM20-241	Carb	4372	54.6	33.2	16.5	30.7	44.8	36.5	1110	143
VM10-88	RC†	4971	207	53.7	76.3	178	184	89.8	159	271
AT181-1	Carb	3895	1.41	14.9	0.26	4.71	12.6	0.097	2900	9.83
RC21-02	RC	3895	123	60.2	15.3	30.2	39.5	115	284	474
VM22-212	RC†	6081	244	89.2	73.4	209	152	99.9	137	320
VM10-87	GC	5329	117	90.9	14.0	35.3	24.5	146	117	457
D11805_7-S1	GC	6129	73.1	71.4	9.48	36.9	44.0	56.9	991	485
D11805_7-S2	GC	6129	74.0	71.0	9.40	38.5	44.6	58.5	1000	488
D10311-S1	RC	6133	137	101	39.8	110	87.1	108	145	357
D10311-S2	RC	6133	141	90.6	51.4	106	124	110	167	347
D11805_5-S1	GC	5554	70.2	70.2	9.79	38.9	45.8	57.9	983	483
D11805_5-S2	GC	5554	73.7	73.1	9.59	38.0	45.0	56.7	988	480
VM27-255	RC	5554	131	95.0	15.3	55.9	92.4	113	149	380
VM32-52	Carb	5220	125	88.5	28.3	76.5	107	105	222	433
KA74-0046	RC	4838	88.0	71.6	18.7	47.5	72.1	72.7	735	366
VM23-99	Carb	4118	58.3	71.4	7.08	37.6	62.2	47.2	936	842
VM29-170	Carb	4455	41.9	27.5	6.50	17.0	35.8	28.3	1400	230
VM30-54	Carb	3506	41.7	36.1	5.34	28.7	28.0	33.1	1090	490
KM1-046P	GC	1221	30.4	36.6	2.71	18.7	10.6	27.9	947	233

Table 3: Concentrations (ppm) of minor elements in North Atlantic deep-sea sediments. *Carb = carbonate; RC = red clay; RC† = red clay with micronodules; GC = grey clay.

2.3.4 Laser ablation ICP-MS analyses of micronodules

Thick sections were made of consolidated sediments containing micronodules, and these were mounted onto a glass sample holder along with polished chips of NIST 610 and NIST 612 glass standard reference materials. Figure 3 shows the distribution of micronodules in some of these thick sections.

Laser ablation ICP-MS analyses of these materials were conducted at the University of Southampton using a 193 nm excimer laser (New Wave Research model UP193X) coupled to a quadrupole ICP-MS (Thermo X-Series II). Element

concentrations were determined on 50 µm diameter spots on each nodule. Ablations were conducted with a laser power of ~75% and a repetition rate of 5 Hz, in a He atmosphere. For each analysis, the gas blank was measured first with the laser beam blocked by a shutter. The shutter was then removed, and the transient signals from the analyte were collected for the ablation period. Data was acquired for Mn, Fe, Cu, Ti, V, Co, Ni, Ba, U, Th and the REYs. Raw counts were processed off line using standard spreadsheet software, and measurements were calibrated using the NIST 612 and NIST 610 glass standards. The reproducibility of the analyses (assessed by multiple (n = 30) measurements of the NIST-612 standard) was better than ±5 % for all elements except Cu (± 17 %) and V (± 13 %). The accuracy of the analyses (assessed by measuring NIST-610 as an unknown) was better than ±5 % for all elements except Sm and Ho (better than ± 10 %).

2.4 Results

Concentrations of major, minor and REY elements in the sediment samples are given, respectively, in Tables 2, 3 and 4. Results of laser ablation analyses of metal and REY concentrations in 3 representative micronodules from each of the micronodule-containing samples (VM10-88, VM20-242, VM25-033, VM25-032 and VM22-212) are given in Tables 5 and 6. A total of 14 micronodules were analysed from sample VM10-88, 49 from VM20-242, 86 from VM25-033, 19 from VM25-032 and 49 from VM22-212.

2.4.1 Chemical composition of North Atlantic deep-sea sediments

The red and grey clays are characterised by relatively high concentrations of elements associated with detrital material, including Ti (0.14-0.64 wt %), Mg (0.81-2.06 wt %), Al (2.19-10.7 wt %), K (0.90-3.15 wt %), Rb (27.9-146 ppm), and Fe (1.23-7.05 wt %), whereas carbonate sediments have relatively high concentrations of Ca (3.02-40.9 wt %) and Sr (222-2990 ppm). The $CaCO_3$ content of the sediments generally decreases with increasing water depth, but is relatively lower close to the continental shelf (~31 to 72 wt %).

Sample	Type*	Depth (m)	La	Ce	Pr	Nd	Sm	Eu	Gd	Tb	Dy	Y	Ho	Er	Tm	Yb	Lu	ΣREY	LREE/ HREE	Ce*
RC10-277	Carb	5407	8.97	42.2	2.22	8.74	1.90	0.47	1.97	0.31	1.82	11.0	0.37	1.06	0.16	1.03	0.16	82.5	0.77	2.36
RC11-243	RC	5407	39.1	86.9	9.63	35.7	6.75	1.36	5.67	0.85	4.80	26.4	0.94	2.59	0.38	2.43	0.36	224	1.38	1.15
VM17-002	RC	5303	48.9	128	12.4	46.3	9.40	2.04	8.32	1.24	6.94	36.8	1.34	3.62	0.52	3.36	0.50	310	1.27	1.33
VM16-015	RC	5809	44.3	115	11.0	40.4	7.99	1.69	6.71	1.01	5.70	29.0	1.10	3.01	0.44	2.84	0.42	270	1.34	1.34
VM9-34	RC	5879	46.0	122	11.4	41.9	8.07	1.66	6.55	0.99	5.60	28.1	1.08	2.98	0.44	2.91	0.43	280	1.38	1.38
RC10-10	RC	5929	48.2	140	11.9	43.7	8.62	1.79	7.12	1.09	6.18	31.0	1.19	3.30	0.48	3.16	0.48	308	1.31	1.52
RC10-13	RC	5300	47.4	129	12.0	43.4	8.60	1.80	7.30	1.09	6.21	33.7	1.20	3.31	0.48	3.10	0.46	298	1.31	1.41
VM25-33	RC†	5009	59.6	101	16.0	62.2	13.4	3.03	12.3	1.87	10.7	58.7	2.08	5.59	0.78	4.89	0.71	352	1.11	0.82
VM25-32	RC†	5464	53.8	156	13.6	51.0	10.3	2.20	8.91	1.34	7.54	39.7	1.45	3.94	0.57	3.67	0.55	355	1.28	1.48
VM25-30	Carb	4096	32.0	61.1	8.53	33.0	6.78	1.46	6.19	0.91	5.10	28.7	0.97	2.58	0.36	2.24	0.32	190	1.29	0.93
VM10-093	Carb	3574	11.4	13.5	2.83	11.3	2.35	0.53	2.46	0.36	2.14	15.3	0.44	1.19	0.16	1.00	0.14	65.3	0.97	0.59
VM31-152	Carb	4174	8.27	9.18	2.11	8.76	1.87	0.44	2.00	0.30	1.74	11.7	0.35	0.94	0.13	0.79	0.11	48.7	0.92	0.53
VM10-89	Carb	3523	13.2	17.5	3.25	13.1	2.72	0.63	2.86	0.42	2.51	18.1	0.51	1.40	0.19	1.20	0.17	77.8	0.94	0.66
TH1-54S	Carb	3840	26.4	45.9	6.71	26.4	5.44	1.20	5.22	0.77	4.40	27.5	0.87	2.35	0.33	2.06	0.30	156	1.12	0.86
VM20-242	RC†	4565	75.0	139	20.5	81.2	17.5	4.01	17.1	2.56	14.4	75.1	2.76	7.26	1.00	6.21	0.90	465	1.11	0.88
AT180-118P	Carb	4500	34.2	72.5	8.53	31.7	6.23	1.31	5.19	0.78	4.44	23.6	0.87	2.41	0.36	2.38	0.35	195	1.27	1.09
VM20-241	Carb	4372	25.4	48.3	6.47	25.0	5.08	1.12	4.80	0.71	4.11	24.8	0.81	2.22	0.31	2.00	0.29	152	1.12	0.95
VM10-88	RC†	4971	85.3	166	22.1	84.9	17.3	3.90	15.9	2.37	13.8	82.3	2.72	7.48	1.07	6.87	1.01	513	1.11	0.96
AT181-1	Carb	3895	1.22	1.03	0.22	0.94	0.19	0.05	0.25	0.04	0.26	3.40	0.06	0.18	0.02	0.13	0.02	7.8	0.62	0.48
RC21-02	RC	3895	33.3	72.0	8.27	30.8	6.12	1.29	5.16	0.78	4.51	25.3	0.88	2.46	0.36	2.40	0.35	194	1.22	1.12
VM22-212	RC†	6081	62.8	117	18.5	72.3	15.7	3.47	14.0	2.09	11.6	59.0	2.18	5.72	0.79	4.89	0.69	391	1.24	0.85
VM10-87	GC	5329	46.8	101	11.5	42.2	8.15	1.58	6.74	1.00	5.65	29.7	1.08	2.94	0.43	2.84	0.42	262	1.43	1.13
D11805_7-S1	GC	6129	24.1	46.5	5.83	21.8	4.24	0.91	3.78	0.56	3.21	18.9	0.64	1.77	0.26	1.67	0.25	134	1.23	1.01
D11805_7-S2	GC	6129	24.5	47.1	5.86	22.0	4.26	0.91	3.75	0.56	3.22	19.7	0.65	1.79	0.26	1.67	0.25	136	1.23	1.01
D10311-S1	RC	6133	47.1	123	11.4	42.0	8.19	1.74	7.12	1.08	6.28	35.2	1.24	3.49	0.51	3.37	0.51	292	1.19	1.37
D10311-S2	RC	6133	49.6	138	12.1	44.5	8.85	1.88	7.55	1.15	6.61	36.3	1.29	3.55	0.52	3.42	0.51	316	1.24	1.46
D11805_5-S1	GC	5554	23.8	46.1	5.70	21.3	4.13	0.89	3.68	0.54	3.13	19.2	0.62	1.73	0.25	1.62	0.24	133	1.23	1.02
D11805_5-S2	GC	5554	24.0	46.3	5.76	21.5	4.18	0.89	3.70	0.55	3.15	19.1	0.62	1.74	0.25	1.64	0.24	134	1.24	1.01
VM27-255	RC	5554	47.0	117	11.3	41.3	8.01	1.67	6.68	1.02	5.75	30.8	1.11	3.09	0.45	3.00	0.45	278	1.33	1.32
VM32-52	Carb	5220	43.5	110	10.7	39.5	7.81	1.65	6.61	1.01	5.78	31.6	1.13	3.13	0.46	3.00	0.45	267	1.25	1.32
KA74-0046	RC	4838	36.2	73.7	9.21	34.7	6.94	1.53	6.10	0.91	5.10	28.2	0.98	2.63	0.38	2.47	0.36	209	1.30	1.03
VM23-99	Carb	4118	21.4	35.7	5.12	19.7	3.86	0.84	3.55	0.53	3.15	19.8	0.64	1.78	0.26	1.70	0.26	118	1.07	0.86
VM29-170	Carb	4455	19.3	30.9	4.53	17.4	3.42	0.78	3.21	0.47	2.70	16.8	0.54	1.46	0.21	1.32	0.20	103	1.20	0.84
VM30-54	Carb	3506	14.7	25.2	3.53	13.5	2.61	0.57	2.40	0.35	2.04	13.4	0.41	1.15	0.17	1.10	0.17	81.2	1.14	0.89
KM1-046P	GC	1221	11.8	21.3	2.97	11.4	2.14	0.46	1.83	0.26	1.54	10.1	0.32	0.92	0.14	0.92	0.14	66.2	1.15	0.91

Table 4: Concentrations (ppm) of rare earth elements and yttrium (REY) in North Atlantic deep-sea sediments. *Carb = carbonate; RC = red clay; RC† = red clay with micronodules; GC = grey clay. $Ce^* = (2 \times Ce/Ce_{NASC})/(La/La_{NASC} + Nd/Nd_{NASC})$; $LREE/HREE = (La/La_{NASC} + 2 \times Pr/Pr_{NASC} + Nd/Nd_{NASC})/(Er/Er_{NASC} + Tm/Tm_{NASC} + Yb/Yb_{NASC} + Lu/Lu_{NASC})$.

The red clays have the highest Fe concentrations (3.88-7.05 wt %), and the micronodule-rich red clays are notably Fe- (6.46-8.87 wt %) and Mn- (0.62-1.04 wt %) rich compared to the other red clay samples. The red clays also have the highest concentrations of V (88.0-268 ppm), Cr (53.7-101 ppm), Co (12.7-131 ppm), Ni (30.2-466 ppm) and Cu (39.5-205 ppm); the micronodule-rich red clays have higher V (133-268 ppm), Co (64.3-131 ppm), Ni (136-466 ppm) and Cu (148-205 ppm) (but not Cr (53.7-89.2 ppm)) compared to the red clays that do not contain micronodules.

Similarly, ΣREY concentrations are highest in the red clays and lower in the grey clays that contain significant terrigenous material transported by turbidites (Thomson et al., 1984), and lowest in carbonate ooze. ΣREY concentrations in the red clays (Table 4) vary from 194 to 513 ppm, and the average value is 310 ppm. Highest ΣREY concentrations are found in the red clay samples that contain micronodules (up to 513 ppm). The total HREE (Eu, Gd, Tb, Dy, Ho, Er, Tm, Yb and Lu) content of the red clays is 18-55 ppm. For the grey clays, ΣREY concentrations vary between 66 to ~262 ppm (average 145 ppm), and HREE concentrations are 13-23 ppm. Carbonate-rich sediments have ΣREY concentrations of between 7.8 and 267 ppm (average 120 ppm) and HREE concentrations vary from ~7 to 30 ppm.

Red clays containing micronodules that were observable in hand specimen are variably enriched or depleted in Ce relative to La and Nd. There is a positive Ce anomaly in sample VM25-32 (1.48; Table 6) but the Ce anomaly is slightly negative (0.82-0.96) in the rest of the micronodule-containing samples. All the red clay samples without micronodules have positive Ce anomalies (1.03 to 1.52), whereas Ce is variably enriched or depleted relative to La and Nd in the grey clays (Ce* = 0.91 to 1.13). Most of the carbonate-rich samples have negative Ce anomalies, as low as 0.53. However samples RC10-277 and VM32-52, which are located close to the continental slope, have positive Ce anomalies. LREE/HREE ratios indicate that grey and red clays, including the micronodule-rich red clays, are enriched in the LREE relative to the HREE, whereas most of the carbonates are enriched in the HREE relative to the LREE.

2.4.2 Chemical composition of micronodules

Micronodules that were observable in hand specimen were found in samples VM20-242, VM10-088 (Central Atlantic), VM25-32, VM25-33 (North America

Basin), and VM22-212 (Canary Basin). The nodules are Fe-Mn rich, with Mn concentrations up to ~35.6 wt%, and Fe concentrations up to ~10.5 wt %. Micronodules from the Central Atlantic tend to have higher Fe/Mn ratios (~0.3) compared to the other sites (~0.1), higher concentrations of V, Ba and Ti, and lower concentrations of Ni and Cu.

Sample	Nodule #	Mn wt%	Fe wt%	Ti ppm	Cr ppm	Cu ppm	V ppm	Co ppm	Ni ppm	Ba ppm
VM10-088	1	35.6	5.26	4140	8.67	1630	1110	4330	3700	5640
	2	14.3	1.29	1140	29.2	2450	194	1090	15100	441
	3	11.8	1.59	1320	34.3	1790	195	1400	9890	632
	Avg	12.8	2.43	2710	38.2	1540	389	1550	5450	1480
	SD (n=14)	10.3	1.19	1920	19.1	952	306	1270	4290	1780
VM20-242	1	30.6	10.5	5870	20.9	953	1560	6900	2480	2390
	2	14.6	6.60	3540	14.7	686	940	2630	1290	1220
	3	19.4	6.50	3660	17.6	746	927	3610	2220	1200
	Avg	24.2	8.50	4950	25.1	844	1210	4610	2050	1610
	SD (n=49)	21.6	7.13	765	17.1	144	187	1660	426	311
VM25-033	1	14.9	1.48	1080	21.7	1530	209	756	7430	596
	2	16.0	2.40	2700	90.5	1620	390	1870	7570	558
	3	15.3	2.52	2040	40.4	1480	298	1310	6340	544
	Avg	21.1	1.98	1500	38.7	2740	293	1910	15300	665
	SD (n=86)	7.17	0.77	507	28.9	1250	101	953	8920	167
VM25-032	1	8.26	0.94	1710	32.1	1560	140	116	4890	400
	2	8.50	1.12	1840	38.6	1440	166	143	4520	461
	3	5.90	1.74	2780	108	882	242	202	2980	389
	Avg	7.55	1.16	1940	44.1	1330	161	189	4110	415
	SD (n=19)	1.91	0.27	455	18.0	467	38.1	123	1210	63.1
VM22-212	1	16.8	1.15	877	29.3	1220	263	2140	8440	935
	2	10.9	1.66	1590	51.4	934	314	1270	5280	624
	3	11.9	6.87	4450	31.1	903	2230	584	1150	4410
	Avg	18.2	1.46	1200	30.8	1290	423	2040	8280	1070
	SD (n=49)	7.57	1.37	893	16.3	337	453	870	3300	850

Table 5: Concentrations of metals in micronodules.

The ΣREY content of the micronodules ranges from ~200 to 3620 ppm. Nodules from sample VM20-242 have highest ΣREY (average = 2710 ppm) while the average ΣREY content of the other samples is lower (VM10-088 = 728 ppm, VM25-033 = 516 ppm, VM25-032 = 248 ppm and VM22-212 = 487 ppm). ΣHREE concentrations range from ~20 to ~200 ppm, and are also much higher in sample VM20-242 (average 162 ppm) than the average of the other samples (18.3 to 31.7 ppm).

Most of the micronodules have positive Ce anomalies; the average Ce anomaly in micronodules from sample VM22-212 (1.14) is slightly lower than it is in the other samples (2.51-8.36). Some of the nodules in sample VM10-088 have negative Ce anomalies (~0.78). Many of the micronodules from samples VM25-033, VM25-032, VM10-088 and VM22-212 are slightly enriched in the MREE (Fig. 8) but this is not true for most of the micronodules from VM20-242. Many of the micronodules from VM20-242 are also depleted in Y relative to Ho, but most of

the other micronodules have a positive Y anomaly. Most of the micronodules are slightly enriched in the HREE relative to the LREE (average LREE/HREE = 0.78-0.95) but, on average, micronodules from sample VM25-032 are slightly enriched in the LREE (LREE/HREE = 1.08).

Sample	Nodule #	La	Ce	Pr	Nd	Sm	Eu	Gd	Tb	Dy	Y	Ho	Er	Tm	Yb	Lu	ΣREY	LREE/ HREE	Ce*	Y/Ho
VM10-088	**1**	48.8	2440	5.58	20.6	3.54	0.90	5.22	0.60	4.29	15.8	0.92	3.11	0.49	4.34	0.83	2560	0.64	36.2	0.81
	2	49.2	99.9	12.0	46.6	9.98	2.50	9.19	1.57	10.5	60.4	1.92	6.03	0.92	5.71	0.84	317	0.74	1.03	1.48
	3	77.5	140	20.3	97.8	21.8	4.52	19.7	2.99	18.6	118	3.86	11.4	1.53	10.4	1.35	550	0.75	0.78	1.43
	Avg.	46.4	542	10.6	42.7	9.30	2.01	8.68	1.29	7.87	44.8	1.53	4.61	0.66	4.41	0.68	728	0.89	8.36	1.32
	SD (n=14)	14.8	797	4.59	21.4	5.11	1.05	4.48	0.71	4.08	27.0	0.81	2.35	0.30	1.87	0.24	761	0.16	13.3	0.23
VM20-242	**1**	413	2500	60.6	235	45.0	10.9	50.8	8.24	51.6	168	10.1	29.8	4.54	30.0	4.75	3620	0.84	3.92	0.78
	2	223	1280	33.3	128	25.8	5.97	31.3	4.70	30.7	106	5.79	17.1	2.53	16.9	2.69	1910	0.81	3.70	0.86
	3	244	1460	37.1	150	30.1	7.70	34.8	5.24	33.6	125	6.83	20.6	3.12	20.3	3.39	2180	0.74	3.75	0.86
	Avg.	314	1827	45.1	181	36.4	8.23	41.4	6.37	41.2	144	8.14	24.4	3.61	24.7	4.05	2710	0.78	3.80	0.84
	SD (n=49)	63.6	407	8.28	32.2	6.65	1.41	7.43	1.21	7.65	24.7	1.58	4.72	0.72	4.82	0.80	560	0.04	0.25	0.06
VM25-033	**1**	49.5	234	12.7	58.4	14.0	3.24	15.0	2.05	11.9	69.4	2.49	7.01	0.78	4.70	0.65	486	0.89	2.13	1.31
	2	52.0	263	16.0	58.1	17.7	3.40	13.8	2.22	12.4	63.7	2.44	6.85	0.71	4.86	0.67	518	1.01	2.35	1.22
	3	42.0	401	8.31	33.1	7.11	1.73	8.03	1.14	7.25	32.1	1.25	3.89	0.61	4.28	0.64	552	0.78	5.34	1.20
	Avg.	40.2	346	9.91	39.3	9.01	1.97	8.92	1.29	8.08	40.1	1.56	4.50	0.61	3.87	0.58	516	0.95	4.20	1.22
	SD (n=86)	11.3	123	3.71	15.8	3.98	0.90	4.29	0.63	3.92	19.9	0.72	1.95	0.24	1.35	0.19	144	0.17	1.18	0.15
VM25-032	**1**	25.5	127	5.00	20.1	4.06	0.83	3.84	0.64	3.65	17.7	0.77	2.22	0.27	1.76	0.31	214	0.98	2.80	1.08
	2	30.0	137	5.44	18.6	4.72	0.94	3.60	0.61	3.32	17.4	0.62	1.89	0.29	1.66	0.18	226	1.24	2.84	1.33
	3	47.1	158	12.2	56.4	12.6	2.45	12.0	1.49	8.86	41.4	1.52	4.25	0.59	3.72	0.54	363	1.18	1.50	1.28
	Avg.	29.9	138	6.50	26.4	5.76	1.18	5.39	0.81	4.58	23.4	0.88	2.54	0.36	2.24	0.35	248	1.08	2.51	1.25
	SD (n=19)	6.20	21.0	1.83	8.30	1.94	0.36	1.90	0.25	1.37	7.40	0.27	0.75	0.13	1.03	0.17	42.0	0.20	0.43	0.10
VM22-212	**1**	30.5	135	8.95	33.6	7.68	1.65	7.23	0.95	6.11	29.2	1.12	3.91	0.43	2.99	0.51	270	0.93	2.08	0.87
	2	26.5	116	5.47	21.6	4.43	0.95	4.61	0.69	3.56	16.3	0.70	2.50	0.30	2.21	0.29	206	0.95	2.40	0.54
	3	209	1620	55.9	242	51.0	10.8	57.2	7.75	46.4	154	9.47	26.6	3.59	20.1	3.17	2520	0.89	3.53	0.76
	Avg.	30.4	201	7.80	32.1	7.10	1.51	7.19	1.02	6.14	24.4	1.23	3.58	0.48	3.08	0.46	487	0.87	1.14	1.03
	SD (n=49)	43.7	345	11.8	51.3	10.7	2.27	12.2	1.64	9.84	32.0	2.01	5.63	0.76	4.15	0.67	533	1.27	1.54	0.12

Table 6: Concentrations (ppm) of rare earth elements and yttrium (REY) in micronodules. $Ce^* = (2 \times Ce/Ce_{NASC})/(La/La_{NASC} + Nd/Nd_{NASC})$; $LREE/HREE = (La/La_{NASC} + 2 \times Pr/Pr_{NASC} + Nd/Nd_{NASC})/(Er/Er_{NASC} + Tm/Tm_{NASC} + Yb/Yb_{NASC} + Lu/Lu_{NASC})$; $Y/Ho = (Y/Y_{NASC})/(Ho/HY_{NASC})$.

2.4.3 Factor analysis

To better quantify and understand the processes that control the chemical composition of the sediment samples, the elemental data were subjected to statistical factor analysis (Winters & Buckley, 1992) using the RStudio.Ink Varimax rotation scheme with Kaiser normalisation. The results of this analysis are shown in Tables 7 and 8. Differences in the chemical composition of the sediment samples can be accounted for statistically by changes in the relative proportions of three principal factors (with eigenvalues, or sums of squared (SS) loadings, of >1) which together account for 92% of the sample variance.

	Factor 1	Factor 2	Factor 3
Na	0.229	**0.680**	
Al	0.420	**0.878**	0.179
K	0.359	**0.906**	0.146
Ca	-0.421	**-0.871**	-0.163
Ti	0.447	**0.859**	
Mn	**0.787**	0.160	0.590
Fe	0.674	**0.684**	0.227
Co	**0.755**	0.208	0.605
Ni	**0.683**	0.230	0.326
Cu	**0.803**	0.291	0.414
La	**0.822**	0.533	0.134
Ce	0.597	**0.674**	0.322
Pr	**0.863**	0.474	0.136
Nd	**0.886**	0.432	0.135
Sm	**0.909**	0.382	0.147
Eu	**0.931**	0.325	0.151
Gd	**0.942**	0.293	0.149
Tb	**0.939**	0.302	0.155
Dy	**0.941**	0.300	0.149
Y	**0.962**	0.243	
Ho	**0.943**	0.298	0.144
Er	**0.937**	0.318	0.139
Tm	**0.923**	0.354	0.138
Yb	**0.908**	0.387	0.134
Lu	**0.896**	0.407	0.141
Th	0.414	**0.825**	0.259
U	**0.492**	-0.117	-0.169
Eigen value (SS loading)	15.75	7.50	1.59
Total variance (%)	58.3	27.8	5.9
Acum. variance (%)	58.3	86.1	92

Table 7: Varimax rotated factor matrix for North Atlantic deep-sea sediments. Numbers in bold denote elements that appear to be loaded in the factor.

Factor 1 is the main factor controlling REY concentrations, with the exception of Ce, and it accounts for 58.3% of the sample variance. Factor 1 also has a high loading for Mn, Co, Ni and Cu, and all of the REY (including Ce) show a significant ($p < 0.05$; Table 8) positive correlation with Mn, Co and Cu and also Fe. Mn, Fe, Cu, Co and Ni are generally considered to have a significant hydrogenous source in deep-sea sediments (e.g. Thomson et al., 1984).

	Na	Al	K	Ca	Ti	Mn	Fe	Co	Ni	Cu	La	Ce	Pr	Nd	Sm	Eu	Gd	Tb	Dy	Y	Ho	Er	Tm	Yb	Lu	Th	U
Na																											
Al	0.68																										
K	0.71	**0.97**																									
Ca	-0.69	**-0.97**	**-0.97**																								
Ti	0.67	**0.96**	**0.93**	**-0.94**																							
Mn	0.31	0.57	0.51	-0.57	0.51																						
Fe	0.62	**0.92**	**0.90**	**-0.91**	**0.89**	**0.77**																					
Co	0.34	0.61	0.56	-0.60	0.55	**0.98**	**0.79**																				
Ni	0.51	0.51	0.48	-0.53	0.45	**0.78**	0.70	0.71																			
Cu	0.50	0.66	0.60	-0.64	0.63	**0.92**	**0.85**	**0.91**	**0.83**																		
La	0.54	**0.85**	**0.80**	**-0.84**	**0.84**	**0.81**	**0.94**	**0.82**	0.68	**0.87**																	
Ce	0.59	**0.92**	**0.88**	**-0.90**	**0.89**	**0.76**	**0.93**	**0.80**	0.57	**0.82**	**0.93**																
Pr	0.52	**0.81**	**0.77**	**-0.80**	**0.80**	**0.83**	**0.94**	**0.84**	0.71	**0.88**	**0.99**	**0.90**															
Nd	0.49	**0.78**	0.74	**-0.78**	**0.77**	**0.84**	**0.92**	**0.85**	0.72	**0.89**	**0.99**	**0.88**	**1.00**														
Sm	0.47	0.74	0.70	-0.74	0.73	**0.86**	**0.91**	**0.86**	0.74	**0.90**	**0.97**	**0.85**	**0.99**	**1.00**													
Eu	0.44	0.70	0.66	-0.70	0.70	**0.87**	**0.89**	**0.86**	**0.75**	**0.90**	**0.96**	**0.83**	**0.98**	**0.99**	**1.00**												
Gd	0.42	0.68	0.63	-0.68	0.68	**0.88**	**0.87**	**0.87**	**0.75**	**0.90**	**0.95**	**0.81**	**0.98**	**0.98**	**0.99**	**1.00**											
Tb	0.43	0.69	0.64	-0.69	0.68	**0.88**	**0.87**	**0.87**	**0.75**	**0.90**	**0.95**	**0.82**	**0.98**	**0.99**	**0.99**	**1.00**	**1.00**										
Dy	0.43	0.69	0.63	-0.68	0.68	**0.88**	**0.87**	**0.87**	**0.75**	**0.90**	**0.95**	**0.81**	**0.98**	**0.99**	**0.99**	**1.00**	**1.00**	**1.00**									
Y	0.39	0.64	0.57	-0.63	0.65	**0.85**	**0.83**	**0.83**	0.74	**0.89**	**0.94**	**0.78**	**0.96**	**0.97**	**0.98**	**0.99**	**0.99**	**0.99**	**0.99**								
Ho	0.42	0.68	0.63	-0.68	0.69	**0.87**	**0.87**	**0.86**	**0.76**	**0.90**	**0.95**	**0.81**	**0.98**	**0.98**	**0.99**	**1.00**	**1.00**	**1.00**	**1.00**	**0.99**							
Er	0.44	0.70	0.64	-0.69	0.70	**0.87**	**0.88**	**0.86**	**0.75**	**0.90**	**0.96**	**0.82**	**0.98**	**0.99**	**0.99**	**1.00**	**1.00**	**1.00**	**1.00**	**0.99**	**1.00**						
Tm	0.45	0.73	0.67	-0.72	0.73	**0.86**	**0.89**	**0.85**	**0.75**	**0.90**	**0.97**	**0.84**	**0.98**	**0.99**	**0.99**	**0.99**	**0.99**	**1.00**	**0.99**	**0.99**	**1.00**	**1.00**					
Yb	0.47	**0.75**	0.69	-0.74	**0.76**	**0.85**	**0.90**	**0.85**	0.74	**0.90**	**0.98**	**0.86**	**0.99**	**0.99**	**0.99**	**0.99**	**0.99**	**0.99**	**0.99**	**0.99**	**0.99**	**1.00**	**1.00**				
Lu	0.48	**0.76**	0.70	**-0.75**	**0.77**	**0.85**	**0.91**	**0.85**	0.73	**0.90**	**0.98**	**0.87**	**0.99**	**0.99**	**0.99**	**0.98**	**0.98**	**0.98**	**0.98**	**0.98**	**0.99**	**0.99**	**1.00**	**1.00**			
Th	0.65	**0.97**	**0.93**	**-0.94**	**0.93**	0.61	**0.88**	0.65	0.49	0.68	**0.85**	**0.96**	**0.81**	**0.78**	0.73	0.69	0.67	0.68	0.68	0.63	0.68	0.69	0.72	0.74	**0.76**		
U	0.41	0.38	0.41	-0.42	0.37	-0.02	0.25	0.01	0.03	0.06	0.19	0.22	0.17	0.15	0.12	0.10	0.08	0.08	0.08	0.06	0.08	0.10	0.12	0.13	0.15	0.30	

Table 8: Correlation coefficients between elements in deep Atlantic sediments. Significant ($p < 0.05$) correlations are highlighted in bold.

Factor 2 has high loading factors for Na, Al, K, Ti, Fe and Th, and also for Ce. The light REY (La-Nd) have a higher loading in this factor than the heavy REYs, and they show a significant positive correlation with Al, K and Ti ($p > 0.05$; Table 8). Ca has a negative loading in this factor. Factor 2 can be considered to represent the detrital component, and it accounts for the 27.8% of the sample variance.

Factor 3 accounts for the 5.9% of the sample variance. It has an eigenvalue of >1, so it is statistically significant, but no element is dominantly loaded in this factor. However, slightly higher loadings are found for Mn and Co.

2.5 Discussion

2.5.1 REY carrier phases in North Atlantic deep-sea sediments

ΣREY concentrations are positively correlated with Al, K and Ti which are enriched in detrital minerals (Table 8), and negatively correlated with elements that are relatively enriched in $CaCO_3$, such as Ca (Tables 7 and 8, Fig. 6). Partitioning of REE, especially LREE, into the carbonate lattice is directly influenced by REE concentrations in seawater (Zhong & Mucci, 1995). Consequently, the REY concentration of carbonates is low relative to detrital minerals and carbonates actively dilute the REY resource in deep-sea sediments (de Lange & Poorter, 1992; Dubinin & Rozanov, 2001, Kato et al., 2011).

However, the relative proportions of detrital vs. carbonate material only accounts for ~28% of the total variance in the chemical composition of the North Atlantic deep-sea sediments, and the factor analysis reveals that the REY are also located in association with Mn, Fe, Cu, Co and Ni (Tables 7 and 8) that are generally considered to have a significant hydrogenous source in deep-sea sediments (e.g. Thomson et al., 1984).

REY distribution patterns for the red clays show a mirror image of the seawater distribution pattern, with LREE enrichment relative to the HREE and a positive Ce anomaly (Fig. 4). This supports the idea that the red clays acquire at least part of their REY from seawater (Thomson et al., 1984; Dubinin & Rozanov, 2001; Kato et al., 2011). The red clays are also enriched in other elements that have a hydrogenous source (e.g. Fe, Mn, Cu, Co, Ni and V: Turekian & Imbrie, 1966; Chester and Messiha-Hanna, 1970; Thomson et al., 1984) relative to NASC (Fig. 5). Significant enrichment of the REY in red clays, due to input of hydrogenous

material, has also been noted in the Brazil Basin (Dubinin & Rimskaya-Korsakova, 2011), and for mesopelagic clays from the western part of the North Equatorial Pacific (Dubinin & & Uspenskaya, 2006).

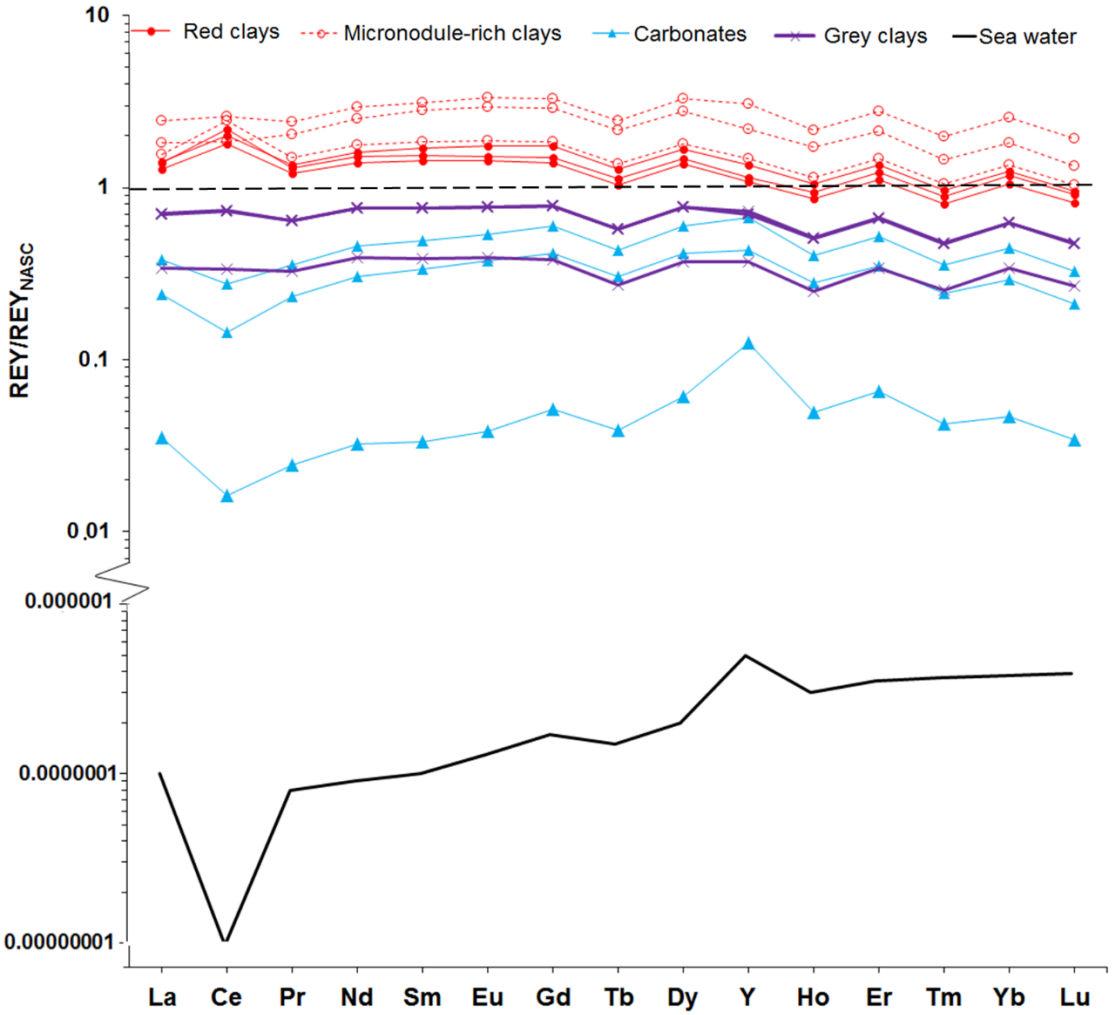

Figure 4. REY distribution patterns, normalised to North America Shale Composite (NASC; Gromet et al., 1984), for North Atlantic deep-sea sediments and comparison with a sea water-like pattern (Douville et al., 1999). Three representative samples from each sediment type are shown. The REY distribution pattern for deep Atlantic seawater is also shown for comparison (Douville et al., 1999). Black dashed line shows values for NASC; samples with REY/REY$_{NASC}$ >1 are enriched in the REY relative to NASC; samples with REY/REY$_{NASC}$ <1 are depleted in the REY relative to NASC.

By contrast, REY distribution patterns for the grey clays are closer to shale, though they are slightly depleted in the HREE possibly because my dissolution procedure underestimated the contribution of refractory minerals (Sholkovitz, 1990). Although they are slightly enriched in Mn relative to NASC, they show no

enrichment in other metals that have a hydrogenous source (Fig. 5). This supports the idea that the REYs in grey clays are dominated by terrigenous input because they are deposited relatively rapidly and therefore contain an insignificant hydrogenous component (Thomson et al., 1984).

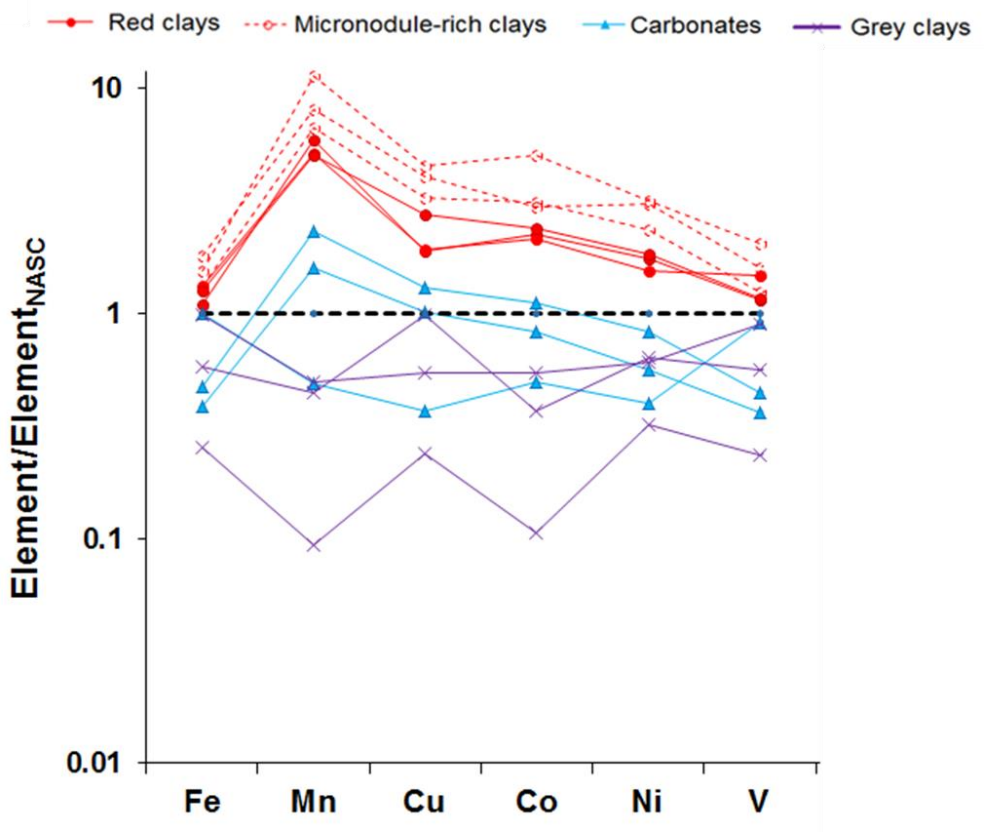

Figure 5. Distribution of transition metals in North Atlantic deep-sea sediments relative to NASC. Black dashed line shows values for NASC.

REY distribution patterns for the carbonate-rich sediments are similar to the seawater pattern, with enrichment of the HREE relative to the LREE, a negative Ce anomaly and a positive Ho anomaly (Fig. 4). The HREE are relatively enriched in seawater because they form stable complexes with CO_3^{2-} compared to the LREE (Cantrell & Byrne, 1987; Lee & Byrne, 1992). Carbonates that precipitate from seawater inherit the REY distribution pattern, and ancient carbonates can provide important information about palaeoceanographic environments (e.g. Nagarajan et al., 2011).

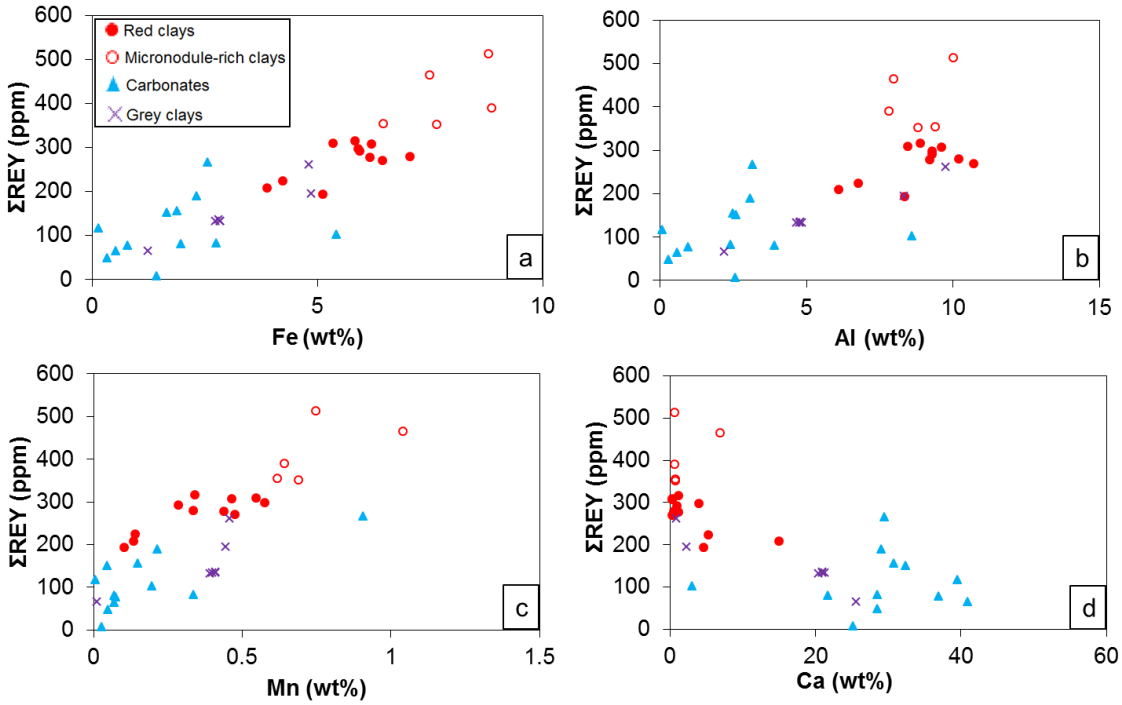

Figure 6. Relationship between ΣREY content and (a) Fe, (b) Al, (c) Mn and (d) Ca in North Atlantic deep-sea sediments. Note that the micronodule-rich red clays are enriched in Fe and Mn, as well as the REY.

Uptake of REY from seawater is widely considered to occur via scavenging by Fe-Mn (oxyhdr)oxide phases (Piper, 1974; Li, 1981; German et al., 1991; De Carlo & Green, 2002; Dubinin & Rimskaya-Korsakova, 2011; Bau & Koschinsky, 2009). Sequential leaching of suspended particles reveals that REE concentrations are high in Mn oxides (Sholkovitz et al., 1994), but also in hydrous Fe oxides (Bau & Koschinsky, 2009), which is consistent with analyses of suboxic porewaters in sediments from the Peru and California margins that show the REYs are released during reduction of Fe-oxides, but not Mn-oxides (Haley et al., 2004). My data for North Atlantic deep-sea sediments supports the participation of both Mn- and Fe-(oxyhydr)oxide phases and, furthermore, they indicate that the LREE and HREE show a greater affinity for Fe-oxides whereas, in general, the MREE appear to have a greater affinity for Mn-oxide phases (Table 8).

2.5.2 Accummulation of REYs in micronodules

Fe-Mn rich micronodules are common in pelagic sediments, and they are morphologically, mineralogically and chemically similar to larger Fe-Mn nodules found at the sediment surface in sediment-starved deep-ocean basins (Addy, 1979; Dubinin and Sval'nov, 2003; Pattan et al., 1994; Sval'nov et al., 1991).

Micronodules can have a hydrogenous, diagenetic, or hydrothermal source. Hydrogenous micronodules precipitate from seawater, whereas diagenetic nodules form from metal ions in sub-oxic pore waters, and hydrothermal nodules form from metals supplied by hydrothermal vent fluids. These different types of nodule can be distinguished by the field on which they plot on a Mn-Fe-(Ni + Co + Cu) ternary diagram (Bonatti et al., 1972) (Fig. 7), which delimitates the diagenetic, hydrogenous and hydrothermal fields according to the relative proportions of these groups of elements. According to this, hydrogenous deposits will show higher Fe/Mn ratios, and lower (Ni + Co + Cu) than diagenetic nodules, whereas hydrothermal nodules will have the lowest (Ni + Co + Cu) content.

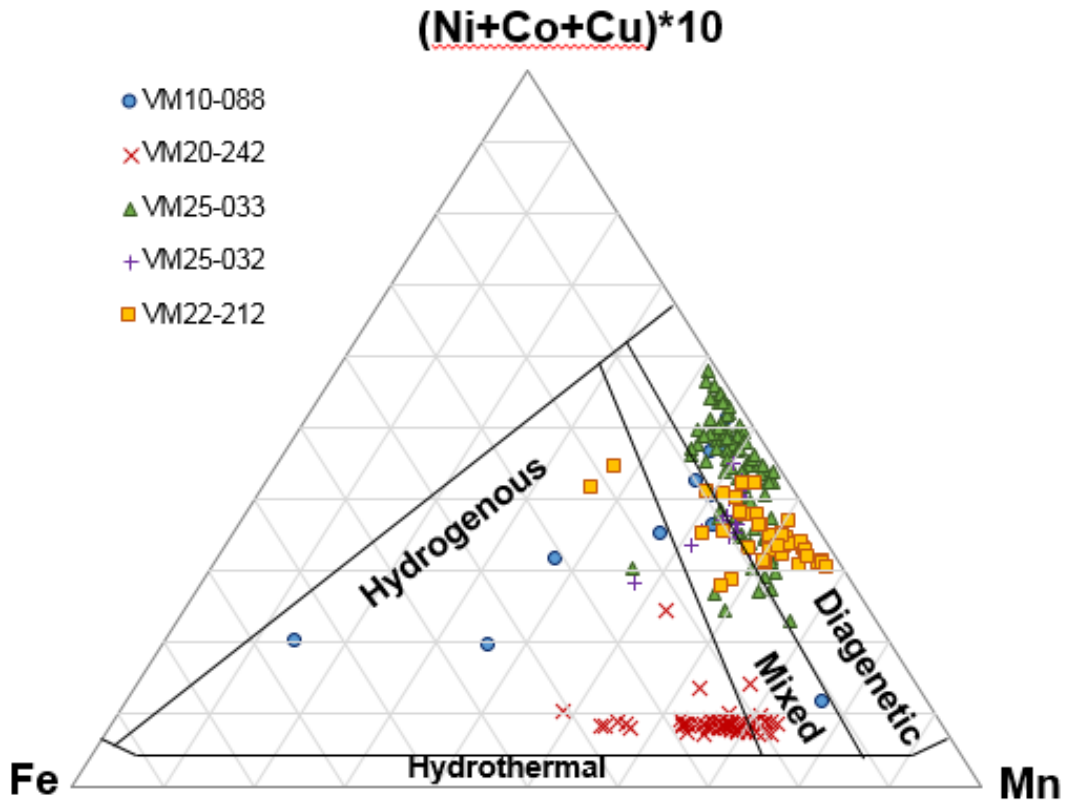

Figure 7. Ratio of Fe:Mn:Cu + Ni + Co in micronodules from red clay sediments in the North Atlantic, . Black lines define different nodule fields, according to Bonatti et al. (1972) and Wegorzewski and Kuhn (2014).

Most of the micronodules in deep-sea North Atlantic red clays have a diagenetic or mixed (hydrogenous and diagenetic) source (Fig. 7), but micronodules from sample VM20-242, and some micronodules from sample VM10-088, have a mainly hydrogenous source. None of the sediment samples appear to contain micronodules with a hydrothermal signature, even though some of the

micronodule-containing sediments (VM20-242 and VM10-88) were from close to the Mid-Atlantic Ridge.

REY distribution patterns (Fig. 8) shows that the hydrogenous micronodules (e.g. from sample VM20-242) have higher ΣREY and Nd concentrations than the diagenetic micronodules, which is consistent with data compiled by Bau et al. (2014) for regular Fe-Mn nodules. This, together with the positive Ce anomalies is indicative of a hydrogenous origin for these nodules (Piper, 1974; Addy, 1979; de Lange & Poorter, 1992; Nath et al., 1992; Kasten et al., 1998). However, the same authors report that diagenetic nodules are characterised by no or negative Ce anomalies, whereas most of my micronodules have small positive Ce anomalies. This may indicate that the 'diagenetic' micronodules also contain a small hydrogenous component.

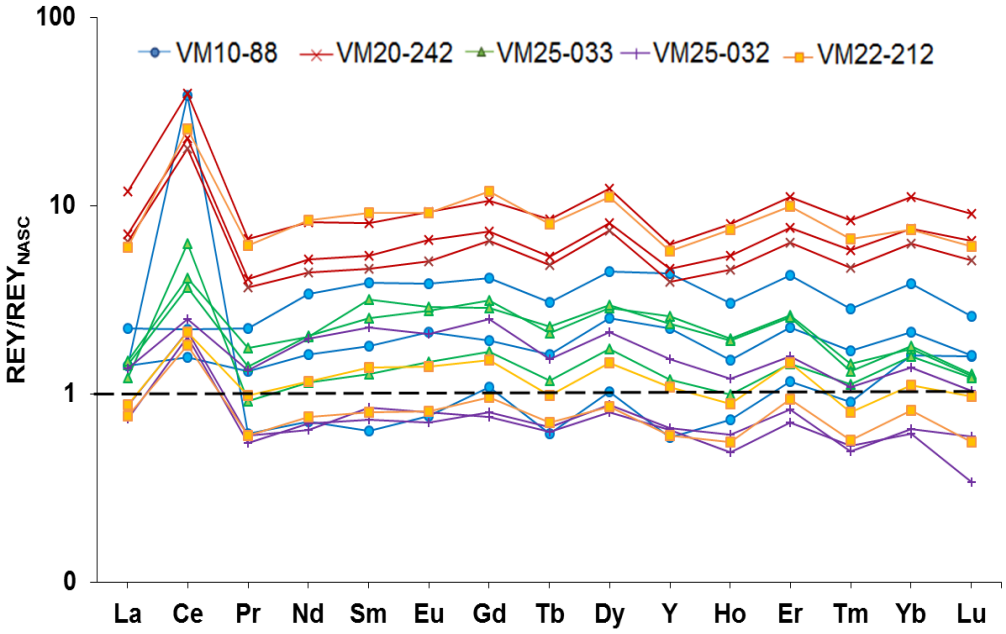

Figure 8. REY distribution patterns, normalised to NASC for 3 representative micronodules from red clay samples VM20-242, VM10-088, VM22-212 and VM25-033.

Y is depleted with respect to its geochemical twin Ho in most micronodules from sample VM20-242 and some from VM10-088 and VM22-212. Y^{3+} and Ho^{3+} have very similar ionic radii, but Y forms less stable surface complexes, so Ho is preferentially scavenged by metal (oxyhydr)oxide phases (Bau et al., 1995, 1996, 1997; Bau & Dulski, 1999; Schijf & Marshall, 2011). Thus, hydrogenous nodules can be expected to be enriched in Ho. By contrast, micronodules from sample VM25-032 and most micronodules from VM25-033 and VM10-088 have shale-normalised Y/Ho ratios ≥ 1, as is typical for seawater (Douville et al., 1999). Positive Y anomalies are usually characteristic of hydrothermal Fe-Mn nodules, or

nodules that have become phosphatized (Bau et al., 2014). While I did not assess the P content of the micronodules, as discussed above I see no evidence for a hydrothermal signature on the basis of their (Cu + Ni + Co) content (Fig. 8). However, sequential leaching experiments on Fe-Mn crusts have shown that Mn-oxides have shale-normalised Y/Ho ratios of ≥1 whereas Fe-oxides have negative Y anomalies (Bau & Koschinsky, 2009); in this connection, micronodules with shale-normalised Y/Ho ratios of >1 tend to have higher Mn/Fe (Mn/Fe > ~5). Thus, the positive Y anomaly in the micronodules with high Mn/Fe may suggest that REY scavenging from ambient seawater by Mn-oxides is very rapid and produces a disequilibrium REY distribution (Bau et al., 2014).

There is a positive correlation between the Fe and Mn content of the micronodules and ΣREY (Fig. 9). However, the diagenetic nodules, which have higher Mn relative to Fe (~10, compared to ~4.5 in hydrogenous nodules), have lower ΣREY. Although some studies suggest that diagenetic nodules have low ΣREY concentrations because of REY loss due to dissolution of Fe- and Mn-(oxyhydr)oxide carrier phases (Nath et al., 1992), I note that the diagenetic nodules in the North Atlantic deep-sea clays have similar Mn concentrations to the hydrogenous nodules, although the hydrogenous nodules have higher Fe. The hydrogenous micronodules are also enriched in V and Co, and depleted in Cu and Ni, compared to the diagenetic nodules. In a study of ferromanganese micronodules in sediments in the northeast Pacific basin (Dubinin et al., 2008), two populations of micronodules were found, one relatively enriched in Mn, Ni and Cu and depleted in Fe, in Ce and Co, which is suggested to form under suboxic conditions, and the other with higher concentrations of Fe, ΣREY (especially Ce) and Co, but similar Mn, that formed under oxic conditions.

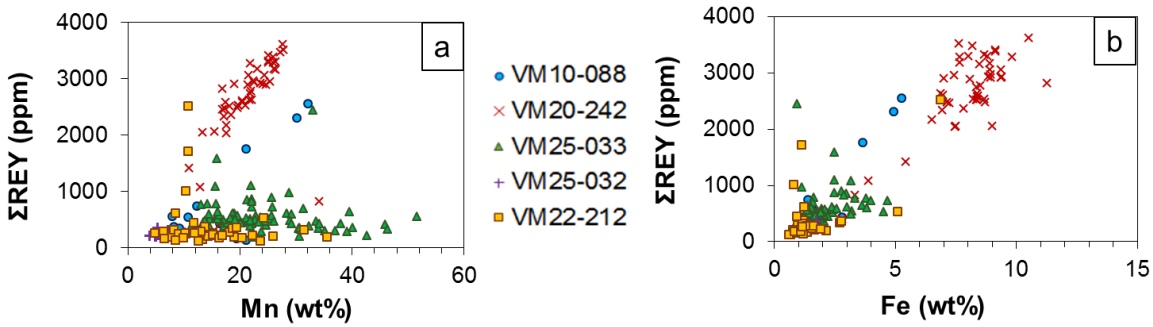

Figure 9. Relationship between ∑REY content and (a) Fe and (b) Mn in micronodules recovered from North Atlantic deep-sea sediments.

Although some of the micronodule-rich sediments were collected in close proximity to the Mid-Atlantic Ridge, the micronodules do not appear to contain a

significant hydrothermal component (Fig. 7), which supports the conclusions of previous studies conducted in the North Atlantic (Dubinin & Rozanov, 2001). This may be because hydrothermal plumes tend to be confined to the axial valley due to the topography of slow spreading ridges (e.g. Charlou & Donval, 1993). By contrast, in the Pacific Ocean, hydrothermal sediments can be found several hundreds of kilometres away from the fast-spreading East Pacific Rise (Dymond, 1981).

2.5.3 Comparison between Atlantic and Pacific deep-sea sediments

On average, the total REY abundances for my North Atlantic deep-sea sediments (ΣREY up to 512 ppm) are lower than reported values for the Pacific (ΣREY up to 2230 ppm) (de Baar et al., 1985; Kato et al., 2011). This difference is likely to be, in part, due to differences in sedimentation rate; in general, sedimentation rates are higher in the Atlantic as most of the seafloor lies above the carbonate compensation depth (Sverdrup et al., 1970; Berger, 1975; Biscaye et al., 1976). The REY content of the deep-sea clays is principally controlled by scavenging of the REYs from seawater, so the lower the sedimentation rate, the greater the uptake of the REY during sedimentation. Differences in sediment lithology could also be a factor; in the Pacific, deep-sea sediments are often rich in fish bone debris which is composed of biogenic calcium phosphate that readily accumulates REYs from seawater (Toyoda et al, 1990; Dubinin & Rozanov, 2001; Dubinin, 2004). Similarly, widely distributed iron and manganese oxyhydroxides of hydrothermal origin in the Pacific scavenge dissolved phosphate (Feely et al., 1996); in deep-sea sediments this P is converted to calcium-iron hydroxophosphates that have high REY concentrations (Dubinin, 2001). The REY content of the clays may also be affected by differences in the REY concentration of seawater. REY concentrations are higher in the deep Pacific than they are in the deep Atlantic, partly because of dissolution of sinking biogenic particles from surface waters (de Baar et al., 1985), and partly because deep Pacific waters have lower carbonate ion concentrations which enhances uptake of the REY onto particle surfaces (Sholkovitz, 1995; Byrne, 2002; Luo & Byrne, 2004).

Although the North Atlantic deep-sea clays have lower REY contents than in the Pacific, they have a much more pronounced Ce anomaly (up to 2.4 in the Atlantic, compared to up to 1.4 in the Pacific; Toyoda et al., 1990). It is likely that this is related to higher levels of bottom water oxygenation in the Atlantic than in the

Pacific, which lies at the end of the ocean conveyor (Reid, 1997; Mantyla & Reid, 1983).

2.5.4 Resource potential of Atlantic deep-sea sediments

The average ΣREY content of the red clay samples analysed in this study is 257 ± 86 ppm (Table 9). Given a dry bulk density of 0.65 g cm^{-3} (Thomson et al., 1984), and assuming that mining will remove the upper ~1 m of seafloor sediments (based on specifications for the Nautilus Minerals seafloor mining tool; Coffey Natural Systems, 2008), 1 km^2 of red clay in the North Atlantic Ocean has the potential to yield 167 ± 56 tonnes of REY oxides (Table 9). This represents a <1 % of the global annual consumption of the REY in 2010 (105,000 tonnes; Hatch, 2012). Similarly, mining of 1 km^2 of grey clay (which has an average ΣREY content of 130 ± 61 ppm (Table 9), will yield 85 ± 40 tonnes of REY oxides.

Area/ sediment type	Av. ΣREY content ppm	Mass REY oxides[1] tonnes/km^2	Mining area[2] km^2 yr^{-1}	Reference
North Atlantic red clay	257	167	63	This study
North Atlantic grey clay	130	84.5	124	This study
Eastern South Pacific red clay	1180	767	17	Kato et al. (2011)
Central North Pacific red clay	640	416	32	Kato et al. (2011)

Table 9. Average ΣREY content of North Atlantic deep sea sediments, compared to deep sea clays from the Pacific Ocean. [1]Assumes removal of upper 1m of sediment, and dry bulk density of 0.65 g cm^{-3}. [2]Area of seafloor to be mined per year to meet 10% of the global annual REY demand.

The area of North Atlantic red clay (~1 m thick) required to provide ~10% of the global annual demand for the REYs is of the order of ~60 km^2. This is a tiny fraction (<0.0001%) of the total area of the Atlantic Ocean seafloor, but is nevertheless much greater than the area of seafloor calculated to produce the same quantity of REYs in the eastern South Pacific (~1.5 km^2; for an average clay thickness of 10 m) or the central North Pacific (~0.5 km^2; for an average clay thickness of 70 m) (Kato et al., 2011).

As Kato et al. (2011) estimate seafloor REE resources for far greater depths of sediment removal than I assume in this study, the areal extent of sediment extraction required to meet 10% of the global annual demand for a sediment depth of 1 m is provided for comparison with my study in Table 9. Whatever

thickness of sediment is removed, it is clear from Table 9 that the higher ΣREY content of Pacific red clays means that the area of seafloor impacted by mining will be less than it is in the Atlantic Ocean. Nevertheless, I caution that mining will almost certainly result in long-term changes to the ecosystem structure, functions and services in the deep sea (e.g. Miljutin et al., 2011) that will extend far beyond the area of sediment removal (Jankowski & Zielke, 2001).

2.6 Conclusions

Geochemical analyses of a suite of deep-sea sediments from a transect across the North Atlantic at ~24 °N indicates that the REY are enriched in slowly-deposited red clays from the Nares Abyssal Plain and the Canary Basin, with highest concentrations found in red clays that contain micronodules of ferromanganese oxides (up to 513 ppm ΣREY). Grey clays that contain significant terrigenous material transported by turbidites contain lower ΣREY (~150 ppm), and carbonate-rich sediments contain lowest ΣREY concentrations (~120 ppm). REY distribution patterns of the red clays mirror that of seawater, with positive Ce anomalies and enrichment in the LREE relative to the HREE. Compared to NASC, the red clays are also enriched in Fe, Mn, Cu, Co, Ni and V, which are typically associated with hydrogenous material. Results of factor analysis confirm that the red clays acquire REY from seawater.

In situ analysis of individual micronodules confirms that they have very high ΣREY (up to 3620 ppm). The micronodules consist of two distinct groups: one with relatively high Fe/Mn and higher V and Co concentrations, and one with relatively lower Fe/Mn and higher Cu and Ni concentrations. The former group appears to have a mostly hydrogenous source, while the latter group has a stronger diagenetic source. The hydrogenous micronodules have highest ΣREY and are significantly enriched in Ce relative to La and Nd (Ce* up to 36.2).

Total REY concentrations in North Atlantic deep-sea sediments are lower than those measured in Pacific deep-sea sediments, by a factor of ~4. This may, in part, be due to overall lower sedimentation rates, higher concentrations of fish bone debris and ferromanganese oxyhydroxides of hydrothermal origin, and higher seawater REY concentrations, in the Pacific. Because of its lower ΣREY concentrations, the area of the seafloor impacted by future mining of deep-sea sediments will be greater in the Atlantic than it would be in the Pacific.

Chapter 3: Evaluation of leaching techniques and their environmental implications for commercial extraction of metals and REY from deep-sea sediments and polymetallic nodules

Abstract

Deep sea sediments and nodules could be economically interesting sources of metals and rare earth elements and yttrium (REY). In this study we assess the efficacy of extraction of these elements in cold, low strength acids and the potential for release of unwanted elements in a hypothetical mining scenario where the leached residue is returned to the seafloor.

Leaching of REY-rich Atlantic sediments in oxalic acid effectively releases Mn, Co, Ni and Cu (>~80%). In turn, HCl efficiently extracts P and Ca (presumably from apatite), but only moderate amounts of REY (~50%). This suggests that, in contrast to Pacific REY-rich sediments, a greater proportion of the REY are hosted in recalcitrant detrital phases. While oxalic acid extracts >50% of Mn, Fe, Co and Cu from Atlantic nodules, it was ineffective at extracting metals from Pacific nodules. HCl leaching extracted >~80% of the REY from Pacific nodules but only ~40% from Atlantic nodules, and was generally ineffective for extracting most transition metals.

Return of leached sediment and nodule residues to seawater has the potential to increase trace metal concentrations in seawater by up to four orders of magnitude. This might represent an important source of toxicity to the benthic ecosystem in prospective mining areas.

3.1 Introduction

Rare earth elements and yttrium (REY) are essential components in modern technologies such as magnets, computer hard drives, electric motors and liquid crystal displays (Kingsnorth, 2008). They also play a vital role in environmental

protection, as they are key in the improvement of energy efficiency and in many 'green' carbon-reducing technologies (Castor and Hedrick, 2006).

World REY production is currently dominated by mining of alkaline and carbonatite deposits in China; these accounted for 90% of the total REY supply in 2013 (USGS, 2014). The REY are relatively easily extracted from residual deposits of REY-bearing clays by leaching with sulfide and chloride salts at ambient temperature (Tran, 1991; Ru'an, 1998; Moldoveanu & Papangelakis, 2012), followed by purification using solvent extraction (Li et al., 2006 ; Preston et al., 1996) or ion-exchange techniques (Ochsenkühn-Petropoulou et al., 2002). However, most REE deposits must first undergo physical beneficiation and then leaching in hot, concentrated acid or alkali solutions that requires a high consumption of energy (e.g. Haque et al., 2014). Additionally, some ores can be highly radioactive (e.g. Meor Yusoff & Latifah, 2002) and processing of REE deposits on land has seen significant release of chemical waste into local farmlands and rivers (Hilsum, 2009).

Because of these concerns, and as demand for REY increases, additional sources of REY have been sought. These include marine REY resources, in the form of deep sea sediments and polymetallic nodules. High concentrations (up to 2230 ppm) of REY have been reported in sediments from the eastern South Pacific and central North Pacific, leading to the suggestion that removal of just ~1 km^2 of a ~70-m thick layer of mud could meet one-fifth of a year's supply of the world's current REY demand (Kato et al., 2011). High concentrations (up to 5000 ppm) of REY have also been reported in sediments from the western Pacific (Iijima et al., 2016), although marine sediments from the North Atlantic (Menendez et al., 2016) and Indian Oceans (Pattan & Parthiban, 2011;Yasukawa et al., 2015) appear to have rather lower REY concentrations (<1000 ppm).

Polymetallic nodules have long been considered a potential resource of metals such as Mn, Co, Ni, Cu, Li and Te (Mero, 1965; Hein et al., 2013) and they also contain high concentrations of the REYs (up to 1082 ppm; Bau et al., 2014). A number of exploration licenses for large nodule fields have been granted by the International Seabed Authority (ISA) since 2013; most of these are located within the Clarion Clipperton Fracture Zone (CCFZ) in the eastern equatorial Pacific Ocean. Preliminary work shows that a significant potential advantage of both marine sediments and polymetallic nodules is that metals and the REY are relatively easily extracted from them. For example, it has been shown that the REY can be efficiently leached from polymetallic nodules in weak (0.2 M) H_2SO_4

(Parhi et al., 2013), and recent studies of Pacific deep-sea sediments indicate that the REY can be quantitatively extracted from them by leaching in dilute HCl and H_2SO_4 for periods of as short as 2-5 minutes at room temperature (Kato et al., 2011; Takaya et al., 2015). Similarly, studies of marine ferromanganese precipitates including crusts and nodules show that transition metals (Mn, Co, Ni, Cu, Zn and Pb) can easily be extracted at room temperature using low concentration solutions of hydroxylamine hydrochloride and oxalic acid/ammonia oxalate buffer (Koschinsky & Halbach, 1995). Co, Cu, Ni and Mn have also been successfully extracted within a short time from polymetallic nodules using a mixture of $FeSO_4$-H_2SO_4-H_2O (Vu et al., 2005). However, this method requires heating to ~90˚C. The relative simplicity of these methods has obvious and considerable benefits over extraction from land-based REY deposits. In this study I develop these ideas and test the efficacy of a number of different inexpensive techniques for fast extraction of REY and metals from deep-sea sediments and polymetallic nodules. In addition, I investigate the potential for release of potentially harmful elements if leached residues are returned to the ocean as part of the mining operation (Angel & Rice, 1996; Ahnert & Borowski, 2000; Thiel et al., 2005).

3.2 Sample material

Three sediment samples and five nodule samples were selected for the leaching experiments (Table 1). The sediment samples are red clays from the North Atlantic Ocean that have relatively high REY concentrations (up to 513 ppm). One of these samples (VM10-88) contains small Fe-Mn-rich micronodules that have high REY concentrations (up to 2560 ppm; Menendez et al., 2016). The nodule samples include two USGS certified reference materials from the Atlantic (NOD-A-1) and Pacific (NOD-P-1) oceans, as well as three samples collected from the UK Claim Area (~13.3˚N, 116.4˚W) in the CCFZ during RRS James Cook cruise JC120 in 2015.

3.3 Analytical methods

A variety of methods were tested to evaluate their potential for release of resource metals and the REY. These included leaching in dilute HCl and H_2SO_4 at room temperature which has previously been shown to release significant amounts of REY from deep sea sediments and nodules (e.g. Zhang et al., 2001; Parhi et al., 2013; Kato et al., 2011; Takaya et al., 2015), and use of a low

Sample	Sample type	Location#	Lat. (°N)	Long. (°E)	Water depth (m)	Source*
VM10-88	Micronodule-rich brown clay	Central Atlantic	23.0	-38.2	4971	LDEO
RC10-10	Brown clay	Nares Abyssal Plain	25.2	-56.1	5929	LDEO
D10311-S2	Red clay	Canary Basin	25.7	-31.0	6133	BOSCORF
NOD-A-1	Mn nodule CRM	Blake Plateau	31.0	-78.2	788	USGS
NOD-P-1	Mn nodule CRM	CCFZ	14.5	-124.3	4300	USGS
JC120-104-02	Mn-nodule	CCFZ (UK claim area)	13.3	-116.3	4130	JC120
JC120-104-03	Mn-nodule	CCFZ (UK claim area)	13.3	-116.3	4130	JC120
JC120-104-04	Mn-nodule	CCFZ (UK claim area)	13.3	-116.3	4130	JC120

Table 1: Location and description of sediment and nodule samples used in this study. CRM = certified reference material. #CCFZ = Clarion Clipperton Fault Zone; *LDEO = Lamont-Doherty Earth Observatory; BOSCORF = British Ocean Sediment Core Facility; USGS = U.S. Geological Survey.

concentration oxalic acid/ammonia oxalate buffer solution that is expected to target moderately reducible Fe (oxyhydr)oxides and associated resource metals including Ni and Cu (Koschinsky & Halback, 1995). The bulk chemical composition of the sediments and nodules was also determined. Finally, unwashed and washed residues from the leaching experiments were suspended in seawater to assess the potential for release of metals and the REY.

3.3.1 Bulk analysis

Prior to acid leaching, the bulk composition of the nodules and sediments was measured. For this, the samples were ground in an agate mortar, washed with Milli-Q water, oven-dried at 40 °C and then dissolved in a mixture of hydrofluoric (HF), perchloric ($HClO_4$) and hydrochloric (HCl) acids, and aqua regia. For each sample, ~50 mg of powdered material was transferred to a 15 mL PTFE screw-cap vial and weighed. 5 mL of aqua regia was added to each vial, which was capped and refluxed on a hotplate at 90 °C overnight. The solution was then evaporated to near dryness, 3 mL of HF and 2.25 mL of $HClO_4$ was added and then heated on a hotplate at 150 °C overnight. The cap was removed and the samples were

heated to 170 ˚C until white fumes were observed. The temperature was then increased to 180 ˚C and the sample was evaporated to near-dryness. 2 mL of HClO4 was added, the cap was replaced and the solution was heated overnight on a hotplate at 150 ˚C. After evaporating to near-dryness, 10 mL of 6M HCl was added and the sample was heated on a hotplate at 130 ˚C. The solution was then evaporated to near dryness, and made up to 100 cm^3 in 0.5 M HNO_3 in a volumetric flask. A sub-sample of 1 mL of this solution was dried down, spiked with an internal standard consisting of 5 ppm Re and In and 20 ppm Be, and made up to 13 mL with 0.5 M HNO_3 for trace element and REY analyses. For analysis of the major elements, 0.25 mL of the solution was spiked, and made up to 5 mL with 0.5 M HNO_3.

3.3.2 Leaching experiments

1g of every ground sample was weighed and transferred to a 15 mL PTFE screw-cap vial. 10 mL of either i) 0.5 M HCl, ii) 0.2 M H_2SO_4 or iii) 0.2 M oxalic acid/ammonia oxalate buffer solution (pH 3.5) was added to the vial, and the vials were shaken on a shaker table at room temperature for 12 hours. 100 µl aliquots of the leachate solution were extracted after 15 minutes, 1 hour, 4 hours and 12 hours. The leachate solutions were spiked with an internal standard consisting of 5 ppm Re and In and 20 ppm Be, and made up to 5 ml with 0.5 M HNO3. A 1 mL sub-sample of this solution was further diluted with 4 mL of 0.5 M HNO3 spiked with Re, In and Be. This solution was used to measure the concentrations of major elements in leachates extracted after 15 minutes and 1 hour. For the rest of the leachates (i.e. those extracted after 4 hours and 12 hours), this solution was further diluted by a factor of 5 for analysis of the major elements. All of the leaching experiments were carried out in duplicate.

3.3.3 Release of metals from residue into seawater

10 mL of certified seawater reference material NASS-6 were added to the solid residues remaining after the acid leaching experiments. One of the two replicates of each sample/acid pair was washed with Milli-Q water before the seawater was added, while the other was left unwashed. Samples were then shaken on a shaker table for 24 hours. A sub-sample of 0.67 mL of the seawater was extracted and spiked with an internal standard consisting of 5 ppm Re and In and 20 ppm Be, and made up to 20 ml with 0.5 M HNO_3. This solution was used to determine the major element concentrations in all of the HCl and H_2SO_4-leached samples; for the

samples leached with oxalic acid, this solution was further diluted by a factor of 10.

3.3.4 Analysis of major elements, trace elements and REYs

Major element (Fe and Mn), trace element (Co, Ni, Cu, Th and U), and REY (La, Ce, Pr, Nd, Sm, Eu, Gd, Tb, Dy, Y, Ho, Er, Tm and Lu) concentrations were determined by inductively coupled plasma mass spectrometry (ICP-MS; Thermo Scientific X-Series II) at the University of Southampton. Measurements were calibrated against 6 artificial standards of different concentrations, and the accuracy and reproducibility of the measurements was assessed by multiple (n=9) analyses of MAG-1, BCSS-1 and MESS-1 certified reference materials, analysed as unknowns alongside the samples. Instrument drift was assessed by addition of internal standards (Re, In and Be), and analysis of an internal standard every 10 samples. The external reproducibility of the analyses was better than ±5 % for the major elements, and better than ±3 % for most of the trace elements and REEs; the reproducibility of Cu and Y analyses was ±8 % and ±15 %, respectively. Measured concentrations were within ±5% of the certified or recommended values for all elements except Tb (±20 %) and Y (±15 %). The reproducibility of duplicate experiments was better than ±7% for REY and ±10% for major elements.

3.4 Results

3.4.1 Bulk composition of sediments and nodules

Concentrations of major, minor and REY elements in the nodules and sediments are given in Table 2. Deep sea red clays are relatively enriched in Fe (~5.9-8.8 wt. %) and REY (~308-513 ppm) with respect to grey clays and carbonate-rich sediments, and the micronodule-rich red clay shows the highest contents in Mn (~0.7 wt. %), Co (~76 ppm), Ni (~178 ppm) and Cu (~184 ppm). Although I have not determined the chemical composition of red clays from the Pacific in this study, I note that compared to the REY-rich red clays analysed by Kato et al. (2010), the Atlantic clays have lower concentrations of Mn, Ca, P and ΣREY (Table 2).

Element	Nodules					Sediments			
	NOD-A-1	NOD-P-1	JC120-104-02	JC120-104-03	JC120-104-04	RC10-10	VM10-88	D10311-S2	Pacific REY-rich*
Mn (wt %)	18.7	33.6	36.1	38.7	35.4	0.46	0.75	0.34	1.67
Fe	9.49	5.05	4.03	3.55	4.27	6.19	8.79	5.84	7.32
Ca	11.1	1.95	1.24	0.70	0.96	0.29	0.62	0.91	2.89
P (ppm)	7510	1910	1560	1700	1270	865	885	517	4910
Cr	19400	14400	9050	8880	10800	81.2	53.7	90.6	-
Co	3010	2160	1130	1080	1100	61.3	76.3	51.4	142
Ni	5900	12700	13100	10300	13700	107	178	110	299
Cu	987	10700	11100	8000	1100	124	184	124	573
La	107	98.7	82.1	73.2	79.9	48.2	85.3	49.6	113
Ce	840	350	237	234	274	140	166	138	96.4
Pr	23.6	30.2	25.7	21.6	24.8	11.9	22.1	12.1	31.3
Nd	96.7	126	109	90.3	103	43.7	84.9	44.5	131
Sm	21.4	30.4	26.7	21.9	25.7	8.61	17.3	8.85	29.7
Eu	5.30	7.80	6.76	5.43	6.38	1.78	3.90	1.88	7.35
Gd	26.9	28.8	25.1	20.9	24.4	7.12	15.9	7.55	33.3
Tb	3.95	4.89	3.94	3.26	3.84	1.09	2.37	1.15	5.01
Dy	22.3	24.8	22.2	18.2	21.6	6.18	13.8	6.61	31.4
Ho	4.95	5.06	4.19	3.45	4.08	1.12	2.72	1.29	6.52
Er	13.6	12.7	11.3	9.30	11.0	3.30	7.48	3.55	18.6
Tm	2.05	1.96	1.68	1.37	1.66	0.48	1.07	0.52	2.57
Yb	13.3	12.4	11.3	9.20	11.1	3.16	6.88	3.41	16.2
Lu	2.15	1.89	1.70	1.40	1.67	0.48	1.01	0.51	2.48
Y	116	84.6	71.6	59.7	69.3	31.0	82.3	36.3	198
ΣREY	1299	818	640	573	662	308	513	316	723
ΣHREE	94.0	98.9	88.2	72.6	85.8	24.8	55.1	26.5	124
Th	22.5	15.2	10.6	9.89	13.7	15.9	15.4	15.1	7.99
U	7.00	4.10	3.78	4.24	3.91	2.39	2.43	2.37	2.17

Table 2: Bulk elemental composition of sediment and nodule samples. *Average data from REY-rich muds from Kato et al., (2011).

Compared to the Atlantic nodule, the Pacific nodules have higher Mn (~34-39 wt. % vs 18.7 wt% in the Atlantic), Ni (~13000 ppm vs 5900 ppm in the Atlantic) and Cu (~10000 ppm vs 987 ppm in the Atlantic). In turn, the Atlantic nodule has higher Fe (~9.5 wt % vs ~ 4.5 wt % in the Pacific), Co (~3000 ppm compared to ~ 1500 ppm in the Pacific) and ΣREY (1300 ppm vs ~700 ppm in the Pacific). Hence the Pacific nodules have higher Mn/Fe ratios (~8) than the Atlantic nodule (~2), and higher concentrations of Ni + Cu + Co (~25000 ppm vs ~10000 ppm in the Atlantic nodules). This suggests that they acquired a greater part of their metals from sediment pore waters (diagenetic sources) relative to the overlying seawater (hydrogenous sources), compared to the Atlantic nodules (Bonatti et al., 1972; Wegorzewski & Kuhn, 2014).

3.4.2 Sediment leaching experiments

Concentrations of metals and REY released from the Atlantic sediments by weak acid leaching are shown in Appendixes A.1 and A.2. The proportion of each element released relative to the bulk sediment is also given. Release of the REYs by HCl and H_2SO_4 is relatively fast at first but slows significantly after ~1 hour. The total amount of the REY released by these acids is similar, between ~30 and ~50% after 24 hours. The quantity of the REY released by buffered oxalic acid is lower (<20% after 24 hours). The proportion of middle REE (MREE=Sm, Eu and Gd) released is generally higher than the proportion of light- and heavy-REEs (Figure 1). The amount of Ce released, however, is much smaller than the other REEs, up to ~34% with HCl and up to ~31% for H_2SO_4; release of Ce from the micronodule-rich sediment (VM10-88) was even lower (18 %). Buffered oxalic acid appears to preferentially leach the heavy REE (HREE= Eu, Gd, Tb, Dy, Ho, Er, Tm, Yb and Lu), and is more effective at releasing Ce, with recoveries of ~10-21%.Recovery of Fe, Cr and Co is low with HCl and H_2SO_4 (usually <10% after 24 hours, with the exception of Co in sample D10311-S1). Concentrations of Mn, Ni and Cu leached by these acids increase over time but less than ~55% of these elements is recovered after 24 hours. HCl and H_2SO_4 are however relatively successful at releasing Ca and P, with ~ 31-79 % and ~64-77 % released during the first 15 minutes, and almost all after 24 hours (Figure 2). Leaching with buffered oxalic acid releases proportionally more Mn, Co and Ni after 12 hours, with recoveries of ~71-98%, ~77-88%, ~67-72%, respectively. Relatively high release rates are achieved after only 15 minutes, up to ~58%, ~44% and ~31%, respectively, of Mn, Co and Ni. Release of Cu is lower after 12 hours (~27-55%), and only minor amounts of Fe are recovered (~5-14%). Recovery of Ca and P is much lower than it is from leaching in HCl and H2SO4, ~0.3-11% and ~3-26%, respectively (Figure 2).The weak acid leaches release small quantities of Th and U from the sediments after 12 hours, up to ~10% and ~27%, respectively with HCl; up to ~37% and ~31% with H_2SO_4; and up to ~40% and ~21% with oxalic acid (Figure 1).

Figure 1: REY, Th and U recovery from Atlantic sediments with 0.5 M HCl, 0.2 M H_2SO_4 and 0.2 M oxalic acid/ammonia oxalate buffer leaching after 15 mins, 1 hour, 4 hours and 12 hours

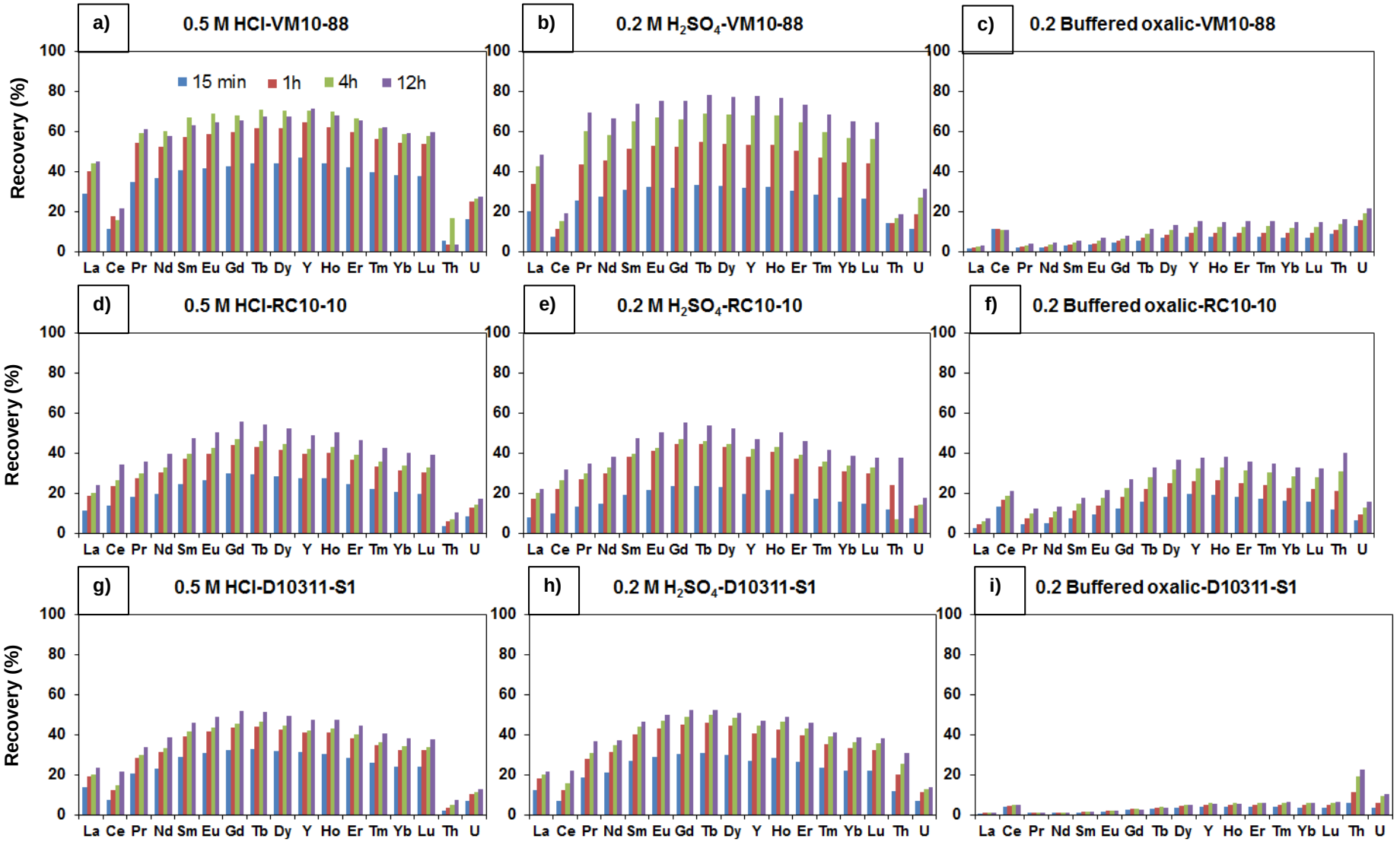
a)
0.5 M HCl-VM10-88
15 min
1h
4h
12h
b)
0.2 M H2SO4-VM10-88
c)
0.2 Buffered oxalic-VM10-88
d)
0.5 M HCl-RC10-10
e)
0.2 M H2SO4-RC10-10
f)
0.2 Buffered oxalic-RC10-10
g)
0.5 M HCl-D10311-S1
h)
0.2 M H2SO4-D10311-S1
i)
0.2 Buffered oxalic-D10311-S1
Recovery (%)
0
20
40
60
80
100
La Ce Pr Nd Sm Eu Gd Tb Dy Y Ho Er Tm Yb Lu Th U

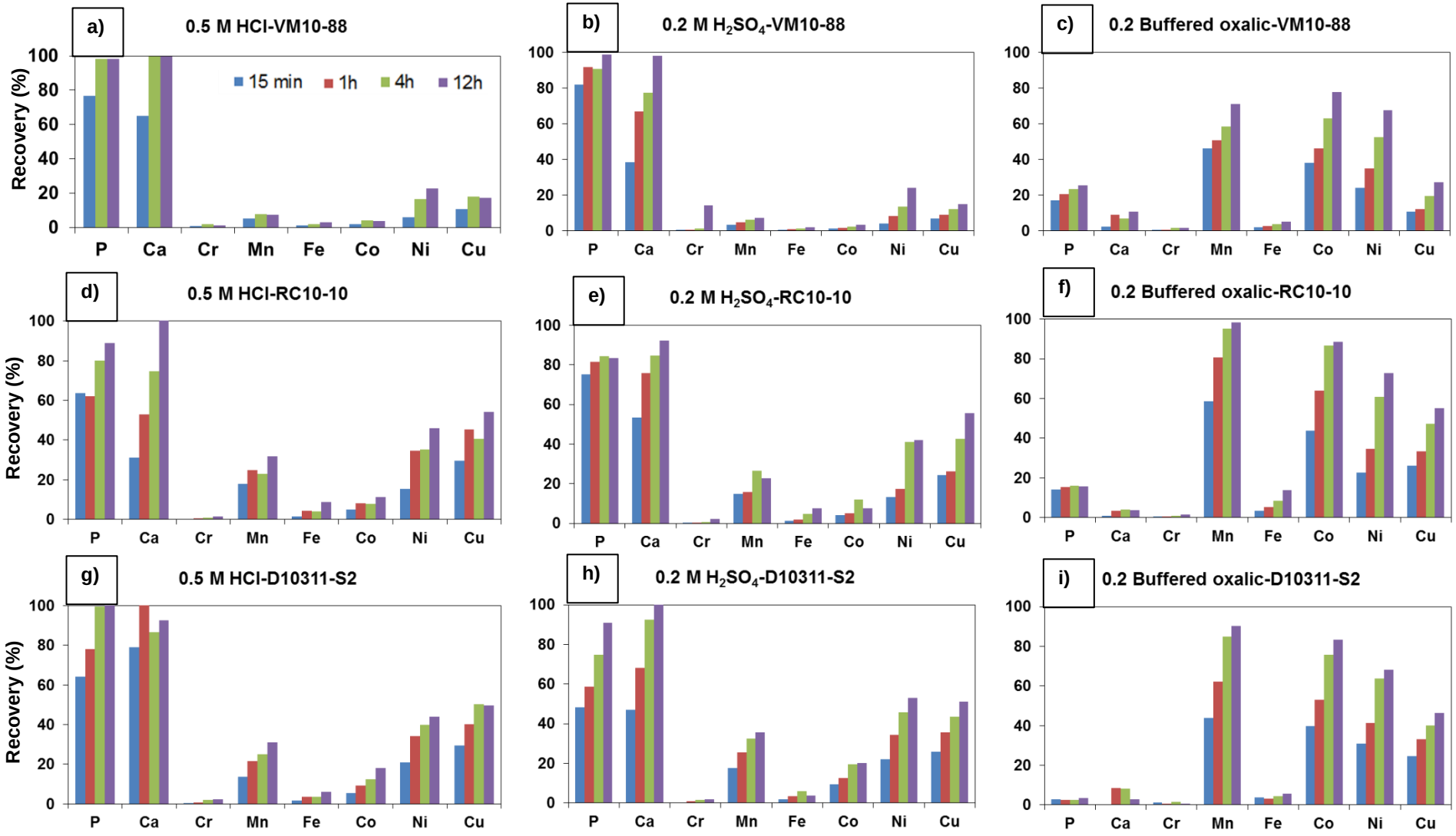
a)
0.5 M HCl-VM10-88
15 min
1h
4h
12h
b)
0.2 M H2SO4-VM10-88
c)
0.2 Buffered oxalic-VM10-88
d)
0.5 M HCl-RC10-10
e)
0.2 M H2SO4-RC10-10
f)
0.2 Buffered oxalic-RC10-10
g)
0.5 M HCl-D10311-S2
h)
0.2 M H2SO4-D10311-S2
i)
0.2 Buffered oxalic-D10311-S2
Recovery (%)
0
20
40
60
80
100
P
Ca
Cr
Mn
Fe
Co
Ni
Cu

Figure 2: Major and trace metals recovery from Atlantic sediments with 0.5 M HCl, 0.2 M H_2SO_4 and 0.2 M oxalic acid/ammonia oxalate buffer.

3.4.3 Nodule leaching experiments

Concentrations of metals and REY released from leaching the Atlantic and Pacific nodules in weak acid are shown in Appendixes A.3 and A.4 and the % recovery is shown in Figures 3 and 4. Release of REY from most of the Pacific nodules gradually increases over time in HCl and moderate amounts (~52-63%) of ΣREY are released after 12 hours (Figure 3). However, the quantity of REYs released from the Atlantic nodule is much lower (< ~19%). In general, slightly higher quantities of the light REE (up to 90%) are leached using HCl compared to the heavy REE (up to 81%). Y shows the highest recovery in all the nodules, ~81-97% in Pacific nodules, and up to ~41% in the Atlantic nodule, whereas Ce shows the lowest recovery (~6 to 26%). Leaching in buffered oxalic acid releases only minor quantities of the REY, between ~0.41and 4%. In general, the buffered oxalic acid is more effective at leaching the HREE relative to the LREE.

Fe and Mn are poorly recovered with HCl, 5-32% and ~0.3-17%, respectively: highest values correspond to the Atlantic nodule (Figure 4). Release of Co (~0.13-11%), Ni (~7-49%) and Cu (22-46%) after 12 hours is similar or slightly higher. Overall higher quantities of Ca (23 – 100%), and moderate quantities of P (17-67 %) are released after 12 hours. Leaching in buffered oxalic acid released negligible amounts (<8 %) of Mn and Fe from the Pacific nodules, but after 12 hours, ~72% of Mn and almost all Fe is released from the Atlantic nodule (Figure 4). Recovery of Co, Ni and Cu was also low from the Pacific nodules, but higher (up to 42%, 27% and 19%, respectively) from the Atlantic nodule. Recovery of Ca and P was also low for all nodules, ~0.03-19% and <5%, respectively.

Th was not significantly released (<5%) from the nodules by any of the acids (Figure 3). U, however, was significantly released by leaching in dilute HCl, up to ~31% in the Atlantic nodule, and up to ~74% in nodules from the Pacific. Release of U with oxalic acid was low and only slightly increased over time, up to ~16% for the Atlantic nodule, and up to ~10% for the Pacific nodules.

Figure 3: REY, Th and U recovery from Atlantic and Pacific nodules with 0.5 M HCl and 0.2 M oxalic acid/ammonia oxalate buffer leaching after 15 mins, 1 hour, 4 hours and 12 hours.

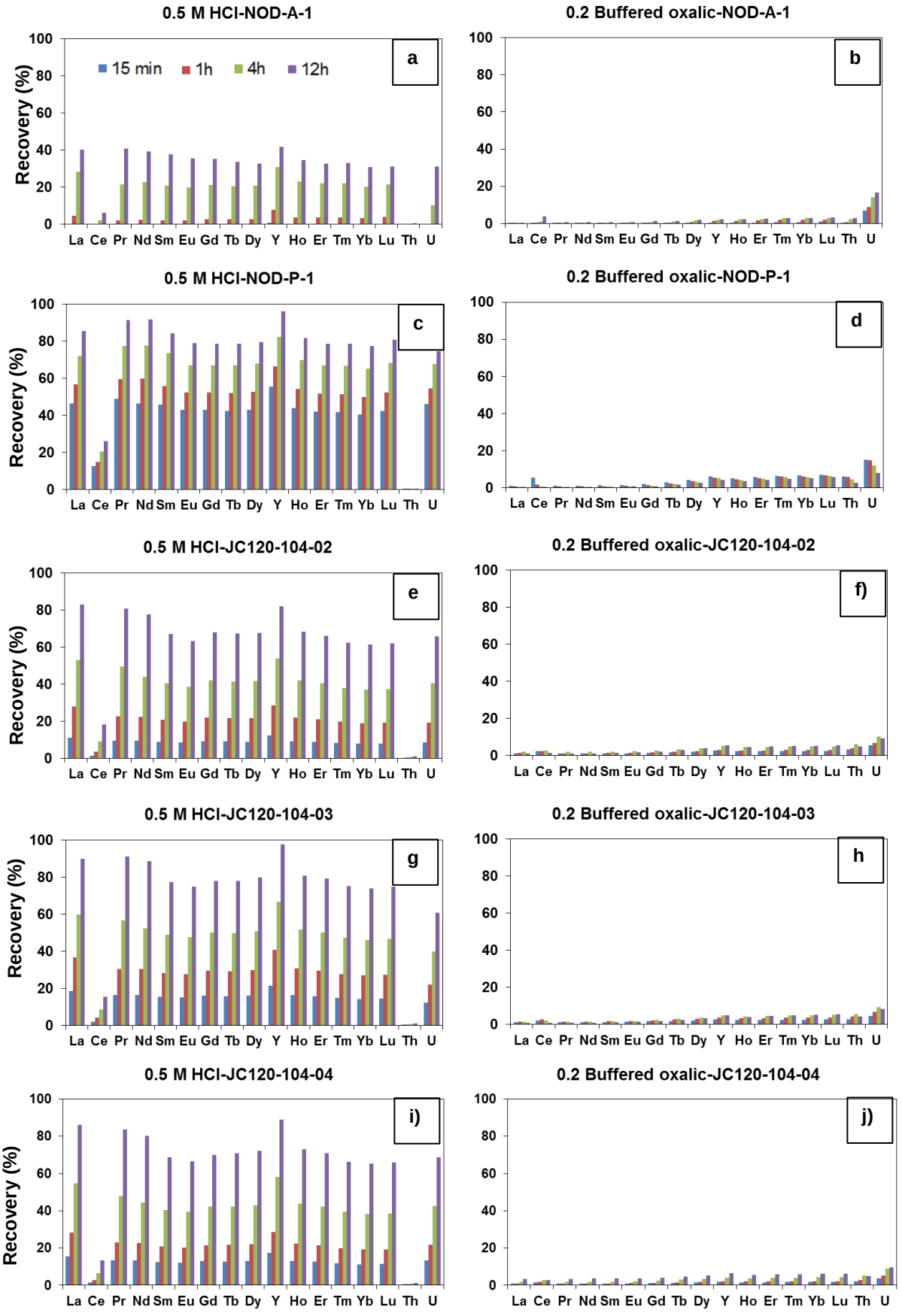
0.5 M HCl-NOD-A-1
0.2 Buffered oxalic-NOD-A-1
0.5 M HCl-NOD-P-1
0.2 Buffered oxalic-NOD-P-1
0.5 M HCl-JC120-104-02
0.2 Buffered oxalic-JC120-104-02
0.5 M HCl-JC120-104-03
0.2 Buffered oxalic-JC120-104-03
0.5 M HCl-JC120-104-04
0.2 Buffered oxalic-JC120-104-04
Recovery (%)
15 min
1h
4h
12h
a
b
c
d
e
f)
g
h
i)
j)
La Ce Pr Nd Sm Eu Gd Tb Dy Y Ho Er Tm Yb Lu Th U

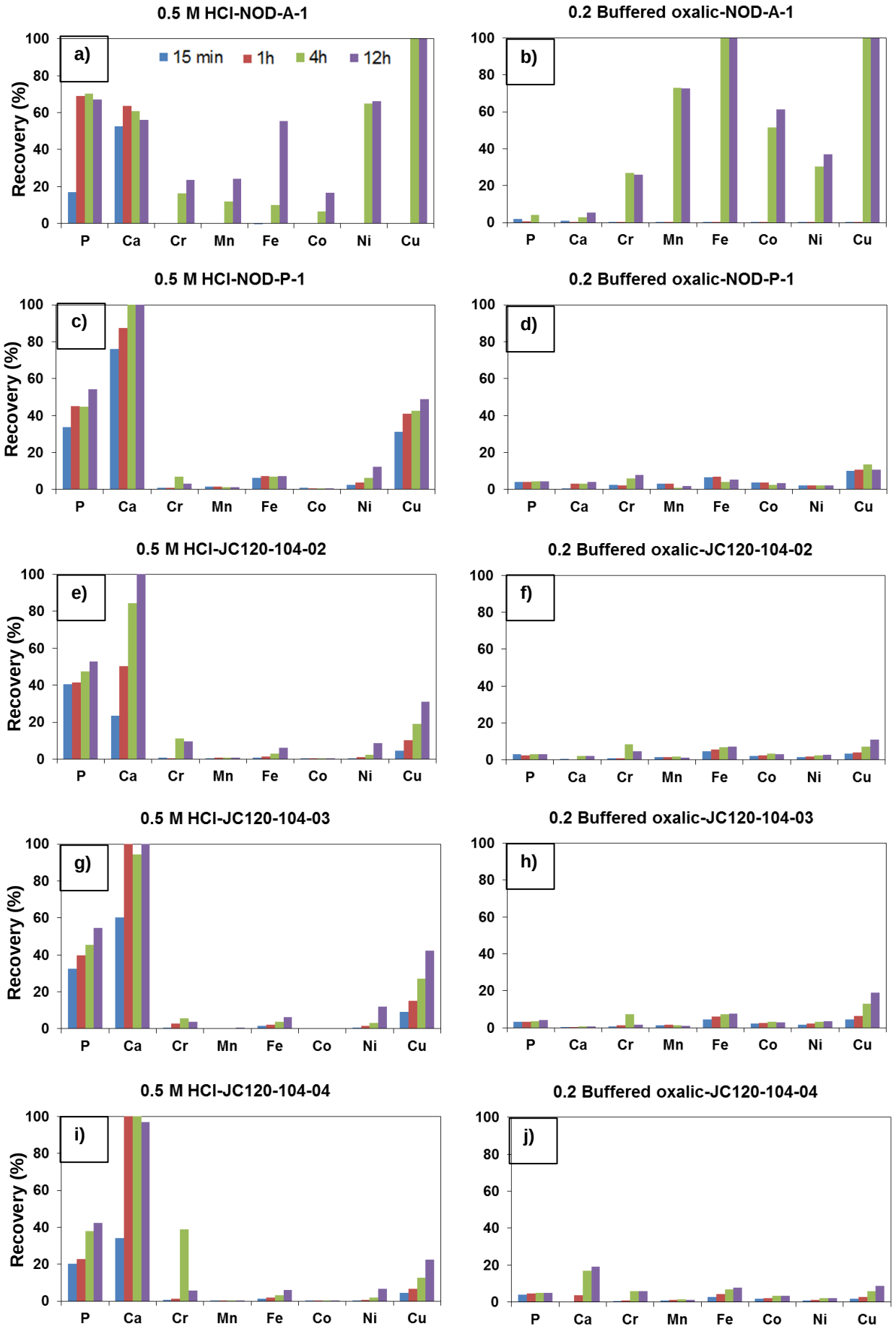
0.5 M HCl-NOD-A-1
0.2 Buffered oxalic-NOD-A-1
0.5 M HCl-NOD-P-1
0.2 Buffered oxalic-NOD-P-1
0.5 M HCl-JC120-104-02
0.2 Buffered oxalic-JC120-104-02
0.5 M HCl-JC120-104-03
0.2 Buffered oxalic-JC120-104-03
0.5 M HCl-JC120-104-04
0.2 Buffered oxalic-JC120-104-04
a)
b)
c)
d)
e)
f)
g)
h)
i)
j)
15 min
1h
4h
12h
Recovery (%)
0
20
40
60
80
100
P
Ca
Cr
Mn
Fe
Co
Ni
Cu

Figure 4: Major and trace metals recovery from Atlantic and Pacific nodules with 0.5 M HCl and 0.2 M oxalic acid/ammonia oxalate buffer leaching after 15 mins, 1 hour, 4 hours and 12 hours.

3.4.4 Seawater release experiments

Concentrations and percentage recovery of metals released into seawater from washed and unwashed leached residues are shown in Table 7. Only a small part (< 3.5 %) of the total content of major and trace metals and REY in sediment and nodules was released from their acid-leached residues into seawater. The relative amount released from the sediments was slightly higher than that released from the nodules, and the washed residues generally released lower quantities of metals than the unwashed residues.

3.4.4.1. Solid residues from leached sediments

HCl and H_2SO_4-leached sediment residues released up to ~1% of the total REY inventory from the unwashed residues, and ~0.5% from their washed equivalents. The amount of REY released from the oxalic acid-leached residues was lower, up to ~0.08% and ~1.5 % from the unwashed and washed sediments, respectively.

Release of Fe and Mn was highest from the unwashed HCl-leached residues, reaching up to ~0.3 and ~0.7%, respectively, whereas the proportion released from the washed samples was lower, <~0.2 % and <~0.2%, respectively. Sediments leached with oxalic acid released greater amounts of Fe and Mn, up to ~0.5 % and ~3%, respectively from unwashed residues and ~0.15 % and ~3% from washed residues.

The amounts of Co, Ni and Cu released from all of the acid-leached residues were similar, up to ~1.3 %, ~2 % and ~1.2% of the total from unwashed residues, respectively. Washed samples generally released lower amounts of all of these elements. Return of U and Th to seawater from both the acid-washed residues and the unwashed residues was low, <0.6% of the total.

3.4.4.2. Solid residues from leached nodules

Only small quantities of the REY were released from both the washed and unwashed residues, < ~0.4% of the total for HCl-leached residues and < ~0.001 % of the total for the oxalic acid-leached residues. The proportion of Fe and Mn released into seawater from the washed residues (~0.001 % and ~0.007%, respectively) was slightly lower than their unwashed counterparts (~0.005 % Fe

and ~0.01 % Mn), whereas washing made no significant difference to the amounts of Co, Ni, Cu, U and Th released (~0.001 %, ~0.8 %, ~0.4 %, ~0.4 % and 0.005 %, respectively).

		Mn		Fe		Co		Ni		Cu		Σ REY		Th		U	
		ppm	%	ppm	%	ppm	%	ppm	%	ppm	%	ppm	%	ppm	%	ppm	%
Non washed																	
RC10-10	HCl	30.1	0.65	170	0.28	0.22	0.35	1.06	0.99	1.01	0.81	2.66	0.86	0.11	0.67	0.01	0.33
	H_2SO_4	32.5	0.70	198	0.32	0.18	0.30	1.56	1.45	1.49	1.20	3.21	1.04	0.08	0.51	0.01	0.39
	Oxalic	116	2.49	302	0.49	0.78	1.27	1.09	1.02	1.25	1.00	0.24	0.08	0.01	0.06	0.01	0.42
D10311-S1	HCl	36.9	1.09	128	0.22	0.31	0.61	1.31	1.23	1.03	0.83	2.31	0.73	0.05	0.35	0.01	0.28
	H_2SO_4	27.8	0.82	90.2	0.15	0.50	0.97	1.24	1.17	0.86	0.69	2.56	0.81	0.09	0.61	0.01	0.31
	Oxalic	101	2.98	149	0.25	0.69	1.34	1.10	1.03	0.89	0.72	0.01	0.005	0.001	0.005	0.005	0.20
NOD-P-1	HCl	31.7	0.01	2.76	0.01	0.01	< 0.001	95.8	0.75	41.9	0.39	0.005	0.001	< 0.001	0.001	< 0.001	0.001
	Oxalic	6.71	0.002	0.15	< 0.001	0.04	0.002	0.65	0.01	0.19	0.002	2.99	0.37	0.001	0.01	0.02	0.37
Non washed																	
RC10-10	HCl	8.95	0.19	75.1	0.12	0.05	0.08	0.31	0.29	0.14	0.11	1.58	0.51	0.01	0.08	0.003	0.13
	H_2SO_4	9.37	0.20	59.3	0.10	0.06	0.11	0.42	0.39	0.37	0.30	2.01	0.65	0.06	0.39	0.004	0.15
	Oxalic	139	2.98	90.8	0.15	0.98	1.60	1.35	1.26	0.55	0.44	4.70	1.53	0.02	0.14	0.01	0.21
D10311-S1	HCl	34.5	1.02	116	0.20	0.08	0.16	1.21	1.14	0.90	0.72	1.38	0.44	0.02	0.11	0.003	0.13
	H_2SO_4	7.95	0.23	39.5	0.07	0.08	0.15	0.36	0.34	0.29	0.23	1.38	0.44	0.04	0.29	0.003	0.14
	Oxalic	67.8	2.00	60.8	0.10	0.41	0.79	0.50	0.47	0.24	0.20	0.61	0.19	0.002	0.02	0.004	0.16
NOD-P-1	HCl	26.6	0.01	0.51	0.001	0.04	0.002	102	0.81	37.5	0.35	2.76	0.34	0.001	0.004	0.01	0.31
	Oxalic	18.7	0.01	0.51	0.001	0.02	0.001	1.31	0.01	0.19	0.002	0.01	0.001	< 0.001	0.001	< 0.001	0.001

Table 3: Concentrations (ppm) and percentage of recovery of metals added to seawater from washed and unwashed leached residues.

3.5 Discussion

3.5.1 Efficacy of REY and metal recovery by leaching in cold, dilute acid

The proportion of REYs released from the Atlantic sediments (excluding Ce) after leaching in cold, dilute HCl and H_2SO_4 for 12 hours (59-66%) is far lower than the amount released from REY-rich muds from the Pacific Ocean after 1-3 hours (80-90%; Kato et al., 2011), and even after leaching of similar material from the Pacific for much shorter leaching times (>80% recovery after 2 – 5 minutes; Takaya et al., 2015). This indicates that a greater proportion of the REY in the Atlantic sediments resides in phases that are resilient to attack by dilute acid. These are most likely detrital silicates; the Atlantic receives a higher input of aeolian and riverine terrestrial material compared to the Pacific (de Baar et al., 1985; Dubinin & Rozanov, 2000) and, in support of this, the proportion of REYs recovered by dilute acid attack was lowest from sample D10311, which was collected from the Canary Basin and hence closer to the continental shelf (Table 1).

Kato et al. (2011) suggest that the main hosts for the REY in Pacific muds are a Fe-oxyhydroxide precipitate from hydrothermal plumes, and an aluminosilicate mineral, most likely phillipsite. I have not determined the Al or Si content of our leachates, but although the total Fe content of our Atlantic sediments is higher than in the Pacific sediments, only small quantities of Fe are released by leaching in cold, dilute acid. This suggests that hydrothermal Fe-oxyhydroxide precipitates are unlikely to host significant quantities of REY in the Atlantic sediments. Crucially, however, my data do reveal that leaching in both dilute HCl and dilute H_2SO_4 releases a high proportion of Ca and P and the REYs, whereas leaching in buffered oxalic acid releases little Ca, P and the REYs. This rather implies that in the Atlantic sediments, P-rich phases such as apatite are likely important hosts for the REY (Takaya et al., 2015; Elderfield et al., 1981; Dubinin & Sval'nov 2002; Nath et al., 1992). In this connection, leaching in dilute HCl and H_2SO_4 releases only small quantities of Ce that has a different oxidation state (+4) in seawater compared to the other REYs (3+), and tends to be excluded from the apatite structure (Elderfield et al., 1981). Although the importance of P-rich phases as hosts for the REY in Pacific deep-sea clays was not discussed by Kato et al. (2011), I note that there is a strong correlation between REY and P concentrations in these clays (Suppl Info). I also note that concentrations of P in the Pacific clays, like the REY, are higher than recorded in Atlantic sediments (Table 2; Menendez et al., 2016). Considered together with work presented in Takaya et al. (2015), my data indicate that P-rich phases strongly control REY concentrations in marine sediments, and these phases are efficiently attacked by leaching in cold, dilute acids.

REY distribution patterns for the HCl and H_2SO_4 leachates (Fig. 5) indicate that the P-rich phase is enriched in the middle REEs (MREEs, Sm, Eu, Gd). By contrast, seawater is enriched in the HREE (e.g. Douville et al., 1999), indicating that the REE patterns do not record seawater chemistry. Rather, it seems likely that MREE enrichment is due to incorporation of REY from sediment pore waters, which has been shown to produce MREE enrichment together with high ΣREE, Mn and Y/Ho ratios in conodonts, the skeletal remains of extinct soft-bodied animals that are composed of apatite (Bright et al., 2009; Zhang et al., 2012). Pacific REY-rich clays from have, on average, higher Y/Ho ratios than my Atlantic sediments (30.4 vs. 25.8, respectively), as well as higher Mn and ΣREE contents (Kato et al., 2011).

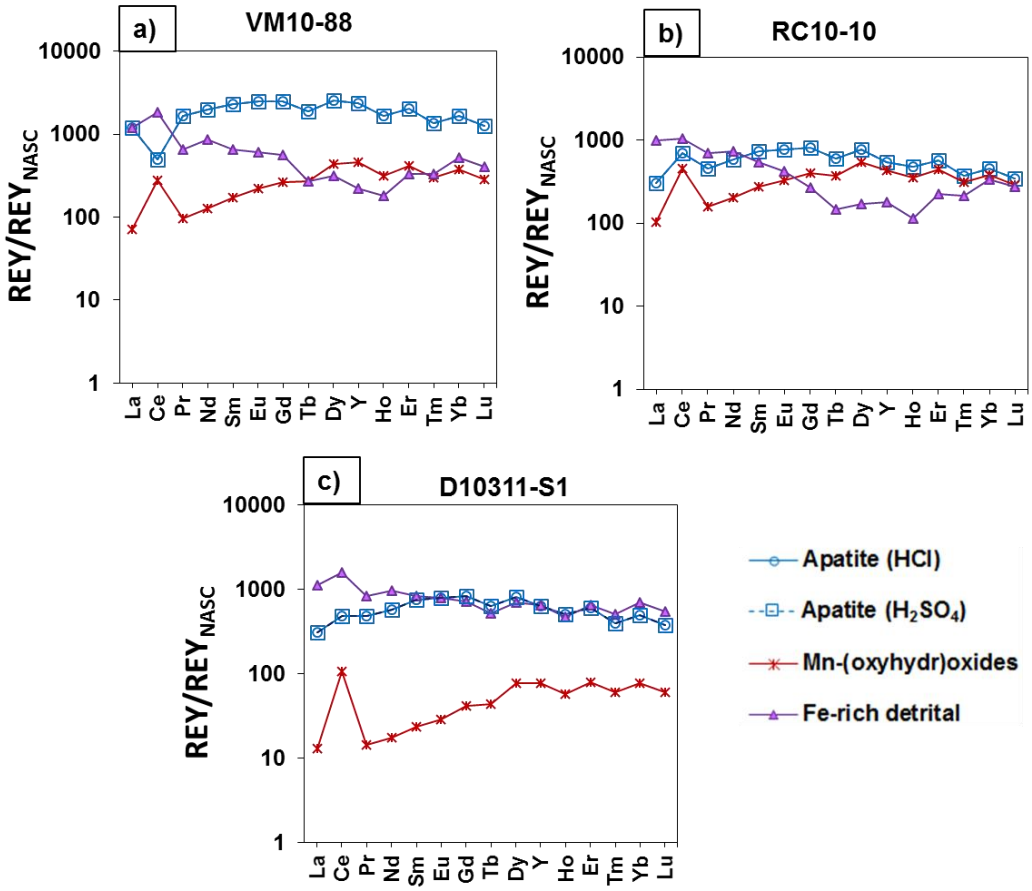

Figure 5: REY distribution patterns, normalised to North America Shale Composite (NASC; Gromet et al., 1984) for HCl, H_2SO_4, buffered oxalic leaches and residual components of Atlantic sediments.

Studies of both Atlantic (Menendez et al., 2016) and Pacific (Kato et al., 2011) deep-sea clays indicate that they are relatively enriched in Mn-Fe-(oxhydr)oxides that are acquired from seawater. Buffered oxalic acid is considered to target moderately reducible Fe- and Mn-(oxyhydr)oxides, releasing Fe and Mn together with associated metals (Koschinsky and Halbach, 1995). Although moderate to high quantities of Mn (71-98%) are released by oxalic acid (together with Co, Ni and Cu) in my experiments, only small quantities of Fe (and the REY) are released. This is consistent with recent work by ourselves (Menendez et al., 2016) and others (Bau et al., 2014) that suggests that the REY have a lower affinity for Mn-oxyhydroxides than for Fe-oxyhydroxides. Thus, although oxalic acid is effective for cheap and efficient removal of Mn, Co, Ni and Cu from deep-sea sediments, it is ineffective at releasing the REY and, by contrast, while dilute HCl and H_2SO_4 are effective for releasing the REY, they release only small quantities of the other economically important elements. Nevertheless, release of the REY from Atlantic sediments is not as effective as it is for Pacific REY-rich clays, as a greater

proportion of the REY are held in detrital mineral phases that are resistant to dilute acid attack.

As for the sediments, dilute HCl is effective for releasing the REY together with P and Ca from polymetallic nodules, but it releases negligible amounts of resource metals (except Cu), at least for nodules from the Pacific. By contrast, dilute HCl releases relatively low amounts of the REY from the Atlantic nodule, but rather higher amounts (> ~50% after 12 hours) of Fe, Ni and Cu. Again, this points to close association of the REY with P-rich phases that are effectively attacked by dilute HCl; a greater proportion of the REY appear to be associated with these phases in the Pacific nodules compared to the Atlantic (Figure 6). Leaching in buffered oxalic acid, by contrast, released negligible amounts of the REY from any of the nodules and negligible amounts of resource metals and P and Ca from the Pacific nodules. Buffered oxalic acid was more successful at releasing Mn, Fe, Co, Ni and Cu from the Atlantic nodule. The amounts of these elements released (~1.4% Mn, ~7.0% Fe, ~3.1% Co, ~2.6% Ni and ~12.3% Cu) are similar to those reported by Koschinsky & Halbach (1995) for nodules that acquire metals from sub-oxic pore water (~0% Mn, ~11.0% Fe, ~0% Co, ~1% Ni and ~2% Cu). These nodules tend to have a relatively higher proportion of Mn-oxyhydroxide phases (todorokite) that form as Mn-rich phases recrystallize during sub-oxic diagenesis. Todorokite is thus relatively stable under reducing conditions and unlikely to be attacked by buffered oxalic acid (Koschinsky & Halbach (1995). Thus metals are not readily released from diagenetic nodules that have high Mn/Fe (i.e. nodules from the Pacific; Table 2) by leaching in weak acid. By contrast, nodules with lower Mn/Fe (i.e. those from the Atlantic; Table 2) contain a greater proportion of amorphous Fe-(oxyhydr)oxides that are readily attacked by leaching in weak acid. While this results in release of other resource metals, it produces negligible quantities of the REY.

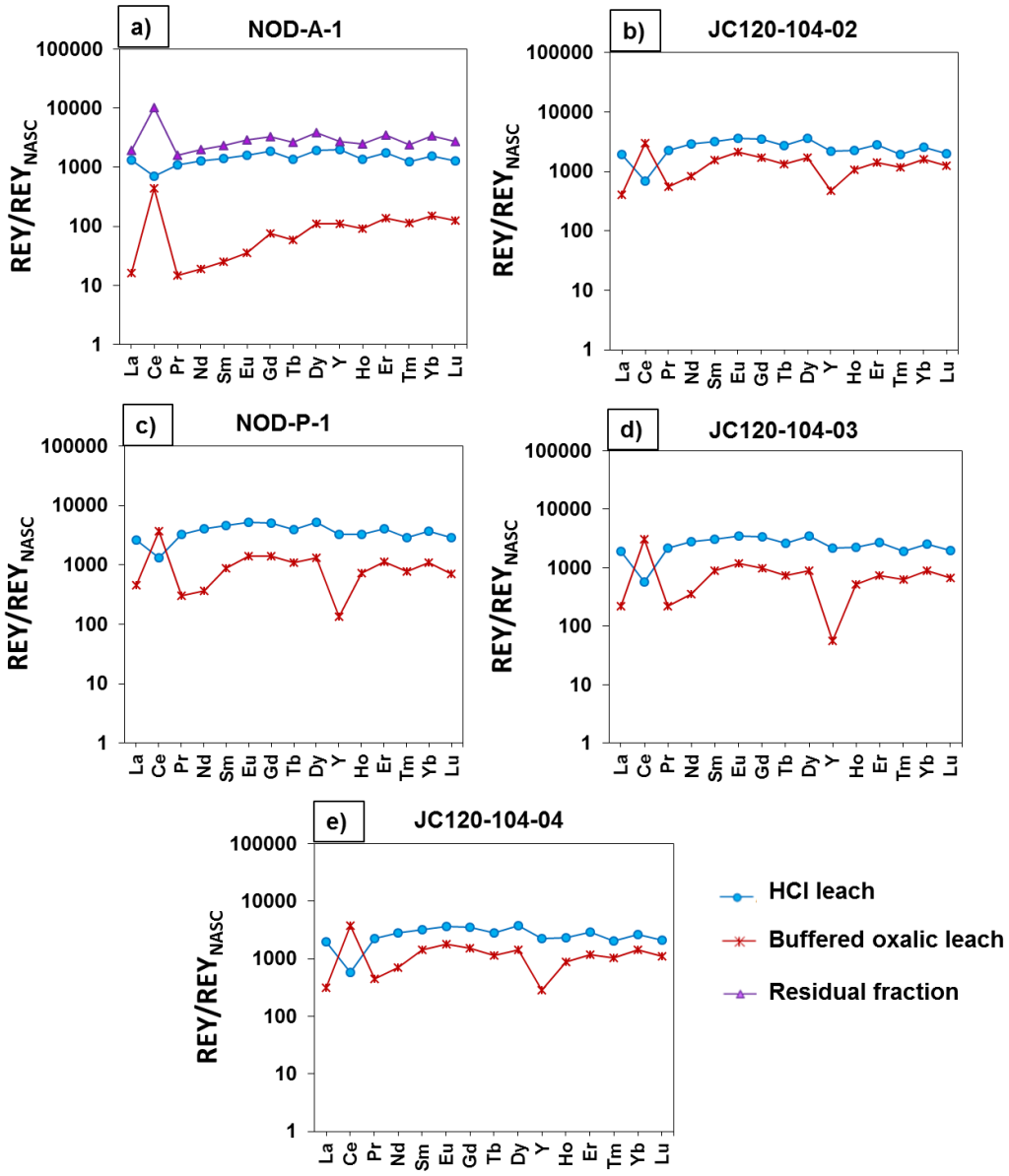

Figure 6: REY distribution patterns, normalised to NASC for HCl, H_2SO_4, buffered oxalic leaches and residual components of Atlantic and Pacific nodules.

3.5.2 Commercial viability of acid leaching of deep sea REY and metal resources

As concentrations of the REY are lower in Atlantic sediments relative to the Pacific (Menendez et al., 2016), this makes them a less attractive source for resource exploitation. By contrast, nodules from the Atlantic Ocean are more REY enriched than their Pacific counterparts (e.g. de Lange & Poorter, 1992; Table 2). However, my study shows that significantly smaller quantities of REY can be extracted with dilute HCl in Atlantic nodules compared to those from the Pacific.

On the other hand, leaching of Atlantic sediments and nodules with buffered oxalic acid over relatively short time periods is effective for economically interesting elements including Mn, Co, Ni and Cu. Appendix A.5. shows that the cost of the volume of buffered oxalic acid required to produce 1T of each of these metals from Atlantic nodules is relatively low for most of them (~< £2.5k for Ni and Cu; and ~ £0.2k for Mn), although slightly higher for Co (~ £19k). These costs are increased by approximately 1-2 orders of magnitude for the Atlantic sediments. These costs are likely to be a maximum, because they are based on purchase of relatively small volumes, rather than wholesale prices. Still, our primary estimations indicate that the extraction cost of 1T of Mn, Ni and Cu from Atlantic nodules represents respectively ~15.4, 9.6 and 45% of their current market prices (see Table S1 Suppl. Info.). Only the extraction of Co exceeds its market price, by ~187%.

Similarly to REY-rich clays (Takaya et al., 2015), the REY in nodules from the Pacific Ocean can be efficiently extracted by leaching in dilute HCl. My nodules from the CCFZ, whose exploitation is likely to occur in the near future, show REY recoveries of up to ~90% (excluding Ce) after 12 hours of leaching. Based on our observed release rates, I estimate that the cost of the acid required to produce 1T of REY from these nodules is ~£0.5k, whereas that the cost of releasing a similar amount of REY in nodules from the Atlantic nodules is of ~£1.2k (Appendix A.5.). In both nodule types, for most of the individual REY this is a considerably cost-effective method, if we compare with their current market prices (i.e. between 5.24-64% of this for Pacific nodules and 13.3-82% for the Atlantic nodule; Appendix A.5.). For the Pacific nodules, only the production cost of Sm and Ho exceed their market price, while La, Ce, Sm, Eu and Ho does it in Atlantic nodule.

While Mn, Fe, Co, Ni and Cu were not successfully recovered by weak acid leaching of Pacific nodules, these are readily released from Atlantic nodules by leaching in buffered oxalic acid over relatively short periods of time. Thus, none of the acids that I have tested in this study are a ‘magic bullet’ that effectively releases both the REY and resource metals from nodules and sediments from both the Atlantic and Pacific Oceans (that have subtly different proportions of different mineral phases).

Although it is more difficult to extract the REY from Atlantic sediments and nodules, Table 4 shows that exploitation of these deep-sea resources may nevertheless be more cost-effective and safer than extraction from land-based resources. Additionally, terrestrial hard-rock REY deposits require complex and

costly processing via labour-intensive drilling, milling or blasting with explosives (e.g. Castor & Hendrick, 2006), whereas nodules are friable and likely to be crushed during the collection process by hydraulic transport systemssuch as the French GEMONOD system that was utilized in 1988. And although mining and processing of low grade, near surface, unconsolidated ion adsorption deposits are simpler, metal extraction pond and pile leaching techniques can cause extensive environmental damage (Kanazawa & Kamitani, 2006). Moreover, after recovery, a series of physical and chemical beneficiation processes are required to extract the metals, often requiring the use of chemicals such as hot caustic soda to remove REE from hard minerals such as monazite and xenotime (Castor & Hedrick, 2006). In comparison, exploitation of deep sea clays requires only mining solutions to recover the ores from great oceanic depths. Seafloor mining tools of this type are already under construction (Nautilus Minerals; Coffey Natural Systems, 2008).

Table 4 shows that the estimated cost to produce 1 tonne of REY blend resource from terrestrial deposits is ~ £6300 k for carbonatite deposits and ~ £12700 for alkaline-based deposits (Avalon Rare Metals Inc. and Rare Element Resources Ltd. in Tyrer & Sykes, 2013). These figures include the costs of labour, grinding, electricity, explosives and reagents, and they are therefore not directly comparable with my estimates for REY production, which solely focus on the REY extraction and do not include the cost of the separation and recovery of the individual REE from the leachate (which can represent up to the ~50% of the total operational cost, e.g. Tyrer & Sykes, (2013)). Nevertheless, Table 4 shows t that extraction of the same amount (1 tonne) of REY from nodules would cost between ~ £23 and ~ £51, and leaching of Atlantic sediments would cost between ~ £16 and £250 to produce 1 tonne of REY. These costs are substantially lower than for land-based deposits.

Crucially, deep sea clays and nodules have been reported to be more enriched in the rarer but economically more interesting heavy REE (HREE) than Chinese terrestrial deposits (e.g. Kato et al., 2011; Hein et al., 2013). The HREE content of large terrestrial REY ores is < 1% of the total REY, while my data show that the HREE content of nodules from the CCFZ comprises up to ~ 14% of the total REY (Table 2). If I consider the total value of the deposits as determined by the abundances of the individual REY with respect to the ΣREY oxide blend, I note that the value of deep sea nodules and clays is equal or higher than that of carbonatites from the Chinese deposit of Bayan Obo (Table 4), whereas the value

of Pacific nodules is slightly lower than that of the Canadian alkaline deposit of Strange Lake.

As shown for Pacific sediments (Takaya et al., 2015), leaching of Atlantic sediments with dilute acid releases negligible amounts of unwanted radioactive elements. The quantity of Th and U released is between ~4 and ~6 orders of magnitude lower when compared to terrestrial deposits (Meor Yusoff & Latifah, 2002). Release of Th from nodules is negligible. Although U is partly released from nodules, nodules contain on average ~4 orders of magnitude lower U than in terrestrial deposits (Meor Yusoff & Latifah, 2002), and ~2 order of magnitude lower U than the maximum recommended values for U exposure (respectively, 0.2 and 0.6 mg/m^3 for long and short term exposures in the UK).

	Terrestrial deposits		Nodules		Atlantic sediments	
Deposit geology	**Strange Lake (alkaline)[a]**	**Bayan Obo (carbonatite)[b]**	**Atlantic nodules**	**Pacific nodules**	**Atlantic sediments**	**Atlantic sediments**
Extraction type	Underground	Open pit	HCl leaching	HCl leaching	H_2SO_4 leaching	HCl leaching
Deposit Resource (terrestrial, nods., t REY), (seds., t REY/km^2) [*]	20020	610000	3800000	3380000	167	167
Op. Cost (£/t REO)[#]	12700	6300	51.1	22.9	15.9	243
REY oxide blend value (£/t)	25800	8580	9850	19000	13600	13600
Profit margin GBP/tonne	13100	2260	9800	19000	13500	13300
cost/benefit (%)	49.2	73.7	0.52	0.12	0.12	1.79

Table 4. Comparison between estimated REY mine costs and benefits in terrestrial ores with underground and open pits methods of extraction and acid leaching of polymetallic nodules and deep sediments, as shown in this study. Value of the REY oxide blend for each deposit estimated with the individual abundances of the individual REY with respect to the ΣREY and their individual market price as in September 2017 (where available from http://mineralprices.com). [a] = Geological data for Strange Lake from Long et al., (2012), [b]= data for Bayan Obo deposit from Fan et al., (2016). [*]= total REY oxide resource estimates for terrestrial deposits from Voncken (2015), for nodules from Menendez et al., (in prep.) and for Atlantic sediments as shown in Menendez et al., (2017). [#] = Operating cost (i.e. fuel, labour, grinding, electricity, explosives and reagents) to produce 1 tonne of REY blend for alkaline and carbonatite-based terrestrial deposits as shown in Tyrer & Sykes (2013). This price does not include separation of individual REY.

3.5.3 Metal release from leached residues into seawater

My experiments show that only a small percentage of the total metal content of the sediments and nodules is released into seawater, following acid leaching (Table 3). This scenario is only slightly improved by washing the residue before its release. Residues that have been leached in buffered oxalic acid release the highest amounts of Mn, Fe, Co, Ni and Cu, whereas the HCl- and H_2SO_4-leached residues generally release greater amounts of Th and U and ∑REY. This directly correlates with the amount of metal released during the leaching process suggesting that part of the leachate remains in the sediment pore space; this residual leachate is partly removed by washing.

The sediment/seawater ratio employed in my experiments was 0.1. Assuming that all of the sediment extracted from a 1 km^2 area of the seafloor, and all of the nodules extracted from the UK Claim area, are returned to the same area of the ocean, at the ocean surface (i.e. disregarding the action of ocean currents), then the sediment/seawater ratio of material returned to the water column is ~1000 times lower than that employed in the experiments utilizing sediments, and ~10,000 times lower than used in the nodule experiments. Table 5 and Figure 7 show the estimated amounts of metals potentially released into the water column on return of the leached residue. Return of both washed and unwashed sediment and nodule residues clearly has the potential to increase the concentrations of most metals in ambient sea water. Concentrations of elements like Mn, Fe, Th and the REY may increase by up to 3-4 orders of magnitude, whereas concentrations of other elements such as Ni and Cu could increase by ~1-2 orders of magnitude. Only U is relatively unaffected. In general, release of metals and the REY from the nodules is lower than it is from the sediments.

It is important to note that these are likely to be upper limits for metal release because, in reality, ocean currents will rapidly disperse material returned to the water column well beyond the immediate area of release, and settling and coagulation of particles will lead to their removal into ocean sediments. Moreover, in my experiments the sediment/seawater solution was continually stirred at rates far higher than can be expected in the ocean.

		Mn	Fe	Co	Ni	Cu	ΣREY	Th	U
		nM	nM	pM	nM	nM	pM	pM	nM
Seawater*		0.2	0.6	15	10	4	470	0.1	14
NASS-6		9.39	8.65	255	5.01	3.81	430	733	12.6
Non-washed samples									
RC10-10	HCl	712	3950	4850	23.4	20.6	25500	600	43.6
	H2SO4	770	4600	3970	34.5	30.5	27500	451	50.8
	Oxalic	2740	**7020**	17200	24.1	25.5	2440	51.7	54.2
D10311-S1	HCl	872	2980	6830	29.0	21.1	22000	513	40.4
	H2SO4	657	2100	11000	27.4	17.6	19700	293	35.9
	Oxalic	2390	3460	15200	24.3	18.2	546	4.01	25.6
NOD-P-1	HCl	43	3.7	12.7	122	49.5	1710	0.29	4.78
	Oxalic	8.4	0.20	50.9	0.83	0.22	2.66	0.03	0.01
Washed samples									
RC10-10	HCl	212	1750	1100	6.86	2.86	17000	350	20.1
	H2SO4	221	1380	1320	9.29	7.56	13600	73.8	17.5
	Oxalic	3290	2110	21600	29.9	11.2	39400	122	27.9
D10311-S1	HCl	816	2700	1760	26.8	18.4	11900	245	17.6
	H2SO4	188	919	1760	7.96	5.93	11700	89.0	17.0
	Oxalic	1600	1410	9040	11.1	4.91	5830	12.8	20.8
NOD-P-1	HCl	36	0.68	50.9	130	44.3	1580	0.21	4.06
	Oxalic	25.5	0.68	25.5	1.67	0.22	5.51	0.04	0.01

Table 5: Theoretical maximum concentrations of metals in seawater resulting from the return of leached tailings compared to 'background' seawater in the deep North Pacific (Nozaki, 1997) and the seawater CRM NASS-6. Calculations for sediments assume removal of upper 1m of sediment (based on specifications for the Nautilus Minerals seafloor mining tool; Coffey Natural Systems, 2008), a dry bulk density of 0.65 g cm^{-3} (Thomson et al., 1984), and 5000 meters water depth. The total nodule resource in the UK Claim area is assumed to be 30 kg/m^2 (ISA, 2003) and the average water depth is ~4000 m. See text for more details.

Concentrations of Mn, Fe and Co similar to those predicted here exceed the available minimum threshold established for lethal toxicity in shallow marine/estuarine benthic ecosystems (Markich et al., 2002; Langdon et al., 2009). However, as both temperature and pressure have been shown to affect the potential toxicity of metals (Brown et al., 2015), it is not clearwhether these toxicity data can be applied to deep sea scenarios. Nevertheless, these data indicate that should these mining and extraction techniques be employed, they should be subject to careful monitoring.

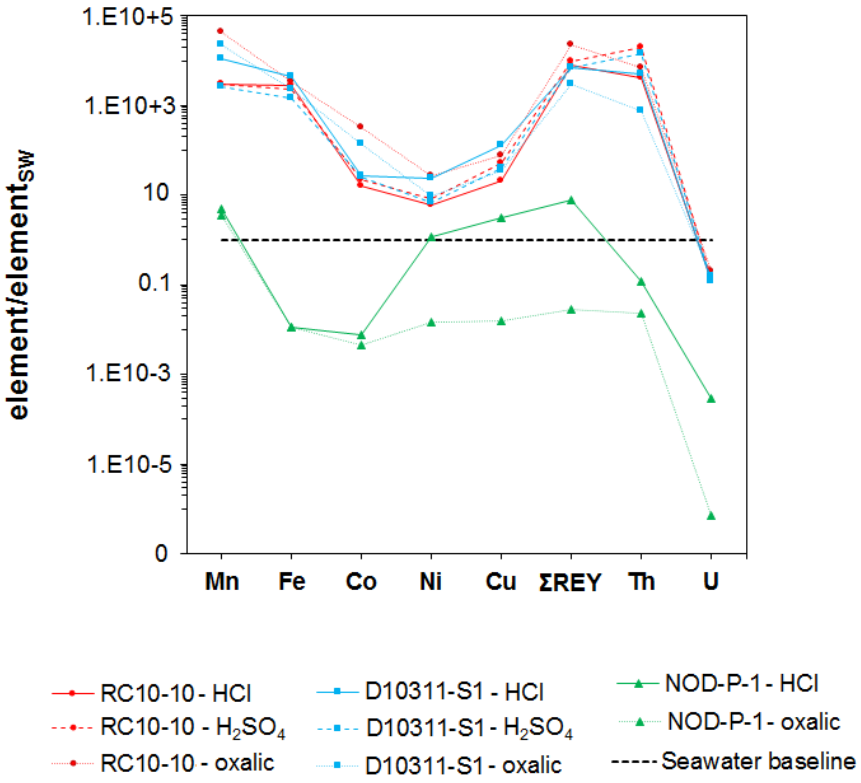

Figure 7. Metals released from nodule and sediment washed leaching residues normalised to the baseline seawater concentrations shown in Nozaki, (1997).

3.6 Conclusions

Dilute acid leaching of Atlantic sediments and nodules reveals significant differences in efficiency with respect to their Pacific counterparts. These differences are likely due to subtle differences in the relative proportions of different mineral phases between sediments and nodules from both areas. My data then indicates that unfortunately there is not a 'universal' solution to effectively release all the resource metals from all deep sea resources. Investigations as to the nature of the mineral phases hosting the metals and the REY are required in order to optimize the leaching procedure.

Due to their lower REY content and greater extraction difficulty, Atlantic sediments will likely constitute a less profitable source for REY and metals when compared with their Pacific counterparts. A similar scenario is found with Atlantic nodules, whose REY are less easily extractable than the nodules from the Pacific, despite of their higher REY content. On the other hand, as their exploitability is still simpler in comparison with terrestrial REY deposits, my estimations reveal that they might still represent a cost-effective resource.

Despite of the simplicity of the metal extraction techniques, return of leached residues to the seafloor may have important consequences in for the marine environment. My experiments show that metal release from leached residues is likely to increase the metal content of seawater by several orders of magnitude in prospective mining areas such as the CCFZ. Ecological studies will be required to quantify the impact of metal release on benthic ecosystems.

Chapter 4: Controls on the chemical composition of ferromanganese nodules in the Clarion-Clipperton Fracture Zone, eastern equatorial Pacific

Abstract

Ferromanganese nodules have long been considered an attractive source for Mn, Co, Ni and Cu and, potentially, for the rare earth elements and yttrium (REY). A number of exploration licenses have recently been granted for the Clarion Clipperton Fracture Zone (CCFZ) in the eastern equatorial Pacific and, because of concern about the environmental impacts of seafloor mining, some parts of the CCFZ have been designated 'Areas of Potential Environmental Interest' (APEI) from which mining will be precluded. As the APEIs were selected based on surface ocean characteristics and seafloor topography, estimated from satellite altimetry, the abundance and composition of nodules in these areas are unknown, and as a result their relevance as an intended baseline for mining disturbance has not been demonstrated.

To fill this gap, I have undertaken a detailed study of the chemical composition of nodules and seafloor sediments in the UK Claim area in the CCFZ and its closest APEI, APEI-6. There are distinct differences between the two sites: nodules from the UK Claim area are larger (10-15 cm in diameter) compared to those from APEI-6 (2-4 cm diameter), and they have faster growth rates (~11 vs ~3 mm/Ma). Because of their larger size, the average nodule resource in the UK Claim area (1.7-57 kg/m^2) is larger than it is in APEI-6 (0.7-2.6 kg/m^2). Nodules from APEI-6 have, on average, higher concentrations of Fe (7.2 vs. 2.7 wt. %), Co (0.28 vs. 0.13 wt. %) and total REY (1120 vs. 715 ppm) relative to those from the UK Claim area. Analyses of individual growth layers reveal that nodules from the UK Claim area contain a greater proportion of Mn-rich phases that are also enriched in Ni and Cu; these layers likely precipitated from sediment pore waters. Sediments from the UK Claim area, in turn, have higher Mn/Al ratios compared to sediments from APEI-6 and have a higher proportion of Mn in easily-reducible phases. Nodules from APEI-6 have a greater proportion of Fe-rich layers that are also enriched in Co and the REY, and likely precipitated from seawater. Nodules of

both types have been sampled in areas that have been licensed for mining in the CCFZ, so APEI-6 provides a relevant geochemical baseline for mining disturbance at least in some areas.

4.1. Introduction

Ferromanganese nodules are small concretions found on the floor of the deep ocean that grow only slowly (~1–6 mm/Ma; Hein, 2004). They usually form either by a) precipitation of metals from overlying oxygenated seawater (hydrogenous source) (Halbach et al. 1988; Koschinsky & Halbach, 1995), or b) precipitation of metals from sediment pore waters, under oxic or suboxic conditions (diagenetic source) (Halbach et al., 1981; Reyss et al., 1985; Wegorzewski and Kuhn 2014). Hydrogenous nodules tend to have a higher proportion of Fe-Mn (oxyhydr)oxide phases such as Fe-vernadite (Wegorzewski et al., 2015), higher concentrations of Fe, Co and the rare earth elements and yttrium (REY), and low Mn/Fe ratios, while diagenetic nodules tend to be more enriched in Mn-oxide phases such as 10 Å phyllomanganates and todorokite, and have higher concentrations of Mn, Ni and Cu and high Mn/Fe ratios (e.g. Halbach et al. 1981; Wegorzewski et al., 2015). However, nodules are complex structures, characterised by irregular, concentrically banded micro-layers around a nucleus. Detailed analyses of these micro-layers have revealed that individual nodules may consist of both hydrogenous and diagenetic layers, depending on the prevailing environmental conditions (Wegorzewski and Kuhn 2014).

Ferromanganese nodules contain economically significant amounts of manganese, iron, copper, cobalt, nickel, molybdenum, lithium, zirconium and the REY (Cronan, 1980; Halbach et al., 1988; Rühlemann et al.2011; Hein et al., 2013). For this reason, there is growing interest in mining them, and a number of exploration licenses for large nodule fields within the Clarion Clipperton Fracture Zone (CCFZ) in the eastern equatorial Pacific Ocean have been granted by the International Seabed Authority (ISA) (Figure 1). Because of concerns about the effects of mining on the functioning of marine ecosystems and biodiversity (Smith & Koslow, 2007), the ISA has identified nine bio-geographic sub-regions within the CCFZ in which no mining will occur. These areas are 400 km × 400 km in size, consisting of a protected core of 200 km x 200 km, surrounded by a buffer zone extending 100 km in each direction. These areas are known as “Areas of Potential Environmental Interest” (APEI), and are distributed across the CCFZ so as to capture the wide range of the different habitat types in the area (Wedding et

al., 2013). As yet, however, the abundance and chemical composition of nodules in these areas is unknown, so their suitability as a reference frame for the effects of future mining operations cannot be confirmed.

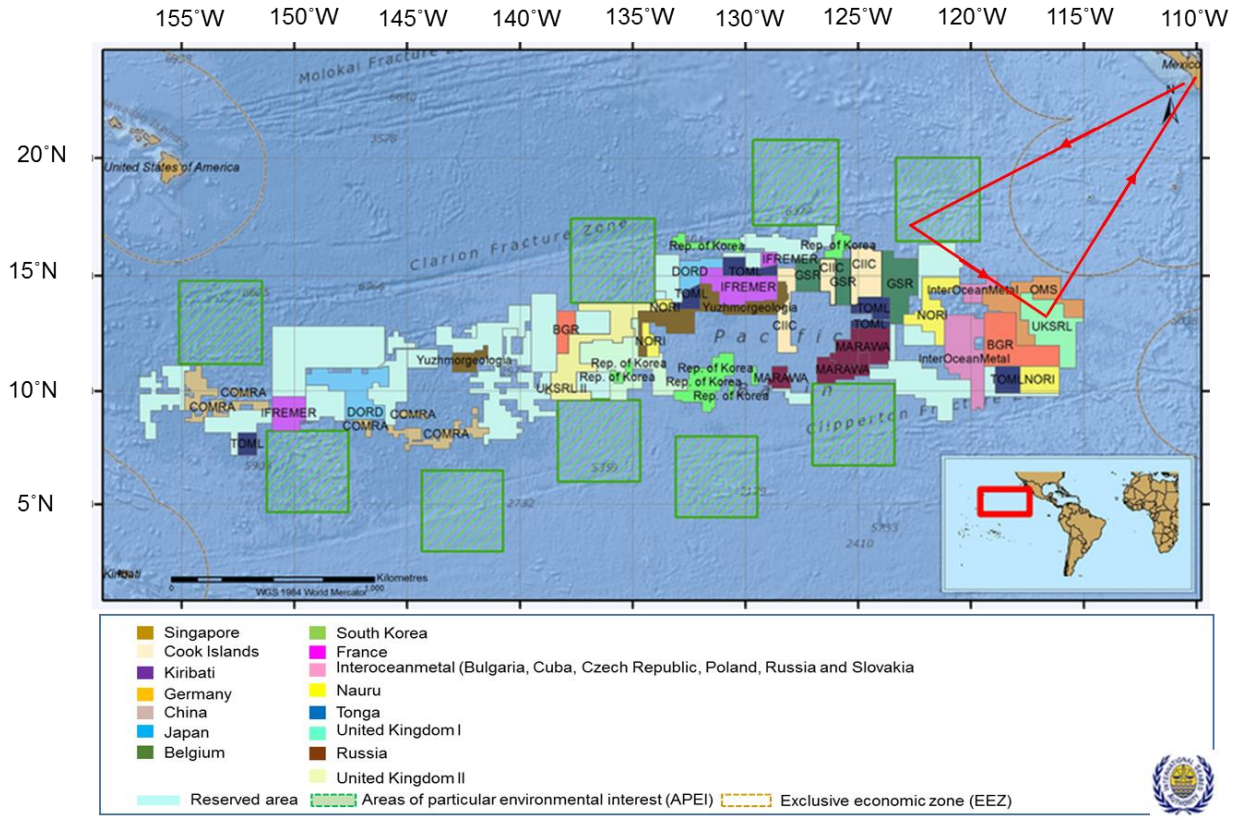

Figure 1. Location of licensed polymetallic nodules exploration areas and Areas of Particular Environmental Interest in the Clarion-Clipperton Fracture Zone (CCFZ). Red line shows the cruise track for JC120.

To fill this gap, I have conducted detailed geochemical analyses on nodules and seafloor sediments from one of the APEIs (APEI-6) and one nodule license area (the UK Claim area) in the CCFZ, collected during RRS James Cook cruise JC120 in 2015 (Figs. 1 and 2). I use the data to evaluate the processes that regulate the formation of the nodules and, in turn, their resource potential. This knowledge is essential for not only future mineral prospecting, but also for managing the environmental impact of mining activities.

4.2. Study area

The Clarion-Clipperton Fracture Zone (CCFZ) is an area located in the Central Eastern Pacific Ocean, north of the equatorial high productivity zone (Antoine et al., 1996). It extends from approximately 20˚N, 120˚W to 5˚N, 160˚W, being limited by the Clarion Fracture Zone to the north and the Clipperton Fracture Zone to the South, with a total length of ~7240 kilometres (Fig. 1). These

fractures are SW-NE trending, as they respond to the north westward migration of the Pacific Plate (Von Stackelberg & Beiersdorf, 1991). This area hosts one of the largest nodule fields in the global ocean (e.g. Halbach et al., 1988).

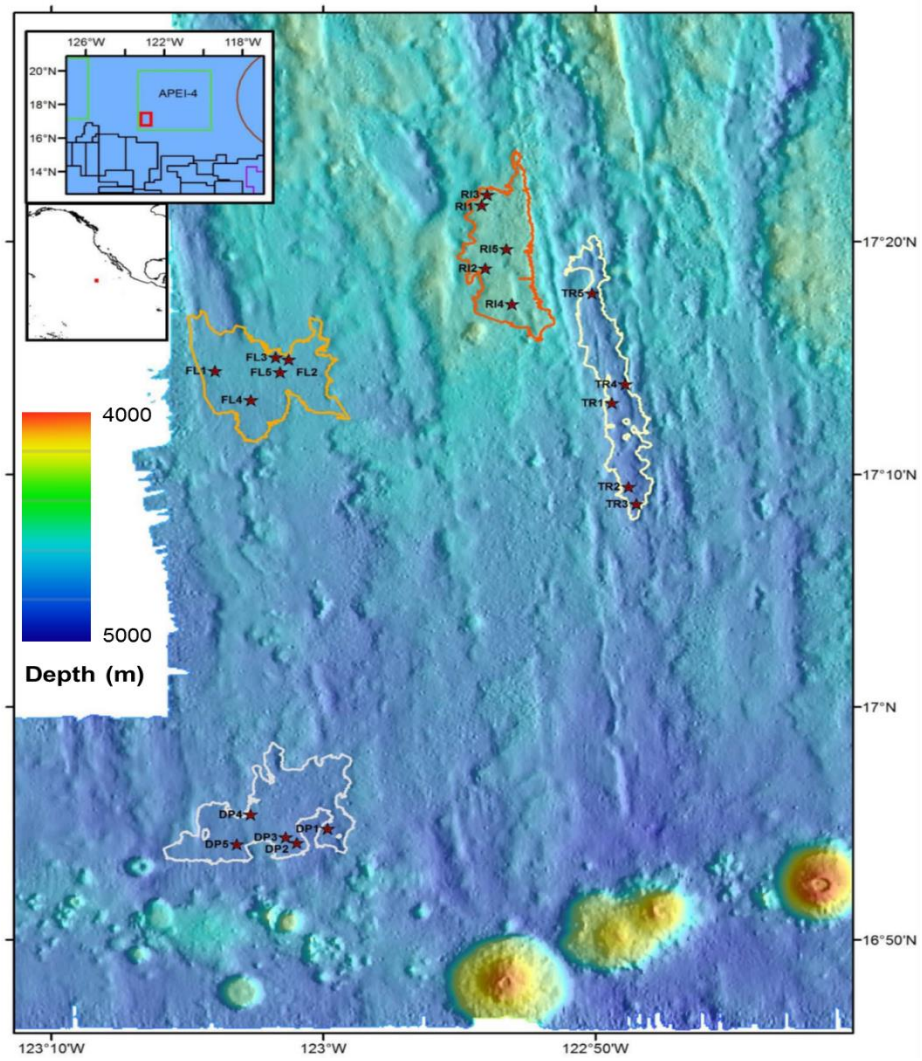

Figure 2. Locations of sampling sites within APEI-6. Coring locations depicted with a red star. DP =Deep Plain; FL = Flat; RI = Ridge; TR = Trough.

Samples for this study were collected during RRS James Cook cruise JC120 to the eastern part of the CCFZ, in the UK Claim zone and APEI-6 (Figures 1 and 2; Table 1). The UK Claim Zone is an area of ~60000 km^2 licensed to UK Seabed Resources Ltd. (UKSRL). APEI-6 comprises an area of ~160000 km^2 located in the northwest part of the CCFZ. It shows an irregular topography, alternating flat areas with ridges and valleys trending NNW-SSE (Figure 2).

Sample	Location#	Lat. (˚N)	Long. (˚E)	Water depth (m)
		Nodules		
JC120-105	UK Claim	13.3	-116.4	4113
JC120-104	UK Claim	13.3	-116.3	4130
JC120-037	APEI-6 (Flat)	17.1	-123.4	4156
JC120-013	APEI-6 (Deep Plain)	16.5	-122.6	4292
J120-061	APEI-6 (Trough)	17.9	-122.5	4280
JC120-048	APEI-6 (Ridge)	17.2	-122.5	4024
		Sediments		
JC120-105	UK Claim	13.3	-116.4	4113
JC120-025	APEI-6 (Flat)	17.1	-123.4	4158
JC120-010	APEI-6 (Deep Plain)	16.5	-122.6	4292
JC120-063	APEI-6 (Trough)	17.1	-122.5	4245
JC120-048	APEI-6 (Ridge)	17.2	-122.5	4024

Table 1. Location and water depth of sample stations

4.3. Methods

Nodules and their associated sediments from both APEI-6 and the UK Claim area were subject to detailed geochemical analyses. These are outlined briefly below; a more detailed description is provided in the Appendix.

Sediments were collected by Mega Corer (MC), which retrieves the uppermost ~40 cm of the sediments, and Gravity Corer (GC), which collects up to ~3 m of the upper sediments. The sediment cores were then sectioned into 1 or 2 cm depth intervals, and sub-samples for geochemical analyses were frozen at -20 ˚C.

Pore waters were extracted from the sediments using Rhizons inserted though pre-drilled holes in the core liner; the Rhizons were connected to a syringe to which a small underpressure was applied. The extent of the oxygen penetration zone in the sediments, or oxygen penetration depth (OPD) was assessed in megacores by using needle-type fiber-optical oxygen microsensors (OXR50-OI, PyroScience©). The measurements were performed at 100 μm depth resolution for up to 5 centimetres below seafloor (cmbsf). Oxygen concentration between 5 and 30 cmbsf were measured at 2 cm intervals by inserting a Robust Oxygen Miniprobe (PyroScience©) through predrilled holes in the core liner into the sediment.

Nodules were obtained by trawling and box coring, and in some cases, they were recovered from the top of the mega cores (MC's) and gravity cores (GC's).

4.3.1. Analysis of bulk nodules and sediments

Nodules and sediments were freeze-dried and ground in an agate mortar. For bulk chemical analysis, ~50 mg of nodules and ~100 mg of sediments were dissolved in a mixture of hydrofluoric (HF), perchloric ($HClO_4$) and hydrochloric (HCl) acids, and aqua regia. The resulting residue was re-dissolved in 10 mL of 6M HCl. 1 mL of this solution was dried down and spiked with an internal standard consisting of 5 ppm Re and In and 20 ppm Be and further made up to 13 mL with 3% HNO_3 for trace element and REY analyses. 0.25 mL of this solution was further diluted (by a factor of 20) for analysis of major elements.

Major element (Li, Na, Mg, Al, K, Ca, Ti, Mn and Fe), trace element (V, Cr, Co, Ni, Cu, Zn, Rb, Sr and Ba), and REY (La, Ce, Pr, Nd, Sm, Eu, Gd, Tb, Dy, Y, Ho, Er, Tm and Lu) concentrations were determined by inductively coupled plasma mass spectrometry (ICP-MS; Thermo Scientific X-Series II) at the University of Southampton. Accuracy and reproducibility were assessed by multiple (n=6) analyses of the NOD-A-1 and NOD-P-1 certified reference materials for the nodules and multiple (n=3) analyses of MESS-1 for the sediments. Instrument drift was assessed by addition of internal standards (Re, In and Be), and analysis of an internal standard every 10 samples. The external reproducibility of the analyses was better than ±4% for the major elements, and better than ±3% for most of the trace elements and the REE; the reproducibility of Ca and Cr analyses was ±9% and ±6%, respectively. Measured concentrations were within ±5% of the certified or recommended values for all elements except Ca (±22%), Ce (±24%), Cr (±26%) and Zn (±26%).

	JC120-104 top (UK Claim)	JC120-104 bottom (UK Claim)	JC120-105 (UK Claim)	JC120-037 (APEI-6 – Flat)	JC120-013 (APEI-6 – Deep Plain)	J120-061 (APEI-6 – Trough)	JC120-048 (APEI-6 – Ridge)
Mn (wt %)	26.0	30.3	28.6	27.0	24.6	26.7	30.3
Fe	6.13	5.98	5.07	6.25	8.59	6.68	7.15
Ca	1.94	1.50	2.06	1.44	2.25	1.64	1.95
Na	2.14	2.24	2.55	2.01	1.89	2.01	1.80
Mg	1.46	1.76	1.70	1.87	1.60	1.77	2.15
Al	1.92	2.15	2.25	2.38	1.97	2.34	2.63
K	0.93	1.11	1.02	1.10	0.94	1.10	1.17
Ni	0.98	1.14	1.35	1.26	1.07	1.16	1.49
Cu	0.75	0.84	1.20	0.96	0.63	1.02	1.08
Co	0.12	0.13	0.14	0.27	0.29	0.25	0.30
P	0.13	0.11	0.14	0.11	0.13	0.12	0.13
Cr (ppm)	16.2	16.8	17.8	19.2	17.1	20.1	21.3
Li	177	170	124	126	66.1	90.0	109
Ti	3030	3160	2340	2910	5060	2920	3250
V	439	529	435	445	503	518	490
Zn	1120	892	1380	1070	783	1820	1130
Rb	18.1	21.4	21.0	26.6	19.4	25.1	28.0
Sr	593	562	559	609	764	598	688
Ba	2530	2670	3080	2540	1940	2740	2580
Hf	3.66	3.63	1.85	2.99	4.96	3.39	3.30
Pb	399	379	247	675	832	656	773
Th	14.1	16.5	9.4.	13.8	21.1	15.0	15.1
U	4.14	4.53	3.64	4.10	5.68	4.20	4.50
La	96.0	102	71.0	110	161	118	129
Ce	352	359	177	453	786	476	511
Pr	28.2	29.9	20.8	31.5	45.2	34.9	36.7
Nd	117	125	87.0	130	184	143	152
Sm	28.3	30.7	21.2	30.6	43.2	34.4	36.1
Eu	7.00	7.61	5.49	7.50	10.3	8.38	8.77
Gd	28.0	30.6	20.9	31.0	44.6	34.3	36.5
Tb	4.18	4.67	3.23	4.47	6.33	5.02	5.30
Dy	22.9	26.0	18.0	24.7	34.5	27.3	29.2
Y	1.69	1.99	1.44	1.73	2.47	1.95	2.11
Ho	72.4	89.9	67.6	82.8	109	85.4	100
Er	4.27	4.91	3.47	4.59	6.43	5.06	5.47
Tm	11.5	13.4	9.50	12.3	17.2	13.5	14.6
Yb	1.70	1.99	1.43	1.80	2.56	2.00	2.15
Lu	11.2	13.2	9.50	11.7	16.6	13.2	14.1
ΣREY	786	841	519	938	1470	1000	1080
GR	12.3	11.9	9.67	3.06	2.66	3.58	3.08

Table 2. Concentrations of major, trace and rare earth elements and yttrium (REY) in APEI-6 and UK Claim nodules. † = Growth Rate = $0.68/(Co_n)^{1.67}$, where Co_n= Co*(50/Fe+Mn), with Co, Fe and Mn in wt. % (Manheim & Lane-Bostwick, 1988).

4.3.2. Leaching of mobilizable Mn from sediments

1g of the freeze-dried sediment was first leached with magnesium chloride, to remove the exchangeable fraction of the sediments, followed by buffered sodium acetate, to remove the fraction bound to carbonates, an d finally 25% hydroxylamine hydrochloride to recover mobilisable Mn, according to procedures given in Tessier et al., (1979). Leaching was done at room temperature, and in duplicate for one of the samples. The residue was washed with Milli-Q water in

between the leaching steps. The chemical composition of the leachates was determined by ICP-MS (Section 3.3.1).

4.3.3. XRF analysis of bulk sediments

Approximately 10 g of freeze-dried sediment was made into a pressed pellet for XRF analysis. Major element oxides (SiO_2, TiO_2, Al_2O_3, Fe_2O_3, MnO, MgO, CaO, K_2O, Na_2O, P_2O_5) and trace element (Co, Cr, V, Ni, Sc, Cu, Zn, Pb, Ba, Rb, Sr, Zr, Nb, Y, La, Ce, Ga, As, Mo, I, S and Cl) concentrations were determined using a Philips® MAGIX-PRO automatic sequential wavelength dispersive X-ray fluorescence spectrometer at the University of Southampton. For clarity, I only discuss Si and P data, as the rest of elements were also acquired by ICP-MS. The agreement between the two methods was better than ± 6% for all elements. Analyses were calibrated using high quality International Geochemical Reference samples (GRS).

	Mn/Fe	Ni + Cu (wt. %)	Co (wt. %)	ΣREE (ppm)	ΣHREE (ppm)	Ce*	LREE/ HREE
JC120-104 (T) (UK Claim)	4.24	1.73	0.12	784	92.0	1.62	0.88
JC120-104 (B) (UK Claim)	5.06	1.98	0.13	839	104	1.55	0.80
JC120-105 (UK Claim)	5.64	2.55	0.14	518	73.0	1.09	0.77
JC120-037 (APEI-6 – Flat)	4.32	2.22	0.27	936	100	1.85	0.94
JC120-013 (APEI-6 – Deep Plain)	2.86	1.7	0.29	1470	141	2.24	0.95
J120-061 (APEI-6 – Trough)	4.00	2.18	0.25	998	111	1.79	0.93
JC120-048 (APEI-6 – Ridge)	4.23	2.57	0.30	1080	118	1.79	0.91
German License area E1a	5.31	2.53	0.15	-	-	-	-
Clarion-Clipperton Zoneb	4.88	2.24	0.22	645	99.3	1.14	0.87
Atlantic Oceanc	0.75	0.46	0.29	2150	148	3.93	0.96
Indian Oceand	3.50	2.14	0.14	981	108	1.86	0.96

Table 3. Bulk chemical composition of APEI-6 and UK Claim nodules compared with published data from the CCFZ and the Atlantic and Indian Oceans. Ce*= $(2*Ce_{SN})/(La_{SN}+Nd_{SN})$. LREE/HREE= $(La_{SN}+2*Pr_{SN}+Nd_{SN})/(Er_{SN}+Tm_{SN}+Yb_{SN}+Lu_{SN})$. SN=shale-normalised. [a]=Wegorzewski & Kuhn (2014), [b]=Dubinin & Sval'nov (2002), [c]=Dubinin & Rozanov (2001), [d]=Pattan & Parthiban (2011).

4.3.4. Scanning electron microscopy (SEM) of nodules

The internal structure of the nodules was investigated using a LEO1450 Variable Pressure Scanning Electron Microscope. Nodules were sectioned, and their microstructure was assessed using a secondary electron detector for topographic imaging and a backscattered electron detector for compositional analysis. Major element concentrations were determined using energy-dispersive X-ray

spectroscopy (EDS; Oxford Instruments X-Act with Silicon Drift detector) combined with Aztec Energy software. Analyses were conducted at 20 kV, using a probe current of 700 pA and a working distance of 15 mm. The probe current was calibrated on a Faraday cup, and element concentrations were calibrated against various mineral standards from Micro-Analysis Consultants Ltd, Cambridge, UK, and the Natural History Museum, UK. A basalt glass standard reference material (BRR-1) was used to assess the accuracy of the analyses. Elemental maps were made using a nominal probe current of 2.5-3.0 nA.

4.3.5. Laser ablation ICP-MS analyses of nodules

The chemical composition of individual microlayers within the nodules was determined by laser ablation ICP-MS. Analyses were carried out on 100 μm-thick polished sections using a 193 nm excimer laser (New Wave Research model UP193X) coupled to a quadrupole ICP-MS (Thermo X-Series II) at the University of Southampton. Concentrations of major elements (Al, Si, K, Ca and Mn), trace elements (V, Cr, Co, Ni, Cu, Sr, Ba, Nb, Hf, Pb, Th and U) and REY (La, Ce, Pr, Nd, Sm, Eu, Gd, Tb, Dy, Ho, Er, Tm, Yb, Lu) were determined on 50 – 75 μm diameter spots. Raw counts were processed off line using standard spreadsheet software, and counts were calibrated using the nodule certified standard reference materials NOD-A-1 and NOD-P-1. The accuracy and reproducibility of the measurements was assessed by multiple (n=120) analyses of NIST 610 and NIST 612 certified reference materials. The external reproducibility of the analyses was better than ±9 % for the major elements, and better than ±7 % for most of the trace elements and REY, except for K, Ti and Ba (±11 %); Cr, Ni and Sr (±10 %), and Co (±12 %). Measured concentrations were within the certified or recommended values for all elements except Al (±37%), Ca (±28%), Ti (±22%), Zr (±17%), Sr (±29%) and Cu (±26%).

	Si wt. %	Mn wt.%	Fe wt.%	Ca wt.%	Na wt.%	Mg wt.%	Al wt.%	K wt.%	P wt.%	Ba wt.%	Cr ppm	Co ppm	Ni ppm	Cu ppm	Ti ppm	V ppm	Zn ppm	Rb ppm	Sr ppm	Hf ppm	Pb ppm	Th ppm	U ppm
NASC†	30.3	0.05	3.99	2.54	0.85	1.72	8.94	3.31	0.09	0.63	124	25.7	58	-	0.63	-	-	125	142	6.30	-	12.3	2.66
JC120-105 - UK Claim																							
(0-1) cm	25.0	0.77	4.48	1.06	6.98	2.13	6.42	2.26	0.08	0.82	65.8	71.5	223	372	3170	119	130	85.2	338	42.2	75.9	12.2	49.8
(1-2) cm	26.7	0.77	3.48	0.75	4.83	1.57	4.97	1.79	0.08	0.63	39.1	59.9	232	350	2510	93.0	104	67.0	258	32.3	59.0	9.30	38.1
(4-5) cm	28.5	0.95	5.06	1.04	5.70	2.09	7.17	2.47	0.07	0.93	66.2	79.9	248	424	3590	132	124	95.6	366	47.6	85.8	13.8	56.0
(7-8) cm	29.6	0.79	5.35	1.05	4.94	2.09	7.61	2.58	0.08	0.97	70.4	81.4	224	394	3890	133	136	102	377	50.5	90.2	14.6	59.7
(9-10) cm	30.1	0.72	5.02	1.04	4.61	1.95	7.17	2.43	0.08	0.91	64.6	75.1	205	360	3640	130	118	95.7	352	46.6	84.0	13.5	54.4
(12-14) cm	29.7	0.56	4.99	0.84	3.87	1.87	7.04	2.39	0.08	0.87	66.1	63.8	168	354	3400	125	124	96.0	340	47.9	85.3	13.6	55.6
JC120-013 - APEI-6 - Deep Plain																							
(0-1) cm	24.7	0.51	4.71	1.04	4.28	2.16	7.76	2.70	0.10	0.69	76.1	101	167	275	4170	126	119	122	297	61.0	111	18.0	73.6
(1-2) cm	32.3	0.48	4.74	1.11	3.28	2.05	7.74	2.64	0.13	0.69	80.9	98.8	155	266	4180	122	114	122	292	61.2	111	18.1	74.0
(4-5) cm	30.0	0.48	4.88	1.06	2.96	2.05	8.04	2.72	0.11	0.72	80.0	102	154	269	4290	128	134	129	299	63.1	115	18.5	75.6
(7-8) cm	33.0	0.44	4.54	0.89	2.76	1.91	7.48	2.57	0.13	0.66	60.0	94.1	138	248	3880	122	102	118	275	57.6	105	16.9	69.2
(9-10) cm	30.2	0.46	4.88	1.06	2.95	2.07	8.10	2.78	0.09	0.71	81.3	94.0	143	259	4440	132	119	126	298	62.1	114	18.1	73.7
(12-14) cm	33.0	0.44	4.98	1.00	3.27	2.14	8.29	2.86	0.12	0.70	80.9	95.2	137	254	4420	134	108	130	297	62.2	114	18.1	73.7
JC120-037 - APEI-6 – Flat																							
(0-1) cm	32.0	0.47	4.35	0.99	3.29	1.90	7.11	2.45	0.15	0.66	58.9	94.7	149	247	3740	114	115	109	281	59.0	103	17.4	71.4
(1-2) cm	29.3	0.54	5.04	1.19	3.38	2.16	8.20	2.77	0.13	0.75	77.8	109	173	283	4400	133	106	127	320	68.1	120	20.1	83.0
(4-5) cm	32.8	0.52	4.94	1.14	3.18	2.05	8.08	2.94	0.15	0.76	75.7	107	168	281	4410	130	119	126	322	69.2	120	20.5	84.3
(7-8) cm	32.9	0.51	4.86	1.18	2.84	2.01	7.91	2.69	0.15	0.74	76.5	104	162	266	4180	132	111	125	311	66.0	117	19.5	79.6
(9-10) cm	33.2	0.53	5.23	1.03	2.87	2.15	8.54	2.88	0.14	0.79	81.3	108	168	279	4710	138	115	133	332	70.8	124	20.8	85.8
(12-14) cm	30.1	0.56	5.21	1.09	2.88	2.16	8.55	2.86	0.13	0.78	81.7	111	177	286	4670	139	118	132	327	70.3	124	20.8	85.0
JC120-061 - APEI-6 – Trough																							
(0-1) cm	28.2	0.48	5.03	1.24	4.58	2.31	8.24	2.85	0.10	0.75	80.8	101	151	269	4540	132	116	124	325	62.7	114	18.5	75.4
(1-2) cm	27.3	0.48	4.98	0.91	3.40	2.12	8.13	2.77	0.10	0.73	87.3	98.4	149	271	4290	127	114	123	312	61.6	112	18.0	73.8
(4-5) cm	32.8	0.42	4.56	0.94	2.77	1.90	7.45	2.56	0.13	0.68	52.0	89.2	127	240	3870	117	103	113	288	56.1	103	16.4	67.5
(7-8) cm	n.m.*	0.44	5.08	1.02	3.14	2.13	8.33	2.83	n.m.*	0.77	82.3	96.4	131	251	4400	133	114	127	323	62.2	114	18.1	74.0
(9-10) cm	30.3	0.46	5.18	1.10	3.34	2.19	8.53	2.91	0.09	0.78	82.1	98.3	136	261	4510	136	113	129	331	63.7	117	18.5	76.3
(12-14) cm	30.1	0.44	5.27	1.16	3.47	2.24	8.67	2.99	0.09	0.79	83.9	107	124	258	4620	139	114	132	333	65.6	119	19.3	78.9
JC120-048 - APEI-6 – Ridge																							
(0-1) cm	27.7	0.54	4.79	1.36	4.80	2.22	7.77	2.71	0.13	0.78	79.3	105	180	268	4220	126	116	118	346	77.0	116	23.1	96.2
(1-2) cm	n.m.*	0.58	5.14	1.42	4.03	2.25	8.32	2.82	n.m.*	0.82	83.1	113	192	291	4490	138	121	127	357	80.6	125	24.1	99.9
(4-5) cm	32.1	0.58	5.25	1.36	3.33	2.20	8.51	2.84	0.18	0.82	82.3	113	189	294	4620	138	107	127	352	81.0	126	24.2	101
(7-8) cm	32.6	0.61	5.52	1.33	3.07	2.28	8.95	2.99	0.18	0.87	61.6	119	203	307	4820	146	124	138	371	87.7	135	26.1	108
(9-10) cm	32.7	0.55	4.91	1.26	2.74	2.02	8.00	2.70	0.19	0.77	78.1	103	175	267	4410	132	115	120	329	75.6	117	22.6	93.8
(12-14) cm	33.1	0.58	5.29	1.02	2.79	2.15	8.60	2.88	0.20	0.86	54.9	115	185	281	4640	140	118	130	360	82.1	127	24.5	102

Table 4. Chemical composition of sediments from APEI-6 and the UK Claim area. Si and P were determined by XRF; all other data were obtained by ICP-MS. *n.m.= not measured. †=NASC data from Gromet et al., (1984).

	La ppm	Ce ppm	Pr ppm	Nd ppm	Sm ppm	Eu ppm	Gd ppm	Tb ppm	Dy ppm	Y ppm	Ho ppm	Er ppm	Tm ppm	Yb ppm	Lu ppm	ΣREY ppm	HREE ppm	Ce*	HREE/LRE
NASC†																			
JC120-105 (UK Claim)																			
(0-1) cm	42.2	75.9	12.2	49.8	11.9	4.01	11.9	1.84	10.9	63.7	2.15	5.94	0.86	5.66	0.86	300	44.0	0.81	0.74
(1-2) cm	32.3	59.0	9.30	38.1	9.04	3.05	9.0	1.40	8.2	47.7	1.64	4.48	0.66	4.29	0.66	229	33.3	0.82	0.75
(4-5) cm	47.6	85.8	13.8	56.0	13.2	4.50	13.2	2.04	11.9	71.2	2.37	6.56	0.95	6.23	0.95	336	48.7	0.81	0.76
(7-8) cm	50.5	90.2	14.6	59.7	14.0	4.75	14.1	2.19	13.0	77.0	2.55	7.06	1.03	6.75	1.02	359	52.5	0.80	0.75
(9-10) cm	46.6	84.0	13.5	54.4	12.9	4.37	13.0	2.01	11.8	70.0	2.32	6.42	0.94	6.15	0.94	329	47.9	0.82	0.75
(12-14) cm	47.9	85.3	13.6	55.6	12.9	4.35	13.1	2.03	11.9	71.6	2.34	6.57	0.95	6.21	0.94	335	48.4	0.81	0.76
JC120-010 (APEI-6 - Deep Plain)																			
(0-1) cm	61.0	111	18.0	73.6	17.4	5.05	17.3	2.69	15.6	90.9	3.08	8.51	1.21	7.91	1.21	434	62.6	0.81	0.78
(1-2) cm	61.2	111	18.1	74.0	17.5	5.06	17.2	2.67	15.6	90.9	3.07	8.47	1.23	7.91	1.20	436	62.5	0.81	0.78
(4-5) cm	63.1	115	18.5	75.6	17.9	5.19	17.6	2.73	15.9	93.7	3.15	8.57	1.24	8.04	1.22	448	63.7	0.82	0.79
(7-8) cm	57.6	105	16.9	69.2	16.3	4.73	16.1	2.50	14.5	84.4	2.84	7.87	1.14	7.34	1.10	408	58.1	0.81	0.79
(9-10) cm	62.1	114	18.1	73.7	17.4	5.07	17.2	2.64	15.4	90.3	3.03	8.31	1.20	7.77	1.17	438	61.8	0.83	0.80
(12-14) cm	62.2	114	18.1	73.7	17.4	5.03	17.3	2.66	15.5	90.9	3.06	8.42	1.21	7.83	1.19	439	62.2	0.83	0.79
JC120-025 (APEI-6 – Flat)																			
(0-1) cm	59.0	103	17.4	71.4	17.0	4.90	16.9	2.62	15.4	90.4	3.01	8.33	1.20	7.74	1.17	420	61.3	0.78	0.77
(1-2) cm	68.1	120	20.1	83.0	19.7	5.68	19.5	3.04	17.8	106	3.49	9.64	1.40	9.01	1.36	487	71.0	0.78	0.76
(4-5) cm	69.2	120	20.5	84.3	20.0	5.76	19.8	3.09	18.0	108	3.54	9.74	1.40	9.05	1.37	494	71.7	0.77	0.77
(7-8) cm	66.0	117	19.5	79.6	18.9	5.46	18.7	2.91	17.0	101	3.37	9.22	1.32	8.57	1.29	470	67.8	0.79	0.78
(9-10) cm	70.8	124	20.8	85.8	20.3	5.88	20.2	3.14	18.3	109	3.60	9.91	1.42	9.27	1.39	504	73.2	0.78	0.77
(12-14) cm	70.3	124	20.8	85.0	20.0	5.82	20.0	3.10	18.1	108	3.56	9.72	1.41	9.10	1.38	500	72.2	0.78	0.78
JC120-063 (APEI-6 – Trough)																			
(0-1) cm	62.7	114	18.5	75.4	17.9	5.24	17.7	2.75	16.0	95.8	3.16	8.70	1.25	8.13	1.22	448	64.2	0.81	0.78
(1-2) cm	61.6	112	18.0	73.8	17.4	5.12	17.4	2.67	15.6	93.0	3.04	8.41	1.21	7.85	1.19	439	62.4	0.82	0.79
(4-5) cm	56.1	103	16.4	67.5	15.8	4.71	15.7	2.44	14.3	84.9	2.80	7.74	1.12	7.15	1.09	401	57.1	0.82	0.78
(7-8) cm	62.2	114	18.1	74.0	17.4	5.17	17.3	2.67	15.5	92.7	3.04	8.38	1.20	7.79	1.17	441	62.2	0.83	0.80
(9-10) cm	63.7	117	18.5	76.3	18.0	5.30	17.8	2.74	16.0	96.3	3.16	8.67	1.24	8.11	1.22	454	64.2	0.82	0.79
(12-14) cm	65.6	119	19.3	78.9	18.6	5.46	18.5	2.84	16.5	99.1	3.23	8.92	1.29	8.32	1.25	467	66.2	0.81	0.79
JC120-048 (APEI-6 – Ridge)																			
(0-1) cm	77.0	116	23.1	96.2	23.1	6.58	23.0	3.64	21.2	129	4.19	11.5	1.65	10.7	1.62	548	84.2	0.66	0.74
(1-2) cm	80.6	125	24.1	99.9	24.0	6.80	24.0	3.75	22.0	134	4.35	11.9	1.72	11.0	1.67	575	87.2	0.68	0.74
(4-5) cm	81.0	126	24.2	101	24.1	6.87	24.1	3.76	22.0	134	4.34	11.9	1.71	11.0	1.68	577	87.4	0.68	0.75
(7-8) cm	87.7	135	26.1	108	25.8	7.32	25.9	4.04	23.7	146	4.65	12.8	1.85	11.9	1.80	623	94.1	0.67	0.75
(9-10) cm	75.6	117	22.6	93.8	22.4	6.40	22.3	3.51	20.6	124	4.06	11.1	1.58	10.2	1.55	537	81.3	0.68	0.75
(12-14) cm	82.1	127	24.5	102	24.3	6.98	24.5	3.80	22.3	137	4.43	12.1	1.75	11.2	1.70	586	88.9	0.67	0.74

Table 5. Concentrations of rare earth elements and yttrium (REY) in sediments from APEI-6 and the UK Claim area. Ce*= $(2*Ce_{SN})/(La_{SN}+Nd_{SN})$. LREE/HREE= $(La_{SN}+2*Pr_{SN}+Nd_{SN})/(Er_{SN}+Tm_{SN}+Yb_{SN}+Lu_{SN})$. SN=shale-normalised. †=NASC data from Gromet et al., (1984).

4.4. Results

Nodules from APEI-6 are relatively small, ~2-4 cm in diameter, and are sub-spherical to discoidal in shape and have a smooth surface. Back scatter images of nodule cross sections (Figs. 4-8) show that internally they consist of a series of approximately concentric layers surrounding one or more accreted older nodules. By contrast, nodules from the UK Claim area are larger, ~10-15 cm in diameter, with multiple lobes giving them a more knobbly shape. The upper surface of the nodule, which is exposed to seawater, is generally smooth, whereas the lower part of the nodule, which is buried in the sediment, is slightly rough and friable, showing signs of geochemical instability. Nodules from the UK Claim area tend to have multiple nucleation centres, and their internal structure is dendritic in appearance in the central part of the nodule, grading into approximately concentric microlayers towards the outer part of the nodule (Fig. 7).

Nodules from both areas sit on top of sediments that consist of brown clay. The oxygen penetration depth in cores from APEI-6 is > 3m whereas it is shallower in cores from the UK Claim area (~1.5m). Concentrations of dissolved Fe, dissolved Mn and ammonium were below detection limit in the uppermost sediments (<100 cmbsf).

4.4.1. Bulk chemistry of sediments and nodules

The chemical composition of the bulk nodules and sediments is given in Tables 2, 3, 4 and 5. Overall, there is little difference in the chemical composition of the nodules from APEI-6 and the UK Claim area. Mn, Ni and Cu are, respectively, ~27, ~1.25 and ~0.92 wt. % in nodules from APEI-6 and nodules from the UK Claim area have ~28.3 wt. % Mn, ~1.16 wt. % Ni and ~0.93 wt. % Cu. There are also no significant differences in concentrations of Ca and P (respectively, ~1.82 wt. % and ~1240 ppm in APEI-6 and ~1.8 wt. % and ~1290 ppm in the UK Claim area). However, concentrations of Fe and Co are higher in nodules from APEI-6 (~7.20 wt. % and ~0.28 wt. %, respectively) compared to the UK Claim area (~5.80 wt. % and ~0.13 wt. %). The Mn content of the lowermost part of the nodule from the UK Claim area is slightly higher (30.3 wt. %) than the Mn content of the upper nodule surface (23.0 wt. %).

Nodules from APEI-6 have higher REY than nodules from the UK Claim area; average ΣREY = 1120 ppm for APEI-6 and average ΣREY = 715 ppm for the UK

Claim area. The total heavy REE (HREE) content of APEI-6 nodules is ~117 ppm, whereas it is ~90 ppm in UK Claim nodules. Nodules from both areas are slightly depleted in the light REE (LREE) compared to the HREE, but this is slightly more marked in the UK Claim nodules (~0.82) compared to APEI-6 nodules (~0.93). APEI-6 nodules also have a higher Ce anomaly (~1.92 compared to ~1.42 in the UK Claim area).

In order to observe trends of chemical variations with depth in the sediments, I have plotted my data as element/Al ratios (Figure 14). Assuming that aluminum is mostly present in clays and detrital aluminosilicates (as suggested by elemental factor analysis; Table 8), and given that Al is immobile, then element/Al ratios can be used to counteract for dilution by other sediment phases (e.g. Turekian & Wedepohl, 1961). There is little change in metal/Al ratios with depth at either site, with the exception of increased Co/Al, Mn/Al, Ni/Al and Cu/Al at 4-5 cmbsf in sediments from the UK Claim area. Sediments from the uppermost 14 cmbsf in the UK Claim area generally have higher concentrations of Fe, Mn, Ni and Cu, and lower concentrations of Co and REY than sediments from the same depth interval from APEI-6 (Fig. 11). Concentrations of P are lower in the UK Claim sediments (~0.08 wt. %) than in the APEI-6 sediments (~0.13 wt. %), and concentrations of Al and Ca are also lower (respectively, ~7 and ~0.96 wt. % in the UK Claim area and ~8 and ~1.12 wt. % in APEI-6).

Like their associated nodules, sediments from APEI-6 also have higher REY concentrations, ~482 ppm compared to ~315 ppm in the UK Claim area. Sediments fron APEI-6 also have higher HREE concentrations, ~70 ppm compared to ~46 ppm in the UK Claim area. Sediments from both areas are depleted in the LREE compared to the HREE, and they have negative Ce anomalies (~0.78).

4.4.2. Composition of individual nodule layers

4.4.2.1. SEM analyses

Representative backscatter images, and Fe-Mn distribution and mineral phase maps for nodule cross-sections are shown in Figs. 3-7, and concentrations of major, trace and rare earth elements and yttrium in representative layers for each nodule are given in Table 5. SEM backscattered electron imaging provides information about the chemical composition of a sample, as backscattered electrons produced by the incident electron beam are sensitive to the atomic mass of the nuclei they interact with. As a result, heavier elements that

backscatter more efficiently appear brighter than heavier elements (e.g. Goldstein et al., 2017). My backscatter images reveal that that the internal structure of the nodules consists of areas with medium to high brightness, and areas that are much darker (dark-grey). Comparison of backscatter images with elemental maps indicates that the brighter dendritic areas tend to be enriched in a single Mn oxide-rich phase, whereas the darker areas correspond to multi-phase assemblages, including Fe-Mn oxides and detrital aluminosilicatesThe dark/light areas are arranged in a variety of different textures; laminated, (Figs. 3, 4 and 6), dendritic (Fig. 7), massive (Figs. 3 and 5) or detrital (Figs. 4 and 5). Any number of these textures are present within an individual nodule, and they vary in extent between different nodules.

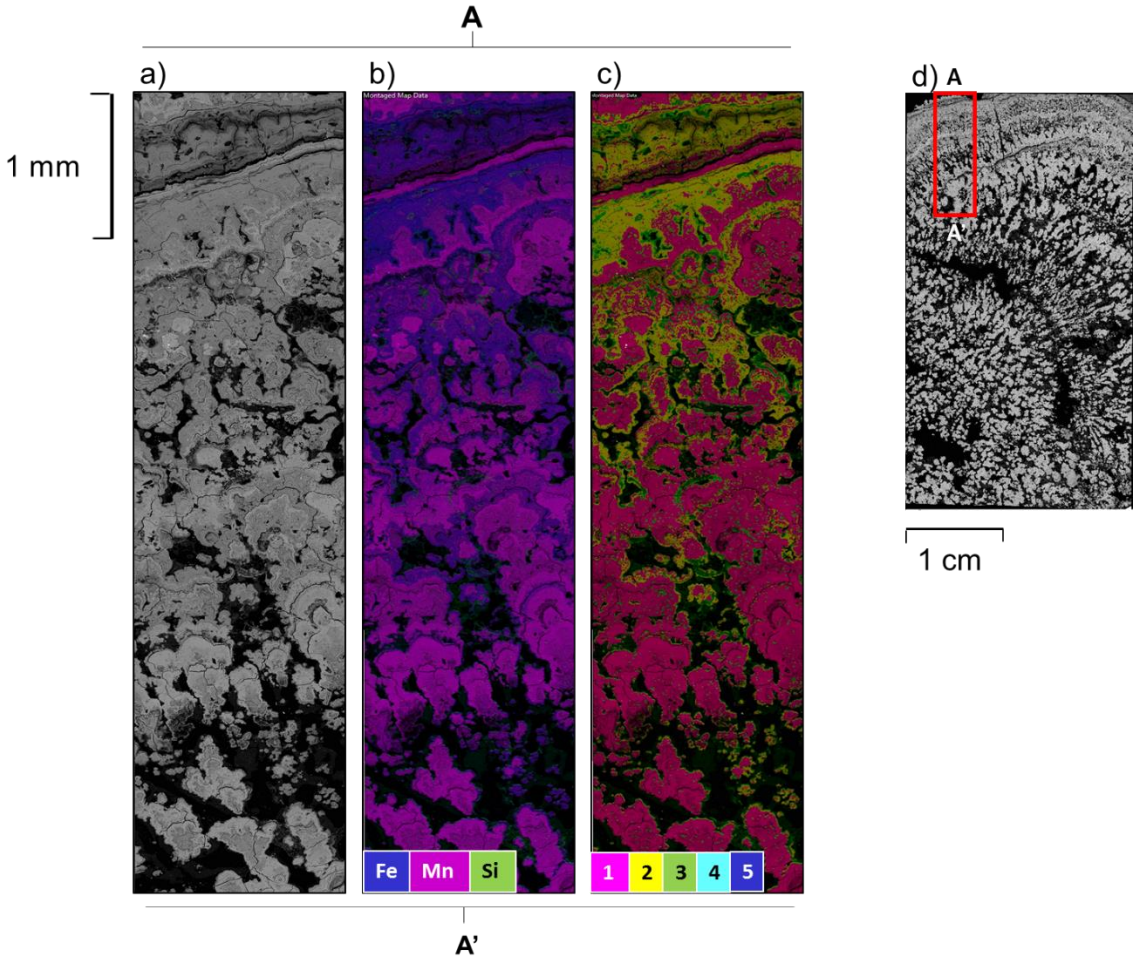

Figure 3. Microtextures and element distribution in nodule sample JC120-104 (UK Claim). a) Backscattered (BSD) image with area of analysis (A to A'); b) Fe-Mn-Si distribution; c) phase association. Magenta (1) = MnO phase. Yellow (2) = FeMnO phase. Green (3) = AlSiO phase (detrital aluminosilicates). Light blue (4) = CaPO phase (biogenic Ca-phosphates). Dark blue FeO phase.

The outer part of most of the nodules is characterized by a parallel or laminated morphology of alternating dark/light layers of similar thickness. Elemental mapping indicates that the darker layers mainly consist of Fe-Mn (oxyhydr)oxides, and the brighter layers mainly consist of Mn-oxides. This texture is characteristic of the small nodules from APEI-6, although it is also present in the outer layers of the uppermost surface of the UK Claim nodules (Fig. 7c). Dendritic textures are characterized by rounded, bulbous discontinuous layers, with pore spaces in between circular growths. These layers generally occur in the inner part of the nodule and they principally consist of Mn-oxides. They are common in larger nodules from the UK Claim area. Massive compacted textures can be found in some of the smaller APEI-6 nodules. These consist of a mixture of finely crystallized Mn-oxides, with the occasional presence of pores containing detrital material. Detrital textures are mainly found in nodules from APEI-6, filling pore spaces and often overprinting FeMnO layers or massive Mn-oxide structures. Detrital material mainly consists of angular grains of aluminosilicate minerals, such as quartz, K-feldspar and phyllosilicates. Biogenic detrital Ca-rich apatite is also present in nodules from both locations. Fe-oxides can also been found within the pore spaces, in trace quantities.

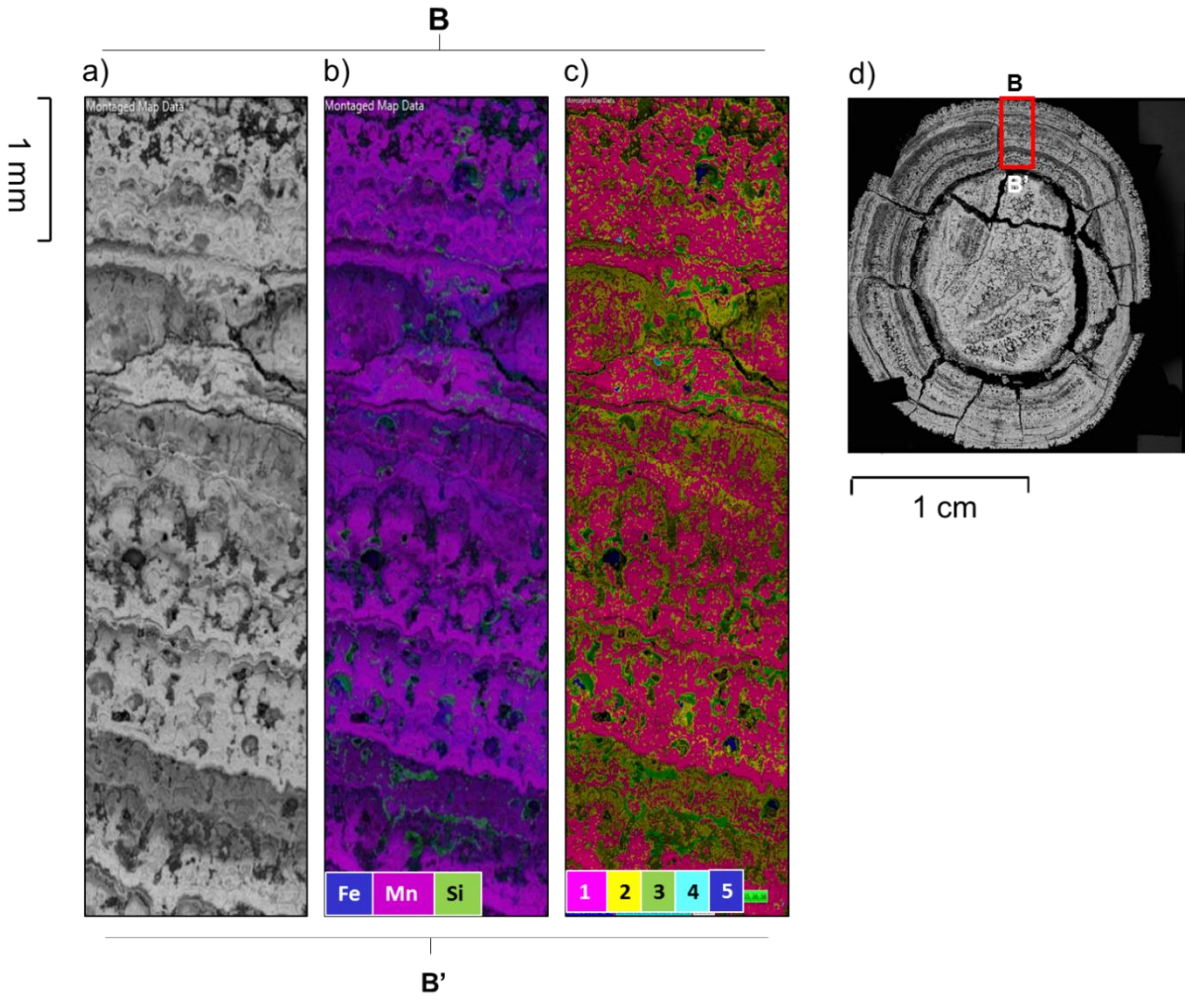

Figure 4. Microtextures and element distribution for nodule sample JC120-037 (APEI-6 – Flat). a) Backscattered (BSD) image with area of analysis (A to A'); b) Fe-Mn-Si distribution; c) phase association. Magenta (1) = MnO phase. Yellow (2) = FeMnO phase. Green (3) = AlSiO phase (detrital aluminosilicates). Light blue (4) = CaPO phase (biogenic Ca-phosphates). Dark blue FeO phase.

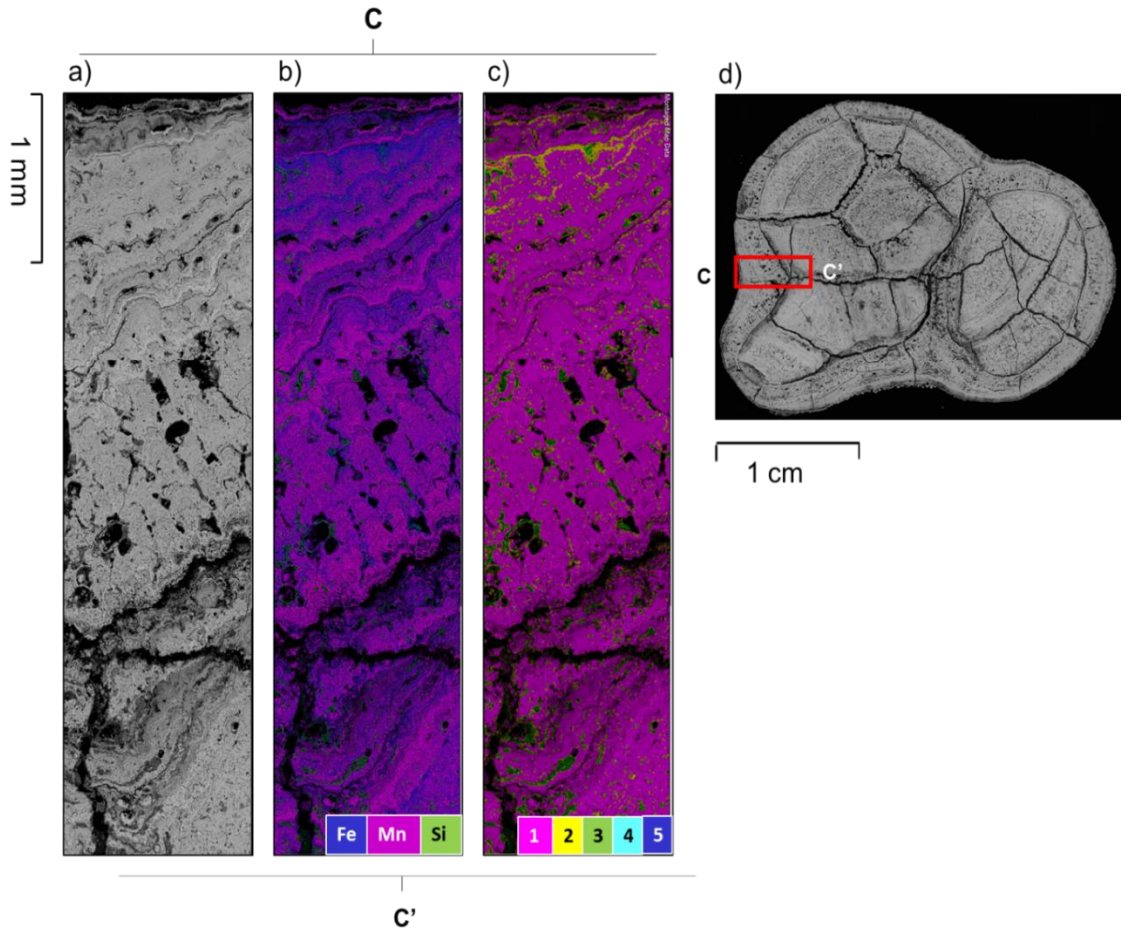

Figure 5. Microtextures and element distribution for nodule sample JC120-013 (APEI-6 – Deep Plain). a) Backscattered (BSD) image with area of analysis (A to A'); b) Fe-Mn-Si distribution; c) phase association. Magenta (1) = MnO phase. Yellow (2) = FeMnO phase. Green (3) = AlSiO phase (detrital aluminosilicates). Light blue (4) = CaPO phase (biogenic Ca-phosphates). Dark blue FeO phase.

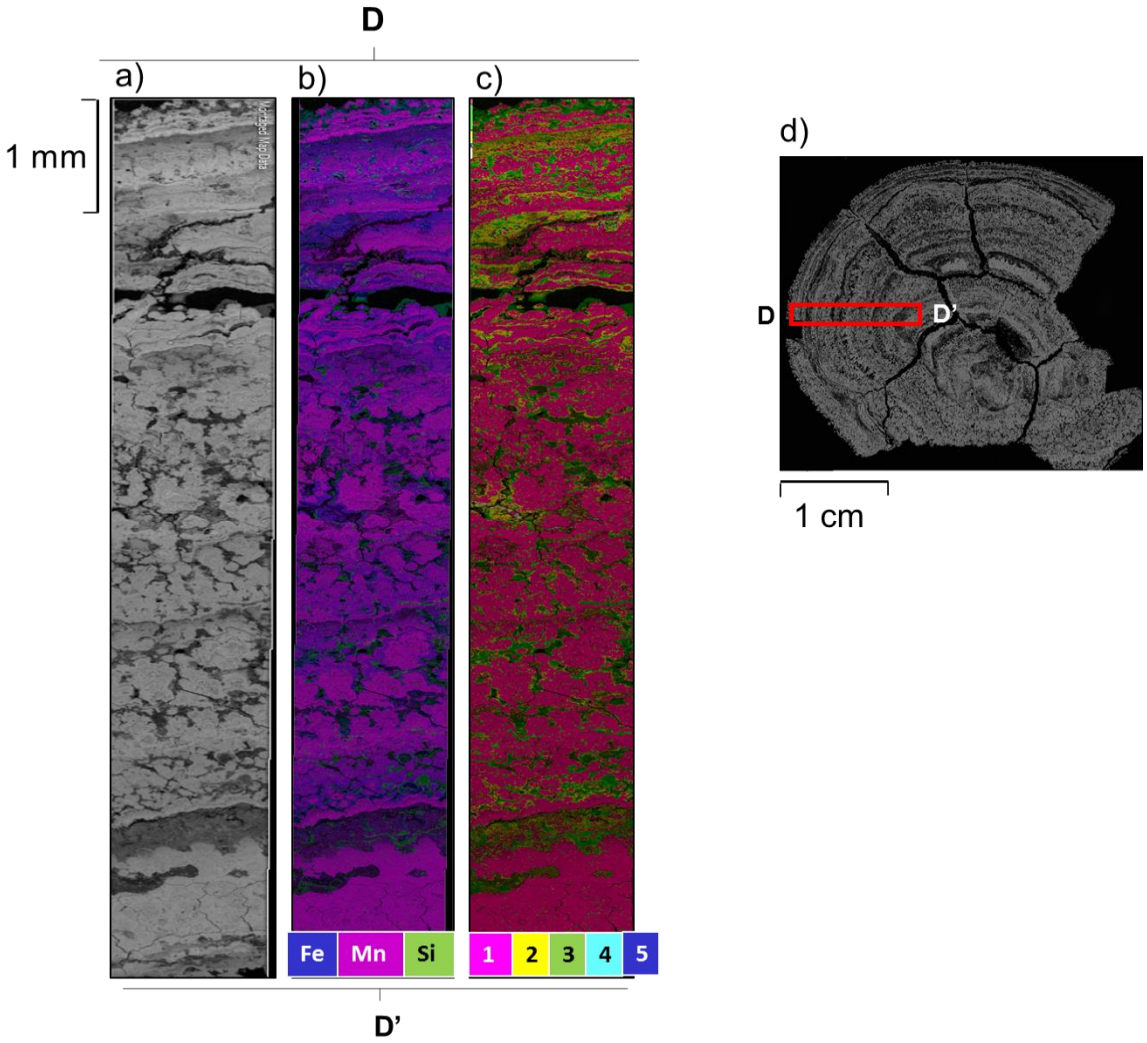

Figure 6. Microtextures and element distribution for nodule sample J120-061 (APEI-6 – Trough). a) Backscattered (BSD) image with area of analysis (A to A'); b) Fe-Mn-Si distribution; c) phase association. Magenta (1) = MnO phase. Yellow (2) = FeMnO phase. Green (3) = AlSiO phase (detrital aluminosilicates). Light blue (4) = CaPO phase (biogenic Ca-phosphates). Dark blue FeO phase.

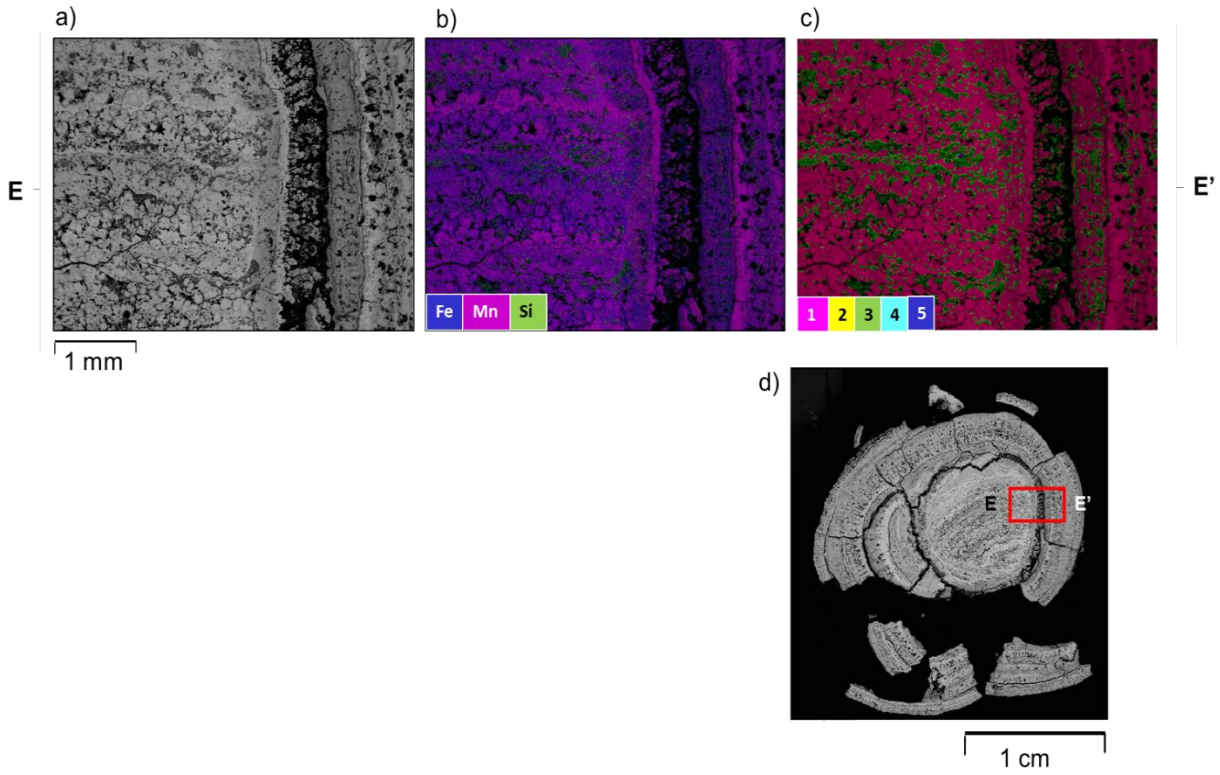

Figure 7. Microtextures and element distribution for nodule sample JC120-048 (APEI-6 – Ridge). a) Backscattered (BSD) image with area of analysis (A to A'); b) Fe-Mn-Si distribution; c) phase association. Magenta (1) = MnO phase. Yellow (2) = FeMnO phase. Green (3) = AlSiO phase (detrital aluminosilicates). Light blue (4) = CaPO phase (biogenic Ca-phosphates). Dark blue FeO phase.

4.4.2.2. Laser ablation ICP-MS analyses

For each individual nodule, ~50 spot analyses of the chemical composition of different nodule layers, identified in back scatter images, were made. Data for 3 selected spots, together with the mean and standard deviation of all analyses, are given in Tables 6 and 7. The data reveal that Mn, Co, Ni and Cu concentrations are very variable within individual nodules but, in general, those parts of a nodule that have high Mn also tend to have relatively high concentrations of Cu and Ni. Parts of the nodule from the UK Claim area have very high Mn, up to 40 wt. %, and Cu and Ni concentrations are, respectively, up to 1.04 and 1.61 wt. %. The Mn-rich layers also tend to have relatively low Fe and Co (~0.74 and ~0.27 wt. %, respectively), high Mn/Fe (up to ~ 54) and fast growth rates (up to ~4.30 mm/Ma). Nodules from APEI-6 tend to have a higher proportion of layers with relatively high Fe and Co (respectively, up to ~14 wt. % and ~1 wt. %). These layers have relatively low Mn/Fe (~0.99), and extremely slow growth rates (~0.2 mm/Ma).

The REY content of individual layers is also highly variable, with ΣREY ranging from ~306 to ~4780 ppm. Generally, the lowest ΣREY concentrations are associated with low, or even negative, Ce anomalies (as low as ~0.34). These layers also tend to be more highly depleted in the LREE relative to the HREE (LREE/HREE as low as ~0.7), and they are most abundant in the UK Claim nodule. Nodules from APEI-6 have a higher abundance of layers with high ΣREY concentrations (up to ~4780 ppm), positive Ce anomalies (up to ~2.6), and generally high LREE/HREE ratios (up to ~1.11). Low ΣREY concentrations tend to be associated with layers that have high Mn/Fe, whereas high ΣREY concentrations tend to be associated with layers that have low Mn/Fe. The proportion of layers with high Mn/Fe is greater in the nodule from the UK Claim area relative to the nodules from APEI-6.

Sample	Layer #	Mn wt%	Fe wt%	Ca wt%	Al wt%	K wt%	Ni wt%	Cu wt%	Co wt%	P wt%	Zn ppm	Mn/Fe	GR† (mm/Ma)
JC120-105 (UK Claim)	1	17.2	12.6	1.37	1.27	0.33	0.29	0.17	0.30	0.31	261	1.37	2.14
	2	40.0	0.74	1.26	1.45	1.05	1.61	1.04	0.27	0.12	410	54.1	4.31
	3	23.7	10.4	1.72	1.58	0.66	0.78	0.52	0.40	0.24	473	2.28	1.65
	Avg	17.7	6.45	3.01	1.84	0.51	0.91	0.39	0.22	0.18	1110	12.8	6.53
	SD (n =48)	10.6	4.86	1.42	1.09	0.23	0.60	0.44	0.13	0.13	872	14.8	8.25
JC120-010 (APEI-6 - Deep Plain)	1	15.7	11.8	3.86	3.02	0.34	1.43	0.15	0.30	0.29	739	1.33	1.86
	2	10.7	10.8	5.07	2.56	0.37	0.49	0.09	0.77	0.22	535	0.99	0.26
	3	15.6	10.4	7.06	2.01	0.41	0.73	0.08	1.01	0.37	715	1.49	0.23
	Avg	15.6	10.2	6.25	2.53	0.44	0.82	0.11	0.84	0.29	803	2.18	0.40
	SD (n =51)	4.45	1.52	2.04	0.56	0.10	0.40	0.04	0.36	0.07	225	0.5	0.10
JC120-025 (APEI-6 – Flat)	1	11.4	5.65	5.32	2.20	0.42	0.54	0.10	0.74	0.17	658	2.01	0.19
	2	20.5	6.03	5.65	1.84	0.47	1.11	0.25	0.28	0.14	1140	3.40	1.93
	3	22.1	10.1	3.34	2.40	0.24	1.10	0.25	0.36	0.32	636	2.19	1.78
	Avg	13.9	6.43	4.69	2.11	0.42	0.78	0.16	0.39	0.16	750	3.00	1.80
	SD (n = 50)	5.24	2.24	1.21	0.45	0.11	0.34	0.07	0.18	0.10	326	1.3	2.30
JC120-063 (APEI-6 – Trough)	1	9.81	8.49	3.40	1.75	0.26	0.50	0.08	0.76	0.20	460	1.16	0.20
	2	19.4	2.70	5.75	1.96	0.60	1.02	0.23	0.32	0.12	1560	7.19	1.19
	3	21.9	6.38	4.20	3.55	0.46	1.88	0.28	0.40	0.19	1800	3.43	1.22
	Avg	10.4	5.21	3.26	1.82	0.38	0.65	0.12	0.29	0.15	709	4.99	2.20
	SD (n =50)	5.23	2.38	1.30	0.67	0.12	0.49	0.08	0.19	0.08	463	4.10	1.50
JC120-048 (APEI-6 – Ridge)	1	16.0	11.5	3.91	1.99	0.60	0.92	0.16	0.32	0.25	952	1.39	1.66
	2	18.3	6.02	4.41	3.12	0.34	1.39	0.28	0.40	0.18	1230	3.03	0.93
	3	16.7	13.7	5.26	2.58	0.55	0.83	0.17	0.33	0.38	862	1.22	1.86
	Avg	12.8	6.68	4.24	1.96	0.41	0.70	0.14	0.35	0.19	742	1.92	0.82
	SD (n = 50)	4.98	0.14	1.31	0.70	0.12	0.43	0.07	0.19	0.14	296	36.0	0.25

Table 6. Concentrations of major and trace elements in individual layers of nodules from APEI-6 and the UK Claim area. †= Growth Rate = $0.68/(Co_n)^{1.67}$, where Co_n= Co*(50/Fe+Mn), with Co, Fe and Mn in wt. % (Manheim & Lane-Bostwick, 1988).

Sample	Layer #	La ppm	Ce ppm	Pr ppm	Nd ppm	Sm ppm	Eu ppm	Gd ppm	Tb ppm	Dy ppm	Y ppm	Ho ppm	Er ppm	Tm ppm	Yb ppm	Lu ppm	ΣREY ppm	ΣHREE ppm	Ce*	LREE/ HREE
JC120-105 (UK Claim)	1	117	310	38.8	158	37.5	8.74	30.3	4.62	28.4	80.8	5.26	14.5	2.35	15.4	2.23	854	103	1.10	0.88
	2	55.0	43.9	15.3	69.9	17.8	3.94	16.2	2.59	15.7	43.4	2.83	8.25	1.28	8.46	1.25	306	56.5	0.34	0.67
	3	87.8	245	20.8	94.6	22.1	4.99	24.0	3.42	20.9	62.6	3.75	11.2	1.50	9.69	1.53	614	76.0	1.33	0.77
	Avg	113	367	34.0	133	34.2	8.09	30.7	4.71	28.8	94.8	5.37	14.9	2.11	14.3	2.15	981	111	1.54	0.81
	SD (n =48)	56.3	173	16.4	63.7	16.2	3.90	15.2	2.27	13.5	46.0	2.56	7.02	0.96	6.61	0.99	443	52.7	0.46	0.07
JC120-010 (APEI-6 - Deep Plain)	1	137	292	46.2	184	53.9	11.4	46.4	7.38	43.6	117	7.99	21.3	3.21	22.3	3.01	1110	155	0.89	0.73
	2	381	2007	101	396	95.8	23.3	81.7	12.7	74.8	228	13.9	35.5	4.56	31.2	4.86	3720	259	2.55	1.11
	3	576	2104	153	578	145	32.8	117	17.9	110	329	20.8	53.9	7.96	53.9	7.79	4630	389	1.80	1.01
	Avg	586	2170	156	595	144	33.3	119	18.3	109	311	19.8	52.4	7.46	50.0	7.39	4820	417	1.91	1.03
	SD (n =51)	404	1610	100	376	88.2	19.8	72.3	10.7	62.2	170	11.2	29.0	4.03	26.7	4.03	3060	239	0.63	0.18
JC120-025 (APEI-6 – Flat)	1	511	1754	150	584	151	35.2	132	19.1	115	313	20.5	53.0	7.4	50.7	7.20	4210	405	1.58	1.03
	2	305	428	90.4	352	86.7	20.1	78.0	11.7	73.6	187	13.2	34.2	5.17	37.0	5.01	1730	258	0.64	0.84
	3	286	546	86.4	311	83.1	16.8	58.8	9.64	58.3	151	10.5	29.3	4.47	30.8	4.26	1840	206	0.90	0.98
	Avg	345	979	103	393	102	23.7	86.9	13.5	81.7	224	14.9	40.0	5.80	39.1	5.63	2680	311	1.32	0.92
	SD (n = 50)	160	604	47.3	179	46.3	10.9	38.4	6.15	36.7	94.2	6.82	18.5	2.77	19.3	2.76	1290	142	0.58	0.07
JC120-063 (APEI-6 – Trough)	1	223	1140	61.3	235	61.5	14.8	53.3	8.57	50.9	183	10.1	27.5	3.89	27.2	3.66	2290	185	2.46	0.81
	2	294	717	85.0	316	77.1	18.7	73.1	11.0	64.7	212	12.7	34.0	5.25	34.1	4.87	2170	240	1.16	0.86
	3	175	465	60.0	221	55.8	13.6	48.5	7.72	43.7	149	8.93	23.2	3.53	25.6	3.34	1450	165	1.15	0.83
	Avg	179	616	57.0	221	57.5	13.7	48.9	7.59	45.4	136	8.40	22.8	3.32	22.5	3.22	2000	176	1.50	0.87
	SD (n =50)	115	547	36.7	136	36.0	8.59	30.0	4.75	28.1	78.8	5.20	14.2	2.06	14.1	2.04	3140	109	0.61	0.11
JC120-048 (APEI-6 – Ridge)	1	196	350	52.6	191	48.8	10.1	40.5	6.26	38.3	116	7.03	20.2	3.05	19.4	2.93	1220	138	0.90	0.92
	2	191	325	57.3	214	58.9	12.9	49.3	8.07	48.1	139	9.68	26.3	4.14	27.8	3.89	1310	177	0.79	0.73
	3	340	1886	96.7	374	95.0	22.4	73.9	11.9	73.4	209	13.6	38.9	6.01	40.2	5.77	3490	264	2.60	0.85
	Avg	289	755	83.8	326	81.6	18.4	71.3	10.9	66.7	181	12.4	33.8	5.05	33.8	4.90	2170	257	1.33	0.88
	SD (n = 50)	209	491	57.7	226	55.6	12.6	50.1	7.50	46.1	111	8.52	23.1	3.45	23.6	3.39	1390	178	0.60	0.11

Table 7. Concentrations of rare earth elements and yttrium (REY) in individual layers of nodules from APEI-6 and the UK Claim area. $Ce^* = (2*Ce_{SN})/(La_{SN}+Nd_{SN})$. $LREE/HREE = (La_{SN}+2*Pr_{SN}+Nd_{SN})/(Er_{SN}+Tm_{SN}+Yb_{SN}+Lu_{SN})$.

4.4.2.3. Factor analysis

To better quantify and understand the processes that control the chemical composition of individual layers, the elemental data were subjected to statistical factor analysis (Winters and Buckley, 1992) using the RStudio.Ink Varimax rotation scheme with Kaiser normalisation. Differences in the chemical composition of the layers can be accounted for statistically by changes in the relative proportions of eight principal factors (with eigenvalues, or sums of squared (SS) loadings, of >1) that together account for 93% of the sample variance (Table 8).

Factor 1 is the main factor that controls REY concentrations, and it accounts for the 49% of the sample variance. Ce has a slightly lower loading in this factor. Ca, V, Co and Ba show slightly higher loadings in this factor, and there are relatively good positive correlations between these elements and the LREE ($p < 0.05$; Table 9). Although the overall lack of a clear element association makes it difficult to infer the nature of this phase, this factor likely represents a hydrogenetic and/or detrital biogenic component.

Factor 2 shows high loadings for K, Mn, Ni, Cu and Zn, and negative loadings for the rest of the elements. Elements in this group show a negative correlation with most of the REY. This factor likely represents the Mn oxide fraction, and it accounts for the 15% of the total variance.

Factors 3-8 each account for <6% of the sample variance. Factor 3 shows high loadings for P and Fe, and negative correlations with Mn, Ni and Cu. This factor likely represents a biogenic detrital ferri-phosphate phase. Factor 4 shows high loadings for V and Ba, and likely represents a biogenic detrital component. Factor 5 is the main factor controlling Co and Ce, and Co also shows a moderate correlation with the rest of the REY. This factor most likely represents a hydrogenous component. Factors 6 (high loadings in Si and Ca), 7 (loadings in Si and Ca) and 8 (loadings in Ca and Ti) most likely represent different detrital aluminosilicate phases that are present in small cracks and pore spaces.

	Factor 1	Factor 2	Factor 3	Factor 4	Factor 5	Factor 6	Factor 7	Factor 8
Al		-0.15				**0.97**	0.11	
Si	0.16	-0.45				0.14	**0.77**	-0.15
K		**0.91**	-0.21		-0.16	-0.16	0.18	
Ca	0.33	**-0.47**	0.14	0.15	0.34		0.41	-0.41
Ti		0.33	0.15		0.23	-0.18	-0.14	**0.87**
V	0.43	-0.42		**0.60**	0.30	0.12	0.28	-0.15
P		-0.26	**0.77**	0.12				0.11
Fe		-0.30	**0.88**					
Mn		**0.94**	-0.13				-0.21	0.20
Co	0.27	-0.18		0.12	**0.70**			0.15
Ni	-0.11	**0.59**	-0.25	-0.12	-0.15	0.55		-0.22
Cu		**0.72**	-0.16	-0.13	-0.10		-0.32	0.17
Zn	-0.12	**0.83**	-0.15	-0.22	-0.20		-0.13	
Ba	0.36	-0.11		**0.91**	0.14			
La	**0.87**	-0.10		0.23	0.36		0.19	
Ce	0.49	-0.24		0.18	**0.65**		0.34	
Pr	**0.94**	-0.10		0.17	0.22		0.15	
Nd	**0.98**			0.11	0.15			
Sm	**0.99**							
Eu	**0.98**				0.10			
Gd	**1.00**							
Tb	**0.99**							
Dy	**0.99**							
Y	**0.97**			-0.10			-0.13	
Ho	**0.99**							
Er	**0.99**							
Tm	**0.98**			0.13	0.10			
Yb	**0.97**	-0.11		0.17				
Lu	**0.97**			0.15	0.11			
Eigen value (SS loading)	14.1	4.34	1.59	1.56	1.56	1.36	1.31	1.14
Total variance (%)	0.49	0.15	0.06	0.05	0.05	0.05	0.05	0.04
Acum. variance (%)	0.49	0.63	0.69	0.74	0.80	0.84	0.89	0.93

Table 8. Varimax rotated factor matrix for individual layers of APEI-6 and UK Claim nodules. Numbers in bold denote elements that appear to be loaded in the factor.

	Al	Si	K	Ca	Ti	V	P	Fe	Mn	Co	Ni	Cu	Zn	Ba	La	Ce	Pr	Nd	Sm	Eu	Gd	Tb	Dy	Y	Ho	Er	Tm	Yb	Lu
Al	**1.00**																												
Si	0.31	**1.00**																											
K	-0.28	-0.31	**1.00**																										
Ca	0.15	0.67	-0.50	**1.00**																									
Ti	-0.32	-0.40	0.29	-0.44	**1.00**																								
V	0.23	0.51	-0.43	0.71	-0.26	**1.00**																							
P	0.07	0.06	-0.40	0.16	0.11	0.11	**1.00**																						
Fe	-0.02	0.18	-0.42	0.27	0.04	0.15	0.69	**1.00**																					
Mn	-0.20	-0.62	0.86	-0.61	0.51	-0.45	-0.31	-0.41	**1.00**																				
Co	-0.10	0.08	-0.28	0.35	0.27	0.42	0.04	0.12	-0.07	**1.00**																			
Ni	0.45	-0.27	0.53	-0.37	-0.15	-0.34	-0.34	-0.44	0.55	-0.37	**1.00**																		
Cu	-0.20	-0.58	0.65	-0.65	0.40	-0.55	-0.25	-0.39	**0.79**	-0.12	0.51	**1.00**																	
Zn	-0.10	-0.49	0.72	-0.55	0.16	-0.60	-0.30	-0.43	**0.79**	-0.37	0.57	0.70	**1.00**																
Ba	0.00	0.11	-0.14	0.37	-0.06	**0.77**	0.13	0.01	-0.10	0.32	-0.25	-0.20	-0.38	**1.00**															
La	-0.02	0.32	-0.18	0.59	0.09	0.70	0.01	0.02	-0.12	0.49	-0.27	-0.17	-0.32	0.59	**1.00**														
Ce	0.01	0.40	-0.29	0.63	0.13	0.68	0.03	0.06	-0.25	0.63	-0.39	-0.33	-0.44	0.46	**0.82**	**1.00**													
Pr	0.002	0.31	-0.17	0.54	0.04	0.66	-0.04	0.01	-0.12	0.41	-0.23	-0.13	-0.28	0.54	**0.98**	0.72	**1.00**												
Nd	-0.02	0.23	-0.10	0.44	0.09	0.56	-0.07	-0.02	-0.04	0.37	-0.17	-0.04	-0.20	0.48	**0.95**	0.64	**0.99**	**1.00**											
Sm	-0.01	0.23	-0.10	0.41	0.07	0.54	-0.08	-0.02	-0.04	0.33	-0.15	-0.03	-0.19	0.45	**0.92**	0.58	**0.98**	**1.00**	**1.00**										
Eu	-0.01	0.25	-0.11	0.43	0.06	0.55	-0.08	-0.01	-0.06	0.34	-0.16	-0.04	-0.20	0.44	**0.93**	0.61	**0.98**	**1.00**	**1.00**	**1.00**									
Gd	-0.04	0.15	-0.05	0.34	0.12	0.45	-0.10	-0.03	0.02	0.30	-0.12	0.04	-0.13	0.39	**0.88**	0.52	**0.95**	**0.99**	**0.99**	**0.99**	**1.00**								
Tb	-0.04	0.18	-0.09	0.38	0.10	0.51	-0.09	-0.03	-0.02	0.33	-0.15	0.002	-0.17	0.43	**0.91**	0.57	**0.97**	**0.99**	**1.00**	**0.99**	**1.00**	**1.00**							
Dy	-0.04	0.19	-0.10	0.38	0.10	0.52	-0.07	-0.02	-0.03	0.33	-0.16	-0.01	-0.18	0.44	**0.91**	0.57	**0.97**	**0.99**	**1.00**	**1.00**	**1.00**	**1.00**	**1.00**						
Y	-0.07	0.02	0.00	0.17	0.14	0.26	-0.15	-0.06	0.11	0.23	-0.04	0.17	0.00	0.24	**0.75**	0.35	**0.85**	**0.92**	**0.93**	**0.93**	**0.97**	**0.95**	**0.94**	**1.00**					
Ho	-0.04	0.19	-0.11	0.40	0.10	0.53	-0.07	-0.02	-0.04	0.35	-0.17	-0.02	-0.20	0.45	**0.92**	0.59	**0.98**	**0.99**	**1.00**	**0.99**	**0.99**	**1.00**	**1.00**	**0.94**	**1.00**				
Er	-0.04	0.18	-0.11	0.39	0.10	0.52	-0.07	-0.02	-0.03	0.34	-0.17	-0.02	-0.20	0.45	**0.91**	0.57	**0.97**	**0.99**	**0.99**	**0.99**	**0.99**	**1.00**	**1.00**	**0.94**	**1.00**	**1.00**			
Tm	-0.01	0.23	-0.16	0.45	0.07	0.59	-0.04	0.00	-0.09	0.36	-0.20	-0.07	-0.25	0.49	**0.94**	0.62	**0.98**	**0.99**	**0.99**	**0.99**	**0.98**	**0.99**	**0.99**	**0.91**	**1.00**	**1.00**	**1.00**		
Yb	-0.01	0.23	-0.16	0.46	0.05	0.62	-0.03	-0.01	-0.10	0.36	-0.20	-0.10	-0.27	0.53	**0.94**	0.62	**0.98**	**0.99**	**0.98**	**0.98**	**0.97**	**0.98**	**0.99**	**0.89**	**0.99**	**0.99**	**1.00**	**1.00**	
Lu	-0.02	0.21	-0.15	0.45	0.08	0.59	-0.03	0.002	-0.08	0.37	-0.20	-0.07	-0.25	0.51	**0.94**	0.63	**0.98**	**0.99**	**0.99**	**0.99**	**0.98**	**0.99**	**0.99**	**0.90**	**0.99**	**0.99**	**1.00**	**1.00**	**1.00**

Table 9. Correlation coefficients between elements in individual layers of APEI-6 and UK Claim nodules. Significant ($p < 0.05$) correlations are highlighted in bold.

4.4.3. Composition of sediments

To better assess the composition of the sediments, the elemental data for the sediments were also subjected to statistical factor analysis (Winters and Buckley, 1992). Differences in the chemical composition of the sediments samples can be accounted for by changes in the relative proportions of three principal factors (with eigenvalues, or sums of squared (SS) loadings, of >1) which together account for 92.3% of the sample variance (Table 10).

Factor 1 is the main factor that controls REY concentrations, although it is slightly less important for Ce, and it accounts for the 56.4% of the sample variance. This factor also shows high loadings for Ca, P and Co, and all of the REY except Ce show a significant ($p < 0.05$; Table 11) positive correlation with Ca, P and Co. The REY are also positively correlated with Fe. Mn and Cu show a negative loading in this factor. Factor 1 can be considered to represent the biogenic Ca-phosphate fraction of the sediment.

Factor 2 has high loadings for Fe, Mg, Al, K, Ti, V, and to a lesser extent Ba, Sr and Ce. The light REY (La-Nd) have a slightly higher loading in this factor compared to the heavy REY, and all REY show a positive correlation with Al, K and Ti, and, to a lesser extent, Fe ($p < 0.05$; Table 11). Mn and Ni have a negative loading in this factor. Factor 2 most likely represents the detrital component of the sediment, and it accounts for the 20.6% of the total sample variance.

Factor 3 has the highest loadings for Mn, Ba, Ni, Cu and Sr, and negative loadings for most other elements, including the light REE. Mn shows a strong positive correlation with Ni and Cu, and Ba with Sr. This factor likely represents the Mn oxide fraction of the sediment that is widely considered to have a diagenetic source (Bonatti et al., 1972; Wegorzewski & Kuhn, 2014). Factor 3 accounts for the 15% of the total sample variance.

	Factor1	Factor2	Factor3
Mn	-0.23	-0.15	**0.95**
Fe	0.37	**0.90**	0.16
Ca	**0.74**	0.26	0.15
Mg	0.48	**0.69**	
Al	0.56	**0.77**	-0.28
K	0.54	**0.75**	-0.33
P	**0.88**		-0.13
Ba		0.52	**0.77**
Co	**0.80**	0.41	-0.29
Ni		-0.24	**0.96**
Cu	-0.38		**0.91**
Ti	0.63	**0.68**	-0.32
V	0.47	**0.85**	
Sr	0.32	0.54	**0.69**
La	**0.92**	0.35	-0.16
Ce	**0.75**	0.51	-0.38
Pr	**0.93**	0.32	-0.15
Nd	**0.94**	0.31	-0.14
Sm	**0.94**	0.29	-0.13
Eu	**0.93**	0.34	
Gd	**0.94**	0.29	-0.11
Tb	**0.95**	0.27	
Dy	**0.95**	0.27	
Y	**0.95**	0.27	
Ho	**0.95**	0.27	
Er	**0.95**	0.27	
Tm	**0.95**	0.27	
Yb	**0.95**	0.28	
Lu	**0.95**	0.27	
Eigen value (SS loading)	16.4	5.97	4.44
Total variance (%)	56.4	20.6	15.3
Acum. variance (%)	56.4	77.0	92.3

Table 10. Varimax rotated factor matrix for APEI-6 and UK Claim deep-sea sediments. Numbers in bold denote elements that appear to be loaded in the factor.

	Mn	Fe	Ca	Mg	Al	K	P	Ba	Co	Ni	Cu	Ti	V	Sr	La	Ce	Pr	Nd	Sm	Eu	Gd	Tb	Dy	Y	Ho	Er	Tm	Yb	Lu
Mn	**1.00**																												
Fe	-0.08	**1.00**																											
Ca	-0.06	0.52	**1.00**																										
Mg	-0.17	**0.77**	0.72	**1.00**																									
Al	-0.51	**0.85**	0.57	**0.80**	**1.00**																								
K	-0.54	**0.81**	0.57	**0.81**	**0.98**	**1.00**																							
P	-0.33	0.24	0.47	0.19	0.48	0.45	**1.00**																						
Ba	0.62	0.66	0.28	0.36	0.19	0.13	-0.10	**1.00**																					
Co	-0.49	0.58	0.68	0.70	**0.86**	**0.86**	0.72	-0.06	**1.00**																				
Ni	**0.96**	-0.08	0.08	-0.13	-0.45	-0.49	-0.15	0.57	-0.34	**1.00**																			
Cu	**0.95**	-0.01	-0.16	-0.19	-0.50	-0.53	-0.48	0.69	-0.61	**0.88**	1.00																		
Ti	-0.54	**0.77**	0.61	0.78	**0.98**	**0.98**	0.31	0.08	**0.91**	-0.46	-0.57	**1.00**																	
V	-0.14	**0.96**	0.60	0.82	**0.90**	**0.86**	0.15	0.55	0.69	-0.12	-0.12	**0.84**	**1.00**																
Sr	0.48	**0.76**	0.53	0.58	0.39	0.34	0.09	**0.95**	0.21	0.49	0.50	0.31	0.69	**1.00**															
La	-0.41	0.62	0.74	0.67	**0.83**	**0.82**	**0.81**	0.09	**0.94**	-0.24	-0.51	**0.87**	0.72	0.36	**1.00**														
Ce	-0.60	0.66	0.63	0.70	**0.93**	**0.93**	0.68	-0.04	**0.97**	-0.47	-0.66	**0.96**	**0.75**	0.21	**0.94**	**1.00**													
Pr	-0.40	0.60	**0.75**	0.66	**0.82**	**0.80**	**0.81**	0.08	**0.94**	-0.23	-0.51	**0.86**	0.70	0.36	**1.00**	**0.93**	**1.00**												
Nd	-0.39	0.59	**0.75**	0.65	**0.81**	**0.79**	**0.82**	0.09	**0.93**	-0.21	-0.50	**0.85**	0.69	0.36	**1.00**	**0.92**	**1.00**	**1.00**											
Sm	-0.38	0.58	**0.76**	0.65	**0.80**	**0.78**	**0.82**	0.09	**0.93**	-0.20	-0.49	**0.84**	0.68	0.36	**1.00**	**0.92**	**1.00**	**1.00**	**1.00**										
Eu	-0.26	0.66	**0.78**	0.68	**0.79**	**0.76**	**0.80**	0.24	**0.89**	-0.09	-0.37	**0.82**	0.74	0.50	**0.98**	**0.88**	**0.98**	**0.99**	**0.99**	**1.00**									
Gd	-0.36	0.59	**0.75**	0.65	**0.79**	**0.77**	**0.83**	0.11	**0.92**	-0.18	-0.47	**0.83**	0.69	0.38	**1.00**	**0.91**	**1.00**	**1.00**	**1.00**	**0.99**	**1.00**								
Tb	-0.35	0.58	**0.76**	0.64	**0.78**	**0.76**	**0.83**	0.11	**0.91**	-0.17	-0.47	**0.82**	0.68	0.39	**0.99**	**0.90**	**1.00**	**1.00**	**1.00**	**0.99**	**1.00**	**1.00**							
Dy	-0.34	0.58	**0.76**	0.64	**0.77**	**0.75**	**0.83**	0.12	**0.91**	-0.16	-0.46	**0.82**	0.68	0.39	**0.99**	**0.89**	**1.00**	**1.00**	**1.00**	**0.99**	**1.00**	**1.00**	**1.00**						
Y	-0.31	0.59	**0.77**	0.64	**0.77**	**0.74**	**0.83**	0.15	**0.90**	-0.13	-0.43	**0.80**	0.68	0.43	**0.99**	**0.88**	**0.99**	**0.99**	**1.00**	**0.99**	**1.00**	**1.00**	**1.00**	**1.00**					
Ho	-0.33	0.58	**0.77**	0.64	**0.77**	**0.75**	**0.84**	0.12	**0.91**	-0.15	-0.45	**0.81**	0.67	0.40	**0.99**	**0.89**	**0.99**	**1.00**	**1.00**	**0.99**	**1.00**	**1.00**	**1.00**	**1.00**	**1.00**				
Er	-0.34	0.58	**0.76**	0.64	**0.77**	**0.75**	**0.83**	0.13	**0.91**	-0.15	-0.45	**0.81**	0.68	0.40	**0.99**	**0.89**	**0.99**	**1.00**	**1.00**	**0.99**	**1.00**	**1.00**	**1.00**	**1.00**	**1.00**	**1.00**			
Tm	-0.33	0.59	**0.76**	0.64	**0.77**	**0.75**	**0.83**	0.14	**0.91**	-0.14	-0.44	**0.81**	0.68	0.41	**0.99**	**0.89**	**0.99**	**1.00**	**1.00**	**0.99**	**1.00**	**1.00**	**1.00**	**1.00**	**1.00**	**1.00**	**1.00**		
Yb	-0.32	0.60	**0.77**	0.65	**0.77**	**0.75**	**0.83**	0.15	**0.91**	-0.13	-0.43	**0.81**	0.69	0.42	**0.99**	**0.89**	**0.99**	**1.00**	**1.00**	**0.99**	**1.00**	**1.00**	**1.00**	**1.00**	**1.00**	**1.00**	**1.00**	**1.00**	
Lu	-0.31	0.59	**0.77**	0.64	**0.77**	0.74	**0.83**	0.15	**0.90**	-0.12	-0.43	**0.81**	0.68	0.42	**0.99**	**0.88**	**0.99**	**0.99**	**1.00**	**0.99**	**1.00**	**1.00**	**1.00**	**1.00**	**1.00**	**1.00**	**1.00**	**1.00**	**1.00**

Table 11. Correlation coefficients between elements in deep APEI-6 and UK Claim sediments. Significant ($p < 0.05$) correlations are highlighted in bold.

Significant amounts of Mn were mobilised by leaching in hydroxylamine hydrochloride, especially in the upper part of sediments from the UK Claim area (up to 0.24 wt. % Mn; Fig. 15). High quantities of Cu were also released from these sediments (up to 61 ppm; Table 12). Relative to sediments from the UK Claim area, higher concentrations of Co and ΣREY were released with reducible Mn oxides from sediments from APEI-6. Leaching with hydroxylamine hydrochloride releases only traces quantities of Fe and Al (<0.1 wt. %). The proportion of Ca released by leaching with buffered sodium acetate (~11 %) was similar for both sites.

		JC120-105 (UK Claim)			JC120-025 (APEI-6 – Flat)			JC120-048 (APEI-6 – Ridge)		
		(0-1) cm	(4-5) cm	(12-14) cm	(0-1) cm	(4-5) cm	(12-14) cm	(0-1) cm	(4-5) cm	(12-14) cm
Al	wt. %	0.10	0.10	0.09	0.05	0.04	0.04	0.04	0.04	0.03
	%	1.56	1.34	1.30	0.72	0.54	0.42	0.50	0.44	0.30
K	wt. %	0.07	0.08	0.04	0.03	0.10	0.04	0.07	0.03	0.06
	%	3.22	3.18	1.56	1.33	3.31	1.29	2.55	1.18	2.17
Ca	wt. %	0.06	0.06	0.06	0.12	0.09	0.08	0.14	0.12	0.13
	%	5.34	5.95	7.44	11.8	7.91	7.78	10.1	9.01	12.9
Mn	wt. %	0.22	0.24	0.14	0.19	0.18	0.17	0.15	0.18	0.15
	%	28.0	25.4	24.4	39.9	34.6	29.4	28.1	30.1	26.2
Fe	wt. %	0.10	0.10	0.09	0.07	0.06	0.05	0.05	0.05	0.04
	%	2.31	1.97	1.73	1.54	1.15	0.93	1.05	0.94	0.74
Co	ppm	15.9	18.4	14.1	33.6	29.9	29.4	28.2	30.7	25.9
	%	22.2	23.0	22.1	35.5	28.0	26.4	26.9	27.3	22.6
Ni	ppm	48.3	54.1	27.3	40.5	38.5	33.9	33.4	41.5	36.8
	%	21.6	21.8	16.2	27.1	22.8	19.1	18.5	22.0	19.9
Cu	ppm	53.0	60.8	38.1	32.0	28.0	25.9	24.8	28.1	19.5
	%	14.2	14.3	10.8	13.0	10.1	9.05	9.26	9.58	6.95
Sr	ppm	4.02	5.23	5.16	6.68	5.13	5.20	5.70	6.50	5.13
	%	1.19	1.43	1.52	2.38	1.59	1.59	1.65	1.85	1.43
Ba	ppm	7.40	5.74	11.4	17.0	10.3	13.8	9.40	7.81	13.2
	%	11.2	10.6	12.6	15.1	9.96	9.53	10.6	10.8	7.58
Pb	ppm	2.03	1.80	1.93	1.76	1.45	1.36	1.16	1.02	1.51
	%	5.77	4.65	4.98	5.18	3.74	3.40	3.05	2.54	3.59
U	ppm	0.05	0.07	0.07	0.08	0.07	0.07	0.06	0.08	0.09
	%	3.19	4.17	4.38	4.02	3.00	3.04	2.91	3.57	3.70
La	ppm	3.74	3.89	4.44	6.23	4.86	4.58	5.96	6.26	4.47
	%	8.86	8.16	9.27	10.6	7.03	6.51	7.74	7.72	5.45
Ce	ppm	4.70	4.70	5.65	6.30	4.89	4.73	4.98	5.21	4.40
	%	6.19	5.47	6.57	6.09	4.06	3.83	4.29	4.15	3.50
Pr	ppm	16.6	17.3	20.6	32.3	25.5	24.6	31.0	32.0	23.7
	%	100	100	100	100	100	100	100	100	96.8
Nd	ppm	0.63	0.67	0.81	1.25	0.99	0.98	1.25	1.30	0.98
	%	1.27	1.19	1.45	1.75	1.18	1.15	1.30	1.29	0.97
Sm	ppm	1.40	1.50	1.86	3.01	2.42	2.42	3.02	3.10	2.40
	%	11.8	11.4	14.4	17.7	12.1	12.1	13.04	12.9	9.88
Eu	ppm	0.36	0.39	0.48	0.74	0.60	0.60	0.76	0.79	0.63
	%	8.99	8.70	11.1	15.1	10.4	10.3	11.6	11.6	8.97
Gd	ppm	1.39	1.49	1.82	2.87	2.29	2.25	2.86	3.00	2.26
	%	11.7	11.3	13.9	16.9	11.5	11.3	12.4	12.4	9.21
Tb	ppm	0.24	0.26	0.32	0.46	0.37	0.37	0.48	0.51	0.40
	%	13.3	12.7	15.9	17.6	12.1	11.9	13.3	13.5	10.5
Dy	ppm	1.25	1.31	1.63	2.48	1.96	1.92	2.46	2.58	1.95
	%	11.5	11.0	13.7	16.1	10.9	10.6	11.6	11.7	8.73
Y	ppm	7.15	7.54	9.01	13.7	10.7	10.3	13.6	14.4	10.4
	%	11.2	10.6	12.6	15.1	9.96	9.53	10.6	10.8	7.58
Ho	ppm	0.25	0.27	0.33	0.46	0.37	0.36	0.48	0.51	0.40
	%	11.6	11.3	14.0	15.3	10.3	10.2	11.5	11.7	8.95
Er	ppm	0.86	0.90	1.11	1.65	1.29	1.26	1.63	1.73	1.30
	%	14.4	13.8	16.9	19.8	13.3	13.0	14.2	14.6	10.7
Tm	ppm	0.12	0.13	0.17	0.21	0.17	0.17	0.24	0.25	0.21
	%	14.4	14.1	17.6	17.5	12.2	12.1	14.5	14.7	11.8
Yb	ppm	0.77	0.80	1.01	1.49	1.17	1.15	1.51	1.56	1.19
	%	13.7	12.8	16.3	19.2	12.9	12.7	14.0	14.2	10.6
Lu	ppm	0.13	0.13	0.17	0.21	0.17	0.17	0.24	0.25	0.21
	%	14.7	14.2	17.8	18.1	12.5	12.5	14.8	15.1	12.2
ΣREY	ppm	39.6	41.3	49.4	73.3	57.7	55.8	70.4	73.5	54.9
	%	13.2	12.3	14.7	17.5	11.7	11.2	12.8	12.7	9.38

Table 12. Amount and % of major and trace elements released by sequential leaching of APEI-6 and UK Claim sediments with hydroxylamine hydrochloride ($NH_2OH \cdot HCl$).

4.5. Discussion

Although there are distinct differences in the size, shape and internal structure of nodules from APEI-6 compared to the UK Claim area, the bulk chemical composition of the nodules is similar, and also similar to nodules obtained from other parts of the CCFZ. Table 3 shows that the Mn/Fe ratio and the Ni+Cu of the nodules from the UK Claim area (~5.6 and ~2.5 wt. %, respectively) are in the range of the average values for the CCFZ (Mn/Fe ~5.3 and Ni+Cu ~2.5 wt.%). On the other hand, the nodules from the APEI-6 show lower Mn/Fe ratios, between ~2.8-4.2, as well as lower Ni+Cu (~1.7-2.6 wt.%). These nodules in turn have noticeably higher concentrations of Co (~0.3 wt. %) and REE (~936-1470 ppm) than the average CCFZ nodules (~0.15-0.2 wt. % Co and ~645 ppm REE). Additionally, nodules from APEI-6 also have higher Ce anomalies than average CCFZ nodules (~1.8-2.2 vs ~1.1) and are slightly less depleted in the light REE relative to the heavy REE (LREE/HREE = ~0.91-0.94 vs ~0.87).

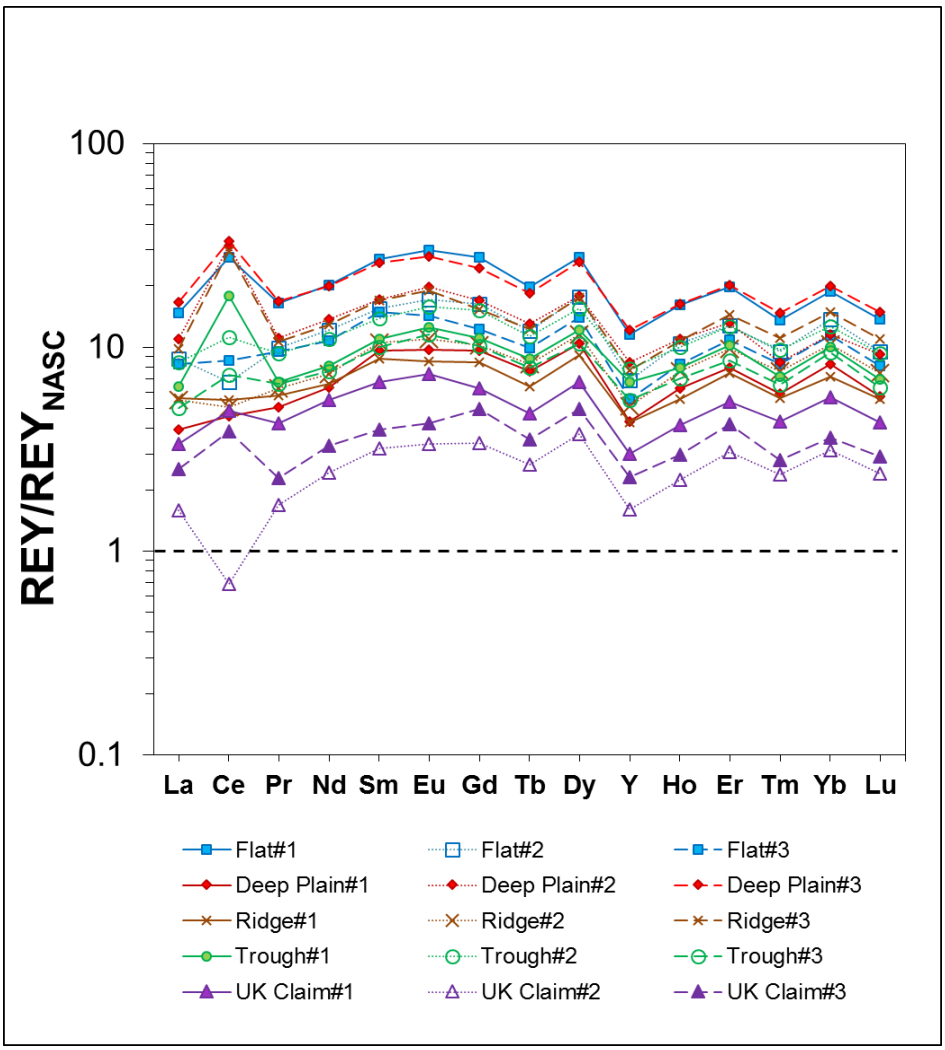

Figure 8. REY distribution patterns of individual layers within nodules, normalised to North America Shale Composite (NASC; Gromet et al., 1984). Layers with Mn/Fe > 3 are shown by open symbols and larger symbol (Ridge).

Generally, the composition of the nodules from the APEI-6 and UK Claim areas are within ranges of values of nodules from the Pacific. Relative to nodules from the Atlantic Ocean (Dubinin & Rozanov, 2001), nodules from the Pacific are characterized by higher Mn/Fe ratios (~4 vs ~0.75 in the Atlantic) and Ni+Cu concentrations (~2.2 ppm vs ~0.5 ppm), but slightly lower Fe (~6.5 wt. % vs ~17 wt. %) and Co (~0.2 wt. % vs ~0.3 wt. %). Their ΣREE content is also generally lower (~950 ppm vs ~2150 ppm), with lower positive Ce anomalies (~1.7 in Pacific nodules vs ~3.9 in Atlantic nodules) and a higher LREE/HREE ratio (~0.88 vs ~1.08). By contrast the nodules from the Indian Ocean show Mn/Fe and Ni+Cu values closer to Pacific nodules (~3.5 and ~2.14 wt. %), and they also have lower Co (~0.14 wt. %) and REY (980 ppm). Nodules from the Indian Ocean however

have slightly higher Ce anomalies than Pacific nodules (~1.9), and they are less depleted in the LREE relative to the HREE (~0.96).

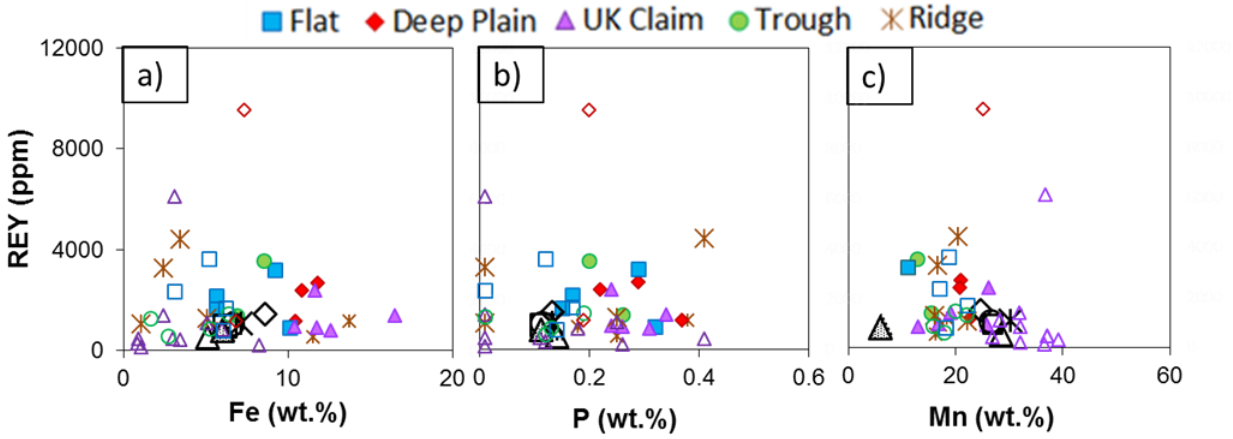

Figure 9. Relationship between ΣREY content and (a) Fe, (b) P and (c) Mn concentration in nodules. Bulk compositions are given by the open black symbols. Layers with Mn/Fe > 3 are shown by open symbols and larger symbol (Ridge).

4.5.1. Controls on the chemical composition of nodules from the UK Claim area and APEI-6

The bulk chemical composition of the nodules from the APEI-6 and UK Claim areas is closely related to the relative abundances of different phases within the nodule microstructures. The outermost part of the nodules from the UK Claim area, and the bulk of nodule material from APEI-6, consists of massive, compacted FeMnO phases, and the inner part of nodules from the UK Claim area is characterized by dendritic MnO phases. The Mn/Fe ratio of these dendritic structures is as high as 54 and Ni + Cu concentrations are up to 2.65 wt. %, whereas the massive areas have lower Mn/Fe, usually between ~1 and ~3, and lower Ni + Cu concentrations (< 1.6 wt. %). The FeMnO-rich layers most likely consist of Fe-bearing vernadite (Halbach and Özkara, 1979; Koschinsky & Halbach, 1995). This phase is often intergrown with amorphous Fe-(oxyhydr)oxide particles in APEI-6 nodules (Figs. 3, 4, 6b and 6c) as well as in the upper surface of the UK Claim nodule. By contrast, layers with Mn/Fe > 3 are considered to consist primarily of Mn-oxides; 10 Å phyllomanganates (named 10 Å vernadite by Bodeï et al. (2007)) can incorporate up to 5 wt. % of Ni + Cu in their structure, whereas the concentration of Ni + Cu in todorokite minerals is generally <2 wt. % (Bodeï et al., 2007). As most laser ablation spots with high Mn/Fe have Ni + Cu of >2 wt% (see appendices IIIa-e Suppl. Info), it is likely that the dendritic Mn-rich structures in the UK Claim nodules are mainly composed of 10 Å phyllomanganates. In support of this, todorokite was not observed in

mineralogical studies of Mn-nodules from the central Pacific Ocean (Wegorzewski et al., 2015).

On the basis of their Fe, Mn, Ni, Cu and Co content, the Mn-rich layers most likely formed from an oxic or sub-oxic diagenetic source, whereas the FeMnO-rich layers are most likely hydrogenous (Figure 10; Bonatti et al., 1972).

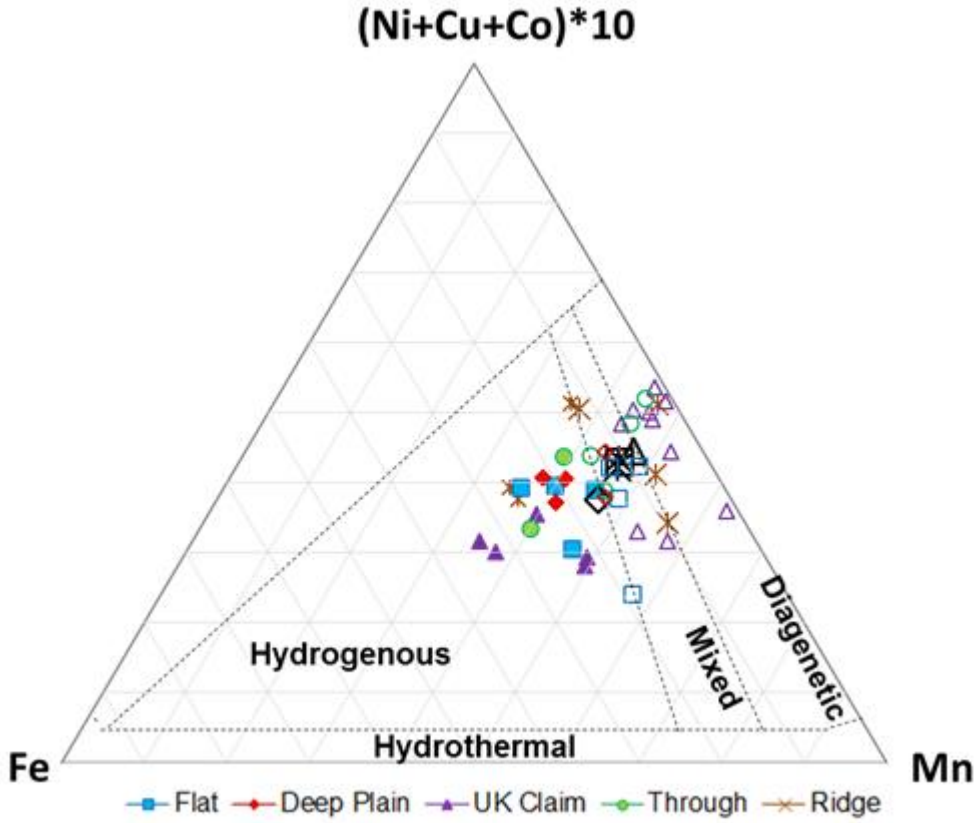

Figure 10. Ratio of Fe:Mn:Cu+Ni+Co for bulk and individual layers compositions of APEI and UK Claim nodules. Black lines define different nodule fields, according to Bonatti et al. (1972) and Wegorzewski and Kuhn (2014). Bulk compositions are shown by the black open symbols, layers with Mn/Fe > 3 are shown by coloured open symbols and larger symbol (Ridge).

As hydrogenetic phases are precipitated from colloidal Fe-Mn-(oxyhydr)oxides in bottom waters, they consist of a fine intergrowth of hydrated Mn and Fe-oxide phases, with low Mn/Fe ratios and high Co (Burns & Burns, 1978). By contrast, diagenetic precipitates form from Mn mobilized under oxic or suboxic conditions that subsequently re-precipitates as Mn-oxides (Halbach et al., 1981). Mn oxides that form under early oxic diagenetic conditions usually have relatively high Ni and Cu (up to 5 wt. %) that are released during the early diagenesis of organic matter (Dymond et al. 1984). By contrast, Mn oxides that form under suboxic conditions tend to have lower Ni and Cu (Hein et al., 2013). Most of our nodule

layers that have high Mn/Fe values (i.e. >3) have relatively low Ni + Cu (<5 wt. %), which suggests that they formed under oxic, rather than sub-oxic, diagenetic conditions. REY data can also provide useful information on the genesis of nodules. Hydrogenous layers tend to have positive Ce anomalies and high REY concentrations, which results from slow surface complexation of REY from ambient seawater into colloidal Fe-Mn-(oxyhydr)oxide particles, with preferential enrichment of tetravalent Ce (Piper, 1974; Addy, 1979; de Lange et al.,1992; Nath et al., 1992; Kasten et al., 1998, Bau et al., 2014). By contrast, fast-growing oxic and suboxic diagenetic phases have lower REY because their limits the opportunity for surface complexation (Kuhn et al., 1998; Ohta et al., 1999). Diagenetic phases also tend to have negative Ce anomalies, as tetravalent Ce does not result mobilised in the pore fluid during diagenesis (Sholkovitz et al., 1994; Schijf et al., 1995; Bau et al., 1997; Bau et al,. 2014). In connection with this, I note that most of my Mn-rich layers from the UK Claim nodule have negative Ce anomalies (Tables 6 and 7 and appendix IVa), which confirms their diagenetic character.

Bau et al. (2014) also suggest that hydrogenous nodules tend to be enriched in Ho relative to Y, because Ho is preferentially scavenged by metal (oxyhydr)oxides due to the lower stability of Y. Figure 11 shows that those parts of a nodule with Mn/Fe <3 also have high Nd concentrations, which confirms they have a hydrogenous source.

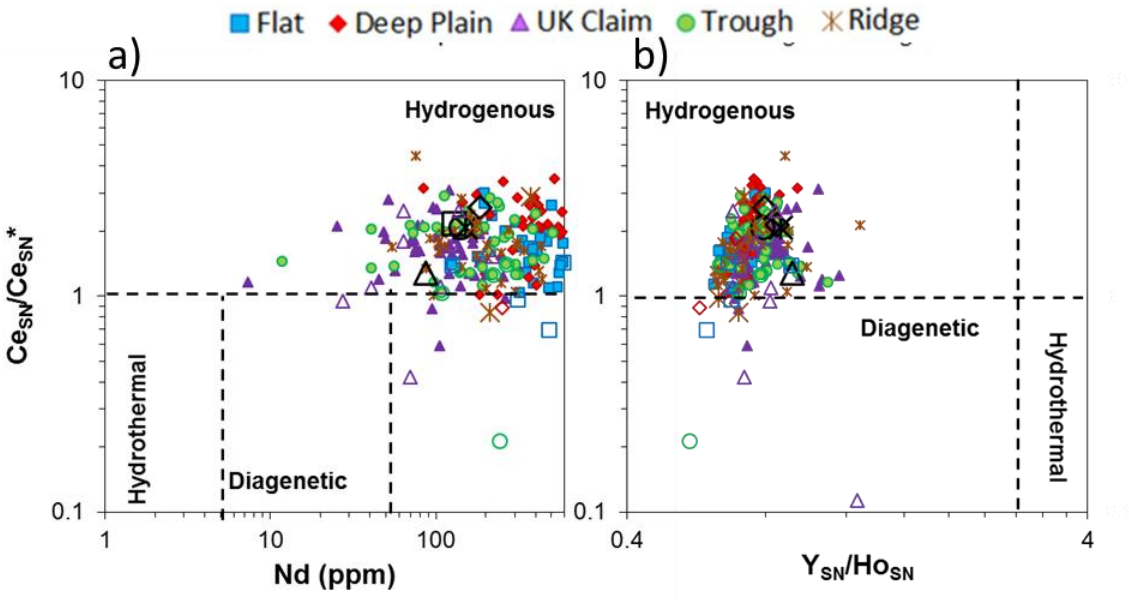

Figure 11. Relationship between (a) Ce_{SN}/Ce_{SN}^* ratio vs Nd concentration and (b) Ce_{SN}/Ce_{SN}^* ratio vs Y_{SN}/Ho_{SN} ratio in individual nodule layers. Bulk compositions are shown by open black symbols. Fields for hydrothermal, hydrogenous and

diagenetic are defined according to Bau et al., (2014). Layers with Mn/Fe > 3 are shown by coloured open symbols and larger symbol (Ridge).

4.5.2. Nodule growth rates

The growth rate of ferromanganese nodules, and the growth rates of their individual layers, can be estimated from their Co concentration (Manheim & Lane-Bostwick, 1988). The idea behind this is that the cobalt flux to Fe-Mn crusts on seamounts is nearly constant at 2.9 μg $cm^{-2}ka^{-1}$ (Halbach et al., 1982), and that the cobalt content of the crusts is inversely related to growth rate because Co^{2+} has a short oceanic residence time and it is incorporated into colloidal Mn-oxide surfaces as Co^{3+}, which is immobile (Koschinsky & Halbach, 1995). This method, however, does not account for hiatuses in Co precipitation (e.g. Banakar & Hein, 2000), so it only provides an estimate of the minimum age of the Fe-Mn deposit.

Using this method it can be estimated that the growth rate of most of the layers from the APEI-6 nodules is between ~0.2 and ~2 mm/Ma; this is rather slow and is indicative of precipitation from a hydrogenous source (Hein et al., 2000; Hein et al., (2015). The slowest average growth rate is recorded in parts of the nodule from the Deep Plain (~0.28 mm/Ma; Table 2); this area also has the highest positive Ce anomaly and ΣREY concentration. By contrast, estimated growth rates for UK Claim nodules are much higher, between ~2 and ~10 mm/Ma (Table 2). Higher growth rates are usually associated with metal precipitation from a diagenetic source, due to the fast mobilization and re-precipitation of Mn in the sediment porewater (Heye & Marchig, 1977, Reyss et al., 1982). As nodules grow faster, they become enriched in the economically interesting elements Mn, Ni and Cu, but there is less time to acquire metals such as Fe, Co and the REY as these are linked to the slow process of colloidal scavenging from seawater (Nath et al., 1992).

4.5.3. Controls on the chemical composition of sediments from the APEI-6 and UK Claim areas

The chemical composition of the sediments from the APEI-6 and UK Claim areas is similar to that of moderately REY-enriched deep sea clays from the North Eastern Pacific (Kato et al., 2011). I do not observe REY concentrations as high as those reported by these authors for the Central South Pacific (1000-2230 ppm). It is likely that the presence of silicate-rich terrigenous material derived from the

closer proximity of these sites to the American component enhances sedimentation rates and reduces the time available for scavenging of REY by hydrogenous phases (Tables 10 and 11).

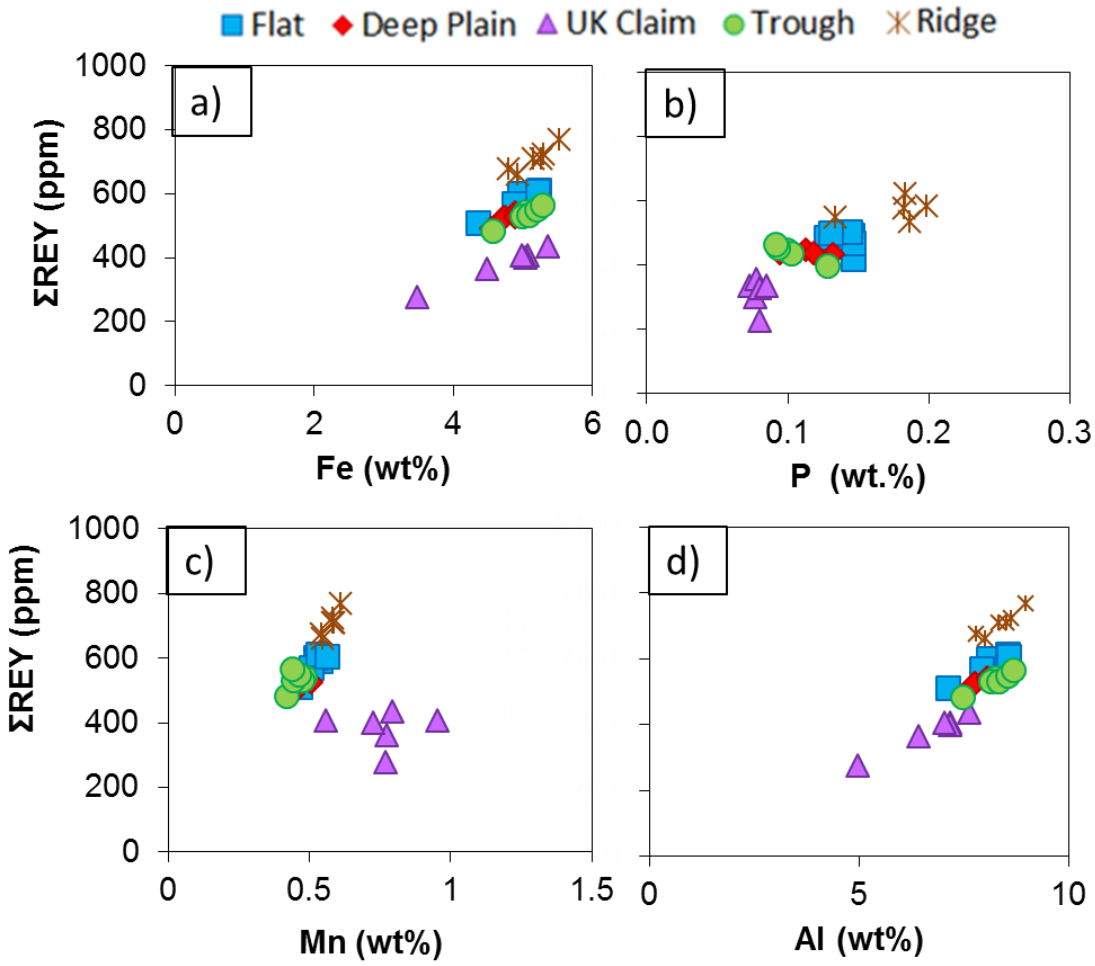

Figure 12. Relationship between ΣREY content and (a) Fe, (b) P, (c) Mn and (d) Al in sediments from the APEI-6 and UK Claim areas.

Surface sediments from the UK Claim area have higher concentrations of Mn, Ni and Cu compared to the APEI-6 sediments, and higher average Mn/Fe ratios (~0.16 vs ~0.10, respectively). This may indicate that they contain a diagenetic Mn (oxyhydr)oxide component due to dissolution of Mn-rich phases in the lower low-oxygen sediments with re-oxidation and precipitation of Mn in the upper oxygen-rich sediments (Bonatti et al., 1972; Wegorzewski & Kuhn, 2014). Similarly the REY are released during diagenesis into the pore waters, and transported upwards to the suboxic-oxic boundary, where they are incorporated into Mn-Fe-(oxyhydr)oxides (Elderfield & Sholkovitz, 1987). The depletion of the REY in my Mn-rich sediments nevertheless suggests that the REY do not have a clear affinity with Mn oxides. By contrast, sediments from APEI-6 have higher

concentrations of Co, Fe and REY, which suggests they have accumulated metals from overlying seawater (e.g. Dubinin & Rimskaya-Korsakova, 2009, Bonatti et al., Bonatti et al., 1972). In support of this, Mn/Al and Ni/Al ratios are higher in our sediments than in NASC, with $(Mn/Al)/(Mn/Al)_{NASC}$ of ~20 in the UK Claim area and ~5 in APEI-6, and $Ni/Al)/(Ni/Al)_{NASC}$ of ~11 in the UK Claim area and ~3 in APEI-6. Co and the REY are also enriched relative to NASC by, respectively, a factor of ~4 and ~3 in the UK Claim area and by a factor of ~5 and ~2 in the sediments from APEI-6. Fe is slightly enriched in sediments from both areas, by a factor of ~1.5 (Figure 13).

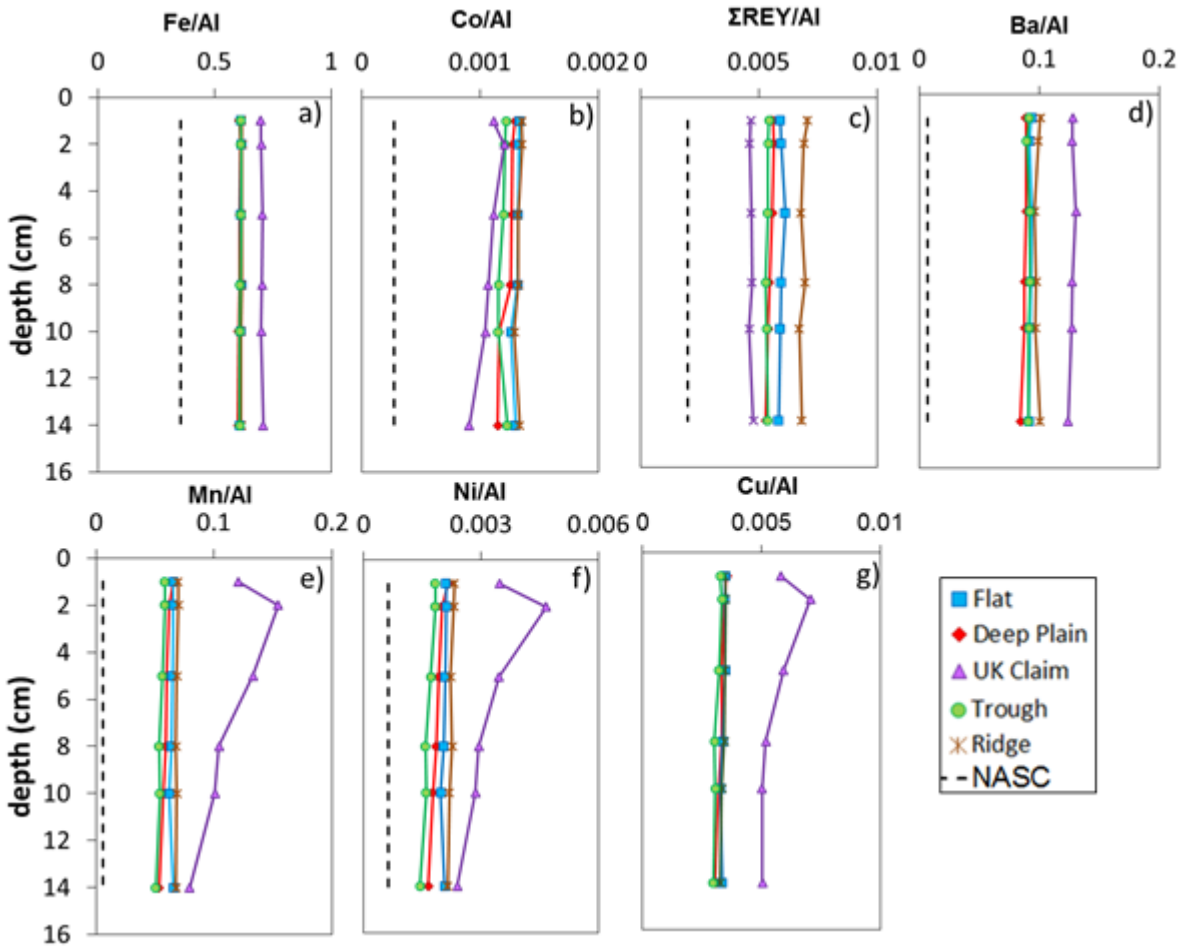

Figure 13. Aluminium-normalised profiles of a) Fe, b) Co, c) ΣREY, d) Ba, e) Mn, f) Ni and g) Cu for the upper 14 cm of the sediment column. Black dashed lines show element/Al ratios for NASC when available (Gromet et al., 1984).

The proportion of Mn that can be easily mobilized from the sediments is highest in the uppermost sediments from the UK Claim area (Figure 16). The Mn/Al ratio of these sediments is also relatively high, which may suggest the proximity of a redox boundary, where Mn^{2+} produced in the lower, oxygen-poor sediments, precipitates. At present, however, the oxic/anoxic boundary within the sediments

from the UK Claim area is located at much deeper depths below the seafloor, around 1 m. Thus this horizon most likely represents a former redox boundary, as observed in sediments from the nearby German Claim Area (Mewes et al., 2014). This Mn-rich layer may represent a former horizon of nodule growth, when the OPD was located at a shallower depth. The depth of the OPD is likely influenced by biological surface productivity (e.g. Halbach et al., 1981; Hein et al., 2015), so fluctuations in primary productivity in the past could have affected the mechanism of nodule growth.

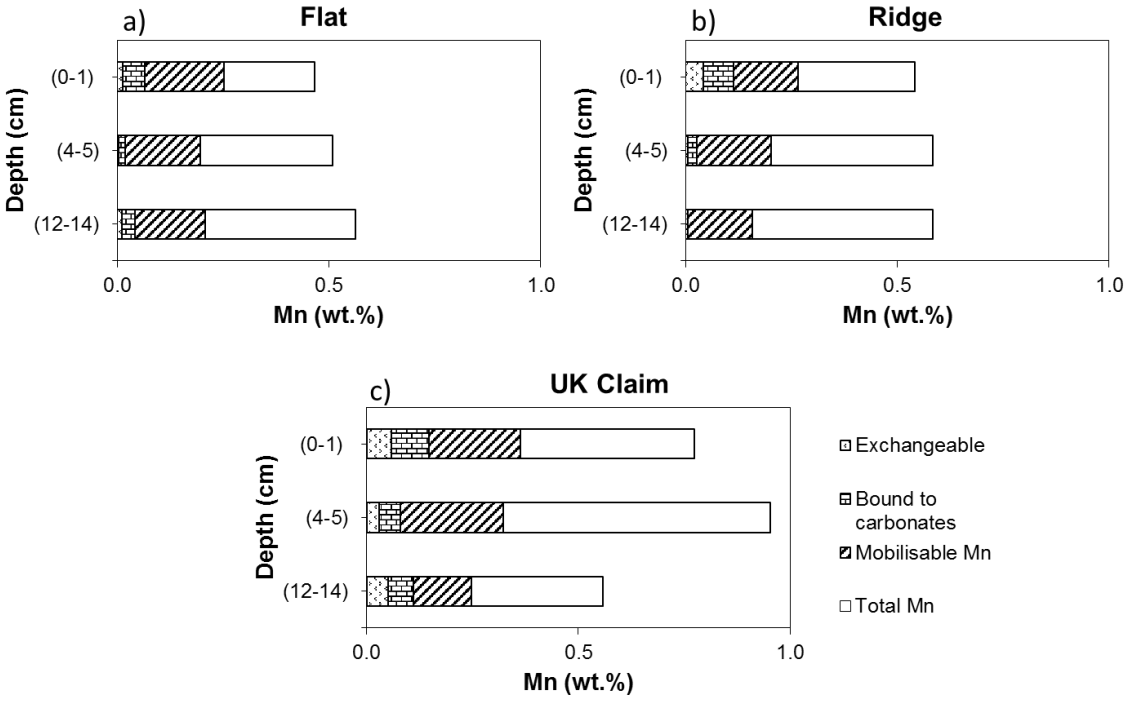

Figure 14. Amount of Mn released during sequential leaching of sediments from a) APEI-6 Flat, b) APEI-6 Ridge and c) the UK Claim area.

The REY distribution pattern in sediments from both areas shows that they must also contain a biogenic Ca-phosphate component (Figure 15). The sediments have a pronounced Ce anomaly, are enriched in the HREE relative to the LREE and have high Y/Ho ratios, equivalent to REY patterns in biogenic apatite (e.g. Elderfield et al., 1981; Dubinin & Sval'nov 2002; Yasukawa et al., 2016). The sediments are also enriched in the middle REEs (MREEs, Sm, Eu, Gd) (Fig. 15), which is likely due to diagenetic reworking of apatite phases (Bright et al., 2009; Zhang et al., 2016). Concentrations of P are highest in the sediments from the ridge are of APEI-6, likely due to better preservation of apatite material (e.g. Yasukawa et al., 2016). The importance of biogenic Ca-phosphates for regulating REY concentrations is

confirmed by statistical factor analysis (Table 7; Figure 12b). I also note that there is a clear positive relationship between REY and P (see Appendix A.6. in Suppl. Info) in other sediments from the Pacific Ocean (Kato et al., 2011).

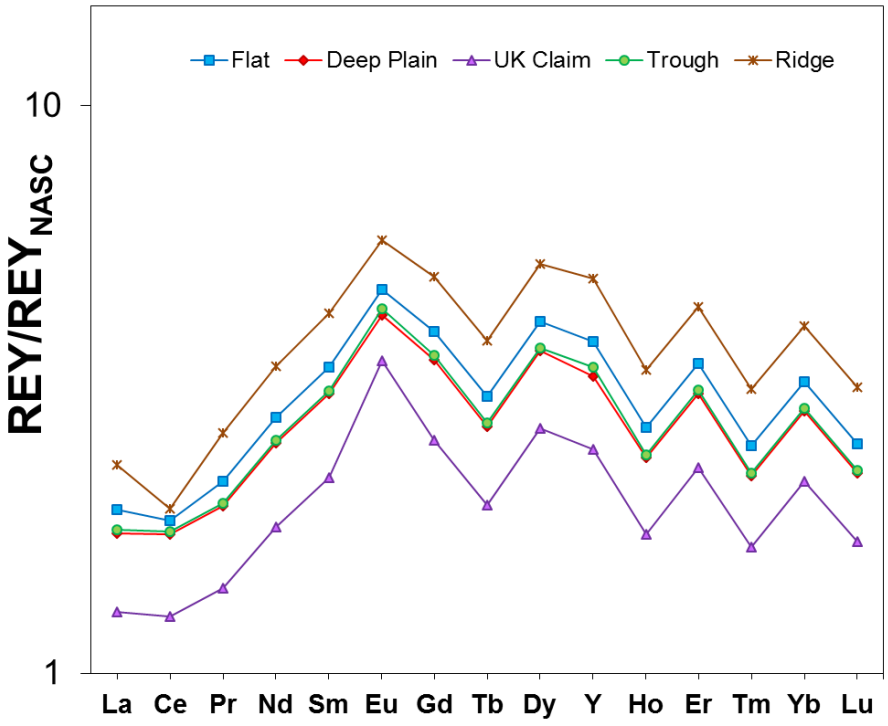

Figure 15. REY distribution patterns in sediments from the UK Claim area and APEI-6, normalised to North America Shale Composite (NASC; Gromet et al., 1984).

There is a positive correlation between the Fe content of the sediments and ΣREY (Fig. 12a), which implies that the REY are incorporated into Fe-(oxyhydr)oxide phases. Notably, sediments from the UK Claim have significantly lower ΣREY, likely due to the presence of oxic diagenetic phases that are less likely to incorporate the REY (Haleyal et al., 2004; Bau et al., 2014). In support of this, statistical factor analysis shows a very poor correlation between Mn and the REY (Table 7), and the leaching experiments show that only up to ~15% of the ΣREY are associated with easily mobilisable Mn-oxides (Figure 14).

4.5.4. Temporal evolution of nodule growth

As discussed in Section 4.5.1, nodules from both APEI-6 and the UK Claim area principally acquire metals from seawater, although some parts of nodules from the UK Claim area also acquire metals from sediment pore waters, facilitated by a shallower OPD, and consequently they have faster growth rates (Lyle, 1982; von Stackelberg, 2000). By contrast, in the German Claim area of the CCFZ, large- and medium- sized nodules are associated with a deeper OPD, and nodules are thought to grow to a larger size because of a lower sedimentation rate (Mewes et al., 2014). We did not assess the sedimentation rates in the UK Claim and APEI-6 areas, but it is likely that the shallower OPD in the UK Claim area is due to a greater availability of organic matter in the sediments due to its proximity to the equatorial belt of high primary productivity (Fig. 16). The Ba content of the sediments can serve as a proxy for the organic matter content due to its strong association with particulate organic carbon (Dymond et al., 1992). To this end, Ba concentrations are higher in sediments from the UK Claim area relative to NASC by a factor of ~18, and by a factor of ~13 in the sediments from APEI-6 (Figure 13d).

This model of nodule growth is similar to that proposed by Hein et al (2015), in which the highest grades of Cu, Mn and Ni in nodules are found in diagenetic nodules in areas of high primary productivity (Cronan, 2006; Verlaan et al., 2004). The high productivity in the surface waters increases the organic carbon content of the seafloor sediments, increasing the rate of oxygen consumption such that the OPD is located relatively close to the sediment-seawater interface (e.g. Koschinsky et al., 2001). At present, bottom waters in the CCFZ are highly oxygenated (~130 µmol/l; (Rühlemann et al., 2010) but the presence of oxic and suboxic diagenetic layers within the nodules from the UK Claim area suggest that this situation may have been different in the past. Based on the average growth rate estimated for nodules from the UK Claim area (~6.53 mm/Ma; Table 6), and their average diameter (~11 cm), the diagenetic growth of the nodules started (assuming there was no hiatus in growth) ~17 Ma ago. By comparison with present-day conditions, diagenetic nodule formation in the vicinity of the UK Claim area would have been most favorable when the area was located closer to the Equator than it is today, at ~9.5˚N (Figure 11; von Stackelberg et al., 1991). This places it closer to the edge of the equatorial belt of high primary productivity that, combined with relatively low sedimentation rates, provides optimal conditions for the growth of diagenetic nodules (von Stackelberg et al., 1991). By

contrast, nodules from APEI-6 have remained outside of the high productivity zone throughout their genesis (Figure 16).

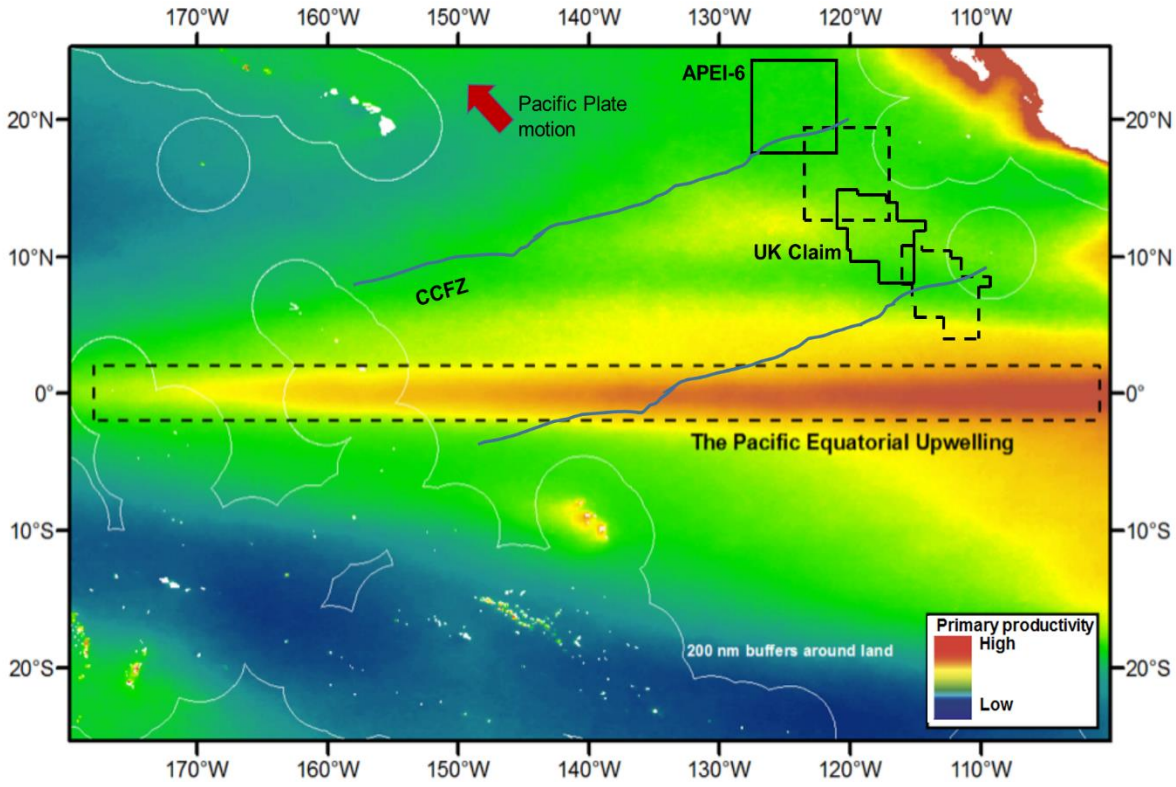

Figure 16. Distribution of primary productivity in the central Pacific Ocean. The present day locations of the UK Claim area and APEI-6 are also shown, together with their approximate locations in the Early-Middle Miocene and the approximate direction of the Pacific Plate motion. Figure modified from www.gobi.org.

Basing on the current spreading rate of the East Pacific Rise (~11 cm/yr; Tyler & Walker, 1996), it can be estimated that the UK Claim area was located in this latitude at ~15 Ma ago. This age is similar to the minimum age of the nodules estimated using the Co-growth method, which provides reassurance that the Co-growth method can be applied to determine nodule growth rates in this area.

4.5.5. Resource potential of nodules

The average ΣREY, Mn, Co, Ni and Cu content of the APEI-6 and UK Claim are nodules is given in Table 13. The average nodule resource in each area can be estimated from box core sampling together with measurements of nodule dimension; these data are also given in Table 13. My calculations indicate that the UK Claim area could supply up to ~66 years of the global demand for Mn, up to ~50 years of the global demand for Co and ~23 years of the global demand of the REY. Nodules from APEI-6 could also make a significant contribution to satisfying

global demands for the REY, Co and Mn, respectively, up to ~4, ~13 and ~7 years. Nodules from both areas yield relatively small quantities of Ni and Cu, providing up to ~3% and ~140% of the global annual demand of these elements.

Resource		APEI-6	UK Claim
	Avg. nodule resource (kg/m^2)	0.7-2.6	1.7-57
	Area (km^2)	160000	60000
Mn	Avg. content (ppm)	271500	309667
	Mass of Mn ($T*10^5$)	304-1130	316-10600
	Years of supply[a]	1.90-7.06	1.97-66.2
REY	Avg. content (ppm)	1120 ± 207	715 ± 141
	Mass of REY ($T*10^5$)	1.26-4.67	0.73-24.4
	Years of supply[b]	1.19-4.44	0.69-23.3
Co	Avg. content (ppm)	2770 ± 200	1300 ± 100
	Mass of Co ($T*10^5$)	3.11-11.5	1.33-44.5
	Years of supply[c]	3.57-13.3	1.52-51.1
Ni	Avg. content (ppm)	12400 ± 1600	11600 ± 1500
	Mass of Ni ($T*10^5$)	13.9-51.8	11.8-396
	Years of supply[d]	$(0.92\text{-}3.53)*10^{-3}$	$(0.08\text{-}2.70)*10^{-2}$
Cu	Avg. content (ppm)	9220 ± 170	9300 ± 190
	Mass of Cu ($T*10^5$)	10.3-38.3	9.49-318
	Years of supply[e]	$(0.4\text{-}1.7)*10^{-1}$	0.04-1.41

Table 13. Average Co, Ni, Cu and ΣREY content of APEI-6 and UK Claim nodules, and estimated resource. [a]=Based on 2015 Global Annual Consumption (GAC) of 16 mT (International Manganese Institute, IMnI, www.manganese.org); [b]=Based on 2012 GAC of 105000 T (Hatch, 2012; Alonso et al., 2012); [c]=Based on 2015 GAC of 87000 T (Cobalt Development Institute, CDI, www.thecdi.com/); [d]= Based on 2010 GAC of 1465 mT (International Nickel Study Group, INSD, www.insg.org); [e]=Based on 2015 GAC of 22.5 mT (CME Group, http://www.cmegroup.com).

Although nodules from APEI-6 have much higher REY concentrations than nodules from the UK Claim area, the larger size of the nodules from the UK Claim area nevertheless makes them a more attractive resource. My study shows that differences in the chemical composition of nodules occurs over distances of less than ~500 km (the distance between APEI-6 and the UK Claim area), which is smaller than the 1000 km length scale previously predicted (Smith & Koslow, 2007).

4.6. Conclusions

The bulk chemical compositions of nodules from APEI-6 and the UK Claim area are similar, but detailed analysis of individual microlayers within the nodules reveals wide variations in their chemistry. Nodules from the UK Claim area contain layers that have relatively high Mn/Fe, and high concentrations of Ni, Cu and Zn, while layers within nodules from APEI-6 tend to be more enriched in Fe, Co and the REY. This reflects differences in the mechanism of nodule growth within the CCFZ; the smaller nodules from APEI-6 mainly form by hydrogenous precipitation, whereas larger nodules from the UK Claim also contain layers that form from oxic and possibly sub-oxic sediment pore waters. These layers are concentrated in the innermost part of the nodules.

Today, the OPD in the UK Claim is located at ~1m below seafloor, and in APEI-6 it is located at >3 m below seafloor. I therefore propose that the innermost, high Mn/Fe layers found in nodules from the UK Claim area formed during the Early-Middle Miocene when the area was located closer to the equatorial belt of high surface biological productivity. This timing is consistent with the estimated growth rate of these nodules.

Because of their larger size, the resource potential of the nodules from the UK Claim is higher than that of nodules from APEI-6. Nevertheless, my data reveal that there are small-scale (<500 km) variations in the chemical composition of nodules and nodule density both within APEI's and individual claim areas. Although the bulk chemistry of nodules from the UK Claim area and APEI-6 are similar, there are subtle differences in their mechanisms of formation that mean that APEI-6 may not represent an effective geochemical baseline for the effects of future mining operations in the UK Claim area. It is, however, suitable for assessing the effects of mining in other areas that contain relatively small nodules, such as parts of the German claim area.

Chapter 5: Genesis of ferromanganese deposits in the Atlantic, Pacific and Arctic Oceans

Abstract

Deep sea polymetallic deposits such as nodules and crusts are known to contain significant amounts of economically interesting metals such as Co, Ni, Cu and ΣREY. Some of these metals are crucial in the development of many emerging and new generation technologies. However, the resource potential of these deposits is variable, and likely related to environmental conditions that prevail as they form. To better assess the environmental controls on the resource potential of ferromanganese deposits, I have undertaken a detailed study of the chemical composition of ferromanganese nodules and one crust sample from different oceanic regions.

Medium-sized nodules from the North Atlantic have a rather constant chemistry and massive compact texture, with Mn/Fe ratios of ~ <1.5 and high ΣREY of ~4000 ppm, which suggests that they acquire metals from a hydrogenous source. On the other hand, nodules from the Pacific Ocean show great variability in their chemistry and textures, with dark, Fe-Mn rich layers alternating with bright areas with Mn/Fe ratios of ~80 and high Ni+Cu (>3 wt. %). The latter parameters are characteristic of diagenetic deposits that acquire metals from sub-oxic sediment pore waters. A nodule from the Arctic Ocean shows the greatest variability in textures; from planar dense layers to dendritic diagenetic areas, all of which incorporate large quantities of detrital silicate material. This nodule has low Ni+Co+Cu and REY. The ferromanganese crust from the Pacific Ocean has relatively constant Mn/Fe (~2) and ΣREY of ~2500 ppm. The sample shows evidence for secondary phosphatization; it is enriched in Y and SEM elemental mapping reveals areas impregnated with Ca-P mineral, likely calcium phosphate. Hydrogenous nodules and crusts represent an economically important source of Co and the REY; these nodules are found in the central deep ocean basins, where the oxygen penetration depth into sediments is deep. Diagenetic nodules have higher concentrations of Ni and Cu, but their relatively fast growth rate means

that they represent a marginal resource of these metals. Shallow water nodules are not an important metal resource.

5.1. Introduction

Marine ferromanganese deposits (including polymetallic nodules and crusts) are important resources of metals such as Co, Ni, Cu, Mo, Li and Te, as well as the rare earth elements and yttrium (REY) (Hein et al., 2013). They are distributed throughout the world's oceanic sedimentary basins, but their chemical and mineralogical compositions, and hence their resource potential can be variable (e.g. Glasby, 1973; Halbach et al., 1981; Cronan, 2000; Hein et al., 2000; Koschinsky & Hein, 2003; Bau et al., 2014).

Polymetallic ferromanganese nodules occur in the deepest parts of the ocean basins, at depths ranging between 4000-6000 m (Zhang et al., 2012). Ferromanganese crusts by contrast usually form on the top of seamounts. Both types of deposits have a complex internal structure, and form extremely slowly (~1 mm/Ma; Opdyke & Foster, 1970) by deposition of Fe- and Mn-rich microlayers around a nucleus. These microlayers have distinct chemical and mineralogical compositions that reflect the environmental conditions in both the ocean and its sediments at the time of deposition. Three different types of deposit have been recognised: (1) hydrogenous, whereby the deposit acquires metals from the overlying oxic water colum (Halbach et al., 1988); (2) diagenetic, whereby metals are acquired from either oxic or suboxic sediment pore waters (Reyss et al., 1985); and (3) hydrothermal, where hydrothermal vent fluids are the principal source of metals (Kuhn et al., 1998). The chemical and mineralogical composition of ferromanganese crusts can also be modified after deposition by diagenetic processes including phosphatization (e.g. Halback & Puteanus, 1984).

Hydrogenous deposits typically have rather low Mn/Fe ratios, ≤ 3, and low quantities of Ni+Cu, whereas diagenetic deposits have higher Mn/Fe (3 to > 10) and high Ni+Cu (Halbach et al., 1981). Hydrothermal deposits, in turn show the lowest average Mn/Fe ratios, of < 1, as well as the lowest content in trace metals (Kuhn et al., 1998; Hein et al., 1997).

The REY composition of the deposits can also be a useful tracer of the environment of deposition. Hydrogenetic nodules and non-phosphatized crusts tend to have positive Ce anomalies, negative Y anomalies and high Nd concentrations (> 100 ppm), whereas diagenetic precipitates usually have

negative Ce anomalies, negative Y anomalies, and intermediate Nd concentrations of between 10 and 100 ppm (Bau et al., 2014).

Although the REY content of hydrothermal deposits is highly variable (e.g. Kuhn et al., 1988), these deposits tend to have negative Ce anomalies, positive Eu and Y anomalies, and are strongly depleted in the light rare earth elements (LREE) relative to the heavy rare earth elements (HREE) (e.g. Mills et al., 2001, Kuhn et al,. 1988). Phosphatized crusts can be identified by positive Ce and positive Y anomalies, and depletion in the light rare earth elements (LREE) relative to the heavy rare earth elements (HREE) (Bau et al., 2014).

Mechanisms of formation of ferromanganese deposits are usually assessed on the basis of analysis of bulk samples. However, it is now clear from studies of nodules from the eastern equatorial Pacific (Clarion-Clipperton Fracture Zone and Peru Basin) that there can be huge differences in the compositions of the individual layers that make up a deposit (Wegorzewski & Kuhn, 2014), due to changes in the environment of deposition over time. Thus, to better evaluate the environmental controls on the resource potential of deep-ocean ferromanganese deposits, I have undertaken detailed geochemical and textural studies of individual layers within deposits from different environmental settings within the North Atlantic, Central and South Pacific and Arctic Oceans.

5.2. Samples and analytical methods

5.2.1. Samples

Nodules and crusts for this study were acquired at a number of locations in the North East and West Atlantic, South and Central Pacific and the Clarion Clipperton Fracture Zone (CCFZ; eastern equatorial Pacific Ocean) and the Kara Sea (Arctic Ocean) (Figure 1; Table 1). Samples E ATL-N4 and NAP-N4 were supplied by the British Ocean Sediment Core Facility (BOSCORF), samples EW9602-09RD and RC12-192GS came from the Lamont-Doherty Earth Observatory, New York (LDEO), sample N29 was supplied courtesy of the P.P. Shirshov Institute of Oceanology (Russia) and sample JC120-104 was collected from CCFZ (UK Claim Area) during the RRS James Cook cruise JC120 in spring 2015.

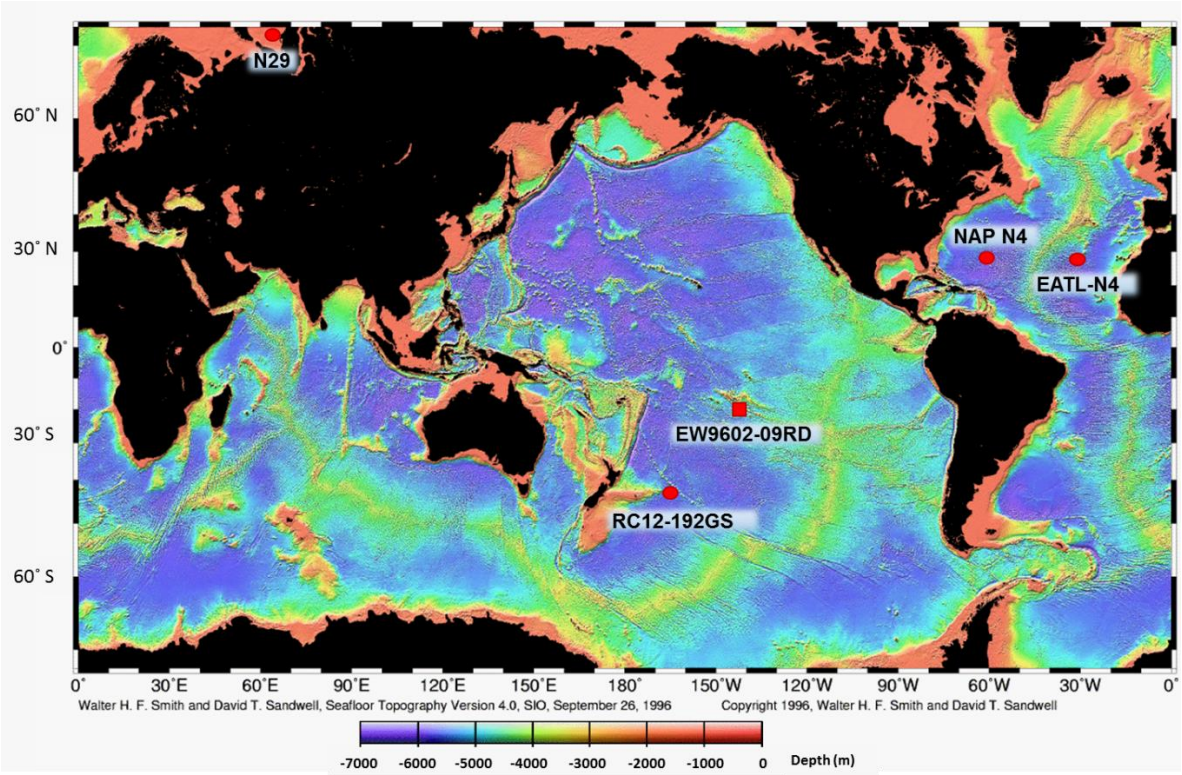

Figure 1. Location of crust and nodule samples used in this study. Seafloor topography is from Smith & Sandwell (1996), National Oceanographic and Atmospheric Administration (NOAA).

Sample	Lat (°N)	Long (° E)	Location	Water depth (m)	OPD (m)	Description
			Pacific			
EW9602-09RD	-27.0	-143.2	Taukina Seamount (Cook-Austral volcanic chain)	1520-1540	~75[a]	~3 cm botryoidal crust around volcanic clast
JC120-104	13.3	-116.3	UK claim area, CCFZ	4130	~1[b]	~15 cm nodule, low sphericity, irregular bottom
RC12-192GS	-39.5	-157.7	Southwest Pacific Basin	4830	~75[a]	~1 cm nodule, low sphericity
			Atlantic			
EATL N4	31.2	-25.2	Great Meteor East	5100-5400	>3[c]	~3cm, round, smooth nodule
NAP N4	23.5	-63.0	NW Atlantic	5900-6200	~18[d]	~3cm, round, smooth nodule
			Arctic			
N29	75.5	89.4	Kara Sea	0-100	~0.5[e]	~5cm flat nodule

Table 1. Location, water depth and description of samples. [a] D'Hont et al., (2015); [b] In situ measurements onboard the JC120 (May 2015); [c] Buckley, (1988); [d] Rutgers & Van der Loeff (1990); [e] Rozanov, (2014).

The nodules range in size from ~1cm to ~15cm in diameter; the smaller nodules are generally rounded and have a smooth surface, whereas the larger nodules have a more lumpy (botryoidal) appearance (Fig. 2). The nodule from the Kara Sea in the Arctic Ocean (sample N29) by contrast is relatively flat and has a discoid shape with a long axis of ~7 cm (Figure 2f).

The ferromanganese crust sample EW9602-09RD (Fig. 2f) was dredged from a seamount from the western part of the Challenger Fracture Zone. It has a botryoidal, slightly irregular appearance.

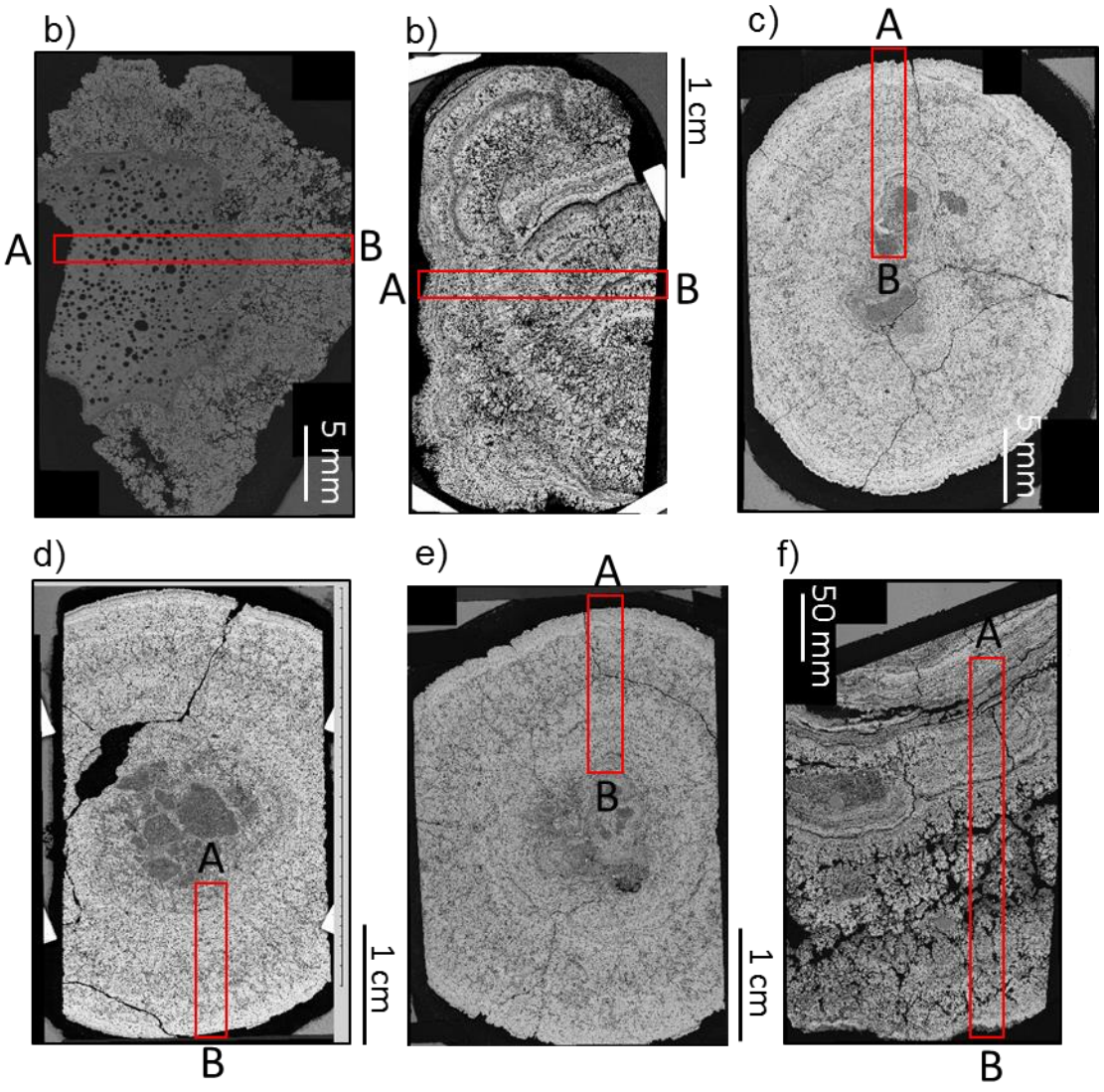

Figure 2. Backscattered (BSD) images of crust and nodule sections: a) EW9602-09RD, b) JC120-104, c) RC12-192GS, d) NAP N4, e) EATL N4, f) N29. Red squares denote A to B areas where SEM elemental mapping was performed.

5.2.2. Analytical methods

5.2.2.1. Scanning electron microscopy

The crust and the nodules were prepared for SEM analysis by sectioning, and grinding and polishing until a flat surface was obtained. Sections were then ground down to a thickness of ~100 mm, and mounted onto a glass sample holder.

SEM work was carried out at the University of Southampton using a LEO1450 Variable Pressure Scanning Electron Microscope. The microstructure of the sectioned crusts and nodules was assessed using both a secondary electron detector (for topographic imaging) and a backscattered electron detector (for compositional analysis). Major element concentrations were determined using energy-dispersive X-ray spectroscopy (EDS; Oxford Instruments X-Act with Silicon Drift detector) combined with Aztec Energy software. Analyses were conducted at 20 kV, using a probe current of 700 pA and a working distance of 15 mm. The probe current was calibrated on a Faraday cup, and element concentrations were calibrated against various mineral standards from Micro-Analysis Consultants Ltd, Cambridge, UK, and the Natural History Museum, UK. A basalt glass standard reference material (BRR-1) was used to monitor the accuracy of the analyses. Elemental maps were made using a nominal probe current of 2.5-3.0 nA.

5.2.2.2. Laser ablation inductively coupled plasmas mass spectrometry (LA ICP-MS) analysis

Laser ablation ICP-MS analyses were used to assess element concentrations in individual layers within the crust and nodules. The analyses were carried out on 100 μm-thick polished sections, prepared as described in Section 2.2.1. Polished chips of NIST 610, NIST 612 and NIST 614 glass standard reference materials were mounted on a glass sample holder. Analyses were conducted at the University of Southampton using a 193 nm excimer laser (New Wave Research model UP193X) coupled to a quadrupole ICP-MS (Thermo X-Series II). Element concentrations of major elements (Mn and Fe) and trace elements (Ti, V, Co, Ni, Cu, Zn, Ba, Th and U) and REY (La, Ce, Pr, Nd, Sm, Eu, Gd, Tb, Dy, Y, Ho, Er, Tm, Yb and Lu) were determined on 50 – 75 μm diameter spots targeting individual layers in the nodules. Ablations were conducted with a laser power of ~75% and a repetition rate of 5 Hz, in a He atmosphere. For each analysis, the gas blank was measured first with the laser beam blocked by a shutter. The shutter was then

removed, and the transient signals from the analyte were collected for the ablation period. Raw counts were processed off line using standard spreadsheet software, and counts were calibrated using pressed pellets of nodule reference materials NOD-A-1 and NOD-P-1. The accuracy and reproducibility of the measurements was assessed by multiple (n=60) analyses of NIST 614, NIST 612 and NIST 610 certified reference material. The external reproducibility of the analyses was better than ±9 % for the major elements, better than ±10 % for most of the trace elements and better than 7± % for most of the REY, except for Ni (±21%), Cu (±17%), Zn (±13%), Nd (±9%), Sm (±8%) and Gd (±10%). Measured concentrations were within the certified or recommended values for all elements except Ti (±20%), Mn (±25%), Fe (±16%), Ni (±11%), and Zn (±27%).

5.3. Results

5.3.1. Internal structure of nodules and crust

Backscatter images (Figs. 3-8) reveal that the nodules and crust have layered growth patterns that tend to be concentric in the smaller nodules (EATL N4, NAP N4 and RC12-192) but more complex and irregular in the larger nodules and the crust. Individual layers are distinguished by differences in reflectivity, with dark, low reflectivity layers alternating with light, highly-reflective layers.

Nodule JC120-104 (Figure 3) is characterised by multiple nucleation centres that result in an irregular distribution of layers. The central part of the section shown in Fig. 3 is characterised by dendritic Mn-rich oxides that appear bright in the backscatter image, surrounded by pore spaces that are generally filled with aluminosilicate or Ca-phosphate detrital material. By contrast, the edge of the nodule consists of parallel layers of Mn-Fe oxides that have low reflectivity and are often intercalated with detrital aluminosilicate material. Aluminosilicate material can also found filling in cracks within the nodule structure.

The crust sample (EW9602-09RD; Figure 4) is composed of a large porous basaltic glass fragment on which finely crystallised Fe-Mn oxides have precipitated in a dendritic pattern. Some of the pores in the basaltic glass are empty and rimmed by aluminosilicate material that is likely a product of alteration. Other pores are filled in with Ca-phosphate. At the contact between the glass and the Fe-Mn crust, there is an Al-rich alteration front (Figure 4c). The Fe-Mn oxides beyond the alteration front are finely crystalline and have high reflectivity (Figure 4a), and Fe-oxides (usually in the form of detrital silicates) can be observed filling the pore

spaces (Figure 4c). Sub angular aluminosilicate clasts are common in the pore spaces towards the outer part of the crust structure.

Nodule samples RC12-192GS (Figure 5), EATL N4 (Figure 6) and NAP N4 (Figure 7) have similar morphological and chemical characteristics. They are composed by finely crystallised Fe-Mn oxides that appear bright in backscatter images, have a massive structure and surround a nucleus composed of multiple silicate-rich (e.g. Figure 5c), aluminosilicate (Figures 5, 6 and 7c) or Ca-phosphate (Figures 5, 6 and 7c) clasts.

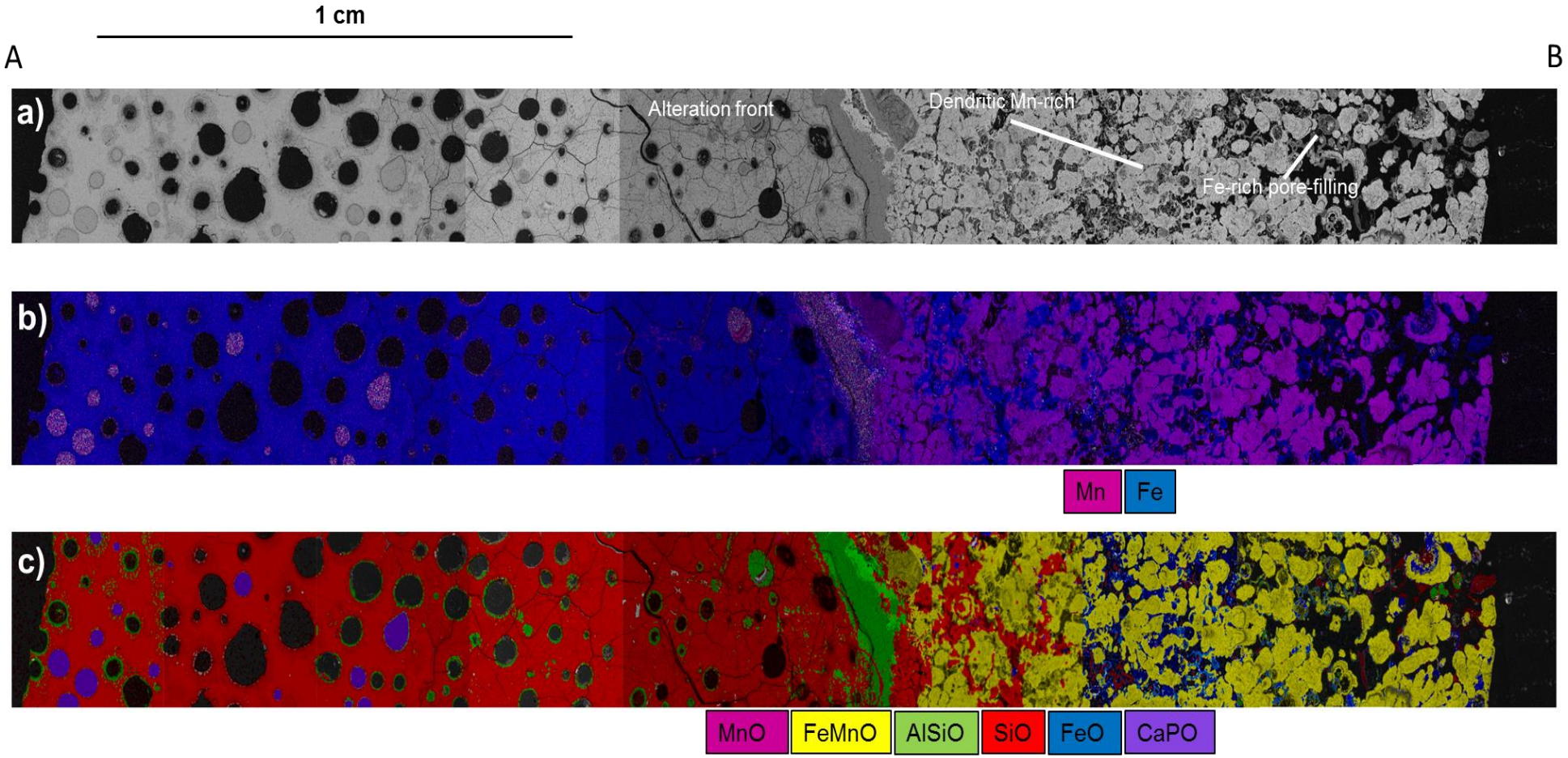

Figure 3. Microtextures and element distribution for crust sample EW9602-09RD (South Pacific Ocean). a) Backscattered (BSD) image; b) Fe-Mn distribution; c) phase distribution.

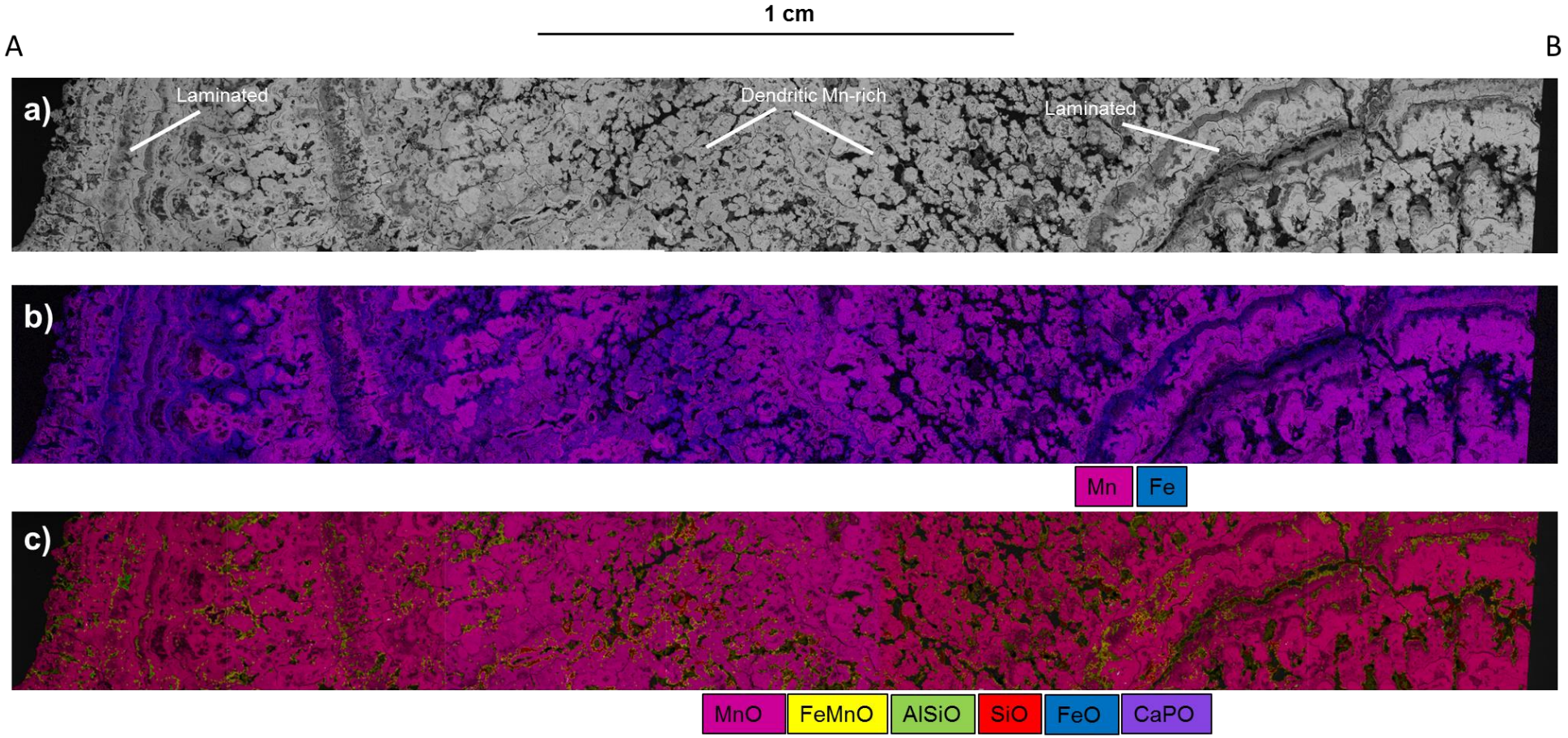

Figure 4. Microtextures and element distribution for nodule sample JC120-104 (CCFZ, Central Pacific Ocean). Side A represents the outer part of the nodule, migrating inwards towards B. a) Backscattered (BSD) image; b) Fe-Mn distribution; c) phase distribution.

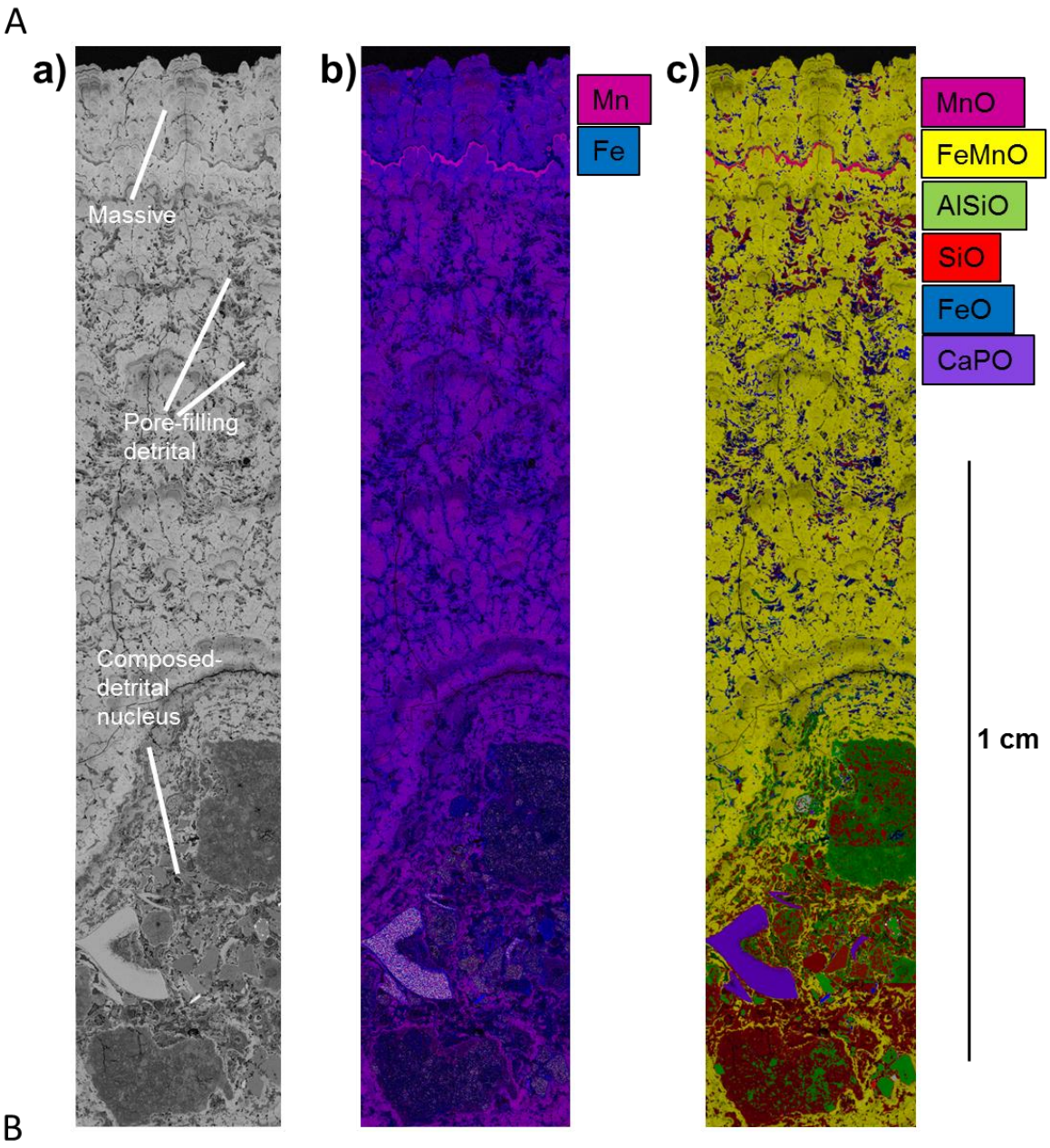

Figure 5. Microtextures and element distribution for nodule sample RC12-192GS (South Pacific Ocean). a) Backscattered (BSD) image; b) Fe-Mn distribution; c) phase distribution.

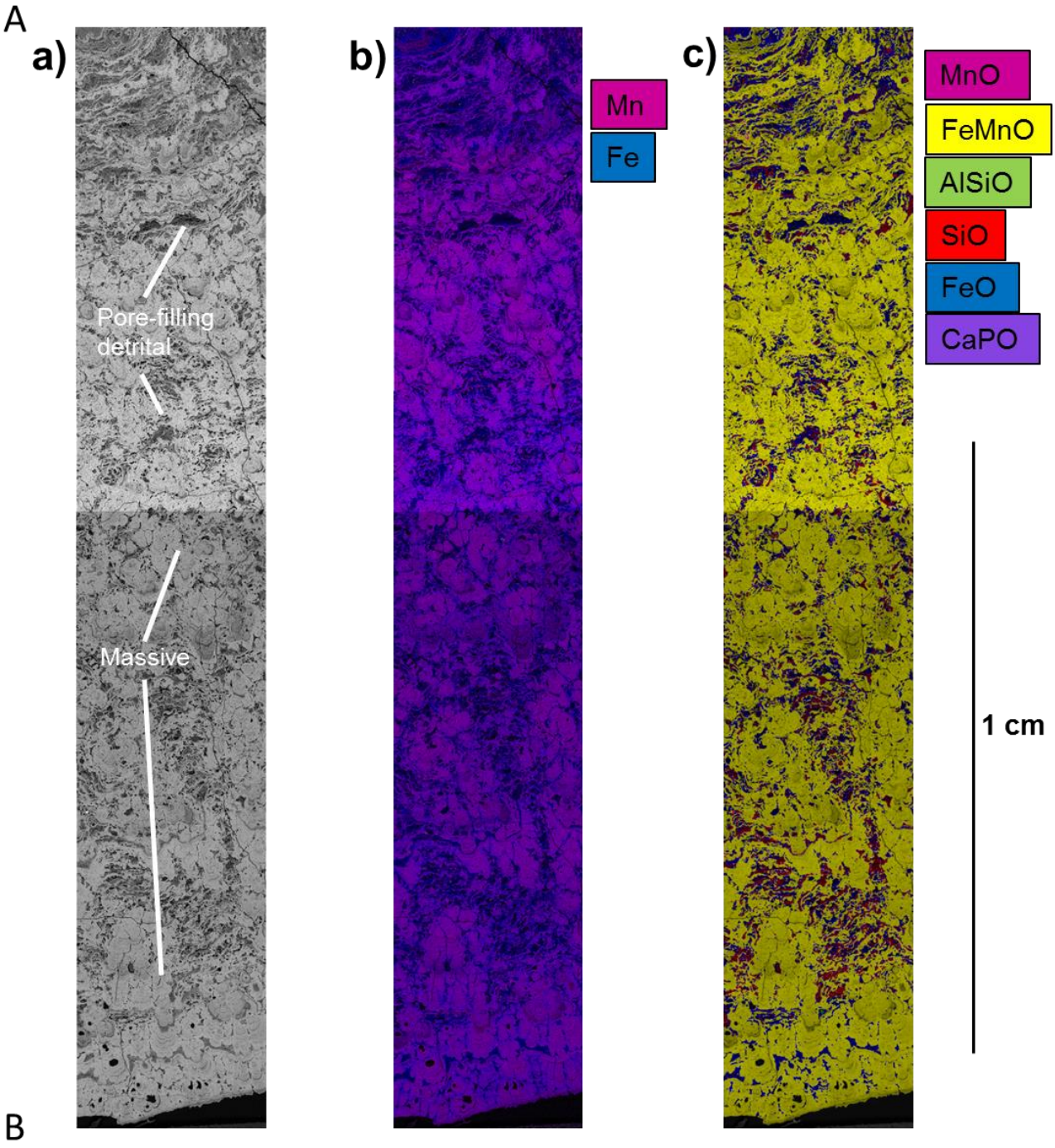

Figure 6. Microtextures and element distribution for nodule sample NAP-N4 (Northwest Atlantic Ocean). a) Backscattered (BSD) image; b) Fe-Mn distribution; c) phase distribution.

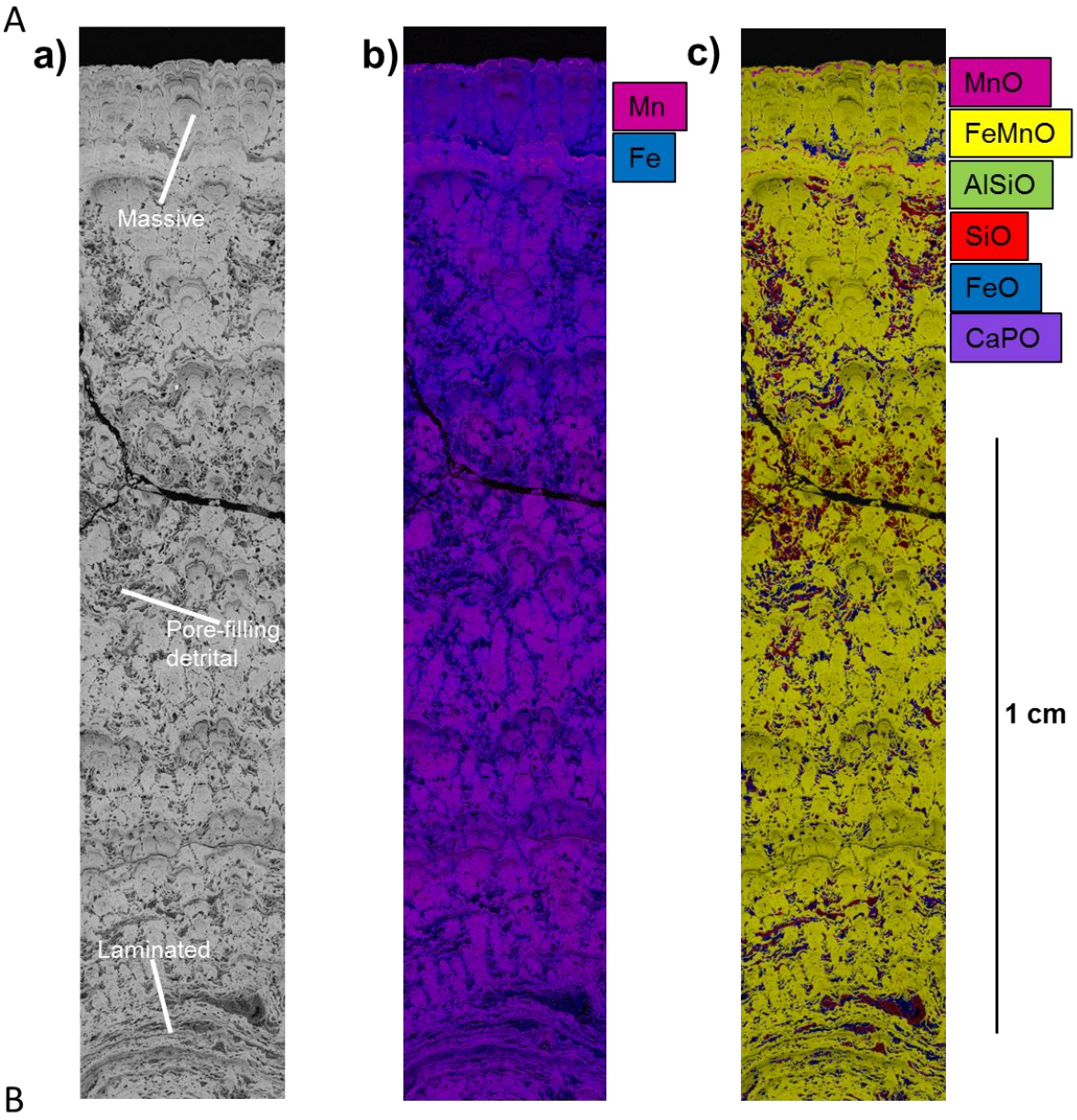

Figure 7. Microtextures and element distribution for nodule sample EATL-N4 (East Atlantic Ocean). a) Backscattered (BSD) image; b) Fe-Mn distribution; c) phase distribution.

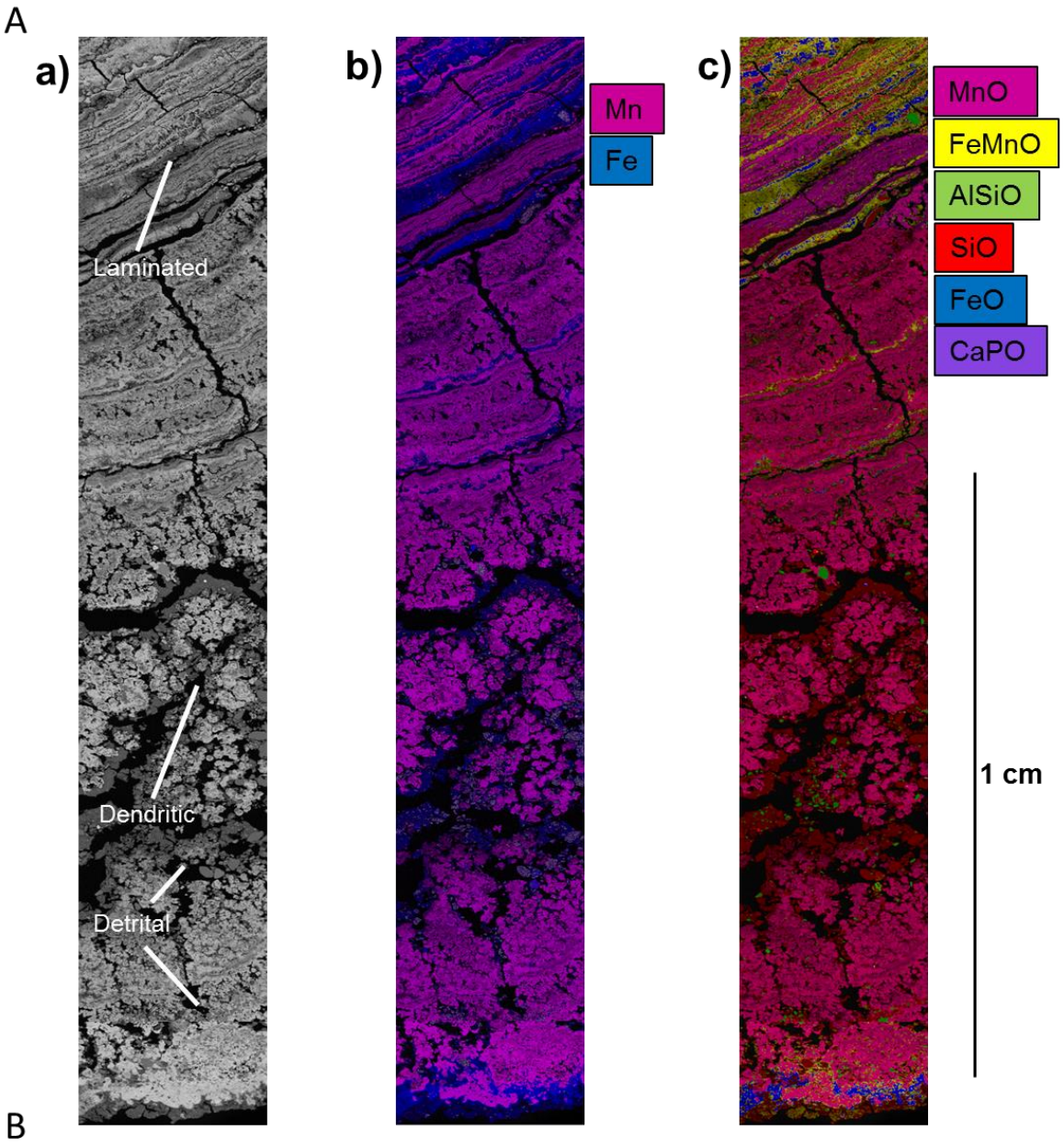

Figure 8. Microtextures and element distribution for nodule sample N29 (Kara Sea, Arctic Ocean). a) Backscattered (BSD) image; b) Fe-Mn distribution; c) phase distribution.

Fe-rich aluminosilicate detrital particles of low reflectivity can be found in pores and cracks throughout the nodule structure. Highly reflective thin Mn-oxide rich layers are also sparsely present in the nodules (Figures 5 and 6c).

Nodule sample N29 (Figure 8) is characterised by large dendritic Mn-rich structures infilled with detrital aluminosilicate material. The Mn-rich oxides overlap the nucleus, and alternate with Fe-Mn oxide-rich layers of lower

reflectivity (Fig. 8c). Fe oxides occur in discrete layers both towards the edge of the nodule and towards the nucleus.

5.3.2. Chemical composition of internal layers

Laser ablation analyses shows that nodule layers with low reflectivity have relatively low Mn/Fe ratios (< 3) and low Ni+Cu (< 1.5 wt. %), and relatively high concentrations of Co (> 0.2 wt. %) and REY (> 1600 ppm). By contrast, layers with high reflectivity have high Mn/Fe ratios (> 3) and high Ni+Cu (> 1 wt. %), but low Co (< 0.2 wt. %) and low REY (< 1600 ppm) (Tables 2 and 3).

The nodule from the CCFZ (JC120-104) has the highest average Mn/Fe ratio (~8.8); this nodule incorporates layers that have extremely high Mn/Fe, up to ~80, as well as layers with lower Mn/Fe, ~1.6. Ni, Cu and Zn also show high concentrations in the high Mn/Fe layers (~1.10 wt. %, ~0.90 wt. % and ~3740 ppm, respectively), and lower concentrations in the low Mn/Fe layers (~0.4 wt. %, 0.18 wt. % and ~617 ppm).

Atlantic nodules NAP N4 and EATL N4 have relatively low average Mn/Fe, ~1.2 and ~1.4 wt. %, respectively. Some layers are moderately enriched in Mn relative to Fe, with Mn/Fe of ~8.9. These nodules have relatively high concentrations of Co (~0.6-0.5 wt. %), Ti (~1.1-1 wt. %), V (~721-680 ppm), Th (~140-130 ppm) and U (11.4-10.4 ppm).

The crust sample has highest concentrations of both Mn (~42 wt. %) and Fe (~24 wt. %), and there is little variation in the Mn/Fe ratio of individual layers, ranging from ~1.3 to ~2.8. The crust has relatively high concentrations of Co (~0.7-3.7 wt. %), Ti (~1.7-2.1 wt. %), V (~840-1170 ppm) and Ba (~2570-2900 ppm).

South Pacific nodule sample RC12-192GS mainly consists of low Mn/Fe layers (~1.5-1.7), although a few layers have slightly higher Mn/Fe (up to ~6). Layers with higher Mn/Fe also tend to have high Ni+Cu and Zn (~3.14 wt. % and ~1310 ppm, respectively), whereas the layers with low Mn/Fe tend to have higher Co (~0.38 wt. %), Ti (~0.7-1.2 wt. %) and Ba (~1290-3510 ppm).

		Mn wt. %	Fe wt. %	Co wt. %	Ni wt. %	Cu wt. %	Ti wt. %	V ppm	Zn ppm	Ba ppm	Th ppm	U ppm	Mn/Fe	GR (mm/Ma)
Sample	**Layer #**													
	1	38.6	29.6	1.27	0.61	0.19	1.66	841	1061	2640	17.3	19.0	1.30	0.77
	2	39.8	27.9	0.67	1.02	0.29	2.12	953	1514	2900	6.77	24.1	1.43	2.21
	3	51.8	18.2	3.67	1.06	0.13	1.87	1166	1367	1710	33.4	23.7	2.84	0.14
EW9602-09RD	**Avg**	42.2	24.5	1.58	0.93	0.23	1.84	888	1248	2570	14.1	21.0	1.88	0.88
(crust)	**SD (n=44)**	6.80	6.10	0.73	0.28	0.05	0.55	175	236	614	7.40	5.76	0.71	0.88
	1	18.4	11.5	0.21	0.41	0.18	0.53	499	617	1040	37.3	7.34	1.60	4.01
	2	34.4	0.51	0.10	0.93	0.91	0.04	172	3770	330	1.27	5.84	67.8	17.3
	3	45.1	0.56	0.17	1.94	1.63	0.05	341	4970	1500	1.41	0.96	80.4	10.9
	Avg	35.9	4.08	0.20	1.10	0.89	0.24	476	3740	1580	18.8	7.54	8.79	6.84
JC120-104	**SD (n=37)**	10.9	4.79	0.16	0.62	0.49	0.22	177	2890	830	16.5	2.71	2.27	2.17
	1	15.6	10.2	0.38	0.26	0.20	0.72	324	418	1290	255	3.75	1.52	1.15
	2	21.4	12.6	0.37	0.24	0.21	1.20	569	512	3510	38.6	8.20	1.70	1.88
	3	31.6	5.27	0.24	2.01	1.13	0.35	359	1310	1250	48.3	3.59	6.00	4.49
	Avg	21.8	11.0	0.34	0.57	0.41	0.92	470	651	2700	79.8	6.49	1.99	2.08
RC12-192GS	**SD (n=92)**	10.1	5.36	0.23	0.49	0.30	0.58	243	310	2290	62.9	3.95	1.88	1.12
	1	21.4	10.3	0.78	0.41	0.15	0.73	555	675	1090	125	10.8	2.07	0.48
	2	26.1	12.2	0.73	0.46	0.16	0.83	752	683	843	201	13.5	2.14	0.73
	3	45.5	5.09	0.37	0.63	0.76	0.37	474	2170	937	53.2	7.19	8.95	3.69
	Avg	17.9	12.6	0.47	0.28	0.16	0.96	680	741	1190	128	10.4	1.42	1.04
EATL N4	**SD (n=61)**	8.84	4.81	0.29	0.18	0.16	0.34	292	373	497	51.1	4.53	1.84	0.60
	1	14.5	17.0	0.40	0.19	0.09	1.21	482	462	1090	136	6.22	0.85	1.45
	2	22.8	17.8	0.80	0.26	0.11	1.43	565	600	1730	158	8.51	1.28	0.70
	3	32.2	19.8	0.61	0.68	0.24	1.04	762	1050	1700	106	13.7	1.63	1.64
	Avg	22.9	19.5	0.62	0.41	0.21	1.12	721	847	1360	139	11.4	1.18	1.15
NAP N4	**SD (n=35)**	6.95	4.40	0.22	0.19	0.14	0.21	198	219	373	28.7	3.75	1.58	0.74
	1	14.8	19.9	0.003	0.01	0.004	0.08	437	56.9	588	12.4	9.18	0.74	8080
	2	29.2	10.8	0.02	0.01	0.004	0.03	224	51.1	1810	4.64	5.79	2.72	226
	3	43.3	4.52	0.03	0.02	0.01	0.09	306	54.8	1110	6.21	5.58	9.57	256
	Avg	23.0	7.51	0.01	0.01	0.01	0.10	228	51.2	773	6.34	4.73	3.06	495
N29	**SD (n=89)**	17.7	9.63	0.01	0.01	0.00	0.06	121	30.9	591	1.28	2.22	1.83	433
Wegorzewski & Kuhn., (2014)	**L.T. 1**	23.1	14.2	0.3	0.46	0.34	0.80	-	900	2600	-	-	1.8	-
	L.T 2.1	44.0	0.81	0.08	1.97	1.92	0.07	-	2600	3300	-	-	95.9	-
	Crust	22.8	17.2	0.4	0.44	0.14	0.89	-	900	2000	-	-	1.38	-
Baturin (2011)		16.5	11.5	155	155	44.0	1.40	325	80	616	4.2	5.9	1.43	-

Table 2. Concentrations of major and trace elements in individual layers of crust and nodules. Layer numbers #1, 2 and 3 were selected as three representative layers within each nodule, being Layer #1 the most hydrogenetic and Layer #3 the most diagenetic. †= Growth Rate = $0.68/(Co_n)^{1.67}$, where Co_n= Co*(50/Fe+Mn), with Co, Fe and Mn in wt. % (Manheim & Lane-Bostwick, 1988). Nodule data from Wegorzewski & Kuhn (2014) and Baturin (2011) has been included for comparison.

The Arctic nodule has a moderate Mn content of ~23 wt. %, but relatively low Fe (~7.5 wt. %). This nodule has relatively low concentrations of other metals, with Co, Ni and Cu concentrations of ~0.01 wt. %, Ti = ~0.1 wt. %, V = ~228 ppm, Zn = ~50 wt. %, Ba = ~770 wt. %, Th = ~6.3 ppm and U = ~4.7 ppm. Some layers have relatively high Mn/Fe (~10), and these tend to have higher concentrations of Co+Ni+Cu.

Nodules from the Atlantic Ocean, EATL N4 and NAP N4, that have relatively low Mn/Fe, have the highest concentrations of REY, with average ΣREY concentrations of, respectively, ~3360 and ~3880 ppm. ΣREY concentrations in the Pacific nodule RC12-192GS and crust EW9602-09RD are lower, ~2670 and ~2500 ppm, respectively, whereas the Pacific nodule that has highest Mn/Fe (JC120-104) has much lower ΣREY (~990 ppm). The Arctic nodule N29 has extremely low ΣREY (~123 ppm). Most of the individual nodule layers have positive Ce anomalies, although high Mn/Fe layers in nodule JC120-104 and most layers in nodule N29 have negative Ce anomalies. All layers are generally depleted in the LREE relative to the HREE, especially in JC120-104 (LREE/HREE = 0.46).

Table 3. Concentrations rare earth elements and yttrium (REY) in individual layers of crust and nodules. $Ce^* = (2*Ce_{SN})/(La_{SN}+Nd_{SN})$, where SN=shale normalised. $LREE/HREE = (La_{SN}+2*Pr_{SN}+Nd_{SN})/(Er_{SN}+Tm_{SN}+Yb_{SN}+Lu_{SN})$. Layer numbers #1, 2 and 3 were selected as three representative layers within each nodule, being Layer #1 the most hydrogenetic and Layer #3 the most diagenetic.

		La	Ce	Pr	Nd	Sm	Eu	Gd	Tb	Dy	Y	Ho	Er	Tm	Yb	Lu	ΣREY	Ce*	LREE/ HREE	Y/Ho
		ppm	ppm	ppm	ppm	ppm	ppm	ppm	ppm	ppm	ppm	ppm	ppm	ppm	ppm	ppm	ppm			
Sample	**Layer #**																			
EW9602-09RD (crust)	**1**	359	1609	41.4	184	34.1	8.17	44.0	6.11	45.9	262	10.7	35.5	5.28	35.6	6.36	2690	3.39	0.53	24.5
	2	233	1407	29.2	134	27.2	7.02	38.8	5.85	44.7	313	11.4	38.6	5.80	42.3	7.51	2350	4.45	0.32	27.5
	3	398	1365	64.9	293	62.0	14.0	74.3	10.3	72.3	325	15.7	47.4	7.01	43.5	6.81	2800	2.31	0.60	20.7
	Avg	302	1561	38.2	175	34.1	8.26	46.1	6.64	48.8	287	11.6	37.8	5.64	38.7	6.73	2610	3.85	0.45	24.9
	SD (n=44)	72.9	410	10.6	48.6	10.4	2.37	13.0	1.84	12.7	64.6	2.84	8.74	1.30	8.55	1.43	600	0.82	0.06	1.52
JC120-104	**1**	195	660	52.4	248	65.4	14.2	68.3	9.95	59.1	175	10.6	29.1	3.96	24.8	3.81	1620	1.46	0.74	16.6
	2	23.3	40.9	6.18	27.5	6.83	1.49	5.91	0.83	4.77	15.6	0.89	2.50	0.35	2.23	0.35	140	0.79	0.97	17.4
	3	50.7	83.3	14.9	64.2	16.7	3.59	13.9	2.23	12.4	35.5	2.17	6.27	0.90	6.12	0.90	314	0.71	0.87	16.3
	Avg	137	292	38.5	181	46.8	10.3	46.2	6.60	39.1	127	7.01	19.5	7.98	24.9	5.06	988	0.90	0.46	18.2
	SD (n=37)	151	285	50.1	242	64.5	14.3	66.9	9.13	53.5	255	9.66	26.7	3.37	21.6	3.25	1250	0.70	0.78	26.4
RC12-192GS	**1**	247	1970	61.6	286	75.3	16.0	72.4	10.6	59.6	162	10.4	27.8	3.72	24.7	3.88	3030	3.64	0.90	15.6
	2	445	1560	103	475	121	27.4	119	17.0	99.3	264	17.8	50.0	6.82	46.0	7.16	3360	1.67	0.84	14.8
	3	94.8	597	28.0	126	34.0	7.57	30.9	4.80	28.6	78.0	4.93	14.4	1.91	13.6	1.97	1070	2.64	0.75	15.8
	Avg	323	1290	78.8	367	93.7	20.7	92.0	13.6	79.2	213	14.1	38.6	5.30	34.9	5.41	2670	1.84	0.83	15.1
	SD (n=92)	227	772	51.5	240	59.5	13.1	59.7	8.71	50.9	133	9.11	25.0	3.42	22.7	3.56	1680	1.63	0.85	14.6
EATL N4	**1**	313	2380	78.0	324	75.9	18.1	77.1	12.3	73.4	238	13.4	37.9	5.42	35.7	5.16	3690	3.69	0.79	17.8
	2	346	2400	85.2	367	83.9	19.0	84.1	12.2	72.8	245	13.5	37.0	5.07	32.4	4.91	3810	3.32	0.93	18.2
	3	130	670	33.7	142	37.0	7.93	36.2	5.25	31.5	113	6.04	16.1	2.20	14.0	2.10	1250	2.42	0.84	18.7
	Avg	308	2020	77.3	336	81.1	18.1	82.8	12.7	75.7	249	14.1	39.3	5.47	34.9	5.31	3360	3.10	0.78	17.6
	SD (n=61)	117	824	30.2	128	30.3	6.87	29.9	4.58	27.3	88.3	5.10	14.3	1.97	13.0	1.94	1320	3.32	0.83	17.3
NAP N4	**1**	328	2000	76.6	343	81.9	18.0	84.3	11.9	72.2	247	13.1	37.1	4.91	32.7	5.04	3360	2.94	0.86	18.8
	3	386	2130	88.0	386	86.1	19.4	86.8	12.3	74.4	254	13.8	39.2	5.37	36.0	5.53	3620	2.73	0.90	18.4
	2	411	2290	104	446	105	24.3	107	15.9	96.9	336	18.2	52.7	7.38	49.4	7.41	4070	2.64	0.76	18.4
	Avg	357	2350	89.2	387	92.9	21.0	94.8	13.9	84.7	283	15.6	44.2	6.06	40.0	5.94	3880	3.11	0.80	18.1
	SD (n=35)	75.7	618	20.5	84.6	20.4	4.96	20.8	3.21	19.8	63.6	3.75	10.9	1.53	10.2	1.47	960	3.80	0.71	17.0
N29	**1**	27.0	32.3	5.34	25.5	5.98	1.37	3.58	1.06	6.88	42.2	1.44	4.22	0.57	3.65	0.53	162	0.61	0.57	29.3
	3	27.6	27.9	6.08	29.5	6.41	1.57	8.43	1.15	6.78	29.3	1.43	3.95	0.54	3.24	0.47	154	0.48	0.69	20.4
	2	19.4	27.9	3.88	18.0	4.01	0.95	2.32	0.66	4.22	20.7	0.84	2.40	0.34	2.02	0.31	108	0.74	0.71	24.6
	Avg	20.8	27.1	4.11	19.4	4.44	1.03	2.60	0.76	4.92	27.7	1.01	2.92	0.40	2.50	0.37	123	0.67	0.63	27.4
	SD (n=89)	11.5	16.8	2.38	11.5	2.78	0.64	3.49	0.50	3.28	20.1	0.69	2.02	0.27	1.74	0.24	70.7	0.72	0.53	29.1

5.3.3. Factor analysis

To assess the controls on the chemical composition of the nodules and crust, the elemental data were subjected to statistical factor analysis (Winters and Buckley, 1992) using the RStudio.Ink Varimax rotation scheme with Kaiser normalisation. The results of this analysis are shown in Table 4, and in Tables S1-6 in the Suppl. Info. Most of the total variance in the chemical composition within nodule JC120-104 and the crust (EW9602-09RD) can be accounted for by 5 factors, and most of the variance in nodules RC12-192GS, EATL N4 and NAP N4 can be accounted for by 4 factors. The variance in the chemical composition of the nodule from the Arctic (N29) is mainly accounted for by 3 factors.

Factor 1 is the most important control on REY concentrations in all samples (excluding Ce in the crust and nodules JC120-104 and N29), and Ti, V, Fe and Co in Atlantic nodules NAP N4 and EATL N4 and the South Pacific nodule RC12-192GS. In the Arctic nodule this factor controls V, Fe and the REY. Factor 1 accounts for 50-77% of the total variance of the samples. In most of the samples it has negative loadings for Mn, Ni, Cu and Zn. This factor likely represents the hydrogenous Fe-Mn-(oxyhydr)oxide fraction of the Atlantic and South Pacific nodules, whereas in the Arctic nodules it likely represents the detrital fraction. In nodule JC120-104 and the crust it most likely represents Ca-rich phosphate in association with Fe-(oxyhydr)oxides, although we cannot confirm this as no Ca or P data were acquired.

Factor 2 controls Mn, Ni, Cu and Zn in the Atlantic nodules NAP N4 and EATL N4, the South Pacific nodule RC12-192GS and the Arctic nodule N29. In these samples it has negative loadings for Fe, Cr and Th. In sample JC120-104 this factor controls Fe, Ce, Th and U, and it has significant negative loadings for Mn and Zn. In the crust this factor controls Fe, Ba and Ce. Factor 2 most likely represents the Mn-rich diagenetic fraction of the nodules, and may also be associated with Fe-oxides in nodule JC120-104. In the crust this factor most likely represents an additional hydrogenous phase. This factor accounts for the 13-24% of the total variance in the chemical composition of all of the ferromanganese deposits sampled in this study.

Factor 3 controls Ti, V, Cr, Fe in most of the nodules, and Co, Ti and U in the crust. This factor likely represents the detrital silicate fraction and it accounts for 4-10 % of the total variance in the chemical composition.

	EW9602-09RD					JC120-104					RC12-192GS			
	Factor1	Factor2	Factor3	Factor4	Factor5	Factor1	Factor2	Factor3	Factor4	Factor5	Factor1	Factor2	Factor3	Factor4
Ti	0.43	**0.86**	0.11				**0.95**	0.16	0.15		**0.97**			
V	0.31	**0.82**	0.27	0.16		0.18	0.29	**0.85**	0.32		**0.95**	0.19		0.20
Cr	**-0.39**	-0.34		-0.17		-0.12					**-0.47**	-0.12		
Mn		**0.40**	0.11	0.34	0.36	-0.17	**-0.92**	0.19			**0.68**	0.67		0.28
Fe	0.17	**0.75**	0.12	-0.20		0.13	**0.91**	0.14	0.26		**0.91**	-0.18	0.30	
Co		**0.86**	0.20	0.11		0.37		0.37		**0.82**	**0.91**	0.11		0.27
Ni		0.24		**0.91**		-0.18	-0.42	-0.18	**-0.78**		-0.30	**0.94**	-0.11	
Cu		-0.13		**0.96**		-0.17	-0.50	-0.11	**-0.81**		-0.24	**0.95**	-0.11	
Zn			0.13	**0.67**		-0.15	**-0.87**		0.13	-0.18	0.13	**0.96**		
Ba	-0.49	**0.62**	0.29	0.11	0.12	0.11		**0.82**		0.23	**0.89**	0.15	-0.23	0.26
La	-0.30	**0.69**	0.64			**0.91**	0.32	0.16	0.15		**0.99**			
Ce		**0.94**	0.23			0.19	**0.91**	0.23	0.20		**0.95**		0.21	
Pr	**0.98**					**0.98**	0.15				**1.00**			
Nd	0.17	0.27	**0.94**	0.13		**0.98**	0.12				**0.99**			
Sm	**1.00**					**0.99**					**0.99**			
Eu	**1.00**					**0.99**					**0.99**			
Gd	0.15	0.24	**0.95**			**0.99**	0.11				**0.99**			
Tb	1.00					**0.99**	0.13				**1.00**			
Dy		0.37	**0.92**			**0.98**	0.14				**1.00**			
Y	**0.93**				0.13	**0.99**					**0.99**			
Ho	**1.00**					**0.98**	0.15				**1.00**			
Er	**1.00**					**0.98**	0.16				**1.00**			
Tm	**0.96**	0.11		-0.18	0.14	**0.98**	0.18				**1.00**			
Yb	**0.79**	0.46	0.41			**0.98**	0.18				**1.00**			
Lu	**0.55**	0.42	0.42	-0.41	0.42	**0.97**	0.20				**1.00**			
Th	**0.92**	0.15	0.20			0.51	**0.80**		0.18			-0.18	**0.98**	
U		**0.94**	0.18	-0.10	0.14	0.14	**0.87**	0.15	0.28		**0.98**			0.16

Table 4. Varimax rotated factor matrix for samples in this study. Numbers in bold denote elements that appear to be loaded in the factor.

	EATL N4				NAP N4				N29		
	Factor1	Factor2	Factor3	Factor4	Factor1	Factor2	Factor3	Factor4	Factor1	Factor2	Factor3
Ti	**0.56**		0.48		**0.97**				0.17	0.13	**0.92**
V	0.59	0.24	**0.71**		**0.95**	0.19		0.20	**0.80**	0.20	
Cr			**0.66**		**-0.47**	-0.12			0.25		**0.29**
Mn	0.46	**0.79**	-0.12	0.32	**0.68**	0.67		0.28	-0.19	**0.81**	
Fe	0.65	0.11	**0.71**		**0.91**	-0.18	0.30		**0.75**	-0.45	
Co	0.45	0.27	-0.24	**0.74**	**0.91**	0.11		0.27		**0.52**	
Ni	0.28	**0.74**	-0.21	0.48	-0.30	**0.94**	-0.11			**0.96**	
Cu		**0.94**			-0.24	**0.95**	-0.11			**0.94**	
Zn	0.26	**0.92**	0.28		0.13	**0.96**			0.39	**0.50**	0.20
Ba	**0.80**	0.34	0.25		**0.89**	0.15	-0.23	0.26	0.14	**0.77**	
La	**0.93**	0.16	0.11	0.13	**0.99**				**0.90**		
Ce	**0.79**	0.17	0.13	0.38	**0.95**		0.21		**0.43**		
Pr	**0.93**	0.19	0.17	0.11	**1.00**				**0.94**		
Nd	**0.94**	0.16	0.16		**0.99**				**0.95**		
Sm	**0.95**	0.16	0.18		**0.99**				**0.96**		
Eu	**0.94**	0.18	0.18	0.11	**0.99**				**0.96**		
Gd	**0.96**	0.14	0.15		**0.99**				**0.98**		
Tb	**0.96**	0.14	0.17	0.11	**1.00**				**0.99**		
Dy	**0.96**	0.14	0.16	0.11	**1.00**				**0.99**		
Y	**0.97**	0.14	0.13	0.13	**0.99**				**0.94**	-0.18	
Ho	**0.97**	0.14	0.14	0.14	**1.00**				**0.99**		
Er	**0.97**	0.13	0.12	0.15	**1.00**				**0.98**		
Tm	**0.97**	0.14	0.12	0.17	**1.00**				**0.97**		
Yb	**0.97**	0.14	0.11	0.18	**1.00**				**0.98**		
Lu	**0.97**	0.12		0.19	**1.00**				**0.96**		
Th	**0.67**		0.11	0.22		-0.18	**0.98**		0.27		0.21
U	**0.74**	0.33	0.40	0.15	**0.98**			0.16	**0.60**		

Table 4 (cont.). Varimax rotated factor matrix for samples in this study. Numbers in bold denote elements that appear to be loaded in the factor.

Factor 4 controls Co in the Atlantic nodule EATL N4, Ni and Cu in JC120-104 and Mn, Ni and Zn in the crust. It does not have a significant loading in any of the other samples. It accounts for the 1-6 % of the total variance. The element associations suggest that Factor 3 represents the pure Mn-oxide fraction. In all of the other samples, this factor likely represents an additional hydrogenous phase.

Factor 5 is only present in the crust sample EW9602-09RD, and it only shows a significant loading for Cr, which might be indicative of the oceanic crust. It accounts for the 5% of the total sample variance.

5.4. Discussion

5.4.1. Genesis of deep-sea ferromanganese deposits

My SEM analyses reveal that the internal structure of deep-sea ferromanganese deposits is highly heterogeneous. In turn, our LA-ICP-MS analyses reveal that the chemical composition of the crust and nodules is also highly heterogeneous, and factor analysis shows that individual deposits can acquire metals and REYs from a variety of different sources, including seawater, sediment pore waters, and detrital aluminosilicate material. Based on the relative abundances of Mn, Fe and Ni+Cu+Co (Bonatti et al., 1972), the ferromanganese crust and nodules from the Atlantic Ocean mainly acquire metals from seawater, whereas different layers within the nodules from the Pacific Ocean acquire metals either from seawater or sediment pore waters (Figure 11), which would not be apparent from measurements of their bulk chemical composition.

High resolution chemical analyses of individual layers within nodules from the German license areas E1 in the easternmost part of the CCFZ also reveal the presence of both dense, dark layers with low average Mn/Fe (1.8) and low average Ni+Cu (0.81 wt. %), and highly reflective dendritic layers with high average Mn/Fe (96) and high Ni+Cu (~4 wt %) (Wegorzewski & Kuhn., 2014). The former are referred to as ‘layer type 1’ and are attributed to hydrogenetic precipitation from oxic waters, whereas the latter are referred to as ‘layer type 2’ and are attributed to metal precipitation from suboxic pore waters. Most of the nodule and crust layers analysed in this study have relatively low Mn/Fe (< ~3; Table 2) and the only layers that have very high Mn/Fe (up to 80.4) come from nodule sample JC120-104, which is also from the CCFZ.

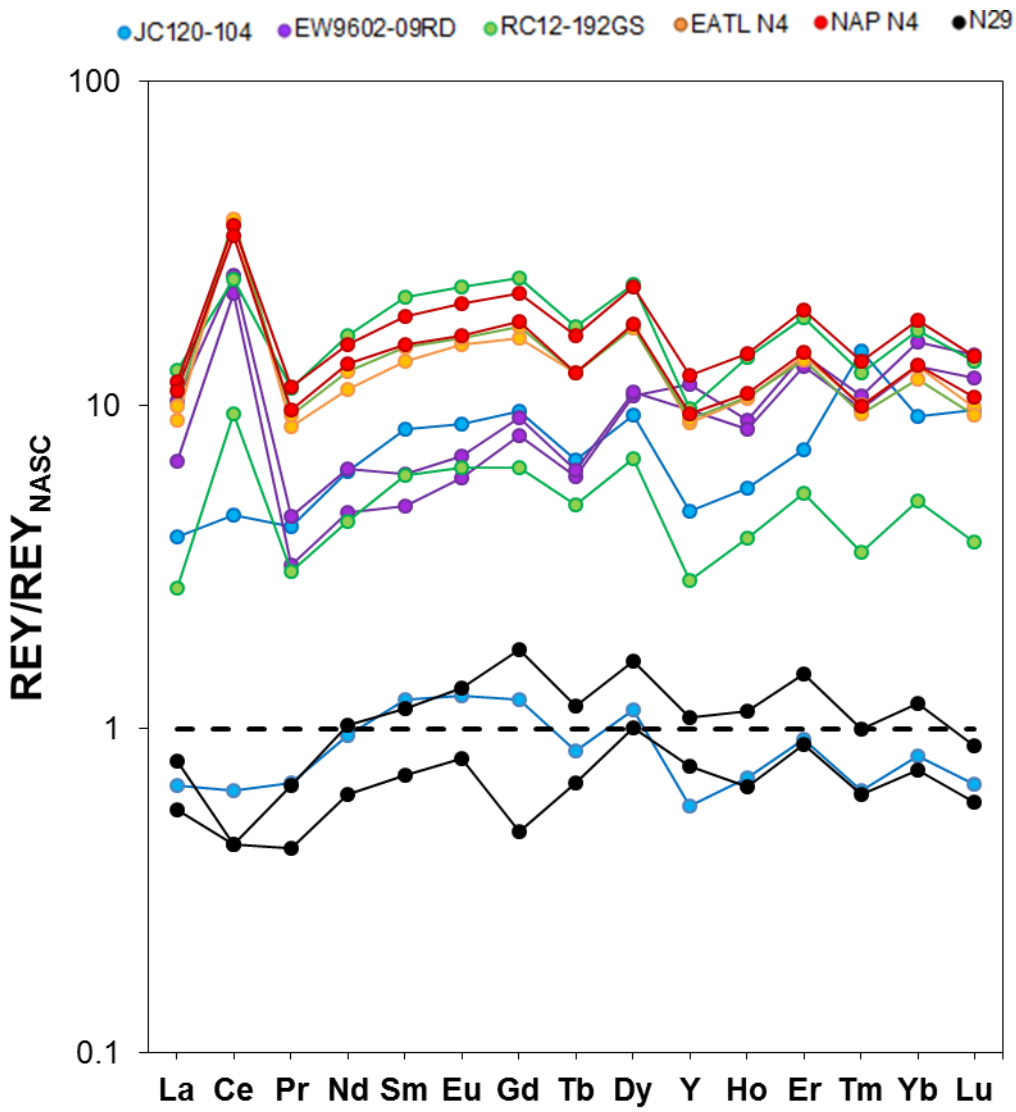

Figure 9. REY distribution patterns of two hydrogenetic-diagenetic end members for each sample, normalised to North America Shale Composite (NASC; Gromet et al., 1984), for 3 selected layers from each sample.

Some of my nodules contain layers with intermediate Mn/Fe values of between 3-10 and intermediate Ni+Cu concentrations, 2-3 wt. %. These are characteristic of deposits that form under oxic diagenetic conditions (Halbach et al., 1981). Although many authors have observed these 'mixed' signals, these are typically attributed to mixing of type 1 and type 2 layers during bulk analysis, we note that some of the layers with relatively low Mn/Fe have higher Cu + Ni, which suggests that these layers form from an oxic diagenetic, rather than a hydrogenous, source.

REY analyses may also be useful for assessing the principal mode of formation of different layers (Bau et al., 2014). REY distribution patterns for different layers within the Atlantic nodules are relatively homogeneous, with strong positive Ce anomalies (~2.5-4), and enrichment of Ho with respect to Y (Figure 9). This

pattern is typical for surface complexation of REY from ambient seawater and subsequent hydrogenetic precipitation (Piper, 1974; Addy, 1979; de Lange et al., 1992; Nath et al., 1992; Kasten et al., 1998, Bau et al., 2014). The crust sample also has a positive Ce anomaly (2.31-4.45), but it is more strongly enriched in the HREE relative to the LREE compared to the Atlantic nodules. This is characteristic of hydrogenetic crusts that are phosphatised (Bau et al., 1996), consistent with our SEM observations of the presence of Ca-phosphate filled cavities within the crust structure (Fig. 4c).

Layers that have relatively high Mn/Fe (principally those within the nodule from the CCFZ, sample JC120-104) by contrast have negative Ce anomalies (~0.75 compared to ~1.5 for layers with low Mn/Fe), as well as lower REY concentrations (~230 vs ~1620 ppm for layers with low Mn/Fe). This is related to the diagenetic origin of these layers, which induces the mobilisation and re-precipitation of the trivalent REYs in the pore fluids. These fluids are not able to transport the Ce^{4+} during this process (Sholkovitz et al., 1994; Schijf et al., 1995; Bau et al., 1997; Bau et al,. 2014), so Ce^{4+} is depleted relative to the trivalent REEs in these precipitates. The lower REY content of these layers is likely due to the relatively fast nature of diagenetic precipitation (Kuhn et al., 1998; Ohta et al., 1999), which depletes the Fe-Mn deposit in slow-precipitating, colloidal related elements such as the REY. Additionally, diagenetic processes likely induce the dissolution of Fe-Mn-(oxyhydr)oxides, releasing their associated REY to sediment pore waters (Nath et al., 1992).

Plots of the Ce anomaly vs Y/Ho and Nd concentration (Fig. 10) support the REY distributions. The only layers that have a diagenetic signature are some of those from the CCFZ nodule; all of the other layers represents hydrogenetic precipitates. As my high resolution data clearly distinguish hydrogenous and diagenetic precipitates, I can better assess their relative growth rates based on Co content (Manheim & Lane-Bostwick, 1988):

$$\text{Growth Rate} = 0.68 / (Co_n)^{1.67} \qquad (1),$$

where Co_n= Co*(50 / Fe+Mn), with Co, Fe and Mn in wt. %. As discussed previously, this method does not account for any hiatuses in precipitation of Co (e.g. Banakar & Hein, 2000) and therefore only provides a minimum age. Bearing this in mind, my data indicate that the hydrogenetic layers have relatively slow growth rates (~1-2 mm/Ma), whereas the diagenetic layers form much more rapidly (up to ~10-17 mm/Ma in the nodule JC120-104). This is consistent with

results of other studies based on bulk compositions (e.g. Reyss et al., 1982, Gonzalez et al., 2009).

A model summarising the different modes of nodule formation revealed in this study is shown in Figure 12. The greater diagenetic component of the nodule from the CCFZ in comparison with the other deposits indicates that more prolonged suboxic conditions occurred at this site during nodule formation. The oxygen penetration depth (OPD) into sediments in the CCFZ is ~1 m (Chapter 3). It is likely, therefore that the area has been more subjected in the past to a greater suboxic signal that promoted the diagenetic signature found in the nodules. A possible explanation for this could be the availability of organic matter in the bottom sediments of the UK Claim area (Figure 12a). This would be derived from its closer proximity to the Pacific equatorial belt of primary productivity, relative to other zones of the eastern CCFZ. By contrast, the typical oxygen penetration depth (OPD) in the deep North Atlantic, is ~18m (Buckley, 1988), because bottom waters are more highly oxygenated as they have formed more recently (Reid, 1997). The OPD in the South Pacific abyssal plain, in proximity to the location of nodule sample RC12-192GS and crust sample EW9602-09RD is also very deep (up to 75 m; D'Hondt et al., 2015) due to low primary productivity in the South Pacific Gyre. Hence, nodules and crusts that form on top of sediments that have a deep OPD tend to have a hydrogenous source, whereas nodules that sit on sediments with a relatively shallow OPD also contain a diagenetic signature (Figure 12).

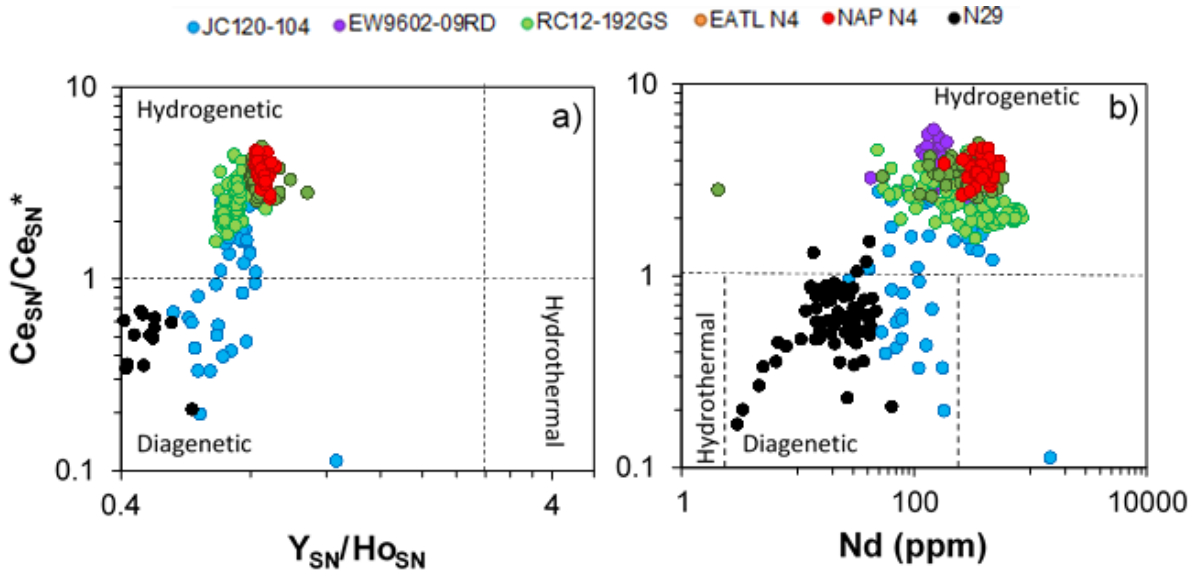

Figure 10. Relationship between (a) Ce_{SN}/Ce_{SN}^* ratio vs Nd concentration and (b) Ce_{SN}/Ce_{SN}^* ratio vs Y_{SN}/Ho_{SN} ratio in layers of samples, where $Ce_{SN}^*= 0.5*La_{SN}+0.5*Pr_{SN}$ and SN=shale normalised. Crust sample EW9602-09RD was not plotted in a) because of its phosphatised state (see text for explanation). Fields

for hydrothermal, hydrogenous and diagenetic are defined according to the data from Fe–Mn (oxyhydr)oxide deposits in Bau et al., (2014).

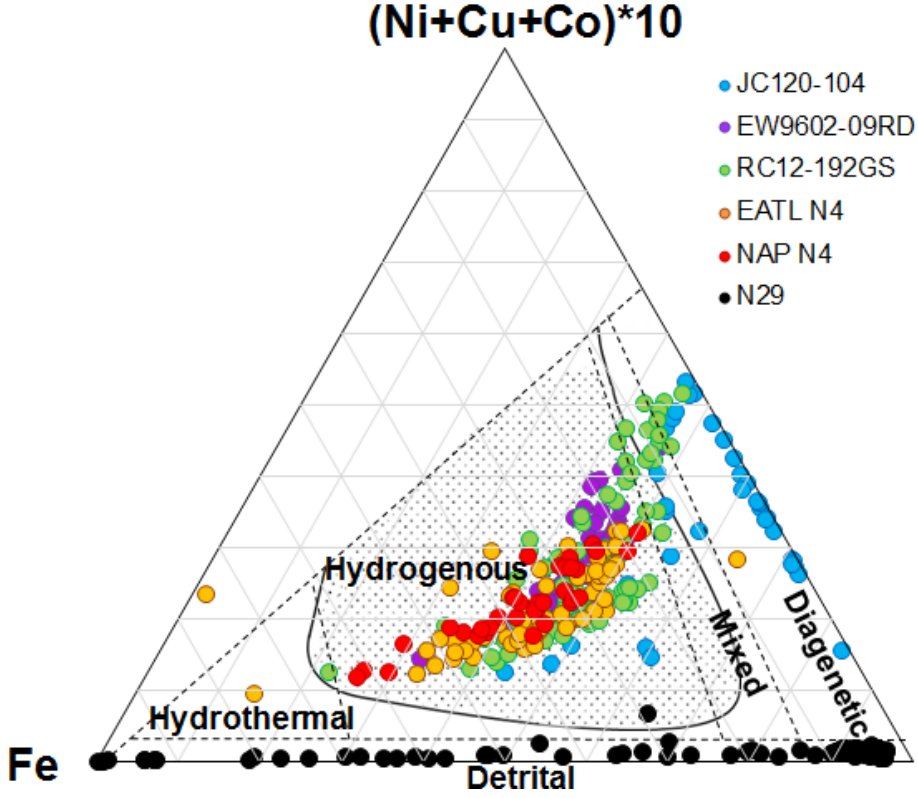

Figure 11. Ratio of Fe:Mn:Cu+Ni+Co for bulk compositions of layers in samples. Black lines define different nodule fields, according to Bonatti et al. (1972), Wegorzewski and Kuhn (2014) and the present study. Dotted area denotes nodules that are REY-enriched.

The transition metal and REY composition of the Arctic nodule is clearly different from the other nodules and the crust (Figs. 9 & 10). This nodule has exceptionally low Ni+Cu+Co and very variable Mn and Fe, similar to the bulk composition of nodules from the Kara Sea (Baturin, 2011). This type of composition is usually attributed to a hydrothermal source (Bonatti et al., 1972), but the nodules have negative, rather than positive, Y anomalies (Fig. 10) that preclude hydrothermal input (Bau et al., 2014). Additionally, the REY distribution pattern and REY concentration of the Arctic nodules is rather similar to shale (Fig. 9), consistent with statistical element associations (Table 3) that indicate that the principal source of the REY is input of detrital material. For this reason, I have delimited a new field to include the detritally-sourced nodules (Figure 11). Mn/Fe ratios within individual nodule layers are highly variable (0.74-10), and much higher than NASC (0.016; Gromet et al., 1984). Together with negative Ce anomalies (Figs. 9 & 10) this is strong evidence for diagenetic precipitation from suboxic pore waters (Bau et al., 2014). In this connection, nodules are only found in those parts of the Kara Sea that host a thin layer of oxic sediments (Figure 12), and they are absent in anoxic sediments presumably because Mn (and Fe) oxyhydroxides

cannot form (Rozanov, 2014). My data also reveal that the Arctic nodule has an extremely high growth rate (Eq. 1; up to ~8080 mm/Ma), similar to that estimated for shallow water nodules from the Gulf of Cadiz (~1400-5000 mm/Ma; Gonzalez et al., (2009). Thus, dilution of the authigenic phases by detrital material, combined with high nodule growth rates and rapid burial rates (Baturin, 2011) preclude significant enrichment in Ni+Cu+Co and the REY; models for the genesis of nodules based on geochemical relationships observed in deep-sea settings cannot therefore be applied to nodules that form in shallow waters.

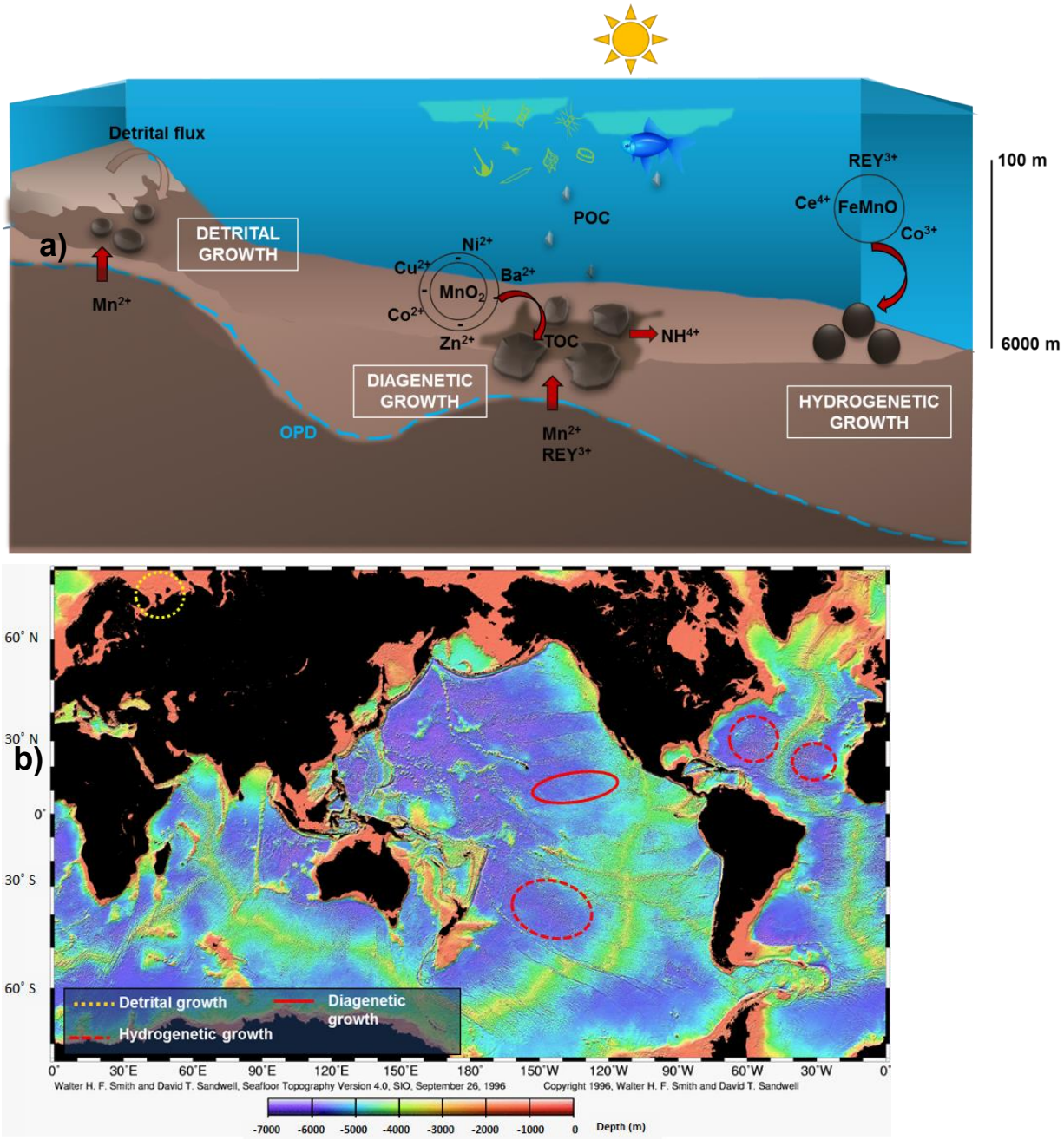

Figure 12. a) Graphic scheme showing detrital, hydrogenetic and diagenetic processes of nodule formation and b) map showing the relative importance of

these processes relative to geographical location of samples analysed in this study. OPD=Oxygen Penetration Depth, separating underlying anoxic sediments from overlying oxygenated sediments. TOC=Total Organic Carbon. POC=Particulate Organic Carbon, linked to surface bioproductivity. See text for a more detailed explanation.

5.4.2. Controls on the resource potential of deep-sea ferromanganese deposits

The economic resource of ferromanganese deposits is mainly based on their high content of Ni, Co and Cu. There is also growing interest in their potential as a REY resource. Our study has shown that the metal content of ferromanganese deposits can be highly variable, depending on their environmental setting, so their resource potential may also vary with location. Hydrogenetic deposits tend to be better resources for Co and REY, while diagenetic-deposits have higher concentrations of Ni and Cu. Shallow-water nodules from the Kara Sea do not contain high quantities of any of these metals, and estimated tonnages are far below their global annual consumption (Table 5).

Resource		Cook-Austral volcanic chain	UK Claim (CCFZ)	SW Pacific Basin	East Atlantic	North West Atlantic	Kara Sea
	Avg. nodule resource (kg/m^2)	50-75[e1]	1.7-57[f1]	0.6-58[g1]	2.6-8.8[h1]	2.6-8.9[i1]	0.5-2.5[j1]
	Area surface (km^2)	1197[e2]	60000 [f2]	20000 [g2]	54000 [h2]	110000 [i2]	30800 [j2]
REY	Avg. content (ppm)	2609	988	2670	3360	3880	123
	Mass of metals (T*10^5)	1.56-2.34	1.01-33.8	3.20-31.0	4.71-16.1	11.1-38.0	≤ 0.09
	Mass/Global annual demand[a]	1.49-2.23	0.96-32.1	3.05-29.5	4.49-15.4	10.6-36.1	≤ 0.09
Co	Avg. content (ppm)	15800	2000	3400	4700	8000	100
	Mass of metals (T*10^5)	9.45-14.2	2.04-68.4	4.08-39.4	6.6-22.6	22.9-72.3	≤ 0.07
	Mass/Global annual demand[b]	10.9-16.3	2.34-78.6	4.69-45.3	7.58-26.0	26.3-90.0	≤ 0.09
Ni	Avg. content (ppm)	9300	11000	5700	2800	2600	100
	Mass of metals (T*10^5)	5.57-8.35	11.2-376	6.84-66.1	3.93-13.5	7.43-25.4	≤ 0.08
	Mass/Global annual demand[c]	≤ 0.001	≤ 0.03	≤ 0.005	≤0.001	≤ 0.002	≤ 5*10^{-6}
Cu	Avg. content (ppm)	2300	8900	4100	1600	1100	100
	Mass of metals (T*10^5)	1.38-2.06	9.08-304	4.92-47.6	2.25-7.69	3.15-10.8	≤ 0.08
	Mass/Global annual demand[d]	≤ 0.009	≤ 1.35	≤ 0.21	≤ 0.03	≤ 0.05	≤ 3*10^{-4}

Table 5. Average Co, Ni, Cu and ΣREY content of the crust and nodules, and estimated average resources. [a]=Based in 2012 G.D.A of 105000 T (Hatch, 2012; Alonso et al., 2012); [b]=Based in 2015 G.D.A of 87000 T (Cobalt Development Institute, CDI, http://www.thecdi.com/); [c]= Based in 2010 G.D.A of 1465 mT (International Nickel Study Group, INSD, www.insg.org); [d]=Based in 2015 G.D.A of 22.5 mT (CME Group, www.cmegroup.com); [e1]=resource characteristics of Western Pacific ferromanganese crusts on submarine seamounts in Zhang et al., (2008); [e2]=seamount dimensions and abundance in Austral Volcanic chain in Jordahl et al.,

(2004); [f1] and [f2]=data collected during JC120 Cruise at the CCFZ in May 2015; [g1]=nodule resource and dimensions in South West Pacific basins from Hein et al., (2015); [h1]=data on nodule distribution in deep Atlantic basins was extremely sparse and numbers given here are based on similar nodules from the Angola Basin in Kasten et al, (1998); [h2]=compiled data in Weaver & Thomson, (1987); [i1]= Kasten et al, (1998); [i2]= dimensions on NW Atlantic basin shown in Addy, 1978; [j1]=density of nodules in the Kara Sea in Baturin, 2009; [j2]=surface estimated from sampled area during the R/V Professir Shtockman cruise in October 2013 (Shulga et al., in prep.).

Nodules from the large-sized North West Atlantic basin represent the best resource for Co (~up to 72 $\cdot 10^5$ T) and REY (~up to 38 $\cdot 10^5$ T), which represents ~90 times the current global annual consumption of Co and ~36 times that of REY (Table 5). As hydrogenetic nodules tend to be smaller, the nodule density is lower, so only very large hydrogenetic nodule fields are likely to represent a viable resource. This is however very unusual in the Atlantic, as nodule fields tend to be confined to relatively small deep basins, as sedimentation rates are too high in the rest of the ocean to support nodule formation (de Lange & Poorter, 1992). On the other hand, lower sedimentation rates and a shallower carbonate compensation depth (CCD) makes nodule-rich deep basins in the Pacific more common and extensive. Because of this, large-sized diagenetic nodules from the CCFZ provide a similar metal tonnage to the hydrogenetic nodules (up to ~68 $\cdot 10^5$ T of Co, and up to ~34 $\cdot 10^5$ T of REY), even though they are less enriched in Co and REY. Similarly, the high quantities of ferromanganese crusts in the Cook-Austral volcanic chain (up to ~75 kg/m^2) provides up to ~14.2 $\cdot 10^5$ T of Co (~16 times the global annual demand) and ~2.3 $\cdot 10^5$ T of REY (~2 times the global annual demand), even though the crusts are only found on the top of seamounts with a maximum area of ~1200 km^2.

The diagenetic-influenced nodules from the CCFZ have the potential to yield the highest tonnages in Ni and Cu, of up to ~376 and ~304 $\cdot 10^5$ T, respectively (Table 5), which represents ~0.03 times the global annual consumption of Ni and ~1.35 times that of Cu. In comparison, the amounts of Cu and Ni contained in hydrogenetic deposits are of ~1 order of magnitude lower.

5.5. Conclusions

Analyses of the structure and chemical composition within individual nodules and crusts reveal great internal variability. Nodules from the Atlantic Ocean, and the ferromanganese crust sample, tend to consist of layers of Fe-Mn-rich oxides with

relatively low Mn/Fe (<3) that precipitate from oxic seawater. These nodules are enriched in ΣREY, Fe and Co, and they grow only slowly (~1 mm/Ma). The crust sample has experienced diagenetic phosphatization. Large nodules from the CCFZ in the Pacific Ocean also contain layers that have much higher Mn/Fe (up to ~60) and Cu, Ni and Zn, that precipitate from suboxic sediment pore waters. These layers grow much faster (~7 mm/Ma) compared to the layers that have low Mn/Fe (~1-2 mm/Ma). Nodules from the shallow Arctic Ocean have highly variable textures, with high concentrations of detrital material and relatively low concentrations of transition metals and ΣREY. The Arctic nodules are extremely fast-growing (~500 mm/Ma).

The mode of genesis of ferromanganese deposits, as well as their growth rate and the oxygen penetration depth of sediments, all affect their final resource potential. Although hydrogenetic deposits are generally better resources of Co and the REY, diagenetic deposits have higher quantities of Ni and Cu, and they also tend to have higher nodule densities because they grow more quickly. Arctic nodules are a poor resource because they have a high detrital component. Deep sea nodules and ferromanganese crusts contain significant quantities of ΣREY and Co with respect to the global annual demand, but are less important resources of Ni and Cu.

Chapter 6: Conclusions and further work

Mining of deep sea resources is likely to take place in the next few years, as world's demand for metals increases. However, the environmental impacts derived from mining activities are still poorly constrained.

In order to provide new insights as to the complex interplay of processes that control metal enrichment in marine resources I have undertaken detailed geochemical mineralogical an geochemical investigations of a series of polymetallic nodules and crusts and deep sea sediments from different oceanic locations. Additionally, I have explored methods for the extraction of metals and the REY from these deposits. The principal outcomes of this work are provided below, and further areas of research that remain to be addressed are provided in Section 6.2.

6.1. Principal outcomes

6.1.1. Controls on the distribution of rare earth elements in deep-sea sediments in the North Atlantic Ocean

Deep sea sediments are now considered a potential resource of the REY, yet the REY content of deep- sea sediments from the Atlantic Ocean is a poorly known, and the processes that lead to the enrichment of the REY are not well understood. To fill this gap, I have determined the REY and major element concentrations of sediments recovered from a transect at ~24 ˚N in the North Atlantic Ocean (Chapter 2). These include fine- grained red and brown clays (some of them containing small micronodules), grey clays, turbidites, carbonate oozes, chalks of different purities and foraminiferal marls, from different marine sedimentary environments such as the Canary, Nares Abyssal Plain and North America deep marine basins, the West African continental slope and the vicinity of the Great Bahama Bank.

This work shows that the slowly-accumulating red clays from the Nares Abyssal Plain and the Canary Basin have the highest ΣREY content, and highest ΣREY concentrations are found in red clays that contain micronodules of ferromanganese oxides (up to ~ 510 ppm ΣREY). In turn, ΣREY concentrations are lower (up to ~150 ppm) in grey clays that contain significant terrigenous material

transported by turbidites, and carbonate-rich sediments contain lowest ΣREY concentrations (~120 ppm).

REY distribution patterns indicate that the principal source of REY enrichment in red clays from the North Atlantic is seawater, through scavenging by Fe-Mn (oxyhydr)oxides. The REY distribution pattern in the red clays mirrors that of seawater, with positive Ce anomalies and enrichment in the LREE relative to the HREE. The red clays are also enriched in some transition metals, elements such as Fe, Mn, Cu, Co, Ni and V, which are also considered to have a hydrogenous (seawater) source.

6.1.2. Evaluation of leaching techniques and their environmental implications for commercial extraction of metals and REY from deep-sea sediments and polymetallic nodules

A potential advantage of deep- sea ferromanganese resources in comparison with land- based ores is that extraction of resource metals is purported to be easier, faster and cheaper. To this end, I have assessed the efficacy of various techniques for the extraction of the REY and the transition metals, as well as their potential for release of unwanted elements such as radionuclides (Chapter 3). Results indicate that leaching Atlantic sediments with dilute HCl and H_2SO_4 extracts P and Ca (presumably from apatite), but only moderate amounts of REY (~50%). This suggests that, in contrast to Pacific REY-rich sediments, a greater proportion of the REY are hosted in recalcitrant detrital phases. Leaching of REY-rich Atlantic sediments in oxalic acid effectively releases Mn, Co, Ni and Cu (> ~80%). Oxalic acid also extracted >50% of Mn, Fe, Co and Cu from Atlantic nodules, but it was ineffective at extracting metals from Pacific nodules. The REY were most effectively extracted from nodules with dilute HCl, with >~80% of the REY leached from Pacific nodules but only ~40% from Atlantic nodules. Dilute HCl was, however, generally ineffective for extracting most of the transition metals.

The potential for release of harmful elements if leached residues are returned to the ocean as part of the mining operation was also investigated. Experiments indicate that metal release from leached residues could increase the metal content of seawater above a mining site by up to four orders of magnitude compared to background values.

6.1.3. Controls on the chemical composition of ferromanganese nodules in the Clarion-Clipperton Fracture Zone, eastern equatorial Pacific

The International Seabed Authority has recently licensed a number of seabed exploration areas in the Clarion Clipperton Fracture Zone (CCFZ) in the eastern equatorial Pacific Ocean. As part of the management plan for this area, and due to concerns about the environmental implications of nodule exploitation, some parts of the CCFZ have been designated 'Areas of Potential Environmental Interest' (APEI). These areas will not be subject to mining and they will be used to monitor the scale of the environmental impacts related to exploitation activities. However, these areas were selected based on surface ocean characteristics and seafloor topography, estimated from satellite altimetry, and the abundance and composition of nodules in these areas are still unknown. As a result, their relevance as an intended baseline for mining disturbance has not been demonstrated.

To fill this gap, I have undertaken a detailed study of the chemical composition of nodules and seafloor sediments collected in the UK Claim area in the CCFZ and its closest APEI, APEI- 6 (Chapter 4). The UK Claim Zone is an area of ~ 60000 km^2 licensed to UK Seabed Resources Ltd. (UKSRL) at the easternmost part of the CCFZ, while the APEI- 6 comprises an area of ~ 160000 km^2 located at the northwest CCFZ.

Nodules from the UK Claim area have higher Mn/Fe ratios, and higher concentrations of Ni, Cu and Zn, while nodules from the APEI-6 area are more enriched in Fe, Co and the REY. Nodules from the UK Claim area acquire a greater proportion of metals and the REY from sediment pore waters than nodules from APEI-6; APEI-6 nodules principally acquire metals and REY from seawater. It is likely that the closer location of the UK Claim to the equatorial Pacific belt of high primary biological productivity during Early-Middle Miocene triggered the growth of diagenetic Mn-rich layers. APEI-6 is located to the north of the UK Claim area, and would not have been located beneath the high productivity zone at any point during nodule growth.

Nodule density is higher in the UK Claim area because diagenetic nodule layers grow relatively rapidly and, for this reason, the UK Claim area represents a better metal resource than the nodules from APEI-6. Nevertheless, there is considerable variation in nodule density within individual areas (on length scales of <500 km).

This may then indicate that APEI-6 is unlikely to represent a suitable baseline for mining disturbance in all parts of the CCFZ.

6.1.4. Genesis of ferromanganese crust and nodules in the Atlantic, Pacific and Indian Oceans

The occurrence of ferromanganese nodules and crusts in different oceanic settings is widely known. Yet, the geochemical processes that regulate the enrichment of these mineral resources in the different oceans are poorly constrained. This is mainly because geochemical and mineralogical data for nodules and crusts from different oceanic basins are sparse, and there is a lack of proper comparison between them.

To address this, I analysed a suite of samples including manganese nodules and ferromanganese crusts from the North East and West Atlantic, South and Central Pacific and the Clarion Clipperton Fracture Zone (CCFZ; eastern equatorial Pacific Ocean) and the Kara Sea (Arctic Ocean) (Chapter 5).

Nodules and crusts from the Atlantic Ocean mainly acquire metals and the REY from hydrogenous sources. For this reason, they tend to consist of compacted Fe- and Mn-rich oxides, have relatively high concentrations of ΣREY, Fe and Co, and relatively slow growth rates (~ 1 mm/Ma). On the other hand, nodules from the CCFZ in the Pacific Ocean tend to be relatively large and have relatively high Mn/Fe ratios and high concentrations of Cu, Ni and Zn, which reveals that they precipitate from oxic or suboxic sediment porewaters. The CCFZ nodules also grow relatively quickly (~ 7 mm/Ma).

Nodules from the Arctic Ocean, by contrast, contain extremely high concentrations of detrital material and therefore have relatively low concentrations of transition metals and ΣREY. They are characterised by extremely fast growth rates (up to ~8080 mm/Ma).

The resource potential of ferromanganese deposits is therefore highly influenced by their mode of formation, as well as by environmental parameters such as the oxygen penetration depth in the associated sediments. Resource estimates show that hydrogenetic deposits tend to be better resources for Co and REY but, as hydrogenetic nodules tend to be smaller, the nodule density is lower, so only very large nodule fields are likely to be viable. On the other hand, large-sized diagenetic nodules from the CCFZ provide a similar metal tonnage to the hydrogenetic nodules in REY and Co, but contain far higher quantities of Ni and

Cu. As large nodule-rich basins are more common in the Pacific than in the Atlantic, Pacific nodules constitute a better resource.

6.2. Areas for further research

6.2.1. Lateral variability in the metal content of nodules within the Clarion Clipperton Fracture Zone (CCFZ)

Chapter 4 reveals that there are small-scale (<500 km) variations in the chemical composition and density of nodules both within APEI-6 and individual claim areas in the Clarion-Clipperton Fracture Zone (CCFZ). As mining impacts in the deep sea are conditioned by the characteristics of the nodule substrate in which benthic communities live in, then monitoring the environmental damage in such a heterogeneous area might be more complex than previously thought.

Areas of Potential Environmental Interest (APEIs) were delimited in the periphery of the CCFZ as part of the management plan for the exploitation of this area, on the assumption that the APEIs were representative of the licensed areas, i.e. both nodules and associated benthic communities are similar. However, Chapter 4 shows that the chemical composition of nodules and their associated sediments in APEI-6 are substantially different from some nodule concession areas like the UK Claim area. This raises concerns as to the suitability of the APEIs as comparison models.

In order to decipher their suitability, more geochemical data are required about nodules and associated sediments in other APEIs within the CCFZ. Especially, Chapter 4 shows that there is a possible relationship between the relative position of the nodule fields with respect to the Equatorial Pacific belt of primary productivity and the size and metal resource of the nodules, so data on the APEIs located further to the south, such as APEI-8 and APEI-9 will be particularly relevant.

6.2.2. Assessment of the toxicity of metals released from nodule residues in deep benthic communities

As shown in Chapter 3, significant quantities of metals could be expected to be released into the marine environment if leached nodule residues are returned to seawater. Although there are significant data regarding toxicity of metals in

shallow-water species, it remains uncertain whether shallow-water species are suitable eco-toxicological proxies for deep-sea species.

Our estimations of the metals released from nodule residues in a nodule mining scenario can then be applied to deep water species in order to test whether or not these levels are potentially harmful for such communities.

6.2.3. More detailed studies on the mineralogy of the nodules and sediments.

In chapters 4 and 5 I have attempted to identify the different mineralogical phases in nodules and crust from elemental association maps obtained by SEM analysis. These analyses are however only semi-quantitative and, although they are useful for assessing the distribution of elements in asample, they do not directly determine mineralogy.

In an attempt to directly assess the mineralogical of the nodules, X-Ray Diffraction analysis (XRD) were performed but this proved inadequate because most of the Fe-Mn-(oxyhydr)oxides that make up the bulk of the sample were amorphous.

To better characterise the mineralogy of the nodules, electron microprobe analyser (EMPA) analyses should be conducted on polished sections. This would have allowed me to accurately characterise the mineralogy of the nodules and sediments and would likely have produced new insights as to the influence of certain minerals in controlling REY concentrations. Additionally, as the role of apatite as a REY source in sediments from the Atlantic Ocean needs to be properly demonstrated, further analysis on the phosphorous content on Atlantic sediments could be performed at the same time.

6.2.4. Assessment of the applicability of the Co-growth method for nodule dating

Nodule growth rates estimated by the Co-growth method (Manheim & Lane-Bostwick, 1988) are utilised in Chapters 4 and 5 but, as discussed previously, this method can only provide minimum age estimates because it does not take into account any hiatuses in nodule growth. Although my estimates of nodule age are in good agreement with the timing of paleogeographical events that triggered nodule formation in the Clarion Clipperton Fracture

Zone (Chapter 4), a more quantitative method to measure ages would produce further reassurance.

A good approach could be to 'calibrate' the validity of the Co-growth equation in the light of techniques developed for nodule dating using isotopic systems. This includes the ^{10}Be-^{9}Be (Somayajulu, 1967) and ^{230}Th-^{232}Th (Bender et al., 1966) methods.

As some studies on isotopic dating on nodules from the Clarion Clipperton Zone are currently being developed, this will provide with a good source of comparison with the ages obtained by my approach in Chapter 4 and 5. Additionally, this will be a good opportunity to re-visit the current applicability of the original empirical formula for Co dating in nodules.

Appendices

Appendix A

A.1. Concentrations (ppm) and percentage of recovery of major and trace elements in solution for sediment leaching

	P		Ca		Cr		Mn		Fe		Co		Ni		Cu		Th		U	
	ppm	%	ppm	%	ppm	%	ppm	%	ppm	%	ppm	%	ppm	%	ppm	%	ppm	%	ppm	%
VM10-88																				
0.5 M HCl																				
15 min	679	76.7	4020	65.0	0.48	0.89	384	5.15	1090	1.24	1.51	1.98	10.7	6.02	19.6	10.7	0.86	5.61	0.39	16.0
4h	870	98.3	6580	100	0.99	1.84	565	7.58	1570	1.78	3.18	4.16	29.0	16.3	32.9	17.9	0.52	16.8	0.64	26.5
12h	868	98.1	6530	100	0.63	1.18	561	7.53	2490	2.83	2.96	3.88	40.3	22.7	31.5	17.1	0.52	3.40	0.67	27.6
0.2 M H_2SO_4																				
15 min	724	10.7	2380	38.5	0.23	0.43	260	3.49	504	0.57	1.04	1.37	7.33	4.13	12.6	6.85	2.20	14.3	0.28	11.3
1h	813	17.9	4130	66.7	0.34	0.64	359	4.81	864	0.98	1.30	1.70	14.5	8.17	16.4	8.94	2.20	14.3	0.46	18.7
4h	803	17.1	4790	77.3	0.71	1.33	463	6.21	1050	1.19	1.71	2.24	24.0	13.5	22.2	12.1	2.56	16.7	0.65	26.7
12h	874	10.7	6060	97.9	7.63	14.2	528	7.08	1900	2.16	2.50	3.28	42.6	24.0	27.6	15.0	2.86	18.6	0.76	31.1
0.2 M Buffered oxalic acid																				
15 min	151	17.0	142	2.30	0.27	0.50	3430	46.1	1820	2.08	28.9	37.9	42.4	23.9	19.8	10.8	1.34	8.72	0.31	12.8
1h	182	20.6	555	8.98	0.31	0.58	3780	50.7	2420	2.76	35.3	46.2	61.8	34.8	22.6	12.3	1.65	10.8	0.38	15.7
4h	207	23.4	435	7.03	0.85	1.58	4350	58.3	3150	3.58	47.9	62.8	93.2	52.5	35.8	19.5	2.13	13.9	0.47	19.3
12h	227	25.6	655	10.6	0.82	1.52	5300	71.0	4540	5.16	59.3	77.8	120	67.5	50.3	27.4	2.51	16.3	0.52	21.4
RC10-10																				
0.5 M HCl																				
15 min	552	63.8	909	31.2	0.18	0.23	827	17.8	866	1.40	3.08	5.03	16.5	15.4	36.9	29.7	0.56	3.55	0.20	8.22
1h	537	62.1	1540	52.9	0.68	0.61	1060	24.7	2470	4.35	4.80	8.23	37.8	34.8	50.6	45.3	0.91	5.74	0.31	12.9
4h	693	80.1	2180	74.8	0.50	0.83	1150	22.9	2690	3.98	5.05	7.83	37.2	35.3	56.3	40.8	1.08	6.77	0.34	14.2
12h	769	88.8	5010	100	1.27	1.56	1480	31.8	5400	8.73	6.93	11.3	49.1	45.9	67.5	54.3	1.65	10.4	0.41	17.2
0.2 M H_2SO_4																				
15 min	650	75.1	1560	53.5	0.23	0.29	689	14.8	882	1.42	2.50	4.07	14.1	13.2	30.1	24.2	1.85	11.6	0.18	7.35
1h	704	81.4	2210	75.9	0.28	0.35	730	15.7	1270	2.06	3.19	5.21	18.7	17.4	32.6	26.3	3.80	23.9	0.33	13.8
4h	729	84.2	2470	84.6	0.66	0.82	1240	26.7	3050	4.93	7.30	11.9	43.9	41.1	53.0	42.7	4.94	31.0	0.38	15.8
12h	722	83.5	2690	92.3	1.94	2.38	1050	22.7	4690	7.58	4.67	7.61	45.1	42.2	69.2	55.7	6.01	37.8	0.42	17.6
0.2 M Buffered oxalic acid																				
15 min	121	14.0	26	0.90	0.35	0.43	2720	58.5	2070	3.34	26.8	43.7	24.2	22.6	32.5	26.2	1.88	11.8	0.15	6.37
1h	132	15.3	98	3.35	0.50	0.61	3750	80.5	3290	5.31	39.2	63.9	37.1	34.7	41.4	33.4	3.33	20.9	0.23	9.43
4h	138	16.0	120	4.10	0.64	0.79	4440	95.3	5200	8.40	53.1	86.6	65.1	60.8	58.7	47.3	4.92	30.9	0.31	12.8
12h	136	15.7	107	3.66	1.20	1.47	4580	98.4	8510	13.8	54.4	88.7	77.7	72.6	68.3	55.0	6.39	40.2	0.38	15.9
D10311-S1																				
0.5 M HCl																				
15 min	332	64.1	7200	79.1	0.37	0.41	467	13.8	1040	1.77	2.75	5.35	22.1	20.8	36.7	29.6	0.30	2.00	0.17	7.00
1h	404	78.1	9750	100	0.70	0.77	728	21.4	2020	3.45	4.75	9.24	36.2	34.2	49.9	40.1	0.55	3.63	0.24	10.1
4h	515	99.7	7890	86.6	1.79	1.98	846	24.9	2160	3.70	6.32	12.3	42.4	40.0	62.5	50.3	0.74	4.92	0.26	11.2
12h	586	110	8440	92.8	2.04	2.25	1050	31.0	3610	6.18	9.27	18.0	46.5	43.8	61.6	49.6	1.08	7.16	0.30	12.8
0.2 M H_2SO_4																				
15 min	250	48.3	4270	46.9	0.34	0.38	598	17.6	1010	1.74	4.88	9.50	23.3	22.0	31.9	25.7	1.74	11.5	0.16	6.80
1h	303	58.6	6210	68.2	0.68	0.75	863	25.4	1960	3.36	6.38	12.4	36.6	34.5	44.1	35.5	3.00	19.9	0.26	11.1
4h	387	74.8	8420	92.5	1.47	1.62	1100	32.4	3390	5.80	10.1	19.6	48.3	45.6	54.2	43.6	3.81	25.2	0.30	12.6
12h	470	90.9	9190	100	1.54	1.70	1210	35.7	2220	3.80	10.4	20.2	56.0	52.9	63.4	51.1	4.61	30.6	0.32	13.6
0.2 M Buffered oxalic acid																				
15 min	15.1	2.93	25.4	0.28	1.10	1.21	1490	43.8	2160	3.70	20.5	39.8	32.8	31.0	30.5	24.5	0.90	5.94	0.08	3.54
1h	12.6	2.43	768	8.43	0.40	0.44	2110	62.3	1850	3.16	27.2	52.9	44.0	41.5	41.2	33.1	1.72	11.4	0.14	5.91
4h	12.4	2.40	733	8.05	1.39	1.53	2880	84.9	2550	4.36	39.0	75.8	67.6	63.8	49.9	40.2	2.87	19.0	0.22	9.14
12h	18.6	3.59	242	2.66	0.65	0.72	3060	90.1	3230	5.53	42.8	83.2	72.1	68.0	57.7	46.4	3.41	22.6	0.25	10.5

A.2. Concentrations (ppm) and percentage of recovery of rare earth elements and yttrium (REY), Th and U in solution for leaching of Atlantic sediment samples

	La		Ce		Pr		Nd		Sm		Eu		Gd		Tb	
	ppm	%	ppm	%	ppm	%	ppm	%	ppm	%	ppm	%	ppm	%	ppm	%
VM10-88																
0.5 M HCl																
15 min	24.6	28.8	18.7	11.3	7.61	34.5	31.2	36.7	7.00	40.5	1.63	41.7	6.74	42.4	1.04	43.9
1h	34.2	40.1	29.4	17.7	12.0	54.4	44.4	52.2	9.90	57.2	2.29	58.7	9.46	59.6	1.46	61.7
4h	37.4	43.9	25.6	15.5	13.0	59.0	50.9	59.9	11.5	66.8	2.68	68.8	10.8	68.0	1.68	70.9
12h	38.3	44.8	35.8	21.6	13.5	61.0	49.1	57.8	10.9	63.0	2.52	64.6	10.4	65.5	1.60	67.5
0.2 M H_2SO_4																
15 min	17.3	20.3	12.1	7.28	5.63	25.5	23.2	27.3	5.32	30.8	1.25	32.1	5.07	31.9	0.78	33.1
1h	28.8	33.8	18.4	11.1	9.60	43.5	38.7	45.5	8.82	51.0	2.05	52.6	8.26	52.0	1.29	54.5
4h	36.1	42.3	25.5	15.4	13.3	60.3	49.3	58.0	11.2	64.9	2.61	66.8	10.5	66.1	1.63	68.7
12h	41.2	48.3	31.3	18.9	15.3	69.1	56.6	66.6	12.7	73.6	2.93	75.1	11.9	75.1	1.84	77.9
0.2 M Buffered oxalic acid																
15 min	1.33	1.56	18.5	11.1	0.45	2.03	1.87	2.21	0.48	2.76	0.13	3.38	0.70	4.43	0.13	5.59
1h	1.61	1.88	18.7	11.3	0.56	2.52	2.30	2.71	0.60	3.45	0.16	4.16	0.84	5.29	0.16	6.91
4h	2.04	2.40	17.7	10.7	0.71	3.22	2.96	3.49	0.77	4.45	0.21	5.39	1.04	6.58	0.21	8.94
12h	2.48	2.90	17.7	10.7	0.88	3.98	3.66	4.31	0.95	5.50	0.26	6.64	1.28	8.05	0.26	11.0
RC10-10																
0.5 M HCl																
15 min	5.52	11.5	18.9	13.5	2.17	18.3	8.57	19.6	2.11	24.5	0.47	26.5	2.12	29.8	0.32	29.4
1h	8.96	18.6	33.1	23.6	3.27	27.5	13.3	30.4	3.19	37.0	0.71	39.5	3.12	43.8	0.47	43.0
4h	9.64	20.0	36.8	26.3	3.53	29.7	14.3	32.7	3.42	39.7	0.76	42.3	3.34	47.0	0.50	46.0
12h	11.5	24.0	48.0	34.3	4.26	35.8	17.2	39.3	4.07	47.3	0.90	50.1	3.95	55.5	0.59	54.1
0.2 M H_2SO_4																
15 min	3.84	7.98	13.8	9.88	1.55	13.0	6.41	14.7	1.66	19.3	0.38	21.3	1.66	23.3	0.32	29.4
1h	8.15	16.9	31.0	22.1	3.20	26.9	13.1	30.0	3.27	37.9	0.73	41.0	3.15	44.3	0.47	43.0
4h	9.36	19.4	37.6	26.8	3.71	31.2	15.1	34.5	3.74	43.4	0.83	46.2	3.59	50.5	0.50	46.0
12h	10.5	21.9	44.2	31.5	4.11	34.6	16.8	38.3	4.06	47.1	0.90	50.4	3.91	55.0	0.59	54.1
0.2 M Buffered oxalic acid																
15 min	1.25	2.60	18.4	13.1	0.53	4.43	2.19	5.01	0.63	7.26	0.17	9.23	0.88	12.3	0.26	23.7
1h	2.10	4.37	23.3	16.6	0.86	7.22	3.54	8.09	0.97	11.3	0.25	13.9	1.27	17.9	0.48	44.2
4h	2.82	5.86	26.1	18.7	1.14	9.62	4.70	10.8	1.27	14.7	0.32	17.8	1.61	22.6	0.54	49.7
12h	3.61	7.50	29.2	20.8	1.43	12.1	5.82	13.3	1.54	17.9	0.38	21.5	1.91	26.8	0.59	53.9
D10311-S1																
0.5 M HCl																
15 min	6.87	13.8	10.0	7.28	2.48	20.5	10.2	23.0	2.55	28.9	0.58	30.8	2.43	32.2	0.38	32.7
1h	9.57	19.3	17.1	12.4	3.39	28.1	13.9	31.3	3.46	39.1	0.78	41.4	3.28	43.4	0.51	43.9
4h	10.1	20.3	20.3	14.7	3.60	29.9	14.8	33.2	3.66	41.3	0.82	43.6	3.44	45.6	0.53	46.2
12h	11.7	23.5	29.6	21.5	4.08	33.9	17.2	38.6	4.08	46.1	0.92	48.8	3.89	51.6	0.59	51.1
0.2 M H_2SO_4																
15 min	6.00	12.1	9.40	6.82	2.23	18.5	9.31	20.9	2.37	26.8	0.55	29.0	2.27	30.1	0.35	30.6
1h	8.97	18.1	17.0	12.3	3.36	27.9	14.0	31.4	3.56	40.2	0.81	43.1	3.38	44.7	0.53	45.9
4h	9.94	20.0	21.8	15.8	3.71	30.8	15.4	34.5	3.89	44.0	0.88	46.9	3.70	48.9	0.58	49.8
12h	10.8	21.7	30.1	21.8	4.41	36.6	16.4	36.9	4.12	46.5	0.93	49.6	3.94	52.2	0.61	52.5
0.2 M Buffered oxalic acid																
15 min	0.29	0.59	5.22	3.78	0.10	0.79	0.38	0.85	0.10	1.18	0.03	1.53	0.17	2.26	0.03	3.01
1h	0.40	0.80	6.22	4.51	0.13	1.08	0.52	1.16	0.14	1.59	0.04	2.01	0.22	2.86	0.04	3.68
4h	0.42	0.84	6.73	4.88	0.13	1.07	0.50	1.12	0.14	1.53	0.04	1.92	0.21	2.79	0.04	3.86
12h	0.45	0.90	6.79	4.92	0.13	1.08	0.50	1.12	0.13	1.46	0.03	1.80	0.20	2.65	0.04	3.64

A.2 (Cont.). Concentrations (ppm) and percentage of recovery of rare earth elements and yttrium (REY), Th and U in solution for leaching of Atlantic sediment samples

	Dy		Y		Ho		Er		Tm		Yb		Lu		Σ REY	
	ppm	%	ppm	%	ppm	%	ppm	%	ppm	%	ppm	%	ppm	%	ppm	%
VM10-88																
0.5 M HCl																
15 min	6.02	43.7	38.7	47.0	1.20	44.1	3.16	42.2	0.42	39.8	2.61	38.0	0.38	37.8	151	29.4
1h	8.48	61.7	52.9	64.2	1.68	61.8	4.46	59.7	0.60	56.3	3.71	54.0	0.55	53.9	215	42.0
4h	9.67	70.2	57.7	70.2	1.90	69.9	4.96	66.3	0.66	61.5	4.01	58.4	0.58	57.8	233	45.5
12h	9.29	67.5	58.8	71.4	1.84	67.9	4.90	65.5	0.66	62.1	4.08	59.3	0.60	59.4	242	47.2
0.2 M H_2SO_4																
15 min	4.49	32.7	26.0	31.6	0.88	32.3	2.28	30.5	0.30	28.3	1.83	26.7	0.27	26.3	107	20.8
1h	7.40	53.8	44.0	53.4	1.45	53.3	3.78	50.5	0.50	46.9	3.05	44.3	0.44	43.8	176	34.4
4h	9.39	68.2	55.9	67.9	1.84	67.8	4.81	64.3	0.64	59.8	3.89	56.7	0.57	56.2	227	44.3
12h	10.6	77.1	63.9	77.7	2.08	76.7	5.48	73.3	0.73	68.3	4.47	65.0	0.65	64.4	262	51.0
0.2 M Buffered oxalic acid																
15 min	0.92	6.66	6.08	7.38	0.20	7.33	0.55	7.32	0.08	7.44	0.49	7.07	0.07	7.01	31.9	6.23
1h	1.15	8.33	7.82	9.50	0.25	9.18	0.70	9.35	0.10	9.56	0.63	9.14	0.09	9.28	35.6	6.95
4h	1.49	10.8	9.96	12.1	0.33	12.1	0.91	12.2	0.13	12.5	0.82	12.0	0.12	12.1	39.5	7.69
12h	1.84	13.4	12.5	15.1	0.40	14.8	1.12	15.0	0.16	15.2	1.01	14.7	0.15	14.8	44.6	8.70
RC10-10																
0.5 M HCl																
15 min	1.76	28.5	8.53	27.5	0.33	27.2	0.81	24.5	0.11	22.0	0.65	20.4	0.09	19.6	52.5	17.0
1h	2.56	41.5	12.3	39.8	0.48	40.0	1.21	36.8	0.16	33.2	0.99	31.2	0.14	30.3	83.9	27.2
4h	2.75	44.4	13.0	42.0	0.51	42.8	1.30	39.3	0.17	35.7	1.06	33.5	0.16	32.7	91.2	29.6
12h	3.22	52.1	15.1	48.8	0.60	50.3	1.53	46.5	0.20	42.3	1.26	40.0	0.19	39.0	113	36.5
0.2 M H_2SO_4																
15 min	1.41	22.8	6.03	19.4	0.26	21.6	0.64	19.4	0.08	17.1	0.49	15.5	0.07	14.8	38.6	12.5
1h	2.65	42.8	11.8	38.1	0.49	40.7	1.22	37.0	0.16	33.3	0.98	30.9	0.14	29.8	80.5	26.1
4h	2.96	47.9	13.3	43.0	0.55	46.0	1.38	41.9	0.18	37.9	1.11	35.2	0.16	34.0	94.1	30.5
12h	3.22	52.1	14.6	47.1	0.60	50.2	1.52	46.0	0.20	41.6	1.22	38.7	0.18	37.7	107	34.6
0.2 M Buffered oxalic acid																
15 min	1.12	18.1	6.05	19.5	0.23	19.0	0.60	18.1	0.08	17.3	0.50	15.9	0.07	15.4	32.9	10.7
1h	1.55	25.1	8.00	25.8	0.31	26.2	0.83	25.1	0.11	23.8	0.71	22.4	0.10	21.8	44.1	14.3
4h	1.95	31.6	10.0	32.3	0.39	32.8	1.03	31.4	0.15	30.2	0.89	28.3	0.13	28.1	52.9	17.2
12h	2.26	36.6	11.6	37.4	0.45	37.9	1.18	35.9	0.17	34.5	1.03	32.6	0.15	32.1	61.0	19.8
D10311-S1																
0.5 M HCl																
15 min	2.10	31.7	11.4	31.3	0.39	30.5	1.01	28.4	0.13	25.7	0.82	24.1	0.12	23.8	51.5	16.3
1h	2.82	42.7	14.9	41.0	0.53	41.2	1.36	38.2	0.18	34.5	1.11	32.4	0.16	32.3	73.0	23.1
4h	2.95	44.6	15.3	42.2	0.56	43.0	1.42	40.1	0.19	36.3	1.16	34.1	0.17	33.8	78.9	25.0
12h	3.27	49.5	17.2	47.4	0.61	47.4	1.58	44.4	0.21	40.3	1.29	37.9	0.19	37.6	96.4	30.5
0.2 M H_2SO_4																
15 min	1.97	29.8	9.70	26.7	0.37	28.5	0.94	26.4	0.12	23.7	0.75	22.0	0.11	21.8	46.5	14.7
1h	2.94	44.6	14.8	40.8	0.55	42.7	1.40	39.4	0.18	35.3	1.13	33.0	0.16	32.5	72.8	23.1
4h	3.20	48.5	16.1	44.3	0.60	46.4	1.52	43.0	0.20	38.9	1.24	36.4	0.18	35.9	82.9	26.3
12h	3.37	51.0	16.9	46.7	0.63	49.1	1.62	45.7	0.21	41.2	1.32	38.7	0.19	38.2	95.6	30.3
0.2 M Buffered oxalic acid																
15 min	0.24	3.60	1.48	4.07	0.05	3.89	0.14	3.88	0.02	3.82	0.12	3.51	0.02	3.48	8.38	2.66
1h	0.30	4.60	1.85	5.09	0.07	5.04	0.18	5.04	0.03	5.04	0.16	4.76	0.02	4.75	10.3	3.26
4h	0.33	4.97	2.10	5.79	0.07	5.77	0.21	5.96	0.03	6.06	0.20	5.82	0.03	5.91	11.2	3.54
12h	0.32	4.82	2.05	5.65	0.07	5.58	0.21	5.98	0.03	6.21	0.21	6.13	0.03	6.25	11.2	3.54

A.3. Concentrations (ppm) and percentage of recovery of major and trace elements in solution for nodules leaching

	P		Ca		Cr		Mn		Fe		Co		Ni		Cu		Th		U	
	ppm	%	ppm	%	ppm	%	ppm	%	ppm	%	ppm	%	ppm	%	ppm	%	ppm	%	ppm	%
NOD-A-1																				
0.5 M HCl																				
15 min	1280	17.0	58500	52.7	0.02	0.13	2.10	0.001	b.d.l.	b.d.l.	0.01	b.d.l.	3.50	0.06	0.21	0.02	2.71	0.01	2.71	0.04
1h	5170	68.9	70700	63.7	0.03	0.15	11.3	0.01	2.32	b.d.l	0.08	b.d.l.	5.07	0.09	0.58	0.06	8.40	0.03	26.8	0.38
4h	5280	70.3	67300	60.7	3.15	16.2	22300	11.9	9360	9.87	198	6.59	3830	64.9	2420	100	42.8	0.18	723	10.3
12h	5040	67.1	62100	56.0	4.57	23.6	45100	24.1	52500	55.3	503	16.7	3910	66.3	4340	100	140	0.58	2180	31.2
0.2 M Buffered oxalic acid																				
15 min	142	1.89	903	0.81	0.03	0.14	15.7	0.01	22.7	0.02	0.74	0.02	1.71	0.03	2.09	0.21	11.1	0.05	491	7.02
1h	53.9	0.72	13.7	0.01	0.01	0.07	47.5	0.03	50.9	0.05	1.10	0.04	1.57	0.03	2.25	0.23	199	0.82	615	8.79
4h	301	4.01	3340	3.01	5.17	26.7	136000	72.9	95700	100	1550	51.5	1790	30.3	2560	100	569	2.35	992	14.2
12h	b.d.l.	b.d.l.	5970	5.38	5.01	25.8	136000	72.5	110000	100	1840	61.2	2180	36.9	3150	100	670	2.76	1150	16.4
NOD-P-1																				
0.5 M HCl																				
15 min	643	33.6	14800	75.9	0.13	0.86	4770	1.42	3160	6.26	16.7	0.77	309	2.44	3340	31.2	83.3	0.50	1890	46.1
1h	865	45.2	17000	87.3	0.14	0.95	5120	1.52	3590	7.11	16.1	0.75	473	3.73	4410	41.1	100	0.60	2230	54.4
4h	859	44.9	22300	100	0.98	6.77	4390	1.31	3550	7.03	13.9	0.64	793	6.25	4560	42.6	93.2	0.56	2780	67.7
12h	1040	54.2	26100	100	0.44	3.00	4560	1.36	3630	7.2	11.6	0.50	1560	12.3	5230	48.8	95.2	0.57	3050	74.4
0.2 M Buffered oxalic acid																				
15 min	78.4	4.10	104	0.53	0.35	2.38	10500	3.14	3390	6.71	83.9	3.88	288	2.27	1070	9.94	1030	6.19	626	15.3
1h	77.9	4.07	589	3.01	0.33	2.30	9950	2.96	3460	6.84	83.2	3.85	292	2.30	1150	10.7	939	5.64	602	14.7
4h	81.2	4.24	590	3.02	1.15	6.10	6260	0.85	2620	4.11	70.8	2.50	273	2.24	1140	13.6	747	4.48	498	12.1
12h	82.6	4.31	783	4.01	0.89	7.94	2860	1.86	2080	5.18	53.9	3.28	285	2.15	1460	10.6	413	2.48	329	8.01

A.3 (cont.): Concentrations (ppm) and percentage of recovery of major and trace elements in solution for nodules leaching

	P		Ca		Cr		Mn		Fe		Co		Ni		Cu		Th		U	
	ppm	%	ppm	%	ppm	%	ppm	%	ppm	%	ppm	%	ppm	%	ppm	%	ppm	%	ppm	%
JC120-104-02																				
0.5 M HCl																				
15 min	633	40.6	2910	23.5	0.05	0.60	982	0.27	342	0.85	1.49	0.13	51.1	0.39	513	4.63	35.5	0.33	327	8.65
1h	648	41.6	6210	50.2	0.04	0.46	2200	0.61	582	1.44	1.65	0.15	146	1.12	1150	10.4	51.5	0.48	731	19.3
4h	739	47.4	10500	84.4	1.01	11.2	2570	0.71	1130	2.81	1.88	0.17	304	2.32	2100	19.0	71.5	0.67	1540	40.6
12h	823	52.8	14600	100	0.87	9.58	2900	0.80	2430	6.04	2.20	0.19	1110	8.49	3400	31.0	114	1.07	2490	65.7
0.2 M Buffered oxalic acid																				
15 min	50.9	3.27	67.0	0.54	0.09	0.97	5160	1.43	1850	4.58	24.9	2.21	190	1.45	370	3.34	356	3.35	209	5.52
1h	39.6	2.54	49.5	0.40	0.09	0.97	6140	1.70	2260	5.61	28.6	2.54	227	1.74	465	4.21	431	4.05	258	6.83
4h	47.3	3.03	281	2.27	0.77	8.54	6540	1.81	2810	6.97	38.9	3.45	329	2.51	796	7.20	660	6.20	384	10.1
12h	49.3	3.17	282	2.28	0.44	4.83	4970	1.38	2940	7.29	35.1	3.11	354	2.71	1210	10.9	545	5.12	358	9.47
JC120-104-03																				
0.5 M HCl																				
15 min	504	32.3	4160	60.2	0.05	0.52	787	0.20	519	1.46	1.80	0.17	69.0	0.67	732	9.15	51.6	0.52	529	12.5
1h	619	39.7	7000	100	0.26	2.94	1110	0.29	749	2.11	1.52	0.14	153	1.49	1220	15.3	55.1	0.56	935	22.0
4h	710	45.6	6520	94.3	0.49	5.56	1470	0.38	1300	3.66	1.34	0.12	332	3.23	2160	27.0	67.2	0.68	1690	39.9
12h	850	54.6	6950	100	0.34	3.81	1720	0.44	2180	6.15	1.69	0.16	1230	12.0	3370	42.1	95.9	0.97	2570	60.7
0.2 M Buffered oxalic acid																				
15 min	49.2	3.16	20.3	0.29	0.08	0.88	5000	1.29	1620	4.57	24.7	2.29	176	1.71	355	4.43	292	2.95	193	4.56
1h	50.9	3.27	24.1	0.35	0.13	1.42	6090	1.57	2200	6.19	29.1	2.70	227	2.21	523	6.53	417	4.22	286	6.74
4h	54.3	3.49	41.3	0.60	0.66	7.41	5710	1.48	2660	7.48	36.1	3.35	323	3.15	1030	12.9	562	5.68	394	9.28
12h	66.0	4.24	48.0	0.70	122	1.77	3870	1.00	2760	7.77	30.0	2.78	359	3.49	1510	18.9	434	4.39	355	8.36
JC120-104-04																				
0.5 M HCl																				
15 min	256	20.2	3290	34.2	0.05	0.51	352	0.10	517	1.21	0.83	0.08	46.5	0.34	486	4.42	79.1	0.58	521	13.3
1h	288	22.7	10300	100	0.14	1.31	504	0.14	802	1.88	1.06	0.10	90.2	0.66	729	6.63	99.3	0.73	849	21.7
4h	482	38.0	10300	100	4.18	38.8	764	0.22	1390	3.26	0.84	0.08	241	1.76	1380	12.6	118	0.86	1670	42.5
12h	535	42.3	9340	97.0	0.62	5.75	1160	0.33	2620	6.13	1.51	0.14	898	6.56	2460	22.4	160	1.17	2690	68.6
0.2 M Buffered oxalic acid																				
15 min	50.1	3.96	3.66	0.04	0.07	0.63	3230	0.91	1220	2.85	18.3	1.66	112	0.82	209	1.90	286	2.09	150	3.84
1h	58.7	4.63	368	3.82	0.10	0.91	3960	1.12	1770	4.15	21.6	1.96	143	1.04	291	2.65	385	2.82	208	5.30
4h	62.9	4.97	1630	16.9	0.62	5.77	5540	1.57	2920	6.83	38.6	3.50	276	2.02	636	5.79	716	5.24	358	9.15
12h	62.2	4.91	1830	19.0	0.63	5.82	4420	1.25	3340	7.81	35.3	3.20	305	2.23	945	8.60	682	4.99	383	9.78

A.4. Concentrations (ppm) and percentage of recovery of rare earth elements and yttrium (REY), Th and U in solution for leaching of nodule samples

	La		Ce		Pr		Nd		Sm		Eu		Gd		Tb	
	ppm	%	ppm	%	ppm	%	ppm	%	ppm	%	ppm	%	ppm	%	ppm	%
NOD-A-1																
0.5 HCl																
15 min	0.40	0.35	0.14	0.02	0.04	0.16	0.17	0.18	0.03	0.14	0.01	0.15	0.05	0.21	0.01	0.18
1h	5.24	4.62	0.93	0.13	0.55	2.25	2.36	2.47	0.42	2.00	0.11	2.11	0.71	2.83	0.10	2.63
4h	32.2	28.3	14.6	1.99	5.28	21.4	21.8	22.8	4.32	20.7	1.06	20.0	5.31	21.1	0.82	20.7
12h	45.6	40.2	45.0	6.2	10.0	40.7	37.6	39.4	7.89	37.8	1.88	35.4	8.86	35.2	1.33	33.6
0.2 M Buffered oxalic acid																
15 min	0.05	0.05	0.25	0.03	0.01	0.06	0.06	0.07	0.02	0.08	b.d.l.	0.08	0.02	0.09	0.01	0.14
1h	0.11	0.10	1.20	0.16	0.03	0.11	0.12	0.13	0.03	0.16	0.01	0.20	0.07	0.28	0.02	0.49
4h	0.35	0.31	8.24	1.13	0.09	0.35	0.36	0.38	0.10	0.46	0.03	0.55	0.20	0.81	0.05	1.15
12h	0.56	0.49	27.7	3.78	0.13	0.54	0.55	0.57	0.14	0.67	0.04	0.78	0.36	1.45	0.06	1.43
NOD-A-1																
0.5 HCl																
15 min	49.8	46.4	39.7	12.5	15.7	49.0	60.0	46.5	14.1	45.8	3.34	42.9	13.3	42.9	2.07	42.4
1h	60.9	56.7	47.4	14.9	19.1	59.6	77.0	59.7	17.1	55.7	4.07	52.2	16.2	52.3	2.54	52.0
4h	77.5	72.1	65.3	20.6	24.7	77.2	100	77.5	22.6	73.6	5.23	67.1	20.8	66.9	3.28	67.0
12h	91.7	85.3	82.5	26.0	29.3	91.4	118	91.7	25.8	84.2	6.14	78.7	24.3	78.4	3.84	78.4
0.2 M Buffered oxalic acid																
15 min	1.03	0.96	17.4	5.48	0.31	0.98	1.29	1.00	0.38	1.23	0.11	1.45	0.63	2.03	0.15	2.99
1h	0.70	0.65	5.46	1.72	0.22	0.69	0.92	0.71	0.27	0.88	0.08	1.03	0.42	1.35	0.12	2.39
4h	0.56	0.52	2.42	0.76	0.18	0.57	0.77	0.59	0.23	0.74	0.07	0.88	0.35	1.12	0.10	2.05
12h	0.39	0.36	1.32	0.42	0.14	0.42	0.59	0.46	0.18	0.59	0.06	0.71	0.27	0.88	0.08	1.64
JC120-104-02																
0.5 HCl																
15 min	9.21	11.2	3.30	1.39	2.48	9.62	10.3	9.52	2.38	8.93	0.58	8.52	2.35	9.34	0.36	9.10
1h	23.1	28.1	8.89	3.75	5.87	22.8	24.4	22.5	5.55	20.8	1.35	19.9	5.50	21.9	0.85	21.7
4h	43.5	53.0	21.9	9.24	12.8	49.6	47.6	43.9	10.8	40.6	2.61	38.5	10.5	41.9	1.64	41.5
12h	68.1	82.9	43.6	18.4	20.7	80.6	84.2	77.6	17.9	67.1	4.28	63.2	17.0	67.8	2.65	67.3
0.2 M Buffered oxalic acid																
15 min	0.96	1.16	5.77	2.44	0.29	1.14	1.22	1.12	0.33	1.25	0.09	1.34	0.40	1.61	0.08	1.93
1h	1.15	1.40	6.02	2.54	0.35	1.37	1.49	1.37	0.40	1.50	0.11	1.58	0.47	1.89	0.09	2.24
4h	1.75	2.13	6.97	2.94	0.55	2.14	2.32	2.14	0.62	2.31	0.17	2.45	0.73	2.89	0.14	3.56
12h	1.06	1.29	3.55	1.50	0.34	1.34	1.48	1.36	0.43	1.61	0.12	1.80	0.57	2.25	0.13	3.18
JC120-104-03																
0.5 HCl																
15 min	13.5	18.5	4.77	2.04	3.57	16.5	14.9	16.5	3.39	15.5	0.83	15.2	3.39	16.2	0.52	15.9
1h	26.9	36.7	9.76	4.17	6.61	30.5	27.5	30.5	6.19	28.2	1.51	27.7	6.18	29.5	0.96	29.3
4h	43.9	59.9	19.9	8.49	12.3	56.8	47.2	52.2	10.7	48.7	2.58	47.5	10.5	50.2	1.63	49.9
12h	65.6	89.6	36.0	15.4	19.7	90.9	80.1	88.7	16.9	77.2	4.07	74.8	16.3	77.9	2.55	77.9
0.2 M Buffered oxalic acid																
15 min	0.86	1.17	5.37	2.30	0.26	1.19	1.07	1.19	0.29	1.32	0.08	1.45	0.36	1.72	0.07	2.01
1h	1.17	1.60	6.38	2.73	0.36	1.65	1.48	1.64	0.40	1.81	0.11	1.98	0.47	2.27	0.09	2.71
4h	1.09	1.48	5.39	2.30	0.33	1.52	1.38	1.53	0.39	1.77	0.11	1.96	0.50	2.37	0.10	3.13
12h	0.67	0.91	2.30	0.98	0.21	0.98	0.90	1.00	0.26	1.19	0.08	1.41	0.36	1.74	0.09	2.63
JC120-104-04																
0.5 HCl																
15 min	12.5	15.6	4.06	1.48	3.35	13.5	13.8	13.4	3.20	12.4	0.78	12.2	3.17	13.0	0.49	12.9
1h	22.7	28.4	7.32	2.68	5.68	22.9	23.3	22.6	5.34	20.8	1.30	20.3	5.28	21.6	0.83	21.6
4h	43.7	54.7	17.8	6.52	11.9	47.9	45.7	44.3	10.4	40.6	2.52	39.4	10.3	42.2	1.63	42.4
12h	68.9	86.3	36.9	13.5	20.7	83.5	82.7	80.1	17.7	68.7	4.25	66.5	17.1	69.9	2.72	70.9
0.2 M Buffered oxalic acid																
15 min	0.66	0.82	4.51	1.65	0.20	0.81	0.83	0.81	0.23	0.88	0.06	0.98	0.28	1.15	0.05	1.35
1h	0.81	1.01	5.21	1.90	0.25	1.00	1.02	0.99	0.28	1.08	0.07	1.17	0.34	1.38	0.06	1.65
4h	1.45	1.82	7.81	2.85	0.45	1.81	1.85	1.79	0.51	1.97	0.14	2.13	0.60	2.48	0.12	3.03
12h	2.77	3.47	7.41	2.71	0.88	3.57	3.75	3.64	0.95	3.70	0.25	3.86	1.01	4.11	0.18	4.64

A.4 (cont.). Concentrations (ppm) and percentage of recovery of rare earth elements and yttrium (REY), Th and U in solution for leaching of nodule samples

	Dy		Y		Ho		Er		Tm		Yb		Lu		ΣREY	
	ppm	%	ppm	%	ppm	%	ppm	%	ppm	%	ppm	%	ppm	%	ppm	%
NOD-A-1																
0.5 HCl																
15 min	0.05	0.19	0.98	0.75	0.01	0.26	0.04	0.26	0.01	0.26	0.03	0.23	0.01	0.28	1.96	0.16
1h	0.70	2.85	10.1	7.78	0.18	3.73	0.55	3.77	0.08	3.75	0.46	3.30	0.08	3.91	22.6	1.87
4h	5.08	20.8	40.1	30.7	1.14	23.0	3.21	22.1	0.45	22.1	2.80	20.3	0.46	21.3	138	11.4
12h	8.00	32.7	54.7	41.9	1.72	34.6	4.76	32.8	0.68	33.0	4.24	30.7	0.67	31.1	233	19.2
0.2 M Buffered oxalic acid																
15 min	0.05	0.21	0.50	0.38	0.02	0.34	0.07	0.46	0.01	0.62	0.10	0.72	0.02	0.85	1.20	0.10
1h	0.20	0.82	1.63	1.25	0.06	1.20	0.21	1.46	0.04	1.81	0.26	1.88	0.04	2.06	4.04	0.33
4h	0.40	1.63	2.68	2.06	0.10	2.11	0.34	2.33	0.06	2.76	0.38	2.77	0.06	2.92	13.4	1.11
12h	0.46	1.87	2.97	2.28	0.12	2.38	0.37	2.55	0.06	2.96	0.41	2.96	0.07	3.09	34.0	2.80
NOD-P-1																
0.5 HCl																
15 min	11.7	42.8	50.2	55.4	2.23	44.0	5.82	42.0	0.82	41.7	5.32	40.6	0.80	42.3	275	33.8
1h	14.4	52.7	60.2	66.5	2.74	54.1	7.18	51.7	1.01	51.5	6.54	49.9	0.99	52.2	337	41.5
4h	18.6	68.0	74.5	82.3	3.54	69.8	9.29	67.0	1.31	66.7	8.54	65.2	1.29	68.3	436	53.6
12h	21.7	79.6	86.8	96.0	4.13	81.6	10.9	78.5	1.54	78.5	10.1	77.2	1.53	80.6	519	63.8
0.2 M Buffered oxalic acid																
15 min	1.15	4.22	5.53	6.11	0.26	5.22	0.79	5.69	0.13	6.49	0.87	6.64	0.13	7.12	30.1	3.70
1h	0.98	3.57	4.87	5.38	0.23	4.59	0.71	5.14	0.12	5.94	0.80	6.14	0.13	6.69	16.0	1.97
4h	0.86	3.15	4.54	5.02	0.21	4.18	0.66	4.76	0.11	5.61	0.77	5.88	0.12	6.46	11.9	1.47
12h	0.70	2.57	3.87	4.27	0.18	3.49	0.57	4.07	0.10	4.88	0.69	5.23	0.11	5.87	9.22	1.13
JC120-104-02																
0.5 HCl																
15 min	2.02	9.08	8.87	12.4	0.39	9.22	1.00	8.82	0.14	8.18	0.89	7.92	0.14	8.05	44.4	6.94
1h	4.80	21.6	20.4	28.5	0.92	22.0	2.40	21.2	0.33	19.7	2.14	19.0	0.33	19.3	107	16.7
4h	9.24	41.6	38.7	54.0	1.76	42.1	4.59	40.6	0.64	37.9	4.16	36.9	0.64	37.5	211	33.0
12h	15.0	67.6	58.7	81.9	2.86	68.1	7.48	66.1	1.05	62.2	6.91	61.4	1.05	61.9	352	54.9
0.2 M Buffered oxalic acid																
15 min	0.49	2.22	1.95	2.72	0.10	2.42	0.28	2.46	0.04	2.57	0.29	2.54	0.04	2.59	12.3	1.93
1h	0.57	2.57	2.28	3.19	0.12	2.81	0.32	2.85	0.05	2.96	0.33	2.97	0.05	3.01	13.8	2.16
4h	0.92	4.14	3.68	5.14	0.19	4.61	0.54	4.74	0.08	4.93	0.55	4.93	0.09	5.06	19.3	3.02
12h	0.89	4.03	3.96	5.54	0.20	4.68	0.57	5.02	0.09	5.32	0.61	5.44	0.10	5.74	14.1	2.20
JC120-104-03																
0.5 HCl																
15 min	2.93	16.1	12.8	21.5	0.57	16.4	1.48	15.9	0.21	14.9	1.32	14.4	0.20	14.6	64.4	11.2
1h	5.44	29.9	24.3	40.6	1.06	30.6	2.76	29.7	0.38	27.8	2.48	26.9	0.38	27.4	122	21.3
4h	9.25	50.8	39.8	66.7	1.79	51.7	4.67	50.2	0.65	47.2	4.24	46.1	0.65	46.7	210	36.6
12h	14.5	79.7	58.2	97.4	2.79	80.9	7.35	79.0	1.04	75.1	6.80	73.9	1.04	74.8	333	58.1
0.2 M Buffered oxalic acid																
15 min	0.42	2.34	1.68	2.81	0.09	2.52	0.24	2.56	0.04	2.64	0.24	2.64	0.04	2.67	11.1	1.94
1h	0.58	3.17	2.26	3.78	0.12	3.43	0.33	3.51	0.05	3.70	0.34	3.66	0.05	3.71	14.2	2.47
4h	0.70	3.86	2.96	4.96	0.15	4.39	0.43	4.64	0.07	4.87	0.46	4.99	0.07	5.21	14.1	2.46
12h	0.64	3.51	2.94	4.93	0.14	4.18	0.43	4.62	0.07	4.99	0.48	5.17	0.08	5.52	9.65	1.68
JC120-104-04																
0.5 HCl																
15 min	2.79	12.9	12.1	17.4	0.54	13.1	1.40	12.6	0.20	11.7	1.25	11.3	0.19	11.5	59.7	9.00
1h	4.73	21.9	19.9	28.7	0.91	22.3	2.37	21.4	0.33	19.9	2.13	19.2	0.32	19.4	102	15.5
4h	9.27	43.0	40.4	58.3	1.79	43.8	4.67	42.3	0.66	39.4	4.24	38.2	0.65	38.7	206	31.1
12h	15.6	72.1	61.6	88.9	2.98	73.0	7.84	71.0	1.10	66.3	7.23	65.2	1.10	66.0	348	52.6
0.2 M Buffered oxalic acid																
15 min	0.33	1.53	1.29	1.86	0.07	1.65	0.19	1.68	0.03	1.72	0.19	1.72	0.03	1.71	8.94	1.35
1h	0.41	1.90	1.58	2.28	0.08	2.06	0.23	2.08	0.04	2.13	0.24	2.16	0.04	2.18	10.7	1.61
4h	0.76	3.53	2.90	4.19	0.16	3.88	0.44	4.03	0.07	4.18	0.47	4.23	0.07	4.32	17.8	2.69
12h	1.12	5.20	4.47	6.45	0.23	5.70	0.65	5.89	0.10	6.02	0.67	6.09	0.11	6.33	24.6	3.71

A.5. Estimate of the volume and price of acids required to produce 1 tonne of metals from leaching of nodules and sediments based on release rates from the leaching experiments, together with the average market price of individual metals in April 2017 (where available; http://mineralprices.com). Calculations were only made performed where metal release was quantitative (>20%). Acid prices from ReAgent (www.chemicals.co.uk).

		La	Ce	Pr	Nd	Sm	Eu	Gd	Tb	Dy	Y	Ho	Er	Tm	Yb	Lu	ΣREY	Mn	Ni	Co	Cu
Acid to release 1 T (kL)		**Atlantic sediments**																			
	HCl	261	280	743	204	919	3970	962	6260	1080	170	5420	2040	15100	2450	16600	204	-	-	-	-
	H2SO4	243	319	655	177	786	3410	839	5430	943	156	4800	1820	13700	2240	15300	38.2	-	-	-	-
	Oxalic	-	-	-	-	-	-	-	-	-	-	-	-	-	-	-	-	1.89	83.4	169	199
		Pacific nodules																			
	HCl	109	121	342	84.5	387	1630	411	2610	460	115	2420	918	6480	989	6550	19.3	-	-	-	-
		Atlantic nodules																			
	HCl	219	222	997	266	1270	5320	1130	7530	1250	183	5830	2100	14800	2360	14900	42.9	-	-	-	-
	Oxalic	-	-	-	-	-	-	-	-	-	-	-	-	-	-	-	-	0.22	2.56	19.9	2.30
Price (k£)		**Atlantic sediments**																			
		La	**Ce**	**Pr**	**Nd**	**Sm**	**Eu**	**Gd**	**Tb**	**Dy**	**Y**	**Ho**	**Er**	**Tm**	**Yb**	**Lu**	**ΣREY**	**Mn**	**Ni**	**Co**	**Cu**
	HCl	7.59	8.11	21.6	5.92	26.7	115	27.9	182	31.2	4.94	157	59.2	438	71.2	483	5.92	-	-	-	-
	H2SO4	9.16	12.0	24.7	6.67	29.7	129	31.7	205	35.6	5.90	181	68.9	518	84.4	579	1.44	-	-	-	-
	Oxalic	-	-	-	-	-	-	-	-	-	-	-	-	-	-	-	-	1.81	80.0	162	191
		Pacific nodules																			
	HCl	3.17	3.52	9.92	2.45	11.2	47.3	11.9	75.7	13.4	3.34	70.2	26.6	188	28.7	190	0.56	-	-	-	-
		Atlantic nodules																			
	HCl	6.36	6.45	28.9	7.72	36.8	154	32.7	219	36.3	5.31	169	61.0	430	68.4	434	1.25	-	-	-	-
	Oxalic	-	-	-	-	-	-	-	-	-	-	-	-	-	-	-	-	0.21	2.45	19.1	2.21
		Market price of metals (k£)																			
		5.46	5.46	66.3	46.8	5.46	117	42.9	429	273	27.3	38.2	74.1	-	-	-	-	1.36	25.5	10.2	4.92

A.6. P_2O_5 versus ΣREY in deep sea sediments from Kato et al., (2011)

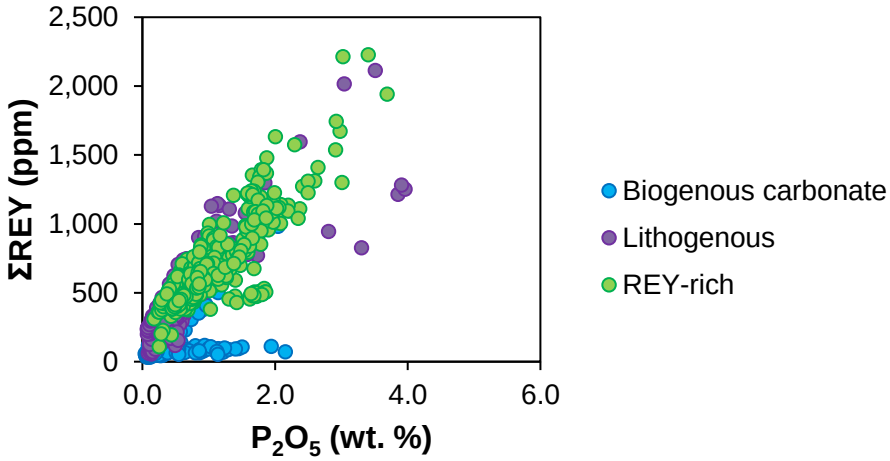

Appendix B

B.1. Methods

B.1.1. Sampling procedures

Sediments, sediment porewaters and manganese nodules were collected from four different topographical areas (Deep Plain, Trough, Ridge and Flat) in the Area of Particular Environmental interest (APEI-6) (Fig. 2), and from one site within the UK license area.

B.1.2. Sample dissolution

For each sample, ~50 mg of powdered material was transferred to a 15 mL PTFE screw-cap vial and weighed. 5 mL of aqua regia was added to each vial, which was capped and refluxed on a hotplate at 90 ˚C overnight. The solution was then evaporated to near dryness, 3 mL of HF and 2.25 mL of $HClO_4$ was added and then heated on a hotplate at 150 ˚C overnight. The cap was removed and the samples were heated to 170 ˚C until white fumes were observed. The temperature was then increased to 180 ˚C and the sample was evaporated to near-dryness. 2 mL of $HClO_4$ was added, the cap was replaced and the solution was heated overnight on a hotplate at 150 ˚C. After evaporating to near-dryness, 10 mL of 6M HCl was added and the sample was heated on a hotplate at 130 ˚C. The solution was then evaporated to near dryness, and made up to 100 cm^3 in 3% HNO_3 in a volumetric flask. A sub-sample of 1 mL of this solution was dried down, spiked with an internal standard consisting of 5 ppm Re and In and 20 ppm Be, and made up to 13 mL with 3% HNO_3 for trace element and REY analyses. For analysis of the major elements, 0.25 mL of the solution was spiked, and made up to 5 mL with 3% HNO_3.

B.1.3. XRF analysis of major element oxides and trace elements

Approximately 10 g of sediment sample were converted into pressed pellets to be used for XRF analysis. Excitation of the elements was made using a 4kW Rh end-window X-ray tube. Element concentrations were determined on a fused bead obtained following fusion with a pure lithium tetraborate flux in a Pt-Au vessel at approximately 1100˚C. A 5:1 dilution factor was chosen

to produce bead. Calibration for powder pellets and fusion beads was made using high quality International Geochemical Reference samples (GRS). Calibration was carried out using SuperQ 4.0 calibration software. During calibration any apparently spurious responses were critically evaluated and eliminated from a calibration line if there was no clear reason for the anomaly (e.g. an interference).

B.1.4. Leaching experiments in sediments

B.1.4.1. Sequential leaching procedure

Three of the sediment samples in three depth intervals were selected for sequential leaching experiments. Experiments were carried out at room temperature, and performed in duplicate for one of the samples. Samples were freeze-dried and ground as in section 3.2. A volume of 8 ml of 1 M magnesium chloride ($MgCl_2$) at pH 7.0 was added to 1g of freeze-dried sediment and shaken in a centrifuge tube for 1 hour, in order to target the exchangeable fraction of the sediments. After this time, the tube was centrifuged for 30 mins and the resulting leachate collected by a pipette. The residue was then washed with 8 ml of Milli-Q water and centrifuged again for 30 mins. This water was discarded. The residue was then added with 8 ml of 1 M sodium acetate (NaOAc) adjusted with 25 % acetic acid (HOAc) to pH 5.0, and shaken for 5 hours, to target the fraction bound to carbonates. The leachate was collected and the sample was washed as in the previous step. This residue was then added with 20 ml of a 25% solution of hydroxylamine hydrochloride ($NH_2OH \cdot HCl$) adjusted with 25 % acetic acid at pH 2.0 and shaken for 6 hours. This reagent is known to target the fraction bound to Fe-Mn oxides. Sample was then centrifuged and leachate collected as in the previous step.

100 µl aliquots of the leachate solutions were spiked with an internal standard consisting of 5 ppm Re and In and 20 ppm Be, and made up to 10 ml with 3% HNO_3. This solution was used to measure the concentrations of trace elements. A 125 µl sub-sample of this solution was further diluted with 10 mL of 3% HNO_3 spiked with Re, In and Be for analysis of the major elements.

B.1.4.2. Analysis of major elements, trace elements and REYs

Major element (Al, K, Ca, Mn, Fe), trace element (Co, Ni, Cu, Sr, Ba, Pb and U), and REY (La, Ce, Pr, Nd, Sm, Eu, Gd, Tb, Dy, Y, Ho, Er, Tm and Lu) concentrations were determined by inductively coupled plasma mass spectrometry (ICP-MS; Thermo Scientific X-Series II) at the University of Southampton. Measurements were calibrated against 6 artificial standards of different concentrations, and the reproducibility of the measurements was assessed by the addition of 2 replicates for each one of the leaching steps. Instrument drift was assessed by addition of internal standards (Re, In and Be), and analysis of an internal standard every 10 samples. The reproducibility of duplicate experiments was better than ±6% for REY, ± 3% for trace elements and ±11% for major elements. The reproducibility of Co, K and Ca was better than ± 10%, ±17% and ±25%, respectively.

B.1.4.3. Laser ablation LA ICP-MS analyses

Laser ablation ICP-MS analyses were used to assess element distribution in individual layers within nodules from both the APEI-6 and UK Claim areas. The analyses were carried out on 100 μm-thick polished sections, prepared as described in Section 2.6. Polished chips of NIST 610 and NIST 612 glass standard reference materials, and pressed pellets of nodule reference material NOD-A-1 and NOD-P-1 were mounted on a glass sample holder. Analyses were conducted at the University of Southampton using a 193 nm excimer laser (New Wave Research model UP193X) coupled to a quadrupole ICP-MS (Thermo X-Series II). Element concentrations of major elements (Al, Si, K, Ca and Mn) and trace elements (V, Cr, Co, Ni, Cu, Sr, Ba, Nb, Hf, Pb, Th and U) and REY (La, Ce, Pr, Nd, Sm, Eu, Gd, Tb, Dy, Ho, Er, Tm, Yb, Lu) were determined on 50 – 75 μm diameter spots targeting individual layers in the nodules. Ablations were conducted with a laser power of ~75% and a repetition rate of 5 Hz, in a He atmosphere. For each analysis, the gas blank was measured first with the laser beam blocked by a shutter. The shutter was then removed, and the transient signals from the analyte were collected for the ablation period. Raw counts were processed off line using standard spreadsheet software, and counts were calibrated using the nodule standards NOD-A-1 and NOD-P-1.

Appendix B

B.2. Chemical composition of cations in all sediment leachates. Leachate 1 = magnesium chloride; leachate 2 = sodium acetate and leachate 3 = hydroxylamine hydrochloride. *b.d.l.= below detection limit

	Al		K		Ca		Mn		Fe		Co		Ni		Cu		Sr		Ba		Pb		U	
	wt. %	%	wt. %	%	wt. %	%	wt. %	%	wt. %	%	ppm	%	ppm	%	ppm	%	ppm	%	ppm	%	ppm	%	ppm	%
JC120-025 (APEI-6 – Flat)																								
(0-1) cm																								
Leachate 1	<0.001	<0.01	0.06	2.31	0.09	8.85	0.01	2.69	b.d.l.	b.d.l.	0.41	0.43	1.83	1.23	0.32	0.13	18.0	6.40	37.6	b.d.l.	b.d.l.	b.d.l.	b.d.l.	b.d.l.
Leachate 2	0.01	0.14	0.05	1.84	0.14	14.1	0.05	11.5	0.002	0.05	3.13	3.30	28.3	18.9	24.0	9.74	24.2	8.61	94.3	12.5	0.06	0.18	0.17	8.23
Leachate 3	0.05	0.72	0.03	1.33	0.12	11.8	0.19	39.9	0.07	1.54	33.6	35.5	40.5	27.1	32.0	13.0	6.68	2.38	17.0	15.1	1.76	5.18	0.08	4.02
(4-5) cm																								
Leachate 1	0.02	0.19	0.06	2.18	0.19	16.5	0.003	0.62	<0.001	<0.01	b.d.l.	b.d.l.	1.84	1.09	0.14	0.05	34.1	10.6	4.89	b.d.l.	b.d.l.	b.d.l.	b.d.l.	b.d.l.
Leachate 2	0.01	0.07	0.05	1.87	0.11	9.76	0.02	3.27	0.001	0.02	0.22	0.21	15.3	9.03	23.2	8.36	20.0	6.20	39.2	8.60	0.02	0.06	0.17	7.30
Leachate 3	0.04	0.54	0.10	3.31	0.09	7.91	0.18	34.6	0.06	1.15	29.9	28.0	38.5	22.8	28.0	10.1	5.13	1.59	10.3	9.96	1.45	3.74	0.07	3.00
(12-14) cm																								
Leachate 1	<0.001	<0.01	0.07	2.43	0.16	14.4	0.01	1.97	b.d.l.	b.d.l.	0.11	0.10	2.47	1.40	0.31	0.11	26.2	7.99	5.66	b.d.l.	b.d.l.	b.d.l.	b.d.l.	b.d.l.
Leachate 2	0.01	0.07	b.d.l.	b.d.l.	0.11	10.5	0.03	5.54	0.001	0.01	0.65	0.59	26.9	15.2	25.6	8.94	20.7	6.33	69.3	9.46	0.03	0.08	0.19	7.98
Leachate 3	0.04	0.42	0.04	1.29	0.08	7.78	0.17	29.4	0.05	0.93	29.4	26.4	33.9	19.1	25.9	9.05	5.20	1.59	13.8	9.53	1.36	3.40	0.07	3.04
JC120-048 (APEI-6 – Ridge)																								
(0-1) cm																								
Leachate 1	<0.001	<0.01	0.06	2.06	0.34	24.7	0.04	7.94	b.d.l.	b.d.l.	0.71	0.68	3.15	1.75	1.61	0.60	54.9	15.9	4.25	b.d.l.	b.d.l.	b.d.l.	<0.001	0.19
Leachate 2	0.01	0.09	0.01	0.40	0.19	14.2	0.07	13.1	0.001	0.03	4.13	3.93	43.5	24.2	31.7	11.8	21.2	6.13	21.6	9.52	0.09	0.23	0.21	9.45
Leachate 3	0.04	0.50	0.07	2.55	0.14	10.1	0.15	28.1	0.05	1.05	28.2	26.9	33.4	18.5	24.8	9.26	5.70	1.65	9.40	10.6	1.16	3.05	0.06	2.91
(4-5) cm																								
Leachate 1	b.d.l.	b.d.l.	0.06	1.94	0.19	13.7	0.01	1.09	<0.001	0.01	0.09	0.08	2.44	1.29	0.28	0.10	34.4	9.76	6.02	b.d.l.	b.d.l.	b.d.l.	b.d.l.	b.d.l.
Leachate 2	0.01	0.06	b.d.l.	b.d.l.	0.10	7.19	0.02	3.53	0.001	0.02	0.41	0.37	17.2	9.1	21.5	7.32	17.4	4.95	35.6	5.93	0.02	0.05	0.15	6.40
Leachate 3	0.04	0.44	0.03	1.18	0.12	9.01	0.18	30.1	0.05	0.94	30.7	27.3	41.5	22.0	28.1	9.58	6.50	1.85	7.81	10.8	1.02	2.54	0.08	3.57
(12-14) cm																								
Leachate 1	<0.001	<0.01	b.d.l.	b.d.l.	0.16	15.6	<0.001	0.08	<0.001	<0.01	0.02	0.01	1.12	0.61	0.05	0.02	32.4	9.01	7.52	<0.01	b.d.l.	b.d.l.	b.d.l.	b.d.l.
Leachate 2	0.00	0.05	0.04	1.34	0.08	8.01	<0.001	0.84	0.001	0.01	0.02	0.02	5.56	3.01	10.0	3.55	13.8	3.84	61.5	5.27	0.00	b.d.l.	0.11	4.70
Leachate 3	0.03	0.30	0.06	2.17	0.13	12.9	0.15	26.2	0.04	0.74	25.9	22.6	36.8	19.9	19.5	6.95	5.13	1.43	13.2	7.58	1.51	3.59	0.09	3.70
JC120-105 (UK Claim)																								
(0-1) cm																								
Leachate 1	b.d.l.	b.d.l.	0.07	3.17	0.31	29.8	0.06	7.61	<0.001	<0.01	0.91	1.27	3.03	1.35	2.69	0.72	54.7	16.2	3.06	b.d.l.	b.d.l.	b.d.l.	<0.001	0.06
Leachate 2	0.01	0.17	b.d.l.	b.d.l.	0.11	10.2	0.09	11.5	0.006	0.13	5.34	7.47	37.3	16.7	48.0	12.9	20.7	6.12	9.73	11.3	0.06	0.18	0.22	14.3
Leachate 3	0.10	1.56	0.07	3.22	0.06	5.34	0.22	28.0	0.10	2.31	15.9	22.2	48.3	21.6	53.0	14.2	4.02	1.19	7.40	11.2	2.03	5.77	0.05	3.19
(4-5) cm																								
Leachate 1	<0.001	b.d.l.	0.07	2.87	0.28	26.5	0.03	3.07	<0.001	0.01	0.35	0.43	2.77	1.12	1.41	0.33	44.6	12.2	2.98	b.d.l.	b.d.l.	b.d.l.	b.d.l.	b.d.l.
Leachate 2	0.01	0.12	0.01	0.43	0.16	15.1	0.05	5.37	0.004	0.08	1.81	2.27	21.7	8.74	34.6	8.15	21.1	5.76	5.11	6.89	0.02	0.05	0.18	10.6
Leachate 3	0.10	1.34	0.08	3.18	0.06	5.95	0.24	25.4	0.10	1.97	18.4	23.0	54.1	21.8	60.8	14.3	5.23	1.43	5.74	10.6	1.80	4.65	0.07	4.17
(12-14) cm																								
Leachate 1	<0.001	<0.01	0.07	3.05	0.23	28.0	0.05	9.04	b.d.l.	b.d.l.	1.10	1.73	2.03	1.21	1.10	0.31	44.9	13.2	4.45	b.d.l.	b.d.l.	b.d.l.	b.d.l.	b.d.l.
Leachate 2	0.01	0.12	0.00	b.d.l.	0.09	10.6	0.06	10.8	0.003	0.07	4.40	6.90	16.6	9.87	28.4	8.02	19.3	5.69	22.8	9.16	0.08	0.20	0.17	10.2
Leachate 3	0.09	1.30	0.04	1.56	0.06	7.44	0.14	24.4	0.09	1.73	14.1	22.1	27.3	16.2	38.1	10.8	5.16	1.52	11.4	12.6	1.93	4.98	0.07	4.38

B.3. Chemical composition of REYs in all sediment leachates. Leachate 1 = magnesium chloride; leachate 2 = sodium acetate and leachate 3 = hydroxylamine hydrochloride. *b.d.l.= below detection limit

	La		Ce		Pr		Nd		Sm		Eu		Gd		Tb	
	ppm	%	ppm	%	ppm	%	ppm	%	ppm	%	ppm	%	ppm	%	ppm	%
JC120-025 (APEI-6 – Flat)																
(0-1) cm																
Leachate 1	b.d.l.	b.d.l.	b.d.l	b.d.l.	b.d.l.	b.d.l	b.d.l.	b.d.l	b.d.l.	b.d.l.	b.d.l.	b.d.l.	b.d.l	b.d.l.	b.d.l	b.d.l
Leachate 2	3.37	5.70	1.97	1.91	13.9	79.9	0.58	0.81	1.56	9.18	0.38	7.84	1.86	11.0	0.23	8.58
Leachate 3	6.23	10.6	6.30	6.09	32.3	100	1.25	1.75	3.01	17.7	0.74	15.1	2.87	16.9	0.46	17.6
(4-5) cm																
Leachate 1	b.d.l.	b.d.l.	b.d.l	b.d.l.	b.d.l.	b.d.l	b.d.l.	b.d.l	b.d.l.	b.d.l.	b.d.l.	b.d.l.	b.d.l	b.d.l.	b.d.l	b.d.l
Leachate 2	2.62	3.79	0.82	0.68	11.1	54.2	0.47	0.55	1.29	6.47	0.31	5.35	1.53	7.74	0.18	5.88
Leachate 3	4.86	7.03	4.89	4.06	25.5	100	0.99	1.18	2.42	12.1	0.60	10.4	2.29	11.5	0.37	12.1
(12-14) cm																
Leachate 1	b.d.l.	b.d.l.	b.d.l	b.d.l.	b.d.l.	b.d.l	b.d.l.	b.d.l	b.d.l.	b.d.l.	b.d.l.	b.d.l.	b.d.l	b.d.l.	b.d.l	b.d.l
Leachate 2	2.76	3.93	1.08	0.87	11.5	55.5	0.50	0.59	1.38	6.88	0.35	5.94	1.70	8.48	0.21	6.65
Leachate 3	4.58	6.51	4.73	3.83	24.6	100	0.98	1.15	2.42	12.1	0.60	10.3	2.25	11.3	0.37	11.9
JC120-048 (APEI-6 – Ridge)																
(0-1) cm																
Leachate 1	b.d.l.	b.d.l.	b.d.l	b.d.l.	b.d.l.	0.14	b.d.l.	b.d.l	b.d.l.	b.d.l.	b.d.l.	b.d.l.	b.d.l	b.d.l.	b.d.l	b.d.l
Leachate 2	3.09	4.01	1.50	1.29	12.8	55.4	0.58	0.61	1.59	6.85	0.42	6.36	1.98	8.57	0.27	7.46
Leachate 3	5.96	7.74	4.98	4.29	31.0	100	1.25	1.30	3.02	13.0	0.76	11.6	2.86	12.4	0.48	13.3
(4-5) cm																
Leachate 1	b.d.l.	b.d.l.	b.d.l	b.d.l.	b.d.l.	0.01	b.d.l.	b.d.l	b.d.l.	b.d.l.	b.d.l.	b.d.l.	b.d.l	b.d.l.	b.d.l	b.d.l
Leachate 2	2.31	2.85	0.79	0.63	9.60	39.6	0.43	0.43	1.13	4.69	0.29	4.23	1.35	5.61	0.18	4.80
Leachate 3	6.26	7.72	5.21	4.15	32.0	100	1.30	1.29	3.10	12.9	0.79	11.6	3.00	12.4	0.51	13.5
(12-14) cm																
Leachate 1	0.001	<0.01	0.01	0.01	0.04	0.14	b.d.l.	b.d.l.	b.d.l.	b.d.l.	b.d.l.	b.d.l.	b.d.l	b.d.l.	b.d.l	b.d.l
Leachate 2	1.98	2.41	0.47	0.4	8.24	33.6	0.37	0.37	0.97	3.99	0.26	3.68	1.18	4.79	0.16	4.33
Leachate 3	4.47	5.45	4.40	3.5	23.7	96.8	0.98	0.97	2.40	9.88	0.63	8.97	2.26	9.21	0.40	10.5
JC120-105 (UK Claim)																
(0-1) cm																
Leachate 1	b.d.l.	b.d.l.	b.d.l	b.d.l.	b.d.l.	b.d.l	b.d.l.	b.d.l	b.d.l.	b.d.l.	b.d.l.	b.d.l.	b.d.l	b.d.l.	b.d.l	b.d.l
Leachate 2	2.66	6.31	1.89	2.49	10.9	89.7	0.43	0.87	1.18	9.85	0.28	6.93	1.33	11.3	0.16	8.80
Leachate 3	3.74	8.86	4.70	6.19	16.6	100	0.63	1.27	1.40	11.8	0.36	8.99	1.39	11.7	0.24	13.3
(4-5) cm																
Leachate 1	b.d.l.	b.d.l.	b.d.l	b.d.l.	b.d.l.	b.d.l	b.d.l.	b.d.l	b.d.l.	b.d.l.	b.d.l.	b.d.l.	b.d.l	b.d.l.	b.d.l	b.d.l
Leachate 2	1.91	4.01	1.11	1.29	7.79	56.6	0.30	0.53	0.80	6.05	0.18	4.06	0.89	6.75	0.10	5.02
Leachate 3	3.89	8.16	4.70	5.47	17.3	100	0.67	1.19	1.50	11.4	0.39	8.70	1.49	11.3	0.26	12.7
(12-14) cm																
Leachate 1	b.d.l.	b.d.l.	b.d.l	b.d.l.	b.d.l.	b.d.l	b.d.l.	b.d.l	b.d.l.	b.d.l.	b.d.l.	b.d.l.	b.d.l	b.d.l.	b.d.l	b.d.l
Leachate 2	2.49	5.19	2.03	2.25	9.97	73.1	0.40	0.72	1.03	7.93	0.25	5.69	1.15	8.80	0.15	7.18
Leachate 3	4.44	9.27	5.65	6.57	20.6	100	0.81	1.45	1.86	14.4	0.48	11.1	1.82	13.9	0.32	15.9

B.3 (cont.). Chemical composition of REYs in all sediment leachates. Leachate 1 = magnesium chloride; leachate 2 = sodium acetate and leachate 3 = hydroxylamine hydrochloride. *b.d.l.= below detection limit.

	Dy		Y		Ho		Er		Tm		Yb		Lu		ΣREY	
	ppm	%	ppm	%	ppm	%	ppm	%	ppm	%	ppm	%	ppm	%	ppm	%
JC120-025 (APEI-6 – Flat)																
(0-1) cm Leachate 1	b.d.l	b.d.l	b.d.l	b.d.l.	b.d.l	b.d.l	b.d.l	b.d.l.	b.d.l	b.d.l	b.d.l	b.d.l	b.d.l	b.d.l	b.d.l	b.d.l
Leachate 2	1.54	10.0	11.3	12.5	0.26	8.72	1.07	12.9	0.06	4.93	0.72	9.34	0.06	5.05	38.9	9.25
Leachate 3	2.48	16.1	13.7	15.1	0.46	15.3	1.65	19.8	0.21	17.5	1.49	19.2	0.21	18.1	73.3	17.5
(4-5) cm Leachate 1	b.d.l	b.d.l	b.d.l	b.d.l.	b.d.l	b.d.l	b.d.l	b.d.l.	b.d.l	b.d.l	b.d.l	b.d.l	b.d.l	b.d.l	b.d.l	b.d.l
Leachate 2	1.27	7.08	9.25	8.60	0.21	6.01	0.87	8.98	0.04	2.95	0.57	6.30	0.04	3.01	30.6	6.20
Leachate 3	1.96	10.9	10.7	9.96	0.37	10.3	1.29	13.3	0.17	12.2	1.17	12.9	0.17	12.5	57.7	11.7
(12-14) cm Leachate 1	b.d.l	b.d.l	b.d.l	b.d.l.	b.d.l	b.d.l	b.d.l	b.d.l.	b.d.l	b.d.l	b.d.l	b.d.l	b.d.l	b.d.l	b.d.l	b.d.l
Leachate 2	1.39	7.70	10.2	9.46	0.25	6.89	0.98	10.1	0.06	3.96	0.63	6.96	0.05	4.00	33.0	6.61
Leachate 3	1.92	10.6	10.3	9.53	0.36	10.2	1.26	13.0	0.17	12.1	1.15	12.7	0.17	12.5	55.8	11.2
JC120-048 (APEI-6 – Ridge)																
(0-1) cm Leachate 1	b.d.l	b.d.l	b.d.l	b.d.l.	b.d.l	b.d.l	b.d.l	b.d.l.	b.d.l	b.d.l	b.d.l	b.d.l	b.d.l	b.d.l	b.d.l	b.d.l
Leachate 2	1.68	7.95	12.2	9.52	0.32	7.73	1.20	10.42	0.10	6.05	0.80	7.45	0.10	6.14	38.7	7.05
Leachate 3	2.46	11.6	13.6	10.6	0.48	11.5	1.63	14.2	0.24	14.5	1.51	14.0	0.24	14.8	70.4	12.8
(4-5) cm Leachate 1	b.d.l	b.d.l	b.d.l	b.d.l.	b.d.l	b.d.l	b.d.l	b.d.l.	b.d.l	b.d.l	b.d.l	b.d.l	b.d.l	b.d.l	b.d.l	b.d.l
Leachate 2	1.12	5.11	7.95	5.93	0.21	4.88	0.79	6.64	0.06	3.70	0.52	4.71	0.06	3.65	26.8	4.65
Leachate 3	2.58	11.7	14.4	10.8	0.51	11.7	1.73	14.6	0.25	14.7	1.56	14.2	0.25	15.1	73.5	12.7
(12-14) cm Leachate 1	b.d.l	b.d.l	b.d.l	<0.01	b.d.l	b.d.l	b.d.l	b.d.l.	b.d.l	b.d.l	b.d.l	b.d.l	b.d.l	b.d.l	b.d.l	b.d.l
Leachate 2	1.01	4.51	7.23	5.27	0.19	4.39	0.74	6.06	0.06	3.65	0.50	4.46	0.06	3.81	23.4	4.00
Leachate 3	1.95	8.73	10.4	7.58	0.40	8.95	1.30	10.7	0.21	11.8	1.19	10.6	0.21	12.2	54.9	9.38
JC120-105 (UK Claim)																
(0-1) cm Leachate 1	b.d.l	b.d.l	b.d.l	b.d.l.	b.d.l	b.d.l	b.d.l	b.d.l.	b.d.l	b.d.l	b.d.l	b.d.l	b.d.l	b.d.l	b.d.l	b.d.l
Leachate 2	1.10	10.1	7.21	11.3	0.18	8.25	0.71	12.0	0.03	3.96	0.48	8.52	0.03	3.86	28.6	9.54
Leachate 3	1.25	11.5	7.15	11.2	0.25	11.6	0.86	14.4	0.12	14.4	0.77	13.7	0.13	14.7	39.6	13.2
(4-5) cm Leachate 1	b.d.l	b.d.l	b.d.l	b.d.l.	b.d.l	b.d.l	b.d.l	b.d.l.	b.d.l	b.d.l	b.d.l	b.d.l	b.d.l	b.d.l	b.d.l	b.d.l
Leachate 2	0.73	6.14	4.90	6.89	0.11	4.75	0.48	7.31	0.02	1.84	0.33	5.31	0.02	1.73	19.7	5.85
Leachate 3	1.31	11.0	7.54	10.6	0.27	11.3	0.90	13.8	0.13	14.1	0.80	12.8	0.13	14.2	41.3	12.3
(12-14) cm Leachate 1	b.d.l	b.d.l.	b.d.l	b.d.l.	b.d.l	b.d.l.	b.d.l	b.d.l.	b.d.l	b.d.l.	b.d.l	b.d.l.	b.d.l	b.d.l.	b.d.l	b.d.l.
Leachate 2	0.96	8.09	6.56	9.16	0.16	6.94	0.65	9.93	0.04	4.20	0.46	7.37	0.04	4.26	26.2	7.82
Leachate 3	1.63	13.7	9.01	12.6	0.33	14.0	1.11	16.9	0.17	17.6	1.01	16.3	0.17	17.8	49.4	14.7

B.4. Concentrations of major and trace elements in individual layers of the JC120-105 nodule (UK Claim area). †= Growth Rate = $0.68/(Co_n)^{1.67}$, where Co_n= Co*(50/Fe+Mn), with Co, Fe and Mn in wt. % (Manheim & Lane-Bostwick, 1988).

JC120-105 (UK Claim)												
	Mn	Fe	Ca	Al	K	Ni	Cu	Co	P	Zn	Mn/Fe	GR† (mm /Ma)
	wt%	wt%	wt%	wt%	wt%	wt%	wt%	wt%	wt%	ppm		
Analysis #												
1	10.5		3.51	1.07	0.34	0.48	0.13	0.32		834		
2	8.02		3.24	2.11	0.36	0.42	0.11	0.11		448		
3	40.0	0.74	1.26	1.45	1.05	1.61	1.04	0.27	0.12	410	54.1	4.30
4	17.2	12.6	1.37	1.27	0.33	0.29	0.17	0.30	0.31	261	1.37	2.14
5	23.7	10.4	1.72	1.58	0.66	0.78	0.52	0.40	0.24	473	2.28	1.66
6	8.12		4.81	2.55	0.43	0.27	0.08	0.23		291		
7	26.2	11.6	1.63	1.32	0.66	0.51	0.55	0.51	0.24	824	2.26	1.31
8	16.8	10.4	5.16	1.90	0.41	0.94	0.24	0.30	0.24	1230	1.62	1.84
9	9.24		3.86	1.29	0.35	0.43	0.11	0.18		532		
10	36.7	3.08	1.35	1.73	0.81	1.96	1.57	0.28	0.01	3000	11.9	3.89
11	37.0	2.98	1.20	1.36	0.94	1.93	1.49	0.59	0.01	1590	12.4	1.13
12	12.4		4.39	1.68	0.31	0.67	0.17	0.25		757		
13	8.09		3.21	1.78	0.37	0.45	0.11	0.18		410		
14	13.0		4.12	1.71	0.43	0.84	0.20	0.15		915		
15	28.2	5.08	1.33	2.42	0.67	1.65	0.95	0.52	0.25	1130	5.55	1.03
16	6.87		1.68	0.90	0.27	0.53	0.12	0.08		672		
17	9.89		2.79	1.34	0.31	0.78	0.15	0.11		716		
18	12.9		2.82	1.51	0.46	0.89	0.17	0.15		1040		
19	6.54		1.64	1.08	0.28	0.56	0.10	0.09		645		
20	36.5	1.04	1.52	2.11	1.00	2.65	1.59	0.10	0.01	3770	35.1	19.7
21	16.8		5.16	1.90	0.41	0.94	0.24	0.30		1230		
22	7.07		2.95	2.75	0.52	0.30	0.09	0.06		300		
23	14.3		3.42	1.74	0.47	0.78	0.17	0.20		794		
24	13.5		4.50	1.40	0.37	0.73	0.17	0.17		991		
25	39.2	0.84	1.26	1.45	1.05	2.65	1.54	0.08	0.12	3350	46.7	31.9
26	37.0	0.90	1.01	1.34	0.91	0.99	0.78	0.35	0.11	3900	41.1	2.47
27	12.6		3.63	1.30	0.37	0.80	0.17	0.13		886		
28	6.95		1.92	1.03	0.30	0.41	0.09	0.07		473		
29	9.39		2.36	1.01	0.28	0.53	0.12	0.12		651		
30	13.9		5.10	1.97	0.47	0.58	0.13	0.25		620		
31	23.7		1.72	1.58	0.66	0.78	0.52	0.40		473		
32	8.12		5.15	2.69	0.36	0.32	0.08	0.15		409		
33	12.6		5.10	1.87	0.42	0.72	0.15	0.14		782		
34	8.24		2.85	1.32	0.27	0.45	0.11	0.17		492		
35	25.8	11.7	1.67	1.22	0.61	0.41	0.59	0.46	0.26	1020	2.21	1.54
36	11.4		3.81	2.06	0.31	0.73	0.16	0.21		706		
37	11.9		4.56	2.98	0.45	0.88	0.18	0.10		927		
38	19.1	16.5	5.28	2.10	0.51	1.00	0.23	0.30	0.34	1230	1.16	2.88
39	6.96		2.63	8.14	0.32	0.5	0.11	0.08		636		
40	9.84		4.06	1.16	0.31	0.68	0.15	0.16		913		
41	31.8	2.41	1.98	2.25	0.92	2.44	0.13	0.16	0.01	1420	13.2	7.70
42	32.1	8.26	1.73	1.00	0.66	0.78	0.84	0.37	0.26	2610	3.89	2.50
43	26.9	3.41	0.65	3.38	0.56	1.77	1.18	0.12	0.41	1970	7.89	10.2
44	32.1	5.98	1.20	1.83	0.79	1.40	0.12	0.24	0.18	2180	5.37	4.68
45	13.0	12.6	4.16	1.71	0.43	0.84	0.20	0.15	0.31	915	1.03	5.28
46	8.44		3.01	0.57	0.20	0.43	0.13	0.12		554		
47	8.65		4.05	1.90	0.40	0.36	0.10	0.33		657		
Avg	17.7	6.70	2.98	1.83	0.51	0.89	0.38	0.23	0.19	1089	13.8	5.89
SD	10.4	4.94	1.43	1.08	0.23	0.60	0.44	0.13	0.12	872	17.0	7.68

B.5. Concentrations of major and trace elements in individual layers of the JC120-025 nodule (APEI-6). †= Growth Rate = $0.68/(Co_n)^{1.67}$, where Co_n= Co*(50/Fe+Mn), with Co, Fe and Mn in wt. % (Manheim & Lane-Bostwick, 1988).

JC120-025 (APEI-6 - Flat)												
	Mn wt%	Fe wt%	Ca wt%	Al wt%	K wt%	Ni wt%	Cu wt%	Co wt%	Zn ppm	P wt%	Mn/Fe	GR† (mm/Ma)
Analysis #												
1	18.2		6.54	1.34	0.56	0.42	0.12	0.23	1530			
2	8.58		3.86	1.45	0.33	0.39	0.06	0.54	526			
3	9.84		4.16	1.39	0.32	0.51	0.07	0.58	613			
4	10.6		4.45	1.86	0.39	0.66	0.12	0.35	684			
5	17.1		6.35	2.06	0.52	1.02	0.18	0.44	1060			
6	10.3		3.60	2.48	0.31	0.61	0.11	0.76	510			
7	7.96		3.82	3.57	0.39	0.47	0.08	0.61	404			
8	6.47		2.51	2.84	0.64	0.35	0.07	0.28	278			
9	21.3		6.44	2.31	0.55	1.14	0.22	0.95	1280			
10	19.7		7.39	2.22	0.60	1.30	0.19	0.73	993			
11	11.4	5.65	5.32	2.20	0.42	0.54	0.10	0.74	658	0.17	2.01	0.19
12	8.03		4.14	2.37	0.24	0.40	0.08	0.49	333			
13	10.5		3.94	2.09	0.38	0.63	0.11	0.54	605			
14	11.1		4.65	1.69	0.43	0.64	0.11	0.35	573			
15	7.47		3.02	1.64	0.34	0.50	0.09	0.21	483			
16	15.1		6.22	2.06	0.44	0.90	0.14	0.55	802			
17	13.4	9.18	5.94	2.06	0.37	0.79	0.13	0.54	673	0.29	1.46	0.51
18	17.0	3.09	5.89	2.27	0.44	1.13	0.25	0.10	825	0.01	5.50	7.33
19	18.1		5.27	3.10	0.53	1.32	0.24	0.16	969			
20	19.1		7.44	2.57	0.45	1.25	0.22	0.27	1020			
21	16.0	5.64	4.58	1.68	0.41	0.96	0.21	0.22	843	0.15	2.83	2.12
22	20.0		5.05	2.36	0.50	1.60	0.28	0.37	1340			
23	14.7		4.62	1.75	0.45	0.68	0.17	0.52	724			
24	18.7	5.16	4.93	2.37	0.45	0.96	0.22	0.58	911	0.12	3.62	0.49
25	15.8		7.54	2.30	0.48	0.48	0.12	0.49	520			
26	18.4		5.19	1.97	0.50	1.04	0.22	0.51	966			
27	8.37		3.83	1.25	0.29	0.29	0.07	0.28	316			
28	9.69		3.61	2.04	0.34	0.42	0.10	0.42	541			
29	20.6		3.84	1.92	0.70	1.07	0.24	0.42	1568			
30	19.0		4.94	1.42	0.50	1.11	0.24	0.16	1140			
31	21.0	6.19	5.52	1.82	0.53	1.05	0.24	0.34	1180	0.17	3.40	1.47
32	20.5	6.03	5.65	1.84	0.47	1.11	0.25	0.28	1140	1530	3.40	1.93
33	17.9		4.57	1.74	0.47	0.91	0.22	0.27	830			
34	17.5		4.47	2.80	0.46	1.16	0.22	0.19	1110			
35	19.7		4.79	1.72	0.51	1.04	0.24	0.22	1140			
36	17.7		4.07	1.71	0.52	0.92	0.23	0.20	1080			
37	22.1	10.1	3.89	2.50	0.53	1.10	0.25	0.36	980	0.32	2.19	0.19
38	8.78		4.06	1.83	0.35	0.41	0.09	0.38	566			
39	11.4		3.34	2.40	0.24	0.86	0.17	0.31	636			
40	6.99		3.75	1.94	0.28	0.26	0.08	0.32	534			
41	12.0		5.03	1.94	0.37	0.69	0.13	0.25	569			
42	7.84		3.55	2.33	0.42	0.41	0.08	0.31	378			
43	6.98		3.64	1.60	0.20	0.34	0.07	0.26	303			
44	4.72		2.57	1.36	0.17	0.26	0.05	0.20	220			
45	10.4		3.60	2.11	0.33	0.54	0.12	0.45	456			
46	8.40		3.94	1.87	0.22	0.43	0.08	0.52	407			
47	5.68		3.60	2.37	0.42	0.32	0.06	0.20	263			
48	11.4		4.35	2.27	0.37	0.59	0.12	0.28	521			
49	22.2		6.81	2.57	0.43	1.12	0.22	0.62	960			
50	20.2		5.04	2.69	0.38	1.26	0.25	0.34	1100			
Avg	13.9	6.38	4.69	2.11	0.42	0.78	0.16	0.39	750	191.40	3.05	1.8
SD	5.24	2.10	1.21	0.45	0.11	0.34	0.07	0.18	326	505.94	1.2	2.2

B.6. Concentrations of major and trace elements in individual layers of the JC120-013 nodule (APEI-6). †= Growth Rate = $0.68/(Co_n)^{1.67}$, where Co_n= Co*(50/Fe+Mn), with Co, Fe and Mn in wt. % (Manheim & Lane-Bostwick, 1988).

JC120-013 (APEI-6 - Deep Plain)												
	Mn	Fe	Ca	Al	K	Ni	Cu	Co	Zn	P	Mn/Fe	GR†
	wt%	wt%	wt%	wt%	wt%	wt%	wt%	wt%	ppm	wt%		(mm/Ma)
Analysis #	16.8		9.40	3.08	0.48	0.42	0.07	1.81	845			
1	18.9		9.17	3.60	0.52	0.67	0.10	1.92	894			
2	10.8		2.24	3.68	0.34	0.98	0.13	0.51	761			
3	10.9		6.43	2.53	0.40	0.37	0.06	1.09	788			
4	8.18		3.27	1.87	0.34	0.45	0.06	0.84	567			
5	11.8		5.72	2.38	0.38	0.60	0.08	0.78	898			
6	19.5		7.63	2.77	0.47	0.87	0.13	1.57	813			
7	19.3		6.87	2.83	0.46	1.50	0.16	0.54	1120			
8	17.8		5.34	3.04	0.49	1.04	0.13	0.87	973			
9	21.0		7.68	3.09	0.64	1.70	0.18	0.37	1070			
10	16.6		6.94	2.52	0.43	1.01	0.11	0.72	797			
11	8.33		2.68	1.04	0.22	0.65	0.09	0.10	553			
12	14.0		7.89	2.27	0.36	0.35	0.07	0.78	772			
13	11.8		5.49	3.02	0.41	0.47	0.09	0.52	725			
14	15.8		7.92	2.15	0.44	0.49	0.08	0.95	800			
15	16.8		8.19	2.15	0.42	0.53	0.08	1.26	720			
16	22.6	7.33	11.0	2.47	0.50	0.77	0.13	0.93	773	0.29	3.09	0.32
17	22.0		9.93	2.52	0.48	0.85	0.13	0.87	831			
18	19.6		10.2	2.41	0.49	0.54	0.10	1.29	694			
19	14.7		7.38	1.87	0.46	0.38	0.07	1.17	560			
20	15.0		7.58	1.93	0.42	0.41	0.07	1.13	566			
21	14.8		8.20	2.28	0.42	0.50	0.07	1.08	788			
22	15.2		8.27	2.29	0.27	0.36	0.06	1.16	688			
23	16.1		7.15	2.57	0.22	0.65	0.08	1.08	796			
24	16.2		4.63	2.84	0.39	1.52	0.15	0.21	637			
25	15.7		3.69	3.02	0.34	1.43	0.15	0.30	739			
26	22.8		5.02	3.21	0.56	1.94	0.24	0.88	1764			
27	20.9	10.8	6.37	2.27	0.53	1.00	0.15	0.72	981	0.22	1.92	0.55
28	9.02		3.63	3.12	0.58	0.38	0.07	0.27	747			
29	14.7		5.88	3.05	0.53	0.85	0.11	0.39	867			
30	10.5		3.73	2.22	0.35	0.55	0.09	0.54	707			
31	17.2		6.63	2.66	0.42	1.09	0.11	0.66	899			
32	8.72		3.23	1.79	0.34	0.54	0.07	0.52	599			
33	9.03		2.81	1.84	0.29	0.69	0.08	0.43	662			
34	16.7		6.48	2.22	0.47	1.06	0.12	0.70	869			
35	21.9		8.68	3.48	0.56	1.25	0.13	1.00	1060			
36	8.03		3.51	1.63	0.34	0.39	0.06	0.66	487			
37	18.8		8.65	3.07	0.53	1.05	0.12	1.00	897			
38	18.3		7.60	2.77	0.51	1.23	0.13	0.88	924			
39	19.1		6.83	3.32	0.55	0.76	0.10	2.06	675			
40	11.3		4.12	2.34	0.36	0.67	0.08	1.02	623			
41	8.76		2.72	2.67	0.36	0.60	0.08	0.62	609			
42	18.1		7.61	3.75	0.47	0.93	0.12	1.14	991			
43	10.7	10.8	5.13	2.56	0.37	0.49	0.09	0.77	535	0.37	0.99	0.26
44	10.7		4.68	2.71	0.38	0.55	0.19	0.53	593			
45	18.6		6.65	2.15	0.53	0.81	0.11	0.84	763			
46	20.9		6.16	2.27	0.53	1.00	0.15	0.72	981			
47	15.6	10.4	7.24	2.01	0.41	0.73	0.08	1.01	715	0.37	1.49	0.10
48	22.6		6.41	2.80	0.62	1.50	0.19	1.05	1250			
49	11.9		4.14	1.90	0.43	0.51	0.06	1.12	571			
50	21.0	11.8	6.17	3.81	0.44	1.49	0.16	1.39	1120	0.22	1.78	0.19
Avg	15.6	10.2	6.25	2.53	0.44	0.82	0.11	0.84	803	0.29	1.85	0.3
SD	4.45	1.52	2.04	0.56	0.10	0.40	0.04	0.36	225	0.07	0.7	0.2

B.7. Conce ntrations of major and trace elements in individual layers of the JC120-061 nodule (APEI-6). †= Growth Rate = $0.68/(Co_n)^{1.67}$, where Co_n= Co*(50/Fe+Mn), with Co, Fe and Mn in wt. % (Manheim & Lane-Bostwick, 1988).

JC120-061 (APEI-6 - Trough)												
	Mn	Fe	Ca	Al	K	Ni	Cu	Co	Zn	P	Mn/Fe	GR†
	wt%	wt%	wt%	wt%	wt%	wt%	wt%	wt%	ppm	wt%		(mm/Ma)
Analysis #												
1	9.84		2.15	0.79	0.39	0.39	0.15	0.07	755			
2	10.4		2.97	1.21	0.45	0.46	0.17	0.07	942			
3	8.61		3.79	1.54	0.30	0.33	0.07	0.65	422			
4	7.43		3.43	1.87	0.34	0.27	0.06	0.51	322			
5	6.22		2.78	1.68	0.35	0.29	0.06	0.26	318			
6	2.09		1.92	1.52	0.16	0.11	0.02	0.07	226			
7	6.81		2.22	1.04	0.29	0.38	0.06	0.25	380			
8	10.4		2.41	1.40	0.31	0.82	0.12	0.35	752			
9	6.02		2.11	1.22	0.25	0.37	0.06	0.25	290			
10	4.69		2.46	1.53	0.34	0.10	0.04	0.21	243			
11	8.09		3.29	1.21	0.25	0.22	0.06	0.67	433			
12	9.33		4.53	1.77	0.30	0.28	0.07	0.71	389			
13	5.65		1.87	0.87	0.20	0.40	0.06	0.16	354			
14	9.00		3.64	1.77	0.27	0.49	0.10	0.28	524			
15	4.40		1.91	1.39	0.27	0.24	0.05	0.20	262			
16	11.4		4.03	2.18	0.31	0.61	0.11	0.71	582			
17	9.81	8.49	3.40	1.75	0.26	0.50	0.08	0.76	460	0.20	1.16	0.20
18	13.8		3.14	1.78	0.57	1.08	0.18	0.24	1350			
19	14.4		5.24	1.39	0.46	0.81	0.16	0.34	1060			
20	19.4	2.70	5.75	1.96	0.60	1.02	0.23	0.32	1560	0.12	7.19	1.19
21	2.37		1.34	1.95	0.42	0.07	0.03	0.17	134			
22	1.06		0.87	1.99	0.41	0.03	0.01	0.07	70.0			
23	5.18		1.58	0.96	0.31	0.32	0.06	0.20	405			
24	10.9		5.98	1.15	0.38	0.32	0.07	0.63	488			
25	6.19		2.46	1.69	0.40	0.34	0.07	0.25	361			
26	12.9		3.09	1.79	0.45	1.03	0.16	0.22	999			
27	14.0		4.75	2.44	0.47	0.99	0.18	0.39	885			
28	17.8		4.54	2.04	0.49	1.53	0.28	0.13	1490			
29	11.5		3.30	1.64	0.42	0.85	0.17	0.15	1000			
30	11.8		3.43	1.79	0.43	0.98	0.18	0.07	1180			
31	6.91		2.84	2.04	0.32	0.28	0.08	0.40	327			
32	3.32		1.52	1.05	0.23	0.11	0.03	0.16	159			
33	3.60		0.85	0.67	0.18	0.32	0.06	0.04	308			
34	7.73		4.72	2.48	0.50	0.24	0.05	0.31	331			
35	9.51		2.34	1.29	0.36	0.81	0.14	0.11	704			
36	19.9		4.28	1.41	0.60	1.23	0.25	0.19	1550			
37	12.8		5.82	1.47	0.38	0.49	0.10	0.48	552			
38	12.0		3.32	3.19	0.41	0.86	0.16	0.46	737			
39	15.5	6.85	3.17	3.36	0.43	1.31	0.21	0.22	884	0.26	2.26	2.21
40	14.2		2.53	3.48	0.49	1.25	0.21	0.46	1110			
41	9.06		5.88	2.27	0.40	0.07	0.03	0.51	362			
42	21.7	1.63	4.66	1.84	0.49	1.95	0.30	0.09	1660	0.01	13.44	11.2
43	5.55		1.76	2.34	0.26	0.37	0.09	0.09	381			
44	18.5		3.73	2.94	0.46	1.32	0.26	0.15	1260			
45	14.8		4.01	2.40	0.38	0.70	0.17	0.19	748			
46	14.4		2.89	1.76	0.38	1.09	0.21	0.08	1120			
47	15.7	5.21	3.39	2.80	0.74	1.40	0.21	0.30	1420	0.13	3.02	1.17
48	21.9	6.38	4.20	3.55	0.46	1.88	0.28	0.40	1800	0.19	3.43	1.22
Avg	10.4	4.98	3.26	1.82	0.38	0.65	0.12	0.29	709	0.14	5.41	2.87
SD	5.23	2.54	1.30	0.67	0.12	0.49	0.08	0.19	463	0.08	4.50	3.78

B.8. Concentrations of major and trace elements in individual layers of the JC120-048 nodule (APEI-6). †= Growth Rate = $0.68/(Co_n)^{1.67}$, where Co_n= Co*(50/Fe+Mn), with Co, Fe and Mn in wt. % (Manheim & Lane-Bostwick, 1988).

JC120-048 (APEI-6 - Ridge)												
	Mn wt%	Fe wt%	Ca wt%	Al wt%	K wt%	Ni wt%	Cu wt%	Co wt%	Zn ppm	P wt%	Mn/Fe	GR† (mm/Ma)
Analysis #												
1	5.37		2.92	1.71	0.40	0.21	0.05	0.21	418			
2	8.56		4.71	2.91	0.64	0.27	0.08	0.31	423			
3	5.20		2.55	1.15	0.29	0.13	0.03	0.42	399			
4	13.3		5.71	2.39	0.46	0.64	0.11	0.53	784			
5	7.37		3.65	1.38	0.33	0.23	0.06	0.34	511			
6	11.6		4.36	1.21	0.36	0.52	0.11	0.34	841			
7	7.03		3.01	0.97	0.29	0.40	0.06	0.34	466			
8	10.1		3.64	2.50	0.41	0.83	0.10	0.21	660			
9	16.0	5.08	5.23	2.23	0.41	1.29	0.16	0.70	1110	0.25	3.15	0.29
10	22.1	1.04	6.87	2.50	0.63	1.68	0.22	0.52	1491	0.01	21.3	0.57
11	7.73		2.88	1.68	0.43	0.51	0.09	0.24	559			
12	16.0	11.5	3.91	1.99	0.60	0.92	0.16	0.32	952	0.25	1.39	1.66
13	14.3		3.74	1.85	0.42	0.75	0.18	0.52	889			
14	18.3		4.41	3.12	0.34	1.39	0.28	0.40	1230			
15	1.76	6.02	0.85	0.81	0.14	0.09	0.03	0.09	241	0.18	0.29	1.79
16	17.5		4.36	2.78	0.27	1.33	0.27	0.50	1210			
17	16.7	13.7	5.26	2.58	0.55	0.83	0.17	0.33	862	0.38	1.22	1.86
18	13.5		3.89	2.86	0.51	1.03	0.21	0.12	965			
19	14.6		6.41	1.15	0.41	0.32	0.09	0.89	680			
20	8.55		3.29	0.71	0.22	0.23	0.06	0.35	322			
21	10.0		4.92	1.25	0.32	0.23	0.07	0.46	568			
22	17.1		5.83	1.33	0.49	0.50	0.13	0.66	751			
23	9.48		3.77	0.91	0.35	0.23	0.07	0.45	575			
24	17.1	2.41	7.30	1.27	0.46	0.51	0.13	0.51	608	0.01	7.10	0.43
25	18.8		4.97	2.17	0.50	1.12	0.22	0.28	932			
26	12.9		4.36	1.45	0.46	0.55	0.14	0.39	675			
27	4.68		4.57	3.47	0.20	0.28	0.05	0.08	304			
28	15.0		4.19	1.94	0.50	0.75	0.15	0.30	777			
29	4.33		2.23	1.38	0.22	0.16	0.04	0.16	280			
30	6.62		3.81	1.84	0.24	0.25	0.06	0.21	386			
31	19.1		4.59	2.15	0.52	1.29	0.22	0.14	1060			
32	17.9		4.52	2.02	0.50	1.11	0.22	0.15	992			
33	17.4		5.17	1.82	0.50	0.85	0.18	0.37	840			
34	20.5	3.41	6.81	1.37	0.49	0.65	0.17	0.42	693	0.41	6.00	0.83
35	16.7		5.68	1.35	0.46	0.51	0.14	0.32	575			
36	16.9		4.67	1.93	0.48	0.89	0.21	0.14	896			
37	14.3		5.38	1.88	0.47	0.48	0.13	0.26	534			
38	11.6		4.32	2.28	0.48	0.49	0.12	0.11	520			
39	8.96		2.73	2.64	0.57	0.74	0.11	0.04	558			
40	7.97		3.13	2.77	0.44	0.45	0.12	0.27	584			
41	6.19		3.36	1.77	0.34	0.21	0.06	0.25	350			
42	5.83		2.41	1.50	0.32	0.28	0.06	0.35	497			
43	17.1		4.51	1.87	0.56	1.46	0.23	0.10	1340			
44	14.2		3.35	2.95	0.42	1.02	0.16	0.84	859			
45	12.8		2.92	2.53	0.43	1.16	0.16	0.45	991			
46	16.3		4.37	1.76	0.47	1.24	0.20	0.23	1120			
47	17.2		2.50	3.98	0.17	1.73	0.28	0.43	1270			
48	13.6		2.74	2.18	0.24	1.19	0.20	0.24	945			
49	18.0		5.19	1.79	0.51	0.62	0.17	0.51	844			
50	17.9		6.12	1.71	0.46	0.62	0.14	0.63	743			
Avg	13.1	6.17	4.26	1.94	0.41	0.72	0.14	0.35	755	0.21	5.77	1.06
SD	4.83	4.39	1.31	0.70	0.12	0.43	0.07	0.19	293	0.15	6.75	0.63

B.9. Concentrations of major and trace elements in individual layers of the JC120-105 nodule (UK Claim area). Ce*= $(2*Ce^{SN})/(La^{SN}+Nd^{SN})$. LREE/HREE= $(La^{SN}+2*Pr^{SN}+Nd^{SN})/(Er^{SN}+Tm^{SN}+Yb^{SN}+Lu^{SN})$.

JC120-105 (UK Claim)																	
	La ppm	Ce ppm	Pr ppm	Nd ppm	Sm ppm	Eu ppm	Gd ppm	Tb ppm	Dy ppm	Y ppm	Ho ppm	Er ppm	Tm ppm	Yb ppm	Lu ppm	ΣREY ppm	ΣHREE ppm
An.#																	
1	149	420	44.5	184	45.3	11.0	41.4	6.42	35.8	114	6.62	18.6	2.60	17.2	2.57	1210	142
2	96.8	293	27.2	106	27.3	6.42	23.8	3.90	22.7	74.9	4.10	11.6	1.53	11.2	1.78	788	87.1
3	55	43.9	15.3	69.9	17.8	3.94	16.2	2.59	15.7	43.4	2.83	8.25	1.28	8.46	1.25	306	56.5
4	117	310	38.8	158	37.5	8.74	30.3	4.62	28.4	80.8	5.26	14.5	2.35	15.4	2.23	854	103
5	87.8	245	20.8	94.6	22.1	4.99	24	3.42	20.9	62.6	3.75	11.2	1.5	9.69	1.53	614	76
6	189	583	54.6	214	51.0	12.4	49.8	7.36	45.3	148	8.35	22.5	3.27	22.6	3.42	1560	175
7	202	618	52.1	208	54.3	12.0	47.4	6.95	43.3	143	8.10	21.7	3.13	21.0	3.28	1590	167
8	121	375	36.9	145	39.0	9.21	32.6	4.69	31.7	109	6.15	16.2	2.51	16.7	2.53	1060	122
9	205	511	64.8	255	65.9	17.1	62.6	9.23	52.9	209	10.3	28.3	4.11	26.1	3.76	1730	214
10	197	538	49.4	221	55.3	12.6	56.7	8.5	52.1	141	9.47	27.0	3.72	24.9	3.72	1400	199
11	97.6	317	27.1	106	27.0	6.86	26.5	4.08	22.7	84.5	4.64	12.6	1.84	12.4	1.88	837	93.5
12	152	594	47.2	183	45.6	10.9	40.7	6.66	40.0	124	7.37	21.8	2.94	18.5	3.03	1420	152
13	124	479	37.9	140	34.4	8.47	31.5	5.07	30.2	97.0	5.63	13.9	2.18	15.3	2.30	1120	115
14	100	350	31.2	120	32.0	7.05	27.0	3.90	25.6	90.3	5.01	14.3	2.21	13.7	2.14	914	101
15	122	392	35.1	139	33.8	8.37	30.5	5.19	32.3	100	6.00	16.2	2.40	17.1	2.22	1040	120
16	38.9	152	13.2	49.7	12.8	2.77	9.64	1.72	9.68	30.5	1.67	5.11	0.64	5.21	0.72	364	37.2
17	56.8	212	18.3	73.3	18.6	3.94	15.4	2.26	14.7	43.7	2.54	7.56	1.12	6.90	1.10	522	55.5
18	92.0	239	29.6	120	29.6	7.25	23.5	4.16	25.0	73.4	4.97	13.5	1.92	12.5	1.96	752	94.7
19	52.2	210	18.6	72.1	18.7	4.82	16.6	2.30	14.3	42.7	2.74	7.41	1.13	7.56	1.01	514	57.9
20	48.7	59.0	15.7	79.29	22.7	4.94	20.4	2.93	16.4	33.9	2.73	7.24	0.97	6.47	0.94	322	63.0
21	19.9	84.7	6.32	25.4	6.25	1.39	4.27	0.68	5.02	18.1	1.01	3.00	0.36	2.30	0.46	197	18.5
22	66.7	209	19.6	74.8	19.4	4.82	18.6	2.57	18.1	57.7	3.09	8.58	1.22	9.47	1.35	572	67.8

B.9 (Cont.). Concentrations of major and trace elements in individual layers of the JC120-105 nodule (UK Claim area). Ce*= $(2*Ce^{SN})/(La^{SN}+Nd^{SN})$. LREE/HREE= $(La^{SN}+2*Pr^{SN}+Nd^{SN})/(Er^{SN}+Tm^{SN}+Yb^{SN}+Lu^{SN})$.

	JC120-105 (UK Claim)																
	La ppm	Ce ppm	Pr ppm	Nd ppm	Sm ppm	Eu ppm	Gd ppm	Tb ppm	Dy ppm	Y ppm	Ho ppm	Er ppm	Tm ppm	Yb ppm	Lu ppm	ΣREY ppm	ΣHREE ppm
An.#																	
23	117	310	38.8	158	37.5	8.74	30.3	4.62	28.4	80.8	5.26	14.5	2.35	15.4	2.23	935	112
24	171	695	51.8	194	51.5	11.1	46.8	7.33	44.1	135	7.94	21.0	2.99	22.3	3.18	1600	167
25	38.5	37.4	11.0	52.5	14.2	3.04	12.7	1.84	10.8	27.7	1.94	5.10	0.71	4.67	0.69	223	41.5
26	61.3	214	17.9	71.6	20.1	4.21	14.4	2.69	13.5	44.3	2.98	7.54	1.25	7.38	1.10	529	55.0
27	105	400	34.2	130	32.3	8.11	29.7	4.46	26.5	86.2	4.78	14.2	2.05	14.6	2.10	981	106
28	69.5	127	23.2	94.3	26.8	5.72	19.5	3.14	19.5	54.5	3.65	10.2	1.32	10.1	1.41	524	74.6
29	79.2	99.1	27.5	105	30.8	6.37	27.2	3.68	21.8	56.7	3.64	10.5	1.62	10.6	1.58	542	86.9
30	269	724	81.5	315	80.9	18.9	70.5	11.2	65.6	207	13.3	35.7	4.92	34.1	5.20	2140	259
31	211	420	67.5	262	67.4	16.4	58.4	8.41	55.4	148	10.1	28.2	4.13	28.6	4.18	1540	214
32	194	660	54.8	213	55.2	13.3	48.3	7.76	48.9	152	8.81	24.7	3.37	23.4	3.80	1660	182
33	143	531	43.6	166	43.9	10.8	39.9	6.36	39.1	122	7.12	21.9	2.95	20.3	2.98	1320	151
34	82.3	419	25.8	101	27.4	6.78	27.1	4.06	24.2	87.3	4.60	12.7	1.81	13.0	1.93	927	96.2
35	821	205	306	1485	402	89.2	413	56.3	329	1600	59.4	164	20.7	133	19.8	6100	1280
36	98.5	314	31.5	126	34.8	8.38	30.8	4.59	28.2	80.6	5.40	14.8	1.95	14.3	2.05	876	110
37	45.0	253	14.0	51.8	12.9	2.96	11.1	1.97	11.6	37.5	2.09	6.41	0.94	6.17	0.93	496	44.1
38	100	720	39.8	121	23.0	7.61	19.4	3.50	22.4	92.9	4.19	11.1	1.70	12.1	1.63	1270	83.6
39	130	348	46.0	172	47.9	11.4	47.0	6.96	42.1	189	7.64	23.0	2.92	19.7	3.13	1280	164
40	68.3	279	19.6	82.8	21.8	5.11	21.7	3.28	20.4	66.7	3.77	10.2	1.33	9.80	1.37	681	76.9
41	86.3	74.1	26.1	127	35.0	7.63	29.6	4.18	24.7	53.7	4.25	11.4	1.59	10.3	1.53	498	95.2
42	52.9	23.7	110	29.6	6.17	25.4	3.67	21.4	50.4	3.68	10.1	1.37	9.37	1.39	1.52	351	125
43	67.6	104	26.7	143	41.9	9.42	36.0	5.09	27.6	52.9	4.69	12.1	1.59	10.8	1.64	545	109
44	46.7	61.2	15.6	77.6	22.3	4.91	20.2	2.91	16.9	35.1	2.87	7.68	1.03	6.81	1.16	323	64.5
45	73.3	223	20.1	79.7	19.3	4.65	17.8	2.83	18.8	59.2	3.54	9.15	1.30	9.09	1.34	602	68.5
46	193	457	52.6	201	53.3	11.5	48.8	7.39	47.1	140	8.43	22.5	3.03	18.5	2.82	1410	170
Avg	124	325	41.1	161	41.8	10.26	38.5	6.20	35.7	120.3	6.58	17.6	2.65	16.5	2.49	1023	136
SD	118	196	44.2	207	56.1	12.6	57.9	8.17	45.9	226	8.32	23.0	3.05	18.7	2.78	891	178

B.10. Concentrations of major and trace elements in individual layers of the JC120-025 nodule (APEI-6). Ce*= $(2*Ce^{SN})/(La^{SN}+Nd^{SN})$. LREE/HREE= $(La^{SN}+2*Pr^{SN}+Nd^{SN})/(Er^{SN}+Tm^{SN}+Yb^{SN}+Lu^{SN})$.

JC120-025 (APEI-6 - Flat)																	
	La ppm	Ce ppm	Pr ppm	Nd ppm	Sm ppm	Eu ppm	Gd ppm	Tb ppm	Dy ppm	Y ppm	Ho ppm	Er ppm	Tm ppm	Yb ppm	Lu ppm	ΣREY ppm	ΣHREE ppm
An.#																	
1	110	301	32.7	126	32.0	7.78	30.1	4.49	26.7	96.5	4.99	14.6	1.78	11.6	1.84	898	104
2	204	1030	56.0	196	45.6	11.6	35.2	6.37	38.1	127	7.67	18.4	2.64	18.5	2.69	1920	141
3	179	1010	49.8	190	44.9	12.2	35.7	6.32	37.8	122	7.56	20.2	2.77	17.5	2.58	1860	143
4	183	1070	53.6	197	51.0	12.0	40.4	6.83	43.1	133	7.80	21.4	3.04	17.7	2.91	1970	155
5	268	1140	79.2	305	79.3	20.3	71.6	10.5	66.3	198	12.1	32.4	4.93	30.9	4.26	2520	253
6	243	940	70.1	262	70.4	15.9	60.9	8.77	54.4	166	9.78	25.5	3.49	21.9	3.38	2120	204
7	402	1140	97.4	392	103	22.9	88.5	13.6	77.9	255	13.7	35.4	5.02	33.6	4.94	2939	296
8	158	467	45.9	179	47.9	10.8	44.4	6.54	40.0	122	7.55	20.8	2.92	18.4	2.67	1290	154
9	323	502	99.1	381	97.0	24.0	88.6	13.5	79.2	220	14.2	38.6	5.71	37.5	5.18	2150	307
10	463	1030	146	542	140	33.6	116	18.8	112	298	20.8	56.8	8.24	57.0	8.27	3350	432
11	511	1750	150	584	151	35.2	132	19.1	115	313	20.5	53.0	7.35	50.7	7.20	4210	440
12	371	1160	107	412	107	23.3	95.0	14.3	87.7	248	16.4	40.8	5.67	39.1	5.43	2980	328
13	273	988	83.6	333	85.2	20.2	79.2	12.0	72.9	202	12.6	33.8	5.04	33.2	4.82	2441	274
14	275	943	87.7	325	85.7	20.1	73.7	11.5	67.6	192	12.7	35.0	4.86	33.3	4.86	2360	263
15	162	461	49.0	186	43.8	11.7	43.8	6.64	41.4	106	7.76	19.5	2.77	18.9	2.23	1270	155
16	434	1720	133	503	126	32.1	108	17.0	98.1	271	18.9	47.2	6.62	46.0	6.84	3840	381
17	404	1440	124	466	123	29.7	107	17.0	104	268	18.0	48.0	7.32	48.4	6.99	3481	386
18	396	562	125	482	131	30.3	119	17.7	105	252	19.9	53.2	8.08	56.6	8.28	2620	418
19	316	1050	101	383	101	24.6	77.8	13.0	80.3	201	14.8	41.1	5.76	41.9	5.86	2660	305
20	610	1960	185	687	177	42.1	144	23.1	135	342	25.4	67.7	9.64	66.5	9.46	4830	523
21	268	486	80.0	305	81.4	17.8	67.2	11.0	64.5	175	11.7	32.7	4.75	32.6	4.49	1820	247
22	264	559	84.5	321	87.8	19.6	74.0	10.4	66.1	177	12.2	35.0	5.31	35.5	4.93	1930	263
23	525	1290	148	553	137	32.3	115	17.2	109	282	19.7	48.9	7.51	49.2	7.17	3620	406
24	505	1440	155	590	151	34.2	127	20.0	121	320	22.6	61.9	8.92	60.3	8.72	3950	464

B.10 (cont.). Concentrations of major and trace elements in individual layers of the JC120-025 nodule (APEI-6). Ce*= $(2*Ce^{SN})/(La^{SN}+Nd^{SN})$. LREE/HREE= $(La^{SN}+2*Pr^{SN}+Nd^{SN})/(Er^{SN}+Tm^{SN}+Yb^{SN}+Lu^{SN})$.

JC120-025 (APEI-6 - Flat)																	
	La ppm	Ce ppm	Pr ppm	Nd ppm	Sm ppm	Eu ppm	Gd ppm	Tb ppm	Dy ppm	Y ppm	Ho ppm	Er ppm	Tm ppm	Yb ppm	Lu ppm	ΣREY ppm	ΣHREE ppm
An.#																	
25	947	3360	277	1040	269	63.8	222	36.0	215	562	39.3	108	15.8	108	15.6	7840	824
26	416	915	130	481	126	29.8	102	15.8	95.9	256	17.2	50.6	6.83	46.5	6.46	2950	371
27	543	1650	158	621	158	36.8	136	21.2	131	337	23.5	65.0	9.31	65.0	9.66	4300	497
28	492	1340	146	567	151	33.1	119	19.7	114	284	19.4	53.2	7.45	49.1	8.33	3690	423
29	204	98	64.1	231	63.8	13.0	48.3	7.27	43.3	100	7.76	18.8	2.97	21.3	2.91	1030	165
30	318	496	94.4	352	94.5	19.4	75.7	10.8	68.5	188	12.3	33.2	4.68	29.6	4.37	1990	258
31	346	585	108	402	102	24.3	85.7	13.4	83.8	214	15.3	39.9	6.06	41.0	5.55	2280	315
32	305	428	90.4	352	86.7	20.1	78.0	11.7	73.6	187	13.2	34.2	5.17	37.0	5.01	1910	278
33	311	447	93.7	355	91.9	20.1	75.2	12.1	72.8	190	13.5	36.2	5.54	35.4	5.11	1960	276
34	252	242	79.6	317	84.7	18.0	68.8	10.3	65.7	177	11.2	30.7	4.78	30.6	4.39	1570	244
35	211	234	62.6	234	58.0	13.1	47.1	7.33	48.0	122	8.45	23.4	3.57	23.7	3.09	1220	178
36	193	222	57.5	215	53.4	11.9	45.7	6.95	43.5	104	7.20	19.7	3.11	19.1	2.69	1110	160
37	286	546	86.4	311	83.1	16.8	58.8	9.6	58.3	151	10.5	29.3	4.47	30.8	4.26	1840	223
38	357	1510	118	445	124	29.6	104	16.7	97.3	296	16.8	49.2	7.01	46.2	6.59	3510	373
39	185	887	58.6	219	59.3	13.9	47.1	8.24	49.7	143	8.64	23.7	3.25	23.6	3.21	1880	181
40	451	2320	134	498	127	30.3	109	16.8	100	283	17.3	46.8	6.98	47.4	7.06	4470	381
41	347	1310	110	429	113	28.1	98.1	15.1	94.5	238	16.9	43.5	6.13	39.7	6.00	3130	348
42	317	1050	94.5	364	97.0	23.5	84.8	14.0	80.6	226	14.8	39.0	5.31	36.5	5.36	2680	304
43	327	905	94.9	366	98.9	22.3	87.0	13.3	79.3	219	13.8	36.8	5.06	36.2	5.55	2530	299
44	179	710	50.4	191	47.5	11.2	46.8	6.62	38.9	119	6.45	19.0	2.70	17.2	2.42	1570	151
45	183	334	53.7	209	53.9	11.3	46.5	7.29	46.0	140	8.46	23.3	3.12	21.5	3.03	1280	171
46	353	1110	99.1	386	98.6	22.1	91.2	13.3	77.5	227	14.3	37.9	5.21	33.0	5.27	2800	300
47	301	553	96.2	394	98.9	25.1	104	14.9	82.9	381	15.8	40.8	5.56	35.4	5.42	2530	330
48	325	728	95.3	388	104	23.5	88.6	14.0	83.8	240	15.2	41.4	6.12	41.8	5.75	2440	320
49	836	1850	249	941	244	54.4	200	32.3	197	496	37.6	100	15.6	108	14.7	5870	759
50	434	683	126	461	123	26.0	102	16.2	100	264	19.6	54.5	8.00	54.9	7.79	2740	389
Avg	345	979	103	393	102	23.7	86.9	13.5	81.7	224	14.9	40.0	5.80	39.1	5.63	2680	311
SD	160	604	47.3	179	46.3	10.9	38.4	6.15	36.7	94.2	6.82	18.5	2.77	19.3	2.76	1290	142

B.11. Concentrations of major and trace elements in individual layers of the JC120-025 nodule (APEI-6). Ce*= $(2*Ce^{SN})/(La^{SN}+Nd^{SN})$. LREE/HREE= $(La^{SN}+2*Pr^{SN}+Nd^{SN})/(Er^{SN}+Tm^{SN}+Yb^{SN}+Lu^{SN})$.

JC120-013 (APEI-6 - Deep Plain)																	
	La ppm	Ce ppm	Pr ppm	Nd ppm	Sm ppm	Eu ppm	Gd ppm	Tb ppm	Dy ppm	Y ppm	Ho ppm	Er ppm	Tm ppm	Yb ppm	Lu ppm	ΣREY ppm	ΣHREE ppm
An.#																	
1	1270	6170	336	1260	303	66.8	232	36.5	218	614.0	38.8	103	14.8	94.5	14.5	11390	819
2	1080	4930	285	1040	249	57.7	188	29.3	175	509	32.4	84.9	11.3	80.7	11.1	9270	671
3	71.6	454	22.2	84	22.2	5.55	17.9	3.08	19.8	82.8	4.14	11.5	1.55	10.5	1.64	900	75.7
4	911	5360	239	901	217	49.9	159	26.8	155	443	26.7	70.4	9.49	62.0	9.15	9080	568
5	248	1590	68.7	255	60.9	15.0	50.7	8.04	46.1	142	8.70	23.0	2.91	20.6	3.01	2680	178
6	540	1960	150	562	144	32.4	116	18.4	111	323	19.4	50.6	7.47	48.3	7.14	4410	410
7	594	221	169	616	148	36.4	128	19.4	120	352	20.8	59.4	7.96	55.8	8.19	4900	456
8	319	1300	94.5	373	91.9	21.8	78.8	12.9	77.4	227	14.6	39.5	6.20	40.6	6.22	2930	298
9	382	1810	109	431	107	25.3	94.0	14.2	90.2	271	17.5	45.2	6.48	44.5	6.39	3730	344
10	414	820	127	503	133	30.2	124	17.0	104	293	18.9	51.8	7.62	50.7	6.92	2990	411
11	369	1860	106	416	101	24.2	91.0	13.9	86.8	258	15.7	42.6	6.21	43.0	6.62	3700	330
12	127	180	33.6	129	31.0	7.34	28.6	4.45	26.1	68.6	4.53	12.4	2.00	12.9	1.80	737	100
13	1450	3230	367	1380	327	76.6	288	40.1	231	624	41.0	103	14.5	92.5	13.9	8900	901
14	791	2240	204	776	177	41.6	149	21.9	134	371	23.3	60.5	8.26	54.6	8.03	5430	501
15	1150	80	297	1130	265	61.6	224	33.9	196	542	35.5	91.2	12.9	84.1	12.5	9360	752
16	998	4960	263	980	234	54.8	186	29.0	175	491	32.2	80.9	11.3	77.3	11.1	9070	657
17	1370	4580	347	1310	314	72.7	271	40.7	239	669	45.5	118	17.1	112	16.8	10190	933
18	993	3000	259	998	250	55.4	222	31.4	195	561	36.7	101	14.5	96.0	14.7	7390	767
19	1330	5148	344	1300	318	70.6	251	38.6	226	614	40.5	108	15.1	104	15.7	10540	869
20	1060	3900	275	1030	240	56.3	197	31.2	176	479	31.0	81.1	11.8	80.4	11.9	8130	676
21	986	3530	256	982	227	52.4	184	28.4	169	463	29.6	77.8	10.9	73.9	10.9	7550	637
22	1080	3400	278	1060	250	58.0	209	30.0	183	490	32.4	84.1	11.7	80.1	11.6	7760	700
23	1480	5850	359	1360	326	69.7	259	37.8	227	627	39.7	107	14.1	92.6	14.7	11490	861
24	1260	3510	318	1220	283	63.5	240	35.4	204	574	37.0	93.3	13.6	89.9	13.1	8530	790
25	144	380	47.7	199	51.9	12.9	52.2	7.60	47.0	116	8.22	22.7	3.40	21.7	3.28	1230	179

B.11 (cont.). Concentrations of major and trace elements in individual layers of the JC120-025 nodule (APEI-6). Ce*= $(2*Ce^{SN})/(La^{SN}+Nd^{SN})$. LREE/HREE= $(La^{SN}+2*Pr^{SN}+Nd^{SN})/(Er^{SN}+Tm^{SN}+Yb^{SN}+Lu^{SN})$.

JC120-013 (APEI-6 - Deep Plain)																	
	La ppm	Ce ppm	Pr ppm	Nd ppm	Sm ppm	Eu ppm	Gd ppm	Tb ppm	Dy ppm	Y ppm	Ho ppm	Er ppm	Tm ppm	Yb ppm	Lu ppm	ΣREY ppm	ΣHREE ppm
An.#																	
26	137	292	46.2	184	53.9	11.4	46.4	7.38	43.6	117	7.99	21.3	3.21	22.3	3.01	1110	167
27	162	315	59.8	251	71.9	16.0	55.5	8.19	50.9	114	9.26	25.3	3.58	25.2	3.62	1280	198
28	164	366	59.4	235	66.1	15.4	49.8	7.62	48.7	115	8.22	24.0	3.69	25.5	3.85	1310	187
29	439	1690	118	435	99.1	24.4	78.8	12.1	74.6	199	12.7	33.0	4.70	29.9	4.65	3450	275
30	605	2110	161	608	152	33.7	123	19.2	110	286	19.0	49.9	7.01	52.2	7.60	4630	421
31	267	819	72.7	290	77.2	17.9	73.9	11.0	63.1	210	11.8	32.2	4.79	31.9	4.62	2200	251
32	337	1590	95.9	365	92.2	22.3	76.6	12.1	73.1	220	13.9	39.3	5.37	39.6	5.83	3210	288
33	193	888	55.7	213	49.7	11.5	43.4	6.86	38.0	130	7.25	18.1	2.65	18.8	2.94	1810	150
34	124	644	35.3	145	32.4	7.86	28.8	4.46	28.3	85.2	5.11	13.8	2.26	14.5	1.93	1260	107
35	362	1570	99.5	385	95.7	23.7	82.3	13.1	77.5	238	15.1	40.4	6.12	40.2	5.93	3290	304
36	484	3240	136	524	126	29.8	100	17.1	104	319	19.8	53.5	7.86	54.0	7.60	5540	393
37	306	1610	79.6	312	79.2	17.8	66.4	9.94	59.6	189	11.1	28.7	4.23	26.0	3.83	2990	227
38	523	2050	143	553	133	31.2	113	17.0	102	304	18.9	50.5	7.57	49.3	7.15	4400	396
39	422	1590	105	418	105	24.9	87.6	14.2	86.3	249	15.7	43.5	6.33	44.4	6.57	3470	329
40	564	2610	155	576	133	30.7	107	16.5	104	303	18.4	49.7	6.88	46.0	6.70	5030	386
41	203	1060	54.0	210	50.3	11.6	34.8	6.15	40.5	119	7.30	18.3	2.77	19.7	2.71	1960	144
42	174	950	46.7	177	42.0	9.56	30.2	4.96	32.0	100	5.48	15.7	2.32	13.3	2.04	1710	116
43	589	3690	169	639	150	35.8	118.5	20.2	117	337	21.2	55.2	8.07	51.8	7.65	6340	435
44	381	2010	101	396	95.8	23.3	81.7	12.7	74.8	228	13.9	35.5	4.56	31.2	4.86	3720	282
45	315	1320	86.4	333	85.1	19.8	67.4	10.9	66.2	197	11.6	29.8	4.39	27.2	4.21	2780	241
46	442	1840	127	478	121	27.3	96.8	15.6	91.7	273	17.2	45.6	6.33	42.7	6.36	3900	350
47	379	823	109	407	103	23.7	88.6	13.6	83.1	257	16.1	43.4	6.27	44.1	6.37	2660	325
48	576	2100	153	578	145	32.8	117.1	17.9	110	329	20.8	53.9	7.96	53.9	7.79	4630	422
49	358	954	102	396	104	24.2	86.9	13.4	84.1	234	15.4	44.6	6.39	45.4	6.26	2710	327
50	366	1810	100	370	88.0	21.6	72.7	11.6	68.1	196	12.6	32.8	4.64	30.4	4.33	3380	259
Avg	586	2170	156	595	144	33.3	119	18.3	109	311	19.8	52.4	7.46	50.0	7.39	4820	417
SD	404	1610	100	376	88.2	19.8	72.3	10.7	62.2	170	11.2	29.0	4.03	26.7	4.03	3060	239

B.12. Concentrations of major and trace elements in individual layers of the JC120-061 nodule (APEI-6). Ce*= $(2*Ce^{SN})/(La^{SN}+Nd^{SN})$. LREE/HREE= $(La^{SN}+2*Pr^{SN}+Nd^{SN})/(Er^{SN}+Tm^{SN}+Yb^{SN}+Lu^{SN})$.

JC120-061 (APEI-6 - Trough)																	
	La ppm	Ce ppm	Pr ppm	Nd ppm	Sm ppm	Eu ppm	Gd ppm	Tb ppm	Dy ppm	Y ppm	Ho ppm	Er ppm	Tm ppm	Yb ppm	Lu ppm	ΣREY ppm	ΣHREE ppm
An.#																	
1	38.9	196	16.1	69.6	20.0	5.1	15.0	2.34	12.3	27.7	1.91	5.5	0.62	4.73	0.64	444	48.2
2	84.0	245	32.4	139	40.7	10.6	39.9	5.16	29.6	115	5.73	15.2	2.12	13.5	1.85	893	124
3	182	1020	54.0	213	55.9	13.5	43.6	6.92	42.2	130	7.70	20.6	2.78	18.8	2.65	1940	159
4	143	667	39.4	156	42.5	9.4	36.8	5.75	33.3	108	6.35	16.5	2.63	16.3	2.18	1390	129
5	130	579	38.2	149	37.0	9.0	34.1	5.45	30.4	107	5.98	15.8	2.43	14.8	2.08	1270	120
6	37.5	151	11.3	40.8	10.8	2.7	10.1	1.38	8.68	27.9	1.67	4.54	0.70	4.48	0.52	342	34.7
7	123	515	35.8	134	32.1	8.6	27.5	4.51	25.9	80.9	4.79	13.4	1.92	13.1	1.89	1100	102
8	96.7	590	32.3	112	29.4	6.7	21.2	3.76	21.8	64.5	4.30	10.8	1.77	11.2	1.59	1070	83.0
9	87.4	350	26.4	107	28.1	6.1	22.8	3.34	22.7	66.9	4.36	10.8	1.47	10.0	1.58	816	83.1
10	224	839	70.2	259	61.0	15.2	57.3	8.50	47.2	141	8.19	23.0	3.16	19.7	2.97	1920	185
11	366	1030	104	384	94.2	22.3	79.8	12.9	77.6	218	12.8	34.2	4.88	32.7	4.86	2690	282
12	423	1200	118	451	110	26.6	102	14.6	84.9	258	15.3	41.3	5.41	37.3	5.29	3150	333
13	72.0	262	19.0	72.3	17.6	4.60	16.6	2.44	16.6	57.8	3.04	8.65	1.36	6.64	1.18	619	61.1
14	192	725	48.4	196	47.5	11.0	45.3	6.50	37.9	140	7.47	19.3	2.65	18.5	2.6	1640	151
15	112	411	29.5	114	30.3	6.69	27.3	4.27	25.0	86.6	4.67	11.8	1.83	12.0	1.7	965	95
16	236	1160	65.5	241	58.9	14.4	51.6	8.64	51.3	172	9.55	26.5	3.71	25.7	3.5	2300	195
17	223	1140	61.3	235	61.5	14.8	53.3	8.57	50.9	183	10.1	27.5	3.89	27.2	3.7	2290	200
18	117	301	35.4	141	34.9	8.96	29.9	4.88	27.8	91.5	5.31	15.0	2.17	16.2	2.4	925	113
19	299	784	81.6	304	75.6	17.2	70.2	10.7	64.3	214	11.8	34.6	4.94	34.2	4.7	22240	253
20	294	717	85.0	316	77.1	18.7	73.1	11.0	64.7	212	12.7	34.0	5.25	34.1	4.9	2170	258
21	86.8	191	24.2	96.7	23.7	5.18	24.2	3.6	22.9	107	4.56	13.0	1.96	12.2	2.1	725	89.7
22	50.7	132	14.1	56.2	13.7	2.87	12.6	2.1	12.1	49.2	2.43	6.03	0.84	4.78	0.71	409	44.4
23	70.8	300	22.5	85.2	24.1	5.67	20.6	3.3	18.7	60.0	3.74	10.0	1.56	9.80	1.24	697	74.5
24	347	1660	107	398	98.7	25.1	84.5	13.4	77.9	251	14.6	41.2	5.99	38.5	5.72	3420	307
25	125	498	38.6	148	39.5	9.31	33.1	4.91	31.1	100	5.85	17.1	2.34	15.4	2.44	1170	122

B.12 (cont.). Concentrations of major and trace elements in individual layers of the JC120-061 nodule (APEI-6). Ce*= $(2*Ce^{SN})/(La^{SN}+Nd^{SN})$. LREE/HREE= $(La^{SN}+2*Pr^{SN}+Nd^{SN})/(Er^{SN}+Tm^{SN}+Yb^{SN}+Lu^{SN})$.

JC120-061 (APEI-6 - Trough)																	
	La ppm	Ce ppm	Pr ppm	Nd ppm	Sm ppm	Eu ppm	Gd ppm	Tb ppm	Dy ppm	Y ppm	Ho ppm	Er ppm	Tm ppm	Yb ppm	Lu ppm	ΣREY ppm	ΣHREE ppm
An.#																	
26	139	586	46.1	178	48.8	11.8	38.7	5.74	37.4	108	6.67	17.7	2.69	18.8	2.69	1360	142
27	193	696	60.3	228	59.6	14.2	50.0	7.80	48.2	140	8.69	23.3	3.67	23.8	3.40	1700	183
28	86.0	190	29.9	108	30.2	7.33	23.8	3.76	24.5	68.0	4.56	11.7	2.06	13.3	1.81	673	92.8
29	147	343	48.7	192	52.0	12.3	47.5	6.98	40.0	119	7.59	20.1	2.90	19.6	2.93	1180	160
30	67.5	131	24.8	102	28.3	6.89	21.4	3.26	20.9	62.5	3.95	10.9	1.73	12.6	1.89	562	83.5
31	171	549	51.9	216	59.1	13.2	51.6	7.63	48.9	147	8.57	23.6	3.27	21.4	3.26	1522	181
32	151	317	32.4	303	36.2	8.47	28.9	4.64	27.5	84.6	5.09	13.4	2.07	13.7	2.06	1110	106
33	34.9	96.2	11.2	40.8	12.2	2.36	9.6	1.44	9.28	25.1	1.67	4.26	0.58	5.30	0.71	281	35.2
34	324	1340	102	384	100	24.7	87.5	13.5	81.5	240	15.0	40.3	5.53	41.6	5.99	3040	316
35	111	319	42.1	161	43.4	10.1	35.2	5.87	33.1	104	6.30	18	2.29	16.9	2.29	1010	130
36	166	547	67.3	267	77.0	17.6	58.1	8.96	55.3	133	9.77	26.0	3.72	27.4	3.64	1600	211
37	399	1640	134	509	134	33.4	112	18.4	110	316	21.3	58.4	8.54	55.0	7.60	3870	424
38	221	899	74.7	278	75.3	17.5	59.7	10.2	61.8	175	11.7	31.2	4.42	31.2	4.55	2130	232
39	227	197	85.9	338	97.6	21.1	74.4	11.8	73.5	168	12.7	37.3	5.80	39.6	5.65	1560	282
40	229	1100	77.8	297	80.2	19.8	61.8	10.1	61.5	163	11.4	30.0	4.22	28.6	4.31	2340	232
41	596	3160	201	744	197	46.3	162	26.0	150	437	28.5	75.4	10.8	73.6	11.1	6360	584
42	228	212	89.8	355	107	26.1	83.9	12.8	79.2	164	13.8	38.5	6.05	43.2	6.08	1630	310
43	93.7	168	35.4	136	39.8	9.69	40.2	5.84	34.4	147	6.43	16.9	2.27	16.4	2.26	902	134
44	154	438	51.5	192	52.3	11.7	44.0	6.33	37.6	106	7.46	19.8	2.89	18.9	2.51	1250	151
45	329	358	108	403	111	23.7	95.1	14.5	92.4	231	16.4	45.8	7.16	48.5	6.90	2120	350
46	84.0	110	28.0	103	26.6	5.61	24.4	3.58	21.6	56.8	3.50	11.0	1.48	11.1	1.54	548	83.9
47	129	70.8	61.0	242	73.5	18.5	57.0	8.56	49.6	97.3	8.35	22.9	3.45	24.2	3.14	966	196
48	175	465	60.0	221	55.8	13.6	48.5	7.72	43.7	149	8.93	23.2	3.53	25.6	3.34	1450	178
Avg	179	616	57.0	221	57.5	13.7	48.9	7.59	45.4	136	8.40	22.8	3.32	22.5	3.22	2000	176
SD	115	547	36.7	136	36.0	8.59	30.0	4.75	28.1	78.8	5.20	14.2	2.06	14.1	2.04	3140	109

B.13. Concentrations of major and trace elements in individual layers of the JC120-048 nodule (APEI-6). Ce*= $(2*Ce^{SN})/(La^{SN}+Nd^{SN})$. LREE/HREE= $(La^{SN}+2*Pr^{SN}+Nd^{SN})/(Er^{SN}+Tm^{SN}+Yb^{SN}+Lu^{SN})$.

JC120-048 (APEI-6 - Ridge)																	
	La ppm	Ce ppm	Pr ppm	Nd ppm	Sm ppm	Eu ppm	Gd ppm	Tb ppm	Dy ppm	Y ppm	Ho ppm	Er ppm	Tm ppm	Yb ppm	Lu ppm	ΣREY ppm	ΣHREE ppm
An.#																	
1	110	319	38.3	143	42.2	8.79	34.3	5.12	31.9	129	6.17	15.5	2.07	13.1	2.07	1030	119
2	154	630	43.7	174	42.9	10.7	38.1	5.66	35.8	174	6.36	18.0	2.63	15.6	2.33	1530	135
3	147	657	40.1	162	41.6	9.40	37.8	5.63	33.5	112	6.25	15.2	2.21	16.3	2.17	1400	129
4	262	995	71.6	278	71.0	15.8	63.4	10.1	58.6	189	11.0	29.9	4.17	27.5	3.94	2280	224
5	159	670	43.7	177	42.1	10.4	40.3	6.03	38.3	123	7.20	18.6	2.78	16.9	2.85	1480	143
6	118	442	32.3	130	33.8	7.84	29.7	4.23	29.9	99.7	5.20	15.9	2.24	14.6	2.24	1070	112
7	199	629	51.8	204	49.7	10.2	44.7	6.78	37.7	121	7.22	20.0	2.72	16.7	2.76	1530	149
8	104	343	30.2	113	29.7	7.11	22.8	3.36	21.6	60.0	4.01	10.5	1.75	10.2	1.40	823	82.7
9	154	639	45.0	173	43.8	10.3	35.4	5.58	35.0	107	6.58	18.0	2.49	16.6	2.58	1400	132
10	175	292	53.5	213	53.7	12.6	44.9	7.07	42.7	120	8.03	22.3	3.43	24.4	3.20	1200	169
11	89.4	312	25.0	92.6	23.8	5.82	19.9	3.00	17.5	54.4	3.45	9.17	1.43	9.24	1.26	723	70.7
12	196	350	52.6	191	48.8	10.1	40.5	6.26	38.3	116	7.03	20.2	3.05	19.4	2.93	1220	148
13	253	522	75.7	302	79.7	17.8	74.5	10.7	65.6	240	12.6	33.7	4.97	32.8	4.77	1970	257
14	191	325	57.3	214	58.9	12.9	49.3	8.07	48.1	139	9.68	26.3	4.14	27.8	3.89	1310	190
15	53	164	13.9	54	13.2	3.21	12.8	1.77	11.2	31	1.96	5.28	0.87	5.25	0.76	403	43.1
16	189	552	55.2	205	55.6	11.4	44.7	7.80	51.3	134	8.77	26.6	3.92	28.5	4.01	1510	187
17	340	1890	96.7	374	95.0	22.4	73.9	11.9	73.4	209	13.6	38.9	6.01	40.2	5.77	3490	286
18	174	365	51.3	201	53.2	11.6	43.9	7.21	42.9	120	8.04	23.0	3.62	22.1	3.22	1250	166
19	848	2110	237	926	227	51.9	204	30.0	179	443	33.1	86.2	12.3	81.7	12.0	5920	691
20	400	913	113	437	108	25.0	103	14.6	93.4	238	17.9	47.7	7.43	49.5	6.92	2810	365
21	675	1430	184	720	180	40.8	160	22.7	139	341	25.4	64.4	9.50	62.2	9.19	4400	533
22	694	1770	200	774	189	42.9	172	25.8	155	398	29.1	78.1	12.3	77.3	11.5	5030	604
23	560	1240	156	600	146	33.6	134	19.0	116	287	20.7	53.7	7.52	50.8	7.68	3720	443
24	715	1710	199	788	200	44.1	178	27.6	172	432	31.3	87.1	12.9	88.5	13.2	5130	654
25	321	576	92.1	356	90.1	20.9	76.8	12.1	75.1	192	14.6	39.3	5.86	41.0	5.83	2110	291

B.13 (cont.). Concentrations of major and trace elements in individual layers of the JC120-048 nodule (APEI-6). Ce*= $(2*Ce^{SN})/(La^{SN}+Nd^{SN})$. LREE/HREE= $(La^{SN}+2*Pr^{SN}+Nd^{SN})/(Er^{SN}+Tm^{SN}+Yb^{SN}+Lu^{SN})$.

JC120-048 (APEI-6 - Ridge)																	
	La ppm	Ce ppm	Pr ppm	Nd ppm	Sm ppm	Eu ppm	Gd ppm	Tb ppm	Dy ppm	Y ppm	Ho ppm	Er ppm	Tm ppm	Yb ppm	Lu ppm	ΣREY ppm	ΣHREE ppm
An.#																	
26	378	946	107	422	107	24.1	88.3	13.8	83.4	212	16.0	43.3	6.51	45.0	6.30	2710	327
27	86	212	22.5	88	20.4	5.52	18.1	2.97	16.6	49.3	3.24	8.95	1.09	8.08	1.26	594	65.8
28	308	945	86.4	341	87.0	18.5	72.5	11.3	68.6	186	13.0	34.5	5.31	34.5	5.36	2400	264
29	168	480	44.8	175	44.9	10.5	40.2	5.82	36.8	97.1	6.74	17.9	2.69	17.2	2.50	1250	140
30	227	681	62.8	248	62.5	14.4	57.6	8.76	51.1	136	9.21	26.3	3.62	24.4	3.61	1750	199
31	246	390	70.6	275	67.5	14.6	58.5	9.01	56.8	153	10.7	29.8	4.60	32.5	4.18	1570	221
32	323	493	98.6	387	100	21.6	86.5	13.3	85.0	263	15.1	41.2	6.39	44.4	5.77	2250	319
33	399	1310	115	435	109	23.5	88.9	14.6	89.8	241	16.9	47.6	6.92	45.8	6.46	3190	340
34	748	1370	206	805	201	44.6	178	28.2	170	434	32.2	90.6	13.2	95.9	13.4	4870	666
35	637	1140	177	690	176	38.5	150	23.9	152	384	28.3	79.0	12.5	83.1	11.9	4160	580
36	230	500	63.6	248	61.8	13.7	53.1	7.90	50.8	143	9.50	24.8	3.64	25.6	3.83	1580	193
37	513	872	142	550	137	31.4	123	18.9	118	307	23.2	63.9	9.77	63.5	9.44	3290	461
38	290	370	78.5	298	75.7	16.7	68.5	10.5	64.5	173	12.2	32.7	5.31	35.9	5.15	1710	251
39	61.7	251	24.3	104	32.8	7.67	24.0	3.63	21.6	50.8	3.70	8.86	1.37	9.15	1.22	657	81.1
40	327	1040	81.3	313	72.2	17.1	61.9	9.53	54.2	158	9.87	25.0	3.70	23.6	3.92	2360	209
41	325	1010	82.6	308	70.0	17.1	65.7	9.61	54.5	188	9.85	26.2	3.69	23.7	3.73	2380	214
42	170	612	45.0	172	44.9	9.70	34.1	5.28	30.8	93.2	5.86	14.9	2.09	13.8	2.13	1350	119
43	80.7	82.5	24.2	99.2	23.9	5.03	19.4	2.91	19.2	58.1	3.70	10.6	1.64	10.9	1.32	501	74.6
44	133	726	38.7	144	33.6	7.57	27.3	4.79	26.8	91.1	5.46	14.2	2.14	13.9	1.97	1360	104
45	93.9	350	27.0	110	26.2	5.83	21.8	3.56	20.5	63.2	3.91	10.9	1.64	11.2	1.79	815	81.2
46	87.6	167	24.3	97.8	25.6	5.37	22.9	3.65	20.8	64.8	4.01	11.3	1.59	10.9	1.54	614	82.0
47	65.8	572	19.5	75.5	18.9	4.70	16.0	3.13	20.0	73.2	3.89	11.6	1.79	11.4	1.68	972	74.3
48	101	304	27.6	104	27.5	5.94	23.3	3.98	23.3	68.9	4.67	12.9	2.11	13.2	1.92	793	91.3
49	560	943	150	581	139	33.1	122	18.4	114	293	20.6	54.9	8.12	53.1	7.61	3390	432
50	617	1720	173	689	169	39.3	152	22.6	139	349	25.2	69.3	9.75	69.2	9.78	4600	536
Avg	289	755	83.8	326	81.6	18.4	71.3	10.9	66.7	181	12.4	33.8	5.05	33.8	4.90	2170	257
SD	209	491	57.7	226	55.6	12.6	50.1	7.50	46.1	111	8.52	23.1	3.45	23.6	3.39	1390	178

Appendix C

C.1. Correlation coefficients between elements in sample JC120-104. Significant ($p < 0.05$) correlations are highlighted in bold.

	JC120-104																								
	Ti	**V**	**Cr**	**Mn**	**Fe**	**Co**	**Ni**	**Cu**	**Zn**	**Ba**	**La**	**Ce**	**Pr**	**Nd**	**Sm**	**Eu**	**Gd**	**Tb**	**Dy**	**Y**	**Ho**	**Er**	**Tm**	**Yb**	**Lu**	**Th**	**U**
Ti	**1.00**																										
V	0.48	**1.00**																									
Cr	0.05	-0.09	**1.00**																								
Mn	**-0.84**	-0.13	-0.17	**1.00**																							
Fe	**0.91**	0.52	-0.01	**-0.82**	**1.00**																						
Co	0.12	0.36	0.19	-0.14	0.09	**1.00**																					
Ni	-0.56	-0.54	0.04	0.39	-0.62	-0.13	**1.00**																				
Cu	-0.62	-0.56	0.01	0.54	-0.70	-0.12	**0.85**	**1.00**																			
Zn	**-0.79**	-0.17	-0.24	**0.92**	-0.71	-0.32	0.26	0.36	**1.00**																		
Ba	0.22	0.69	0.09	0.02	0.18	0.56	-0.23	-0.14	-0.19	**1.00**																	
La	0.40	0.46	-0.17	-0.41	0.50	0.42	-0.45	-0.45	-0.37	0.26	**1.00**																
Ce	**0.95**	0.60	-0.06	**-0.80**	**0.95**	0.22	-0.61	-0.68	-0.74	0.27	0.55	**1.00**															
Pr	0.23	0.32	-0.13	-0.28	0.30	0.44	-0.31	-0.30	-0.26	0.20	**0.97**	0.36	**1.00**														
Nd	0.20	0.31	-0.13	-0.26	0.27	0.44	-0.30	-0.29	-0.25	0.20	**0.96**	0.34	**1.00**	**1.00**													
Sm	0.17	0.29	-0.12	-0.23	0.23	0.44	-0.28	-0.27	-0.22	0.18	**0.95**	0.30	**1.00**	**1.00**	**1.00**												
Eu	0.17	0.28	-0.12	-0.23	0.22	0.44	-0.27	-0.26	-0.22	0.18	**0.95**	0.29	**1.00**	**1.00**	**1.00**	**1.00**											
Gd	0.19	0.28	-0.12	-0.26	0.25	0.44	-0.29	-0.28	-0.24	0.17	**0.95**	0.32	**1.00**	**1.00**	**1.00**	**1.00**	**1.00**										
Tb	0.21	0.29	-0.12	-0.27	0.26	0.43	-0.29	-0.29	-0.25	0.18	**0.96**	0.34	**1.00**	**1.00**	**1.00**	**1.00**	**1.00**	**1.00**									
Dy	0.22	0.30	-0.13	-0.28	0.28	0.43	-0.30	-0.30	-0.27	0.18	**0.96**	0.35	**1.00**	**1.00**	**1.00**	**1.00**	**1.00**	**1.00**	**1.00**								
Y	0.10	0.15	-0.10	-0.20	0.13	0.43	-0.19	-0.17	-0.21	0.11	**0.90**	0.21	**0.98**	**0.98**	**0.99**	**0.99**	**0.99**	**0.98**	**0.98**	**1.00**							
Ho	0.23	0.29	-0.13	-0.29	0.28	0.43	-0.30	-0.29	-0.28	0.18	**0.96**	0.35	**1.00**	**1.00**	**1.00**	**1.00**	**1.00**	**1.00**	**1.00**	**0.98**	**1.00**						
Er	0.24	0.29	-0.13	-0.30	0.28	0.43	-0.29	-0.29	-0.29	0.18	**0.96**	0.36	**1.00**	**1.00**	**0.99**	**1.00**	**1.00**	**1.00**	**1.00**	**0.98**	**1.00**	**1.00**					
Tm	0.26	0.30	-0.13	-0.31	0.30	0.43	-0.30	-0.30	-0.30	0.19	**0.96**	0.38	**0.99**	**0.99**	**0.99**	**0.99**	**0.99**	**1.00**	**1.00**	**0.98**	**1.00**	**1.00**	**1.00**				
Yb	0.27	0.30	-0.13	-0.31	0.30	0.43	-0.30	-0.30	-0.31	0.19	**0.96**	0.38	**0.99**	**0.99**	**0.99**	**0.99**	**0.99**	**1.00**	**1.00**	**0.98**	**1.00**	**1.00**	**1.00**	**1.00**			
Lu	0.28	0.31	-0.13	-0.33	0.32	0.43	-0.31	-0.31	-0.32	0.19	**0.96**	0.40	**0.99**	**0.99**	**0.99**	**0.99**	**0.99**	**0.99**	**1.00**	**0.98**	**1.00**	**1.00**	**1.00**	**1.00**	**1.00**		
Th	**0.84**	0.45	0.00	**-0.80**	**0.86**	0.24	-0.59	-0.62	-0.73	0.16	**0.75**	**0.88**	0.63	0.61	0.58	0.58	0.60	0.61	0.62	0.52	0.63	0.63	0.65	0.65	0.67	**1.00**	
U	**0.88**	0.47	-0.10	**-0.75**	**0.88**	0.14	-0.68	-0.66	-0.72	0.22	0.48	**0.91**	0.31	0.28	0.24	0.24	0.27	0.28	0.30	0.18	0.30	0.31	0.33	0.33	0.35	**0.84**	**1.00**

C.2. Correlation coefficients between elements in sample EW9602-09RD. Significant ($p < 0.05$) correlations are highlighted in bold.

	EW9602-09RD																									
	Ti	**V**	**Cr**	**Mn**	**Fe**	**Co**	**Ni**	**Cu**	**Zn**	**Ba**	**La**	**Ce**	**Pr**	**Nd**	**Sm**	**Eu**	**Gd**	**Tb**	**Dy**	**Y**	**Ho**	**Er**	**Tm**	**Yb**	**Lu**	**Th**	**U**
Ti	**1.00**																										
V	0.55	**1.00**																									
Cr	0.001	**-0.03**	**1.00**																								
Mn	0.38	**0.45**	-0.59	**1.00**																							
Fe	0.19	**0.63**	0.06	-0.002	**1.00**																						
Co	-0.33	**-0.41**	-0.46	0.62	-0.26	**1.00**																					
Ni	-0.20	**-0.34**	-0.30	0.46	-0.65	0.12	**1.00**																				
Cu	0.56	**0.37**	0.08	-0.05	-0.25	-0.40	0.58	**1.00**																			
Zn	0.26	**0.55**	0.30	-0.10	0.36	-0.03	-0.13	0.21	**1.00**																		
Ba	0.28	**0.66**	0.13	0.07	0.88	-0.25	-0.48	-0.09	0.54	**1.00**																	
La	0.39	**0.81**	-0.30	0.43	0.62	0.39	-0.40	-0.62	0.22	0.54	**1.00**																
Ce	0.42	**0.69**	0.04	0.12	0.74	0.13	-0.63	-0.43	0.34	0.74	0.68	**1.00**															
Pr	0.48	**0.80**	-0.22	0.40	0.40	0.58	-0.33	-0.67	0.33	0.36	**0.92**	0.56	**1.00**														
Nd	0.50	**0.79**	-0.19	0.38	0.37	0.57	-0.33	-0.68	0.33	0.35	**0.91**	0.55	**1.00**	**1.00**													
Sm	0.50	**0.75**	-0.14	0.32	0.29	0.59	-0.30	-0.69	0.37	0.29	**0.83**	0.49	**0.98**	**0.99**	**1.00**												
Eu	0.54	**0.78**	-0.12	0.34	0.35	0.57	-0.32	-0.67	0.39	0.35	**0.86**	0.54	**0.98**	**0.99**	**0.99**	**1.00**											
Gd	0.57	**0.76**	-0.10	0.32	0.32	0.56	-0.32	-0.69	0.37	0.33	**0.84**	0.54	**0.96**	**0.98**	**0.99**	**0.99**	**1.00**										
Tb	0.60	**0.78**	-0.08	0.34	0.31	0.56	-0.29	-0.65	0.39	0.34	**0.83**	0.53	**0.95**	**0.97**	**0.98**	**0.99**	**0.99**	**1.00**									
Dy	0.65	**0.80**	-0.09	0.37	0.35	0.56	-0.31	-0.66	0.38	0.38	**0.84**	0.57	**0.95**	**0.96**	**0.96**	**0.98**	**0.99**	**0.99**	**1.00**								
Y	0.69	**0.80**	0.08	0.27	0.53	0.31	-0.42	-0.58	0.40	0.58	**0.79**	0.65	**0.82**	**0.84**	**0.82**	**0.86**	**0.88**	**0.89**	**0.93**	**1.00**							
Ho	0.70	**0.82**	-0.06	0.38	0.40	0.51	-0.33	-0.63	0.37	0.45	**0.84**	0.60	**0.91**	**0.93**	**0.92**	**0.94**	**0.96**	**0.97**	**0.99**	**0.97**	**1.00**						
Er	0.74	**0.84**	-0.03	0.40	0.44	0.49	-0.34	-0.60	0.38	0.50	**0.83**	0.62	**0.89**	**0.90**	**0.89**	**0.91**	**0.93**	**0.95**	**0.97**	**0.97**	**0.99**	**1.00**					
Tm	**0.75**	**0.85**	-0.01	0.40	0.45	0.49	-0.35	-0.59	0.39	0.52	**0.82**	0.64	**0.87**	**0.88**	**0.86**	**0.89**	**0.91**	**0.93**	**0.96**	**0.97**	**0.98**	**0.99**	**1.00**				
Yb	0.73	**0.87**	-0.01	0.40	0.56	**0.39**	-0.38	-0.53	0.41	0.62	**0.83**	0.69	**0.83**	**0.84**	**0.81**	**0.85**	**0.86**	**0.88**	**0.92**	**0.98**	**0.96**	**0.98**	**0.98**	**1.00**			
Lu	0.69	**0.84**	0.04	0.34	0.62	0.25	-0.42	-0.51	0.39	0.68	0.81	0.69	**0.78**	**0.79**	**0.75**	**0.79**	**0.81**	**0.83**	**0.87**	**0.98**	**0.93**	**0.95**	**0.96**	**0.99**	**1.00**		
Th	0.01	0.34	-0.08	0.02	0.32	0.24	-0.35	-0.37	0.28	0.19	0.41	0.43	0.50	0.48	0.50	0.49	0.45	0.41	0.37	0.21	0.29	0.25	0.22	0.20	0.17	**1.00**	
U	**0.90**	**0.75**	-0.04	0.52	0.26	0.62	-0.20	-0.31	0.36	0.37	0.57	0.50	0.63	0.63	0.61	0.65	0.66	0.69	0.74	**0.75**	**0.78**	**0.82**	**0.84**	**0.82**	**0.77**	0.03	**1.00**

C.3. Correlation coefficients between elements in sample RC12-192GS. Significant ($p < 0.05$) correlations are highlighted in bold.

	RC12-192GS																										
	Ti	**V**	**Cr**	**Mn**	**Fe**	**Co**	**Ni**	**Cu**	**Zn**	**Ba**	**La**	**Ce**	**Pr**	**Nd**	**Sm**	**Eu**	**Gd**	**Tb**	**Dy**	**Y**	**Ho**	**Er**	**Tm**	**Yb**	**Lu**	**Th**	**U**
Ti	**1.00**																										
V	**0.89**	**1.00**																									
Cr	-0.47	-0.47	**1.00**																								
Mn	0.59	**0.82**	-0.38	**1.00**																							
Fe	**0.87**	**0.85**	-0.36	0.47	**1.00**																						
Co	**0.90**	**0.92**	-0.43	0.77	**0.78**	**1.00**																					
Ni	-0.38	-0.12	0.03	0.43	-0.48	-0.17	**1.00**																				
Cu	-0.32	-0.05	-0.02	0.48	-0.42	-0.11	**0.98**	**1.00**																			
Zn	0.04	0.30	-0.16	0.72	-0.04	0.21	**0.87**	**0.87**	**1.00**																		
Ba	**0.87**	**0.92**	-0.45	0.79	0.69	**0.92**	-0.10	-0.04	0.24	**1.00**																	
La	**0.98**	**0.91**	-0.46	0.60	**0.90**	**0.89**	-0.38	-0.32	0.04	**0.87**	**1.00**																
Ce	**0.94**	**0.91**	-0.44	0.62	**0.93**	**0.90**	-0.37	-0.32	0.06	**0.83**	**0.95**	**1.00**															
Pr	**0.97**	**0.93**	-0.46	0.62	**0.93**	**0.89**	-0.38	-0.31	0.06	**0.86**	**1.00**	**0.96**	**1.00**														
Nd	**0.97**	**0.92**	-0.46	0.61	**0.92**	**0.89**	-0.39	-0.33	0.04	**0.86**	**1.00**	**0.96**	**1.00**	**1.00**													
Sm	**0.97**	**0.92**	-0.45	0.61	**0.94**	**0.89**	-0.39	-0.33	0.05	**0.85**	**0.99**	**0.97**	**1.00**	**1.00**	**1.00**												
Eu	**0.97**	**0.93**	-0.46	0.62	**0.93**	**0.89**	-0.38	-0.32	0.06	**0.86**	**0.99**	**0.96**	**1.00**	**1.00**	**1.00**	**1.00**											
Gd	**0.97**	**0.92**	-0.45	0.61	**0.93**	**0.89**	-0.39	-0.33	0.04	**0.86**	**0.99**	**0.96**	**1.00**	**1.00**	**1.00**	**1.00**	**1.00**										
Tb	**0.97**	**0.93**	-0.45	0.62	**0.93**	**0.90**	-0.38	-0.32	0.06	**0.86**	**0.99**	**0.96**	**1.00**	**1.00**	**1.00**	**1.00**	**1.00**	**1.00**									
Dy	**0.97**	**0.93**	-0.45	0.63	**0.93**	**0.90**	-0.38	-0.31	0.06	**0.87**	**0.99**	**0.96**	**1.00**	**1.00**	**1.00**	**1.00**	**1.00**	**1.00**	**1.00**								
Y	**0.97**	**0.94**	-0.45	0.63	**0.93**	**0.90**	-0.38	-0.32	0.05	**0.87**	**0.99**	**0.96**	**0.99**	**0.99**	**1.00**	**1.00**	**1.00**	**1.00**	**1.00**	**1.00**							
Ho	**0.97**	**0.94**	-0.45	0.64	**0.92**	**0.91**	-0.37	-0.30	0.07	**0.88**	**0.99**	**0.96**	**1.00**	**1.00**	**1.00**	**1.00**	**1.00**	**1.00**	**1.00**	**1.00**	**1.00**						
Er	**0.97**	**0.94**	-0.45	0.65	**0.92**	**0.91**	-0.36	-0.30	0.07	**0.88**	**0.99**	**0.96**	**1.00**	**0.99**	**1.00**	**1.00**	**1.00**	**1.00**	**1.00**	**1.00**	**1.00**	**1.00**					
Tm	**0.97**	**0.94**	-0.45	0.66	**0.91**	**0.91**	-0.35	-0.29	0.08	**0.89**	**0.99**	**0.95**	**0.99**	**0.99**	**0.99**	**0.99**	**1.00**	**1.00**	**1.00**	**1.00**	**1.00**	**1.00**	**1.00**				
Yb	**0.96**	**0.95**	-0.45	0.66	**0.91**	**0.91**	-0.35	-0.29	0.08	**0.89**	**0.99**	**0.95**	**0.99**	**0.99**	**0.99**	**0.99**	**0.99**	**1.00**	**1.00**	**1.00**	**1.00**	**1.00**	**1.00**	**1.00**			
Lu	**0.97**	**0.94**	-0.45	0.65	**0.91**	**0.91**	-0.36	-0.30	0.07	**0.89**	**0.99**	**0.95**	**0.99**	**0.99**	**0.99**	**0.99**	**0.99**	**1.00**	**1.00**	**1.00**	**1.00**	**1.00**	**1.00**	**1.00**	**1.00**		
Th	0.02	0.03	0.04	-0.15	0.36	-0.01	-0.29	-0.29	-0.19	-0.22	0.03	0.25	0.09	0.08	0.11	0.11	0.10	0.09	0.08	0.10	0.07	0.06	0.05	0.04	0.04	**1.00**	
U	**0.94**	**0.97**	-0.44	0.70	**0.91**	**0.93**	-0.30	-0.24	0.13	**0.90**	**0.96**	**0.95**	**0.97**	**0.97**	**0.97**	**0.98**	**0.97**	**0.98**	**0.98**	**0.98**	**0.98**	**0.98**	**0.98**	**0.98**	**0.98**	**0.05**	**1.00**

C.4. Correlation coefficients between elements in sample E ATL N4. Significant ($p < 0.05$) correlations are highlighted in bold.

	E ATL N4																								
	Ti	**V**	**Cr**	**Mn**	**Fe**	**Co**	**Ni**	**Cu**	**Zn**	**Ba**	**La**	**Ce**	**Pr**	**Nd**	**Sm**	**Eu**	**Gd**	**Tb**	**Dy**	**Y**	**Ho**	**Er**	**Tm**	**Yb**	**Lu**	**Th**	**U**
Ti	**1.00**																										
V	**0.67**	**1.00**																									
Cr	0.32	0.47	**1.00**																								
Mn	0.22	0.38	-0.13	**1.00**																							
Fe	**0.78**	**0.95**	0.46	0.34	**1.00**																						
Co	0.23	0.12	-0.20	0.70	0.19	**1.00**																					
Ni	0.05	0.16	-0.18	**0.90**	**0.12**	**0.72**	**1.00**																				
Cu	-0.03	0.22	0.01	0.67	0.10	0.20	0.68	**1.00**																			
Zn	0.28	0.60	0.17	**0.80**	0.47	0.29	0.67	**0.86**	**1.00**																		
Ba	0.66	**0.75**	0.14	0.67	**0.80**	**0.45**	0.46	0.26	0.57	**1.00**																	
La	0.66	0.69	0.06	0.63	**0.76**	**0.57**	0.42	0.08	0.41	**0.92**	**1.00**																
Ce	0.67	0.62	0.05	0.61	0.70	0.71	0.46	0.12	0.41	**0.80**	**0.90**	**1.00**															
Pr	0.67	**0.75**	0.10	0.62	**0.80**	0.54	0.42	0.11	0.46	**0.91**	**0.99**	**0.90**	**1.00**														
Nd	0.67	0.74	0.10	0.61	**0.79**	0.52	0.40	0.09	0.44	**0.91**	**0.99**	**0.89**	**1.00**	**1.00**													
Sm	0.68	**0.75**	0.12	0.59	**0.80**	0.51	0.39	0.09	0.45	**0.90**	**0.98**	**0.89**	**1.00**	**1.00**	**1.00**												
Eu	0.68	**0.75**	0.11	0.60	**0.79**	0.54	0.41	0.11	0.46	**0.88**	**0.97**	**0.90**	**0.99**	**0.99**	**1.00**	**1.00**											
Gd	0.67	0.72	0.10	0.58	**0.78**	0.52	0.38	0.07	0.42	**0.88**	**0.98**	**0.89**	**0.99**	**0.99**	**1.00**	**0.99**	**1.00**										
Tb	0.67	0.73	0.11	0.56	**0.78**	0.53	0.38	0.07	0.42	**0.86**	**0.96**	**0.89**	**0.98**	**0.98**	**0.99**	**0.99**	**0.99**	**1.00**									
Dy	0.66	0.73	0.11	0.57	**0.77**	0.53	0.39	0.07	0.43	**0.87**	**0.96**	**0.89**	**0.98**	**0.98**	**0.99**	**0.99**	**0.99**	**1.00**	**1.00**								
Y	0.63	0.70	0.08	0.60	**0.76**	0.55	0.41	0.07	0.41	**0.88**	**0.98**	**0.88**	**0.98**	**0.99**	**0.99**	**0.98**	**0.99**	**0.99**	**0.99**	**1.00**							
Ho	0.64	0.71	0.10	0.58	**0.76**	0.55	0.41	0.07	0.41	**0.87**	**0.97**	**0.89**	**0.98**	**0.98**	**0.99**	**0.99**	**0.99**	**0.99**	**1.00**	**0.99**	**1.00**						
Er	0.62	0.69	0.08	0.58	**0.74**	0.56	0.42	0.06	0.40	**0.86**	**0.96**	**0.88**	**0.97**	**0.98**	**0.98**	**0.98**	**0.99**	**0.99**	**0.99**	**0.99**	**1.00**	**1.00**					
Tm	0.61	0.68	0.07	0.59	**0.73**	0.58	0.43	0.06	0.40	**0.85**	**0.95**	**0.89**	**0.97**	**0.97**	**0.97**	**0.98**	**0.98**	**0.99**	**0.99**	**0.99**	**0.99**	**1.00**	**1.00**				
Yb	0.61	0.68	0.07	0.60	**0.73**	0.58	0.44	0.06	0.40	**0.86**	**0.96**	**0.89**	**0.97**	**0.98**	**0.98**	**0.98**	**0.98**	**0.99**	**0.99**	**0.99**	**1.00**	**1.00**	**1.00**	**1.00**			
Lu	0.60	0.62	0.03	0.60	**0.69**	0.59	0.44	0.03	0.36	**0.86**	**0.96**	**0.88**	**0.96**	**0.97**	**0.96**	**0.96**	**0.98**	**0.97**	**0.98**	**0.99**	**0.99**	**0.99**	**0.99**	**0.99**	**1.00**		
Th	0.65	0.53	0.03	0.47	**0.64**	0.55	0.28	0.03	0.28	0.69	**0.80**	**0.86**	**0.80**	**0.80**	**0.79**	**0.78**	**0.79**	**0.77**	**0.75**	**0.75**	**0.74**	**0.73**	0.72	0.73	0.73	**1.00**	
U	0.65	**0.88**	0.22	0.62	**0.84**	0.45	0.44	**0.25**	**0.62**	**0.82**	**0.83**	**0.81**	**0.89**	**0.87**	**0.88**	**0.89**	**0.85**	**0.87**	**0.86**	**0.84**	**0.85**	**0.84**	**0.84**	**0.84**	**0.79**	**0.67**	**1.00**

C.5. Correlation coefficients between elements in sample NAP N4. Significant ($p < 0.05$) correlations are highlighted in bold.

	NAP N4																										
	Ti	**V**	**Cr**	**Mn**	**Fe**	**Co**	**Ni**	**Cu**	**Zn**	**Ba**	**La**	**Ce**	**Pr**	**Nd**	**Sm**	**Eu**	**Gd**	**Tb**	**Dy**	**Y**	**Ho**	**Er**	**Tm**	**Yb**	**Lu**	**Th**	**U**
Ti	**1.00**																										
V	**0.89**	**1.00**																									
Cr	-0.47	-0.47	**1.00**																								
Mn	0.59	**0.82**	-0.38	**1.00**																							
Fe	**0.87**	**0.85**	-0.36	0.47	**1.00**																						
Co	**0.90**	**0.92**	-0.43	0.77	**0.78**	**1.00**																					
Ni	-0.38	-0.12	0.03	0.43	**-0.48**	-0.17	**1.00**																				
Cu	-0.32	**-0.05**	-0.02	0.48	**-0.42**	-0.11	**0.98**	**1.00**																			
Zn	0.04	**0.30**	-0.16	0.72	**-0.04**	0.21	**0.87**	**0.87**	**1.00**																		
Ba	**0.87**	**0.92**	-0.45	**0.79**	**0.69**	**0.92**	-0.10	-0.04	0.24	**1.00**																	
La	**0.98**	**0.91**	-0.46	0.60	**0.90**	**0.89**	-0.38	-0.32	0.04	**0.87**	**1.00**																
Ce	**0.94**	**0.91**	-0.44	0.62	**0.93**	**0.90**	-0.37	-0.32	0.06	**0.83**	**0.95**	**1.00**															
Pr	**0.97**	**0.93**	-0.46	0.62	**0.93**	**0.89**	-0.38	-0.31	0.06	**0.86**	**1.00**	**0.96**	**1.00**														
Nd	**0.97**	**0.92**	-0.46	0.61	**0.92**	**0.89**	-0.39	-0.33	0.04	**0.86**	**1.00**	**0.96**	**1.00**	**1.00**													
Sm	**0.97**	**0.92**	-0.45	0.61	**0.94**	**0.89**	-0.39	-0.33	0.05	**0.85**	**0.99**	**0.97**	**1.00**	**1.00**	**1.00**												
Eu	**0.97**	**0.93**	-0.46	0.62	**0.93**	**0.89**	-0.38	-0.32	0.06	**0.86**	**0.99**	**0.96**	**1.00**	**1.00**	**1.00**	**1.00**											
Gd	**0.97**	**0.92**	-0.45	0.61	**0.93**	**0.89**	-0.39	-0.33	0.04	**0.86**	**0.99**	**0.96**	**1.00**	**1.00**	**1.00**	**1.00**	**1.00**										
Tb	**0.97**	**0.93**	-0.45	0.62	**0.93**	**0.90**	-0.38	-0.32	0.06	**0.86**	**0.99**	**0.96**	**1.00**	**1.00**	**1.00**	**1.00**	**1.00**	**1.00**									
Dy	**0.97**	**0.93**	-0.45	0.63	**0.93**	**0.90**	-0.38	-0.31	0.06	**0.87**	**0.99**	**0.96**	**1.00**	**1.00**	**1.00**	**1.00**	**1.00**	**1.00**	**1.00**								
Y	**0.97**	**0.94**	-0.45	0.63	**0.93**	**0.90**	-0.38	-0.32	0.05	**0.87**	**0.99**	**0.96**	**0.99**	**0.99**	**1.00**	**1.00**	**1.00**	**1.00**	**1.00**	**1.00**							
Ho	**0.97**	**0.94**	-0.45	0.64	**0.92**	**0.91**	-0.37	-0.30	0.07	**0.88**	**0.99**	**0.96**	**1.00**	**1.00**	**1.00**	**1.00**	**1.00**	**1.00**	**1.00**	**1.00**	**1.00**						
Er	**0.97**	**0.94**	-0.45	0.65	**0.92**	**0.91**	-0.36	-0.30	0.07	**0.88**	**0.99**	**0.96**	**1.00**	**0.99**	**1.00**	**1.00**	**1.00**	**1.00**	**1.00**	**1.00**	**1.00**	**1.00**					
Tm	**0.97**	**0.94**	-0.45	0.66	**0.91**	**0.91**	-0.35	-0.29	0.08	**0.89**	**0.99**	**0.95**	**0.99**	**0.99**	**0.99**	**0.99**	**1.00**	**1.00**	**1.00**	**1.00**	**1.00**	**1.00**	**1.00**				
Yb	**0.96**	**0.95**	-0.45	0.66	**0.91**	**0.91**	-0.35	-0.29	0.08	**0.89**	**0.99**	**0.95**	**0.99**	**0.99**	**0.99**	**0.99**	**0.99**	**1.00**	**1.00**	**1.00**	**1.00**	**1.00**	**1.00**	**1.00**			
Lu	**0.97**	**0.94**	-0.45	0.65	**0.91**	**0.91**	-0.36	-0.30	0.07	**0.89**	**0.99**	**0.95**	**0.99**	**0.99**	**0.99**	**0.99**	**0.99**	**1.00**	**1.00**	**1.00**	**1.00**	**1.00**	**1.00**	**1.00**	**1.00**		
Th	0.02	0.03	0.04	-0.15	0.36	-0.01	-0.29	-0.29	-0.19	-0.22	0.03	0.25	0.09	0.08	0.11	0.11	0.10	0.09	0.08	0.10	0.07	0.06	0.05	0.04	0.04	**1.00**	
U	**0.94**	**0.97**	-0.44	**0.70**	**0.91**	**0.93**	-0.30	-0.24	0.13	**0.90**	**0.96**	**0.95**	**0.97**	**0.97**	**0.97**	**0.98**	**0.97**	**0.98**	**0.98**	**0.98**	**0.98**	**0.98**	**0.98**	**0.98**	**0.98**	**0.05**	**1.00**

C.6. Correlation coefficients between elements in sample N29. Significant ($p < 0.05$) correlations are highlighted in bold.

	N29																										
	Ti	**V**	**Cr**	**Mn**	**Fe**	**Co**	**Ni**	**Cu**	**Zn**	**Ba**	**La**	**Ce**	**Pr**	**Nd**	**Sm**	**Eu**	**Gd**	**Tb**	**Dy**	**Y**	**Ho**	**Er**	**Tm**	**Yb**	**Lu**	**Th**	**U**
Ti	**1.00**																										
V	0.30	**1.00**																									
Cr	0.57	0.35	**1.00**																								
Mn	0.07	0.11	-0.05	**1.00**																							
Fe	0.12	0.63	0.22	-0.57	**1.00**																						
Co	0.04	0.20	0.01	0.66	-0.30	**1.00**																					
Ni	0.22	0.15	0.05	0.73	-0.45	0.45	**1.00**																				
Cu	0.10	0.10	-0.04	**0.75**	-0.48	0.52	**0.86**	**1.00**																			
Zn	0.44	0.62	0.36	0.37	0.15	0.42	0.50	0.47	**1.00**																		
Ba	0.19	0.40	0.03	0.66	-0.23	0.69	0.70	0.68	0.66	**1.00**																	
La	0.26	**0.86**	0.38	-0.07	0.74	0.20	0.03	-0.03	0.54	0.30	**1.00**																
Ce	0.24	0.57	0.47	0.08	0.35	0.29	0.08	0.06	0.42	0.23	0.63	**1.00**															
Pr	0.30	**0.85**	0.40	-0.06	0.70	0.17	0.08	0.01	0.53	0.27	**0.97**	0.64	**1.00**														
Nd	0.31	**0.85**	0.40	-0.07	0.69	0.16	0.08	0.01	0.53	0.25	**0.95**	0.62	**0.99**	**1.00**													
Sm	0.27	**0.82**	0.36	-0.12	0.68	0.12	0.06	-0.01	0.48	0.21	**0.91**	0.58	**0.97**	**0.99**	**1.00**												
Eu	0.25	**0.83**	**0.35**	**-0.09**	0.69	0.15	0.07	0.00	0.49	0.25	**0.93**	0.60	**0.98**	**0.99**	**0.99**	**1.00**											
Gd	0.26	**0.85**	**0.35**	**-0.13**	0.72	0.09	0.04	-0.02	0.49	0.22	**0.93**	0.52	**0.97**	**0.98**	**0.98**	**0.98**	**1.00**										
Tb	0.25	**0.83**	**0.33**	**-0.17**	0.74	0.07	0.01	-0.06	0.45	0.18	**0.92**	0.52	**0.96**	**0.98**	**0.98**	**0.98**	**0.99**	**1.00**									
Dy	0.25	**0.83**	**0.34**	**-0.18**	**0.75**	0.05	-0.02	-0.08	0.44	0.16	**0.92**	0.50	**0.96**	**0.97**	**0.98**	**0.97**	**0.99**	**0.99**	**1.00**								
Y	0.19	**0.83**	**0.31**	**-0.33**	**0.88**	-0.09	-0.20	-0.24	0.39	0.05	**0.90**	0.42	**0.89**	**0.90**	**0.89**	**0.89**	**0.93**	**0.94**	**0.95**	**1.00**							
Ho	0.24	**0.84**	**0.34**	**-0.22**	**0.78**	0.01	-0.05	-0.11	0.44	0.13	**0.92**	0.48	**0.95**	**0.96**	**0.96**	**0.96**	**0.98**	**0.99**	**0.99**	**0.97**	**1.00**						
Er	0.24	**0.84**	**0.33**	**-0.24**	**0.81**	-0.01	-0.08	-0.14	0.43	0.12	**0.92**	0.47	**0.94**	**0.95**	**0.95**	**0.95**	**0.97**	**0.98**	**0.99**	**0.98**	**0.99**	**1.00**					
Tm	0.22	**0.84**	**0.32**	**-0.21**	**0.77**	0.02	-0.07	-0.13	0.42	0.13	**0.90**	0.46	**0.92**	**0.93**	**0.93**	**0.93**	**0.96**	**0.96**	**0.97**	**0.96**	**0.97**	**0.98**	**1.00**				
Yb	0.24	**0.83**	**0.32**	**-0.26**	**0.81**	-0.04	-0.10	-0.16	0.41	0.10	**0.90**	0.43	**0.92**	**0.93**	**0.93**	**0.93**	**0.96**	**0.97**	**0.98**	**0.98**	**0.99**	**0.99**	**0.98**	**1.00**			
Lu	0.25	**0.85**	**0.32**	**-0.23**	**0.82**	0.01	-0.09	-0.13	0.45	0.14	**0.92**	0.47	**0.92**	**0.93**	**0.92**	**0.93**	**0.96**	**0.96**	**0.97**	**0.98**	**0.98**	**0.99**	**0.97**	**0.99**	**1.00**		
Th	0.47	0.43	0.54	0.00	0.25	0.05	0.09	0.01	0.41	0.09	0.41	0.40	0.44	0.41	0.38	0.38	0.37	0.36	0.36	0.34	0.37	0.36	0.34	0.35	0.35	**1.00**	
U	0.11	**0.78**	0.15	0.05	0.55	0.17	-0.12	-0.10	0.43	0.33	0.67	0.35	0.65	0.64	0.60	0.63	0.64	0.63	0.64	0.71	0.66	0.68	0.66	0.66	0.69	0.31	**1.00**

List of References

Addy, S.K. (1979). Rare earth element patterns in manganese nodules and micronodules from northwest Atlantic. Geochimica et Cosmochimica Acta, 43:1105-1115.

Ahnert, A., & Borowski, C. (2000). Environmental risk assessment of anthropogenic activity in the deep-sea. Journal of Aquatic Ecosystem Stress and Recovery (Formerly Journal of Aquatic Ecosystem Health), 7(4):299-315.

Alonso, E., Sherman, A. M., Wallington, T. J., Everson, M. P., Field, F. R., Roth, R., & Kirchain, R. E. (2012). Evaluating rare earth element availability: A case with revolutionary demand from clean technologies. Environmental Science & Technology, 46(6):3406-3414.

Angel, M. V., & Rice, T. L. (1996). The ecology of the deep ocean and its relevance to global waste management. Journal of Applied Ecology, 915-926.

Antoine, D., André, J.M., Morel, A., (1996). Oceanic primary production 2. Estimation at global scale from satellite (castal zone color scanner) chlorophyll. Global Biogeochemical Cycles, 10:57–69.

Bao, Z., & Zhao, Z. (2008). Geochemistry of mineralization with exchangeable REY in the weathering crusts of granitic rocks in South China. Ore Geology Reviews, 33(3):519-535.

Baturin, G. N. (2011). Variations in the composition of the ferromanganese concretions of the Kara Sea. Oceanology, 51(1):148-156.

Baturin, G. N., & Dubinchuk, V. T. (2009). Composition of ferromanganese nodules from Riga Bay (Baltic Sea). Oceanology, 49(1):111-120.

Baturin, G. N., Gorshkov, A. I., Magazina, L. O., & Bogdanova, O. Y. (2002). Structure and composition of ferromanganese–phosphate nodules from the Black Sea. Lithology and Mineral Resources, 37(4):374-385.

Bau, M. & Dulski, P. (1999). Comparing yttrium and rare earths in hydrothermal fluids from the Mid-Atlantic Ridge: implications for Y and REE behaviour during near-vent mixing and for the Y/Ho ratio of Proterozoic seawater. Chemical Geology, 155:77-90.

Bau, M., Dulski, P. & Möller, P. (1995). Yttrium and holmium in South Pacific seawater: vertical distribution and possible fractionation mechanisms. Chemie der Erde, 55:1-15.

Bau, M. & Koschinsky, A., (2009). Oxidative scavenging of cerium on hydrous Fe oxide: evidence from the distribution of rare earth elements and yttrium between Fe oxides and Mn oxides in hydrogenetic ferromanganese crusts. Geochemical Journal, 43:37-47.

Bau, M., Koschinsky, A. Dulski, P. & Hein, JR. (1996). Comparison of the partitioning behaviours of yttrium, rare earth elements, and titanium between hydrogenetic marine ferromanganese crusts and seawater. Geochimica et Cosmochimica Acta, 60:1709-1725.

Bau, M., Möller, P. & Dulski, P. (1997). Yttrium and lanthanides in eastern Mediterranean seawater and their fractionation during redox-cycling. Marine Chemistry, 56:123-131.

Bau, M., Schmidt, K., Koschinsky, A., Hein, J., Kuhn, T. & Usui, A. (2014). Discriminating between different genetic types of marine ferro-manganese crusts and nodules based on rare earth elements and yttrium. Chemical Geology 381:1-9.

Berndt, C. (2014). World ocean review: Marine Resources-Oportunities and risks.

Biscaye, P. E., Kolla, V., & Turekian, K. K. (1976). Distribution of calcium carbonate in surface sediments of the Atlantic Ocean. Journal of Geophysical Research, 81(15):2595-2603.

Bodeï, S.,Manceau, A.,Geoffroy, N.,Baronnet, A.,Buatier,M. (2007). Formation of todorokite from vernadite in Ni-rich hemipelagic sediments. Geochimica et Cosmochimica Acta 71:5698-5716.

Bollmann, M. (2010). World ocean review: living with the oceans.

Bonatti, E., Kraemer, T., Rydell, H. (1972). Classification and genesis of submarine iron-manganese deposits. In: Horn, D. R. (Ed.), Papers from a Conference on Ferromanganese Deposits on the Ocean Floor. National Science Foundation, 149-166.

Bender, M. L., Ku, T. L., & Broecker, W. S. (1966). Manganese nodules: their evolution. Science, 151(3708):325-328.

Berger, W. H. (1975). Deep-sea carbonates: dissolution profiles from foraminiferal calcite. In: W. V. Sliter, A. W. H. Bé, W. H. Berger (Eds.): Dissolution in Deep-Sea Carbonates. Cushman Found. Foraminiferal Research Special Publication, 13:82-86.

Biscaye, P. E., Kolla, V. & Turekian, K. K. (1976). Distribution of calcium carbonate in surface sediments of the Atlantic Ocean. Journal of Geophysical Research, 81:2595-2603.

Bonatti, E., Kraemer, T., Rydell, H. (1972). Classification and genesis of submarine iron-manganese deposits. In: Horn, D. R. (Ed.), Papers from a Conference on Ferromanganese Deposits on the Ocean Floor. National Science Foundation, 149-166.

Bright, C. A., Cruse, A. M., Lyons, T. W., MacLeod, K. G., Glascock, M. D., & Ethington, R. L. (2009). Seawater rare-earth element patterns preserved in apatite of Pennsylvanian conodonts? Geochimica et Cosmochimica Acta, 73(6):1609-1624.

Brown, A., S. Thatje, C. Hauton (in revision). The effects of temperature and hydrostatic pressure on metal toxicity: Insights into toxicity in the deep sea.

Buckley, H. A., Johnson, L. R., Shackleton, N. J., & Blow, R. A. (1982). Late glacial to recent cores from the eastern Mediterranean. Deep Sea Research Part A. Oceanographic Research Papers, 29(6):739-766.

Burns, V.M., Burns, R.G., (1978). Authigenic todorokite and phillipsite inside deep-sea manganese nodules. American Mineralogist 63:827–831.

Byrne, R. H. (2002). Inorganic speciation of dissolved elements in seawater: the influence of pH on concentration ratios. Geochemical Transactions, 2(2):11.

Cantrell K. J. & Byrne J. H. (1987). Rare earth element complexation by carbonate and oxalate ions. Geochimica et Cosmochimica Acta, 51:597-605.

Castor, S. B., & Hedrick, J. B. (2006). Rare earth elements. Industrial minerals volume, 7th edition: Society for mining, metallurgy, and exploration, Littleton, Colorado, 769-792.

Charlou J. L. & Donval J. P. (1993). Hydrothermal methane venting between 12° and 26°N along the Mid-Atlantic Ridge. Journal of Geophysical Research, 98:9625-9642.

Chester R. & Messiha-Hanna, R. G. (1970). Trace element partition patterns in North Atlantic deep-sea sediments. Geochimica et Comochimica Acta, 34:1121-l 128.

Coffey Natural Systems (2008). Solwara 1 Project Environmental Impact Assessment. Nautilus Minerals Niugini Limited.

Cordier, D. (2011). Rare earths, Mineral Commodity Summary. United States Geological Survey.

Cronan, D.S., (2000). Handbook of marine mineral deposits. CRC Marine Science Series, 17. CRC Press, Boca Roton.

Cronan, D.S., 2006. Processes in the formation of central Pacific manganese nodule deposits. Journal of Marine Science Environment, C4:41–48.

De Baar, H. J. W., Bacon, M. P. & Brewer, P. G. (1985). Rare earth elements in the Pacific and Atlantic Oceans. Geochimica et Cosmochimica Acta, 49:1943-1959.

De Carlo E. H. & Green W. J. (2002). Rare earth elements in the water column of Lake Vanda, McMurdo Dry Valleys, Antarctica. Geochimica et Cosmochimica Acta, 66:1323-1333.

De Lange, G. J., van Os, B. & Poorter, R. (1992). Geochemical composition and inferred accretion rates of sediments and manganese nodules from a submarine hill in the Madeira Abyssal Plain, eastern North Atlantic. Marine Geology, 109:171-194.

Dietz, R.S. (1995). Manganese deposits on the northeast Pacific sea floor. California Journal of Mines and Geology, 51:209-220.

D'hondt, S., Inagaki, F., Zarikian, C. A., Abrams, L. J., Dubois, N., Engelhardt, T., ... & Hoppie, B. W. (2015). Presence of oxygen and aerobic communities from sea floor to basement in deep-sea sediments. Nature Geoscience, 8(4):299-304.

Douville, E., Bienvenu, P. Charlou, J. L., Donval, J. P., Fouquet, Y., Appriou, P., Gamo, T. (1999). Yttrium and rare earth elements in fluids from various deep-sea hydrothermal systems. Geochimica et Cosmochimica Acta, 63:627-643.

Dubinin, A. V. (2001). Geochemistry of iron–calcium hydroxophosphates in pelagic sediments: origin and compositional evolution in the course of diagenesis. Geochemistry International, 39:585-596.

Dubinin, A. V. (2004). Geochemistry of rare earths in the ocean. Lithology and Mineral Resources, 39:289-307.

Dubinin, A. V. & Rimskaya-Korsakova, M. N. (2011). Geochemistry of rare earth elements in bottom sediments of the Brazil Basin, Atlantic Ocean. Lithology and Mineral Resources, 46:1-16.

Dubinin, A.V. & Rozanov, A. G. (2001). Geochemistry of rare earth elements and thorium in sediments and ferromanganese nodules of the Atlantic Ocean. Lithology and Mineral Resources, 36:268-279.

Dubinin, A. V. & Sval'nov, V. N. (2003). Geochemistry of the manganese ore process in the ocean: evidence from rare earth elements. Lithology and Mineral Resources, 38:91-100.

Dubinin, A. V., Sval'nov, V. N., Berezhnaya, E. D., Rimskaya-Korsakova, M. N., & Demidova, T. P. (2013). Geochemistry of trace and minor elements in sediments and manganese micronodules from the Angola Basin. Lithology and Mineral Resources, 48(3):175-197.

Dubinin, A. V., Sval'nov, V. N. & Uspenskaya, T. Y. (2008). Geochemistry of the authigenic ferromanganese ore formation in sediments of the Northeast Pacific Basin. Lithology and Mineral Resources, 43:99-110.

Dubinin, A. V. & Uspenskaya T. Y. (2006). Geochemistry and specific features of manganese ore formation in sediments of oceanic bioproductive zones. Lithology and Mineral Resources, 41:1-14.

Dymond, J. (1981). Geochemistry of Nazca Plate surface sediments – an evaluation of hydrothermal, biogenic, detrital and hydrogenous sources. Geological Society of America Memoir, 154:133-173.

Dymond, J., Lyle, M., Finney, B., Piper, D.Z.,Murphy, K.,Conard, R., Pisoas, N., (1984). Ferromanganese nodules from the MANOP Sites H, S, and R-Control of mineralogical and chemical composition bymultiple accretionary processes. Geochimica et Cosmochimica Acta, 48:931–949.

Elderfield, H., Hawkesworth, C.J., Greaves, M.J. and Calvert, S.E., (1981). Rare earth element geochemistry of oceanic ferromanganese

nodules and associated sediments. Geochimica et Cosmochimica Acta, 45(4):513-528.

Fan, H. R., Yang, K. F., Hu, F. F., Liu, S., & Wang, K. Y. (2016). The giant Bayan Obo REE-Nb-Fe deposit, China: controversy and ore genesis. Geoscience Frontiers, 7(3):335-344.

Farr, H. K. (1980). Multibeam bathymetric sonar: Sea beam and hydro chart. Marine Geodesy, 4(2):77-93.

Feely, R. A., Baker, E. T., Marumo, K., Urabe, T., Ishibashi, J., Gendron, J., Lebon, G. T., & Okamura, K. (1996). Hydrothermal plume particles and dissolved phosphate over the superfast-spreading southern East Pacific Rise. Geochimica et Cosmochimica Acta, 60(13):2297-2323.

Fuerstenau, D. W., & Han, K. N. (1977). Extractive metallurgy. Elsevier Oceanography Series, 15:357-390.

Fujinaga, K., Yasukawa, K., Nakamura, K., Machida, S., Takaya, Y., Ohta, J., Araki, S., Liu, H., Usami, R., Maki, R. and Haraguchi, S., (2016). Geochemistry of REY-rich mud in the Japanese Exclusive Economic Zone around Minamitorishima Island. Geochemical Journal, 50(6):575-590.

Fuyuan, Z., Weiyan, Z., Kechao, Z., Shuitu, G. A. O., Haisheng, Z. H. A. N. G., Xiaoyu, Z. H. A. N. G., & Benduo, Z. H. U. (2008). Distribution Characteristics of Cobalt-rich Ferromanganese Crust Resources on Submarine Seamounts in the Western Pacific. Acta Geologica Sinica (English Edition), 82(4):796-803.

German C.R., Holliday B. P., & Elderfield H. (1991). Redox cycling of rare earth elements in the suboxic zone of the Black Sea. Geochimica et Cosmochimica Acta, 55:3553-3558.

Glasby, G. P. (1973). Mechanisms of enrichment of the rarer elements in marine manganese nodules. Marine Chemistry, 1(2):105-125.

Glasby, G. P. (2000). Lessons learned from deep-sea mining. Science, 289(5479):551-553.

Goldberg, E. D., & Picciotto, E. (1955). Thorium determinations in manganese nodules. Science, 121:613-614.

Goldstein, J. I., Newbury, D. E., Michael, J. R., Ritchie, N. W., Scott, J. H. J., & Joy, D. C. (2017). Scanning electron microscopy and X-ray microanalysis. Springer.

Gonzalez, F. J., Somoza, L., Hein, J. R., Medialdea, T., Leon, R., Urgorri, V., Reyes, J., & Martin-Rubi, J. A. (2016). Phosphorites, Co-rich Mn nodules, and Fe-Mn crusts from Galicia Bank, NE Atlantic: reflections of Cenozoic tectonics and paleoceanography. Geochemistry Geophysics Geosystems, 17:346-374.

Grau, R., & Kudrass, H. R. (1991). Pre-eocene and younger manganese crusts from the manihiki plateau, southwest Pacific-Ocean. Marine Mining, *10*(3):231-246.

Gromet, L.P., Haskin, L.A., Korotev, R.L. & Dymek, R.F. (1984). The “North American shale composite”: Its compilation, major and trace element characteristics. Geochimica et Cosmochimica Acta, 48:2469-2482.

Haque, M. A., Topal, E., & Lilford, E. (2014). A numerical study for a mining project using real options valuation under commodity price uncertainty. Resources Policy, 39:115-123.

Halbach, P., Hebisch, U., Scherhag, C. (1981). Geochemical variations of ferromanganese nodules and crusts from different provinces of the Pacific Ocean and their genetic control. Chemical Geology, 34:3-17.

Halbach, P., Friedrich, G., von Stackelberg, U., (1988). The manganese nodule belt of the Pacific Ocean. Geological Environment, Nodule Formation, and Mining Aspects. Ferdinand Enke Verlag, Stuttgart.

Halbach, P., & Puteanus, D. (1984). The influence of the carbonate dissolution rate on the growth and composition of Co-rich ferromanganese crusts from Central Pacific seamount areas. Earth and Planetary Science Letters, 68(1):73-87.

Halbach, P.E., Sattler, C.D., Teichmann, F., Wahsner, M. (1989). Cobalt-rich and platinum-bearing manganese crust deposits on seamounts: nature, formation, and metal potential. Marine Mining, 8:23-39.

Haley, B. A., Klinkhammer, G. P. & McManus, J. (2004). Rare earth elements in pore waters of marine sediments. Geochimica et Cosmochimica Acta, 68:1265-1279.

Hatch, G. P. (2012). Dynamics in the global market for rare earths. Elements, 8:341-346.

Haymon, R. (1996). The response of 1-crest hydrothermal systems to segmented, episodic magma supply, in Tectonic, Magmatic, Hydrothermal and Biological Segmentation of Mid-Oceanic Ridges, 118:157-168. Geological Society Special Publication.

Hein, J.R., (2004). Cobalt-rich ferromanganese crusts: global distribution, composition, origin and research activities, in: ISA (Ed,), Minerals other tan polymetallic nodules of the International Seabed Area. Workshop Report, Kingston, Jamaica, 188–272.

Hein, J.R. & Koschinsky, A. (2013). Deep-ocean ferromanganese crusts and nodules. Geochemistry of Mineral Deposits, 13:273-291.

Hein, J.R., Koschinsky, A., Bau, M., Manheim, F.T., Kang, J.-K., Roberts, L., (2000). Cobalt-rich ferromanganese crusts in the Pacific. In: Cronan, D.S. (Ed.), Handbook of Marine Mineral Deposits. CRC Press, Boca Raton, Florida, 239–279.

Hein, J. R., Koschinsky, A., & Halliday, A. N. (2003). Global occurrence of tellurium-rich ferromanganese crusts and a model for the enrichment of tellurium. Geochimica et Cosmochimica Acta, 67(6):1117-1127.

Hein, J.R., Mizell, K., Koschinsky, A. & Conrad, T.A. (2013). Deep-ocean mineral deposits as a source of critical metals for high- and green-technology applications: Comparison with land-based resources. Ore Geology Reviews, 51:1-14.

Hein, J. R., Spinardi, F., Okamoto, N., Mizell, K., Thorburn, D., & Tawake, A. (2015). Critical metals in manganese nodules from the Cook Islands EEZ, abundances and distributions. Ore Geology Reviews, 68:97-116.

Hein, J.R., Yeh, H.-W., Gunn, S. H., Sliter, W. V. Benninger, L. M. and Wang, C.-H. (1993). Two major Cenozoic episodes of phosphogenesis Recorded in Equatorial Pacific seamount deposits. Paleoceanography, 8(2):293–311.

Heye, D., & Marchig, V. (1977). Relationship between the growth rate of manganese nodules from the Central Pacific and their chemical constitution. Marine Geology, 23(1-2):M19-M25.

Hilsum, L. (2009). Chinese pay toxic price for a green world. The Sunday Times, 6 December, 2009.

Hoagland, P., Beaulieu, S., Tivey, M. A., Eggert, R. G., German, C., Glowka, L., & Lin, J. (2010). Deep-sea mining of seafloor massive sulfides. Marine Policy, 34(3):728-732.

Horn, D. R., Horn, B. M., & Delach, M. N. (1972). Ferromanganese deposits of the North Pacific Ocean (Vol. 1). Office for the International Decade of Ocean Exploration, National Science Foundation.

Hüneke, H., & Henrich, R. (2011). Pelagic sedimentation in modern and ancient oceans. Elsevier: Amsterdam, The Netherlands, 215-351

Iijima, K., Yasukawa, K., Fujinaga, K., Nakamura, K., Machida, S., Takaya, Y. & Nozaki, T. (2016). Discovery of extremely REY-rich mud in the western North Pacific Ocean. Geochemical Journal, 50(6):557-573.

ISA, International Seabed Authority, 2008. Biodiversity, species ranges, and gene flow in the abyssal Pacific nodule province: predicting and managing the impacts of deep seabed mining. 38 pp. Kingston, Jamaica: ISA Technical Study, No. 3.

ISA, International Seabed Authority, 2010. A geological model of polymetallic nodule deposits in the Clarion–Clipperton Fracture zone. Kingston, Jamaica: ISA Technical Study No. 6.

Jankowski, J. A. & Zielke, W. (2001). The mesoscale sediment transport due to technical activities in the deep sea. Deep Sea Research II, 48:3487-3521.

Jordahl, K. A., McNutt, M. K., & Caress, D. W. (2004). Multiple episodes of volcanism in the Southern Austral Islands: Flexural constraints from bathymetry, seismic reflection, and gravity data. Journal of Geophysical Research: Solid Earth, 109(B6).

Kanazawa, Y., & Kamitani, M. (2006). Rare earth minerals and resources in the world. Journal of alloys and compounds, 408:1339-1343.

Kashiwabara, T., Toda, R., Fujinaga, K., Honma, T., Takahashi, Y., & Kato, Y. (2013). Determination of host phase of lanthanum in deep-sea REY-rich mud by XAFS and μ-XRF using high-energy synchrotron radiation. Chemistry Letters, 43(2):199-200.

Kasten, S. Glasby, G. P., Schulz, H. D., Friedrich, G., Andreev, S. I. (1998). Rare earth elements in manganese nodules from the South Atlantic Ocean as indicators of oceanic bottom water flow. Marine Geology, 146:33-52.

Kato, Y., Fujinaga, K., Nakamura, K., Takaya, Y., Kitamura, K., Ohta, J., Toda, R., Nakashima, T. & Iwamori, H. (2011). Deep-sea mud in the Pacific Ocean as a potential resource for rare-earth elements. Nature Geoscience, 4:535-539.

Kingsnorth, J.D. (2008). Rare earths at the Crossroads. Industrial minerals, September issue 2008.

Kon, Y., Hoshino, M., Sanematsu, K., Morita, S., Tsunematsu, M., Okamoto, N., ... & Takagi, T. (2014). Geochemical Characteristics of Apatite in Heavy REE-rich Deep-Sea Mud from Minami-Torishima Area, Southeastern Japan. Resource Geology, 64(1):47-57.

Koschinsky, A., Fritsche, U., & Winkler, A. (2001). Sequential leaching of Peru Basin surface sediment for the assessment of aged and fresh heavy metal associations and mobility. Deep Sea Research Part II: Topical Studies in Oceanography, 48(17):3683-3699.

Koschinsky, A., & Halbach, P. (1995). Sequential leaching of marine ferromanganese precipitates: Genetic implications. Geochimica et Cosmochimica Acta, 59(24):5113-5132.

Koschinsky, A., & Hein, J. R. (2003). Uptake of elements from seawater by ferromanganese crusts: solid-phase associations and seawater speciation. Marine Geology, 198(3):331-351.

Koschinsky, A., Stascheit, A., Bau, M., & Halbach, P. (1997). Effects of phosphatization on the geochemical and mineralogical composition of marine ferromanganese crusts. Geochimica et Cosmochimica Acta, 61(19):4079-4094.

Kuhn, T., Bau, M., Blum, N., Halbach, P. (1998). Origin of negative Ce anomalies in mixed hydrothermal-hydrogenetic Fe–Mn crusts from the Central Indian Ridge. Earth and Planetary Science Letters 163:207–220.

Langdon K, Warne M.S.J., Sunderam R.I.M. (2009). A compilation of data on the toxicity of chemicals to species in Australasia. Part 4: metals (2000-2009). Australasian Journal of Ecotoxicology, 15:51-184.

Lee, J. H., & Byrne, R. H. (1992). Examination of comparative rare earth element complexation behavior using linear free-energy relationships. Geochimica et Cosmochimica Acta, 56(3):1127-1137.

Li, Y.-H. (1981). Ultimate removal mechanisms of elements from the ocean. Geochimica et Cosmochimica Acta, 46:1053-1060.

Li, J., Huang, X., Zhu, Long, Z., Peng, X., Cui, D. (2007). Extracting rare earth from D2EHPA-HEHEHP-H2SO4 system. Journal of The Chinese Rare Earth Society, 25:55-58.

Li, Z., Chu, F., Jin, L., Li, X., Dong, Y., Chen, L., & Zhu, J. (2016). Major and trace element composition of surface sediments from the Southwest Indian Ridge: evidence for the incorporation of a hydrothermal component. Acta Oceanologica Sinica, 35(2):101.

Lifton, J. (2009). The lower price hybrid fighter soon to be offered by Toyota. Has Toyota discovered rare metal auditing and conservation? The Chinese society of rare earths.

Long, K. R., Van Gosen, B. S., Foley, N. K., & Cordier, D. (2012). The principal rare earth elements deposits of the United States: a summary of domestic deposits and a global perspective. In Non-Renewable Resource Issues (pp. 131-155). Springer Netherlands.

Luo, Y. R., & Byrne, R. H. (2004). Carbonate complexation of yttrium and the rare earth elements in natural waters. Geochimica et Cosmochimica Acta, 68(4):691-699.

Lyle, M. (1982). Estimating growth rates of ferromanganese nodules from chemical compositions: implications for nodule formation processes. Geochimica et Cosmochimica Acta, 46(11):2301-2306.

Lyle, M., Pälike, H., Nishi, H., Raffi, I., Gamage, K., & Klaus, A. (2010). The pacific equatorial age transect, IODP expeditions 320 and 321: building a 50-million-year-long environmental record of the equatorial pacific. Scientific Drilling, 9:4-15.

Manheim, F.T., Lane-Bostwick, C.M., (1988). Cobalt in ferromanganese crusts as a monitor of hydrothermal discharge on the Pacific sea floor. Nature, 335:59–62.

Mantyla, A. W. & Reid, J. L. (1983). Abyssal characteristics of the World Ocean waters. Deep Sea Research Part A, 30:805-833.

McKelvey, V. E., Wright, N. A., & Rowland, R. W. (1979). Manganese nodule resources in the northeastern equatorial Pacific. In Marine geology and oceanography of the Pacific manganese nodule province, 747-762.

Menendez, A., James, R. H., Roberts, S., Peel, K., & Connelly, D. (2017). Controls on the distribution of rare earth elements in deep-sea sediments in the North Atlantic Ocean. Ore Geology Reviews, 87:100-113.

Meor Yusoff, M.S & Latifah, A. (2002). Rare earth processing in Malaysia: case study of ARE and MAREC plants. Proceedings of the Regional Symposium on Environment and Natural Resources, 10-11 April, Kuala Lumpur, 1:287-295.

Mero, J. L. (1965). The Mineral Resources of the Sea. Elsevier, Amsterdam.

Mewes, K., Mogollón, J. M., Picard, A., Rühlemann, C., Kuhn, T., Nöthen, K., & Kasten, S. (2014). Impact of depositional and biogeochemical processes on small scale variations in nodule abundance in the Clarion-Clipperton Fracture Zone. Deep Sea Research Part I: Oceanographic Research Papers, 91:125-141.

Miljutin, D. M., Miljutina, M. A., Arbizu, P. M., Galeron, J. (2011). Deep-sea nematode assemblage has not recovered 26 years after experimental mining of polymetallic nodules (Clarion Clipperton Fracture Zone, Tropical Eastern Pacific). Deep Sea Research Part I, 58(8):885-897.

Mills, R. A., Wells, D. M., & Roberts, S. (2001). Genesis of ferromanganese crusts from the TAG hydrothermal field. Chemical Geology, 176(1):283-293.

Moldoveanu, G. A., & Papangelakis, V. G. (2012). Recovery of rare earth elements adsorbed on clay minerals: I. Desorption mechanism. Hydrometallurgy, 117:71-78.

Mudd, G. M. (2009). Historical trends in base metal mining: backcasting to understand the sustainability of mining. In Proc." 48th Annual Conference of Metallurgists", Canadian Metallurgical Society, Sudbury, Ontario, Canada.

Murakami, H., & Ishihara, S. (2008). REE mineralization of weathered crust and clay sediment on granitic rocks in the Sanyo Belt, SW Japan and the Southern Jiangxi Province, China. Resource Geology, 58(4):373-401.

Murray, J., & Renard, A. F. (1891). Report on deep-sea deposits based on the specimens collected during the voyage of HMS Challenger in the years 1872 to 1876. HM Stationery Office.

Nagarajan, R., Madhavaraju, J., Armstrong-Altrin, J. S., & Nagendra, R. (2011). Geochemistry of Neoproterozoic limestones of the Shahabad Formation, Bhima Basin, Karnataka, southern India. Geosciences Journal, 15:9-25.

Nakamura, K., Fujinaga, K., Yasukawa, K., Takaya, Y., Ohta, J., Machida, S., ... & Kato, Y. (2015). REY-rich mud: A deep-sea mineral resource for rare earths and yttrium. Handbook on the Physics and Chemistry of Rare Earths, 46:79-127.

Nath, B. N., Balaram, V., Sudhakar, M. & Plüger, W. L. (1992). Rare earth element geochemistry of ferromanganese deposits from the Indian Ocean. Marine Chemistry, 38:185-208.

Ochsenkühn-Petropoulou, M. T., Hatzilyberis, K. S., Mendrinos, L. N., & Salmas, C. E. (2002). Pilot-plant investigation of the leaching process for the recovery of scandium from red mud. Industrial & engineering chemistry research, 41:5794-5801.

Ohta, A., Ishii, S., Sakakibara, M. Mizuno, A., Kawabe, I., 1999. Systematic correlation of the Ce anomaly with the Co/(Ni+Cu) ratio and Y fractionation from Ho in distinct types of Pacific deep-sea nodules. Geochemical Journal 33:399–417.

Opdyke, N. & Foster, J., (1970). The paleomagnetism of cores from the North Pacific. Geological Society of America Memoirs, 126:83-119.

Orris, G. J., & Grauch, R. I. (2002). Rare earth element mines, deposits and occurrences (Vol. 2, No. 189). US Department of the Interior, US Geological Survey.

Parhi, P. K., Park, K. H., Nam, C. W., & Park, J. T. (2015). Liquid-liquid extraction and separation of total rare earth (RE) metals from polymetallic manganese nodule leaching solution. Journal of Rare Earths, 33(2):207-213.

Pattan, J. N., & Parthiban, G. (2011). Geochemistry of ferromanganese nodule–sediment pairs from Central Indian Ocean Basin. Journal of Asian Earth Sciences, 40(2):569-580.

Pattan, J. N., Colley, S., & Higgs, N. C. (1994). Behaviour of rare earth elements in coexisting manganese macronodules, micronodules, and sediments from the Central Indian Basin. Marine Georesources & Geotechnology, 12:283-295.

Piper, D. Z. (1974). Rare earth elements in ferromanganese nodules and other marine phases. Geochimica et Cosmochimica Acta, 38:1007-1022.

Preston, J.S., Cole, P.M., Craig, W.M., Feather, A.M. (1996). The recovery of rare earth oxides from a phosphoric acid by-product. Part I: Leaching of rare earth values and recovery of a mixed rare earth oxide by solvent extraction. Hydrometallurgy, 41:1-19

Piper, D. Z. (1974). Rare earth elements in ferromanganese nodules and other marine phases. Geochimica et Cosmochimica Acta, 38:1007-1022.

Rapin, F., Tessier, A., Campbell, P. G., & Carignan, R. (1986). Potential artifacts in the determination of metal partitioning in sediments by a sequential extraction procedure. Environmental Science & Technology, 20(8):836-840.

Reid, J. L. (1997). On the total geostrophic circulation of the Pacific Ocean: flow patterns, tracers, and transports. Progress in Oceanography, 39:263-352.

Reyss, J.L., Lemaitre, N., KU, T.L., Marchig, V., Southon, J.R., Nelson, D.E., Vogel, J.S., (1985). Growth of amanganese nodule from Peru basin: a radiochemical anatomy. Geochimica et Cosmochimica Acta 49:2401–2408.

Reyss, J. L., Marchig, V., & Ku, T. L. (1982). Rapid growth of a deep-sea manganese nodule. Nature, 295(5848):401-403.

Riley, J. P., & Sinhaseni, P. R. A. P. A. S. (1958). Chemical composition of three manganese nodules from the Pacific Ocean.

Rona, P. A. (2002). Marine minerals for the 21st century. Episodes, 25(1):2-12.

Rozanov, A. G. (2015). Redox system of the bottom sediments of the western Kara Sea. Geochemistry International, 53(11):987-1001.

Rühlemann, C., shipboard scientific party, (2010). Cruise report “MANGAN”, microbiology, paleoceanography and biodiversity in the manganese nodule belt of the Equatorial NE Pacific. Bundesanstalt für Geowissenschaften und Rohstoffe (BGR), Sonne Cruise.

Rühlemann, C.,Kuhn, T.,Wiedicke, M.,Kasten, S.,Mewes, K.,Picard, A., (2011). Current status of manganese nodule exploration in the German license area. Proc. Ninth (2011) ISOPE Ocean Mining Symp. International Society of Offshore and Polar Engineers (ISOPE), Maui, 168–173.

Ru'an, C., (1988). Extraction of rare earths from a low-grade, kaolinitic ore by percolation leaching. In: Bautista, R.G., Wong, M.M. (Eds.), Rare Earths: Extraction, Preparation and Applications. The Minerals, Metals and Materials Society, Warrendale, 227–234.

Schijf, J., De Baar, H.J.W., Millero, F.J., (1995). Vertical distributions and speciation of dissolved rare earth elements in the anoxic brines of

Bannock Basin, eastern Mediterranean Sea. Geochimica et Cosmochimica Acta, 59:3285–3299.

Schijf, J. & Marshall, K. S. (2011). YREE sorption on hydrous ferric oxide in 0.5 M NaCl solutions: a model extension. Marine Chemistry, 123:32-43.

Sholkovitz, E. R. (1990). Rare-earth elements in marine sediments and geochemical standards. Chemical Geology, 88(3-4):333-347.

Sholkovitz, E. R. (1995). The aquatic chemistry of rare earth elements in rivers and estuaries. Aquatic Geochemistry, 1(1):1-34.

Sholkovitz E. R., Landing W. M., and Lewis B. L. (1994). Ocean particle chemistry: The fractionation of rare earth elements between suspended particles and seawater. Geochimica et Cosmochimica Acta, 58:1567-1579.

Smith, C. R. & Koslow, J. T. (2007). Pew Workshop on Design of Marine Protected Areas for Seamounts and the Abyssal Nodule Province in Pacific High Seas. Honolulu, 23-26 October-2007 East West Center - University of Hawaii.

Smith, W. H., & Sandwell, D. T. (1997). Global sea floor topography from satellite altimetry and ship depth soundings. Science, 277(5334):1956-1962.

Somayajulu, B. L. K. (1967). Beryllium-10 in a manganese nodule. Science, 156(3779):1219-1220.

Sørensen, H., Bailey, J. C., & Rose-Hansen, J. (2011). The emplacement and crystallization of the U–Th–REE-rich agpaitic and hyperagpaitic lujavrites at Kvanefjeld, Ilímaussaq alkaline complex, South Greenland. Bulletin of the Geological Society of Denmark, 59:69-92.

Sval'nov, V. N., Lyapin, A. B., & Novikova, Z. T. (1991). Manganese micronodules: communication 2. Composition and origin. Lithology and Mineral Resources, 26(4):32-50.

Sverdrup, H. U., Johnson, M. W. & Fleming, R. H. (1970). The Oceans. Prentice Hall, Englewood Cliffs, N.J., 1087 pp. Takaya, Y., Fujinaga, K., Yamagata, N., Araki, S., Maki, R., Nakamura, K., Iijima, K. and Kato, Y., 2015. Chemical leaching of rare earth elements from highly REY-rich mud. Geochemical Journal, 49(6):637-652.

Takaya, Y., Fujinaga, K., Yamagata, N., Araki, S., Maki, R., Nakamura, K., ... & Kato, Y. (2015). Chemical leaching of rare earth elements from highly REY-rich mud. Geochemical Journal, 49(6):637-652.

Theberge Jr, A. E., & Cherkis, N. Z. (2013). A Note on Fifty Years of Multi-beam. Hydro International.

Thiel, H., Schriever, G. and Foell, E.J. (2005). Polymetallic nodule mining, waste disposal, and species extinction at the abyssal seafloor. Marine Georesources and Geotechnology, 23(3):209-220.

Thomson, J., Carpenter, M.S.N., Colley, S. & Wilson, T.R.S. (1984). Metal accumulation rates in northwest Atlantic pelagic sediments. Geochimica et Cosmochimica Acta, 48:1935-1948.

Toyoda, K., Nakamura, Y. & Masuda, A. (1990). Rare earth elements of Pacific pelagic sediments. Geochimica et Cosmochimica Acta, 54:1093-1103.

Tran, T., (1991). New developments in the processing of rare earths. Materials Science Forum. International Conference on Rare Earth Minerals and Minerals for Electronic Uses, January 23–25, HatYai, Thailand, 1991. Trans Tech Publications, Switzerland, 337–354.

Turekian, K., & Imbrie, J. (1966). The distribution of trace elements in deep-sea sediments of the Atlantic Ocean. Earth & Planetary Science Letters, 1:161-168.

Turekian, K., Wedepohl, K. (1961). Distribution of the elements in some major units of the earth's crust. Geological Society of America Bulletin, 72:175-192.

Tyrer, M., & Sykes, J. P. (2013). The statistics of the rare earths industry. Significance, 10(2), 12-16.

U.S. Geological Survey. (2014). Mineral Commodity Summaries, February 2014.

Usui, A., & Someya, M. (1997). Distribution and composition of marine hydrogenetic and hydrothermal manganese deposits in the northwest Pacific. Geological Society, London, Special Publications, 119(1):177-198.

Van Gosen, B. S., Verplanck, P. L., Long, K. R., Gambogi, J., Robert, R., & Seal, I. I. (2014). The rare-earth elements: vital to modern technologies and lifestyles (No. 2014-3078). US Geological Survey.

Verlaan, P.A., Cronan, D.S., Morgan, C.L., (2004). A comparative analysis of compositional variations in and between marine ferromanganese nodules and crusts in the South Pacific and their environmental controls. Progress in Oceanography, b 63:125–158.

Von Stackelberg, U. & Beiersdorf, H. (1990). The formation of manganese nodules between the Clarion and Clipperton fracture zones southeast of Hawaii. Marine Geology, 98:411-423.

Voncken, J. H. L. (2015). The Rare Earth Elements: An Introduction. Springer.

Vu, H., Jandova, J., Lisa, K., & Vranka, F. (2005). Leaching of manganese deep ocean nodules in $FeSO_4$–H_2SO_4–H_2O solutions. Hydrometallurgy, 77(1):147-153.

Vulcan, T. (2012). Rare earth metals: not so rare, but still valuable. Rare Earth Metals: Not so Rare, but Still Valuable.

Weaver, P.P.E & Thomson, J. (Eds.) (1987). Geology and Geochemistry of Abyssal Plains. Blackwell Scientific Publications.

Wedding, L. M., Friedlander, A. M., Kittinger, J. N., Watling, L., Gaines, S. D., Bennett, M., & Smith, C. R. (2013). From principles to practice: a

spatial approach to systematic conservation planning in the deep sea. Proceedings of the Royal Society of London B: Biological Sciences, 280(1773): 20131684.

Wegorzewski, A. V. & Kuhn, T. (2014). The influence of suboxic diagenesis on the formation of manganese nodules in the Clarion Clipperton nodule belt of the Pacific Ocean. Marine Geology, 357:123-138.

Wegorzewski, A. V., Kuhn, T., Dohrmann, R, Wirth, R., Grangeon, S. (2015). Mineralogical characterization of individual growth structures of Mn-nodules with different Ni+Cu content from the central Pacific Ocean. American Mineralogist, 100:2497-2508.

Winters, G. V. & Buckley, D. E. (1992) Factor analyses as a method of evaluation sediment environmental quality in Halifax Harbour, Nova Scotia. Geological Survey of Canada, Current Research, Part D, Paper 92-1D, 165-171.

Wu, C., Yuan, Z., & Bai, G. (1995). Rare earth deposits in China. mineralogical society series, *7*:281-310.

Yasukawa, K., Nakamura, K., Fujinaga, K., Machida, S., Ohta, J., Takaya, Y., & Kato, Y. (2015). Rare-earth, major, and trace element geochemistry of deep-sea sediments in the Indian Ocean: Implications for the potential distribution of REY-rich mud in the Indian Ocean. Geochemical Journal, 49(6):621-635.

Zhang, Z. G., Du, Y. S., Gao, L. F., Zhang, Y., Shi, G. Y., Liu, C. S., Zhang, P. & Duan, X. K. (2012). Enrichment of REEs in polymetallic nodules and crusts and its potential for exploitation. Journal of Rare Earths, 30:621-626.

Zhang, X., Zhang, F., Xin, C. H. E. N., Zhang, W., & Han, D. E. N. G. (2012). REEs fractionation and sedimentary implication in surface sediments from eastern South China Sea. Journal of Rare Earths, 30(6):614-620.

Zhong, S. J., & Mucci, A. (1995). Partitioning of rare earth elements (REEs) between calcite and seawater solutions at 25 C and 1 atm, and high dissolved REE concentrations. Geochimica et Cosmochimica Acta, 59(3):443-453.

Website links

Anon, (2018). The Global Source for Metals Pricing. [online] Available at: http://mineralprices.com).

Cmegroup.com. (2017). Futures & Options Trading for Risk Management - CME Group. [online] Available at: http://www.cmegroup.com b

Gobi.org. (2017). GOBI – Global Ocean Biodiversity Initiative. [online] Available at: http://gobi.org/

Institute, C. (2017). Promoting the sustainable and responsible use of cobalt in all forms | Cobalt Institute - formerly the Cobalt Development Institute (CDI). [online] Thecdi.com. Available at: http://www.thecdi.com

Insg.org. (2017). International Nickel Study Group. [online] Available at: http://www.insg.org

ISA (2014). Polymetallic nodules. International Seabed Authority Technology brochure. [online] Available at: https://www.isa.org.jm/files/documents/EN/Brochures/ENG7.pdf

Langton, D. (2017). Buy online from the UK's leading B2B chemical suppliers. [online] ReAgent Chemicals. Available at: https://www.chemicals.co.uk/

Manganese.org. (2017). Homepage | International Manganese Institute. [online] Available at: http://www.manganese.org